

Copyright

by

Brian G. McConnell

1999

A COUPLED HEAT TRANSFER AND ELECTROMAGNETIC  
MODEL FOR SIMULATING MICROWAVE HEATING OF  
THIN DIELECTRIC MATERIALS IN A RESONANT CAVITY

by

Brian Gregory McConnell

Thesis submitted to the Faculty of the  
Virginia Polytechnic Institute and State University  
in partial fulfillment of the requirements for the degree of

MASTER OF SCIENCE

in

Mechanical Engineering

APPROVED:

---

James R. Thomas, Jr., Chairman

---

James R. Mahan

---

William A. Davis

December, 1999  
Blacksburg, VA

Keywords: Microwave, Ceramic, Simulation, Heating, Field, Loss

# **A COUPLED HEAT TRANSFER AND ELECTROMAGNETIC MODEL FOR SIMULATING MICROWAVE HEATING OF THIN DIELECTRIC MATERIALS IN A RESONANT CAVITY**

by

Brian Gregory McConnell  
James R. Thomas Jr., Chairman  
Mechanical Engineering

## **ABSTRACT**

Microwave heating is an emerging but still underutilized tool in modern industrial applications. The task of designing microwave applicators for heating industrial materials with temperature-dependent properties is challenging, and trial-and-error system prototyping is an expensive and wasteful means to accomplish this goal. The purpose of this work is to combine existing heat transfer and electromagnetic models to provide a complete simulation for heating dielectric materials in a resonant microwave cavity. The numerical simulation is validated by comparison to several independent sets of experimental data. The ultimate goal is to provide a research tool that will facilitate the industrial microwave applicator design process. With a complete, accurate, and user-friendly numerical simulation, parameters affecting the temperature distribution in stationary and moving process materials can be studied to optimize the results before the first prototype is made. This work also explores the sources of power loss in a microwave system and develops means for quantifying these power losses.

# Acknowledgements

I would like to thank my parents, Mike and Linda McConnell, for providing wisdom, encouragement, and support in good times and bad. No matter what, they have been there to keep me focused and on the path to success. I would not be where I am today without their love.

I must also thank my advisor, Dr. James R. Thomas Jr., for his patience, advice and expertise. His mentorship style, guiding rather than leading, has allowed me to strengthen my intellectual wings and tackle problems on my own. When I needed it, he was always ready with a helpful suggestion and insight that only comes with years of experience.

I would also like to thank Dr. James R. Mahan and Dr. William A. Davis, the other members of my advisory committee. Their knowledge of radiation heat transfer and electromagnetics, respectively, has been essential to my thesis work.

Finally, I would like to thank my bride-to-be, Covey Jean Horn. She has been there for me as a true companion. Her ability to tolerate my incessant ramblings about microwave fields and numerical simulations with a smile on her face speaks volumes of her patience and loving nature. I shall be so lucky to spend the rest of my life with her.

# Table of Contents

<b>Acknowledgements</b> .....	<b>iii</b>
<b>Abstract</b> .....	<b>iv</b>
<b>List of Tables</b> .....	<b>vii</b>
<b>List of Figures</b> .....	<b>viii</b>
<b>Chapter 1 - Introduction</b>	<b>1</b>
1.1 Statement of the Problem .....	1
1.2 Limitations .....	2
1.3 Need of the Study.....	3
1.4 Microwave Fundamentals .....	3
1.4.1 A Brief History of Microwaves.....	3
1.4.2 Benefits of Microwave Heating .....	6
1.4.3 Modern Microwave Applications.....	7
1.4.4 Microwave Basics .....	11
1.4.5 Microwave/Material Interaction.....	27
1.4.6 Waveguides and Resonators.....	35
<b>Chapter 2 - Historical Review</b>	<b>40</b>
2.1 Literature Review .....	40
2.1.1 Challenges in Modeling .....	41
2.1.2 Electromagnetic Field Models .....	41
2.1.3 Heat Transfer Models.....	45
2.1.4 Combined Electromagnetic/Heat Transfer Models.....	49
2.1.5 Summary .....	50
2.2 LANL Experiments .....	51
2.3 Prior Work at Virginia Tech.....	59
<b>Chapter 3 - Method of Investigation</b>	<b>67</b>
3.1 Heat Transfer Model .....	67
3.1.1 Thermophysical Properties.....	75

3.2 Electromagnetic Field Model.....	77
3.2.1 Dielectric Properties.....	84
3.3 Interface Development.....	86
3.4 Data Collection.....	87
<b>Chapter 4 - Interpretation of the Data</b>	<b>90</b>
4.1 Comparison of Simulation to LANL Data.....	90
4.1.1 Microwave Power Losses.....	90
4.1.2 VT305A Simulation Results.....	97
4.1.3 Additional Simulations Based On LANL Parameters.....	99
4.2 Comparison of Simulation to Virginia Tech Data.....	105
4.2.1 Transient Heating Comparison.....	106
4.2.2 Steady-State Heating Comparison.....	108
4.3 Justification of Results.....	116
4.3.1 LANL Comparison.....	116
4.3.2 Virginia Tech Comparison.....	120
<b>Chapter 5 - Conclusions and Recommendations</b>	<b>127</b>
5.1 Conclusions.....	127
5.2 Recommendations.....	128
<b>Bibliography</b>	<b>133</b>
<b>Appendix A - Heat Transfer Simulation Code</b>	<b>140</b>
<b>Appendix B - Field Simulation Code</b>	<b>179</b>
<b>Appendix C - User Interface Code</b>	<b>206</b>
<b>Vita</b>	<b>244</b>

# List of Tables

2.1	Legend items for figure 2.1 .....	52
2.2	Section properties of a WR-284 waveguide.....	54
3.1	Boundary and initial conditions for nodal finite-difference equations.....	73

# List of Figures

1.1	The electromagnetic spectrum .....	12
1.2	A propagating electromagnetic wave .....	14
1.3	Historical development of microwave generators and amplifiers (National Research Council, 1994) .....	16
1.4	Power-frequency output limits of various microwave generators (National Research Council, 1994) .....	17
1.5	Schematic of a magnetron microwave generator .....	18
1.6	The distribution of electrons in the magnetron interaction space (Veley, 1987).....	20
1.7	Schematic of a 4-cavity klystron microwave amplifier .....	21
1.8	Schematic of a helix traveling wave tube (TWT) microwave generator (Gilmour, 1994).....	23
1.9	RF charge and electric field patterns for a helix (Gilmour, 1994) .....	25
1.10	The atomic structure and dipole moment of the water molecule .....	29
1.11	The temperature dependence of $\epsilon''$ in zirconia .....	32
1.12	%TD versus sintering temperature and duration for mullite (Schneider et al., 1994) .....	34
2.1	The LANL experimental microwave applicator .....	52
2.2	Schematic layout of the "beyond-cutoff" variable coupler .....	55
3.1	Schematic representation of the process material for applying boundary conditions (Goodson, 1997).....	73
3.2	Outline of the computations performed by the heat transfer model.....	74
3.3	Emissivity of alumina (Touloukian, 1972) and mullite (Bauer and Steinhardt, 1990) .....	76
3.4	A schematic representation of the electromagnetic solution regions.....	78
3.5	Distribution of the electric and magnetic field components in a TE <sub>10</sub> mode (Veley, 1987) .....	80

3.6	Dielectric constant and dielectric loss of mullite .....	85
4.1	A cavity characterization curve for 190 W forward power.....	93
4.2	Loss versus tuning block position and forward power in the variable coupler .....	95
4.3	Experimental load power versus simulation rod power for LANL vt305a .....	98
4.4	Experimental versus simulated temperatures and % error for LANL vt305a .....	99
4.5	Midpoint steady-state surface temperatures versus absorbed power as predicted for a 4.5 mm mullite rod .....	100
4.6	Midpoint steady-state surface temperatures versus average electric field strength as predicted for a 4.5 mm mullite rod .....	101
4.7	Predicted power-temperature response curve for an alumina sphere (NMAB, p. 37, 1994) .....	102
4.8	Radial temperature distribution at steady-state, 150 W .....	103
4.9	Midpoint transient surface temperature at 150 W absorbed power .....	104
4.10	Transient axial temperature distribution at 150 W absorbed power .....	105
4.11	Transient heating at 5 W, simulated and experimental results.....	108
4.12	Comparison of simulated and measured temperatures at low levels of absorbed power (low temperature pyrometer used).....	109
4.13	Comparison of simulation and experimental electric field intensities at low levels of absorbed power.....	110
4.14	Comparison of simulation and experimental temperatures at high levels of absorbed power (high temperature pyrometer used) .....	111
4.15	Comparison of simulation and experimental electric field intensities at high levels of absorbed power.....	112
4.16	Comparison of steady-state midpoint temperatures and average electric field intensity between enhanced and uniform field simulations .....	114
4.17	Axial temperature and field comparison, uniform and enhanced field models .....	116

4.18	Power absorption and temperature predictions of Goodson's model (Goodson, 1997).....	120
4.19	Standing wave patterns in a WR-284 cavity at two source frequencies .....	122
4.20	Temperature measurement error as a function of temperature, wavelength, and emissivity error (NMAB, 1994).....	126
5.1	Temperature and field asymmetry.....	133

# Chapter 1

## Introduction

The use of microwave heating in many industrial processes today represents the culmination of over a hundred years of effort by scientists and engineers around the globe. The benefits gained through this technology are numerous, as is detailed in the following sections. Indeed, this science is still in its adolescence, for the pace of development proceeds at an ever-growing rate. This work deals with numerical simulation and experimental validation of a very specific microwave heating venue: heating cylindrical dielectric rods in a single-mode resonant cavity. In order for the details of this work to be understandable to a reader without an extensive background in the field of heat transfer and electromagnetic radiation, some fundamental background information must be presented before the specifics can be discussed. However, the specific problem at hand and the purpose for undertaking this work must be given first. In the following sections, the problem is specified further by noting the aspects that are included in this work as well as those that are not.

### 1.1 Statement of the Problem

The purpose of this work is to develop an advanced numerical simulation to model the controlled heating of dielectric materials, such as ceramics and polymers, with microwave power in a rectangular, single-mode resonant cavity. The simulation is

intended for use as a tool to explore the effects of the various parameters on the temperature distribution, power absorption, and heating rate of the process material. These parameters include iris dimensions, source frequency and strength, process material composition, size, properties and velocity, and environment temperatures. By exploring the effects of these parameters, the simulation can be used to develop custom microwave applicators. By eliminating the need for trial-and-error applicator prototyping, considerable savings of time and resources can be achieved. This simulation represents the most current development of the continuing efforts at Virginia Tech to provide the most complete solution to the problem at hand.

This endeavor combines independently developed numerical models of the heat transfer and electromagnetic scenarios to solve for the temperature and electric field distributions iteratively at each time step. By incorporating the results of careful laboratory experiments, this work attempts to account for power losses in the microwave applicator that were not dealt with in previous numerical models. This simulation is verified against several experimental data sets as opposed to analytical models to ensure the accuracy and validity of the current numerical model.

## 1.2 Limitations

The focus of this work is limited to the simulation of rectangular waveguides operating in the  $TE_{10n}$  dominant mode with a single-mode resonant cavity coupled by a rectangular iris. The current work assumes the waveguide to be a uniform WR-284 cross-section with the exception of the dielectric-filled impedance matching section to be discussed in detail later. The process material is assumed to be a cylindrical dielectric material with a circular cross-section, a diameter that is "thin" compared to the wavelength of the propagating microwave energy ( $d_{rod} \ll \lambda$ ), and homogenous material composition. The material thermal, optical, and dielectric properties are allowed to vary axially and radially within the sample due to temperature dependence. As a consequence of the assumptions that the rod is "thin" and of homogeneous composition, it is assumed that there are no variations in the circumferential direction of the rod and that the solid

can be realistically modeled in two dimensions (radial and axial) instead of three. The model assumes the material orientation is in a vertical transverse position at the center of the wide dimension of the waveguide cross-section. Additionally, it assumes that the material is located at a maximum of the electric field standing wave pattern within the resonant cavity. The focus of the current investigation is on the assumption that the power absorption by the load is controlled; previous works have explored this scenario as well as the constant electric field strength option and found that power control is necessary to control thermal runaway phenomena. The material selection is limited to those where sufficient property data are available for accurate numerical simulation and experimental data are available for comparison of the results.

## **1.3 Need of the Study**

An accurate numerical simulation of the problem at hand, properly verified against reliable experimental data, may facilitate process design for industrial applications. The inclusion of an advanced electromagnetic field simulation allows the designer to analyze the effects of aperture shaping to affect the temperature distribution in the process material. This would decrease design time and cost, reducing the need for prototyping many experimental configurations to achieve an acceptable design.

## **1.4 Microwave Fundamentals**

### **1.4.1 A Brief History of Microwaves**

Microwaves have existed since the dawn of our universe some 10 billion years ago. In the year 1965, Arno Penzias and Robert Wilson from the AT&T Bell Laboratory discovered the nearly isotropic and isothermal cosmic background radiation that finally provided conclusive evidence of the validity of the famous Big Bang theory. The

radiation field they discovered consisted of low-energy microwaves (Adams and Laughlin, 1999).

The age of modern electromagnetic devices was ushered in when James Clerk Maxwell published his Treatise on Electricity and Magnetism in the year 1873 (Thuery, 1992). In this work, Maxwell hypothesized that electric and magnetic fields could propagate through a vacuum at the speed of light via coupled wave components aligned perpendicular to one another. This theory was later verified through the experimental works of two equally famous scientists, Hermann Von Helmholtz and Heinrich-Rudolf Hertz, during the years from 1879 to 1887. Hertz was also the first scientist to intentionally generate electromagnetic waves in the form of radio signals in the lower portion of the microwave frequency band (430 MHz) using a simple electric oscillator. Hertz continued in his experimentation with such devices and was able to confirm the speed of propagation postulated by Maxwell and demonstrated such electromagnetic phenomena as refraction, deflection, polarization, and standing waves due to constructive wave interference. The scientific community was quick to join in pioneering this new technology and in the year 1894, Guglielmo Marconi raised the bar by utilizing microwave signals at 1.2 GHz to transmit wireless communications over a distance of 4 km. He went on to extend the range of this feat to over-the-horizon communication by the year 1931. At the time of the first microwave communications, the term 'microwave' had yet to be uttered. Andre Clavier, who later went on to demonstrate wireless telephone communication over a distance of 51 km at 1.7 GHz, was the first scientist to use such a phrase. The exact range of frequencies to be called 'microwaves' is still subject to slight variation from one text to another, although it is generally agreed upon as is discussed in Section 1.4.4.

The next major development in the use of radio frequencies besides communications (which, of course, includes radios people listen to) was the development of systems to detect large metallic objects. The principle was first developed by a scientist named Christian Hulsmeyer in the year 1904 when he observed that reflected radio signals from large metallic objects could be detected at a great distance. The first military application of his studies were not realized until 1934 when a large emitter/antenna array was mounted aboard a naval vessel for the purpose of detecting

other ships under conditions where visual detection would not be possible. A scaled-up version of the device was mounted on a fixed land-based structure the following year for detecting aircraft. These early detectors utilized the same principles of modern radar, but they operated at frequencies below the microwave band due to the power/frequency limitations of the time. However, these early developments paved the way for true microwave band detectors engineered simultaneously in the US and Britain during WWII for installation onboard aircraft. This style of passive detector meant that the information from ground-based radar stations no longer had to be radioed to pilots, thus their presence was no longer compromised unless detected by the enemy.

Until the early 1940's, the uses of microwave frequencies had been limited to communication and detection. Both of these types of applications use modulated beams that carry information in the form of a signal. By 1943, the potential for other uses of microwaves that did not carry signals had been recognized (National Materials Advisory Board, 1994). The following quote summarizes the early realization that microwaves could be used for heating purposes:

High-frequency heating really started when engineers working on short-wave transmitters contracted artificial fevers. The great virtues of this kind of heat are as follows:  
The heat is generated directly in the object itself; no transfer of heat is involved. Associated apparatus need not be heated. The surfaces of the material need not be affected. The people who work with the equipment have cooler working conditions. No gases are involved and thus the likelihood of corroded surfaces is eliminated. The material can be heated from the inside-out. Finally, objects of unusual size or shape can be heated.

Scientific American, 1943

Since microwave generators in the past had utilized modulated beams produced by pulsing sources for generating microwave signals, the doorway to dedicated microwave heating was opened in the year 1944 by W.C. Brown and P. Derby (Theury, 1992). These scientists at Raytheon, a company that helped to develop one of the first military aircraft radar, created the first magnetron generator capable of producing a continuous output wave instead of a pulsed one. It was not until 1951 that the first American patent

for a microwave oven for food heating was issued, although P.W. Morse and H.E. Rivercomb of General Electric had devised the first such device much earlier. The first American restaurant to serve pre-packaged meals heated by microwaves opened in 1962 using a British microwave generator, which at the time were more economical than similar American units. Microwave heating continued to have far greater prevalence in the commercial food preparation industry than in other industrial applications for quite some time. Microwave energy was found to be superior to conventional heating for such tasks as thawing, dehydrating, freeze-drying, and sterilization. Early industrial applications were primarily limited to vulcanization of rubber. Microwaves are used for such tasks to this day as well as many others as shown in Section 1.4.3. Home ovens did not become popular until the 1970's and the market for these units peaked in 1984 when it is estimated that 40% of all households in industrialized nations owned a microwave oven.

## **1.4.2 Benefits of Microwave Heating**

There is a fundamental difference in the nature of microwave heating when compared to conventional methods of heating materials. Conventional heating relies on one or more of the heat transfer mechanisms of convection, conduction, or radiation to transfer thermal energy into the material. In all three cases, the energy is deposited at the surface of the material and the resulting temperature gradient established in the material causes the transfer of heat into the core of the object. Thus, the temperature gradient is always into the material with the highest temperatures being at the surface. In microwave heating, the microwave energy interacts with the surface material but also penetrates the surface and interacts with the core of the material as well. Energy is transferred from the electromagnetic field into thermal energy throughout the entire volume of the material that is penetrated by the radiation. Microwave heating does not rely on conduction from the surface to bring heat into the core region. Since the heating rate is not limited by conduction through the surface layer, the material can be heated more quickly. Another important aspect of microwave heating is that it results in a temperature gradient in the reverse direction compared to conventional heating. That is to say, the highest

temperatures occur at the center of the object and heat is conducted to the outer layers of the material. For operations such as material drying, this effect is highly beneficial. In addition to the reversal of the temperature gradient, the gradient is smaller compared to conventional heating because the heat is generated in all parts of the material that are receiving the radiation. This effect reduces the internal stresses in the material and can help eliminate problems such as cracking that may occur when the internal stresses become too large.

The fundamental differences between conventional and microwave heating may cause microwave heating to be superior in many heating applications, but the economics involved may dictate that conventional heating be used. Unless there is an economic benefit to using the process, usually driven by the need to perform an operation more quickly, the simple fact is that the conversion of fossil fuels into heat energy is more efficient than converting them into microwave energy. In terms of raw energy, microwave heating may only result in 30% of the energy transfer compared to conventional heating methods from a given quantity of fossil fuel (NMAB, 1994). This is due to losses in converting fossil fuels into electricity, converting the electricity to microwave energy, and the conversion of microwave energy into heat within the material. In some cases, the difference in product quality between the two heating methods is sufficient to justify the use of microwave heating. In other cases, the smaller equipment used in microwave heating devices may be essential to fitting a new device within the limited existing space in a factory. In most instances where microwave heating is economically justifiable, the shorter process times afforded by the volumetric heating aspect tips the scales in favor of microwave heating. The bottom line is that microwave heating has more potential than is economically affordable in some instances.

### **1.4.3 Modern Microwave Applications**

The differences between the heating achieved by conventional and microwave devices gives the advantage to microwaves for several industrial and medical heating applications. The two most influential differences are the volumetric heating and

reversed temperature gradients involved in microwave heating. This section will discuss some of the more common situations in which microwaves are used as a favorable alternative to conventional heating methods.

Drying of materials involves the mechanisms of heat and mass transport. Heat must be delivered into the material as a means to drive moisture from the material. Heating the material causes an increase in the saturation vapor pressure within the material so that it is higher at the surface than the partial pressure of the surrounding air. The resulting pressure gradient drives moisture from the material by means of evaporation (Theury, 1992). The drying rate of a material is limited by the rate at which capillary suction draws moisture to the surface from within the material. When using conventional heating methods, the temperature gradient and moisture gradient in the material occur in opposite directions because the material is heated externally. This can result in excessive drying of the surface layers, or "crusting", which in turn inhibits the transfer of heat into the material and the transport of moisture to the surface. Both of these effects are detrimental to the drying rate. Using microwave heating, both the temperature and moisture gradients occur in the same direction. This effect minimizes the likelihood of crusting and optimizes the rate of moisture removal from the material. Increasing the drying rate with the use of microwaves allows for the use of smaller drying units in industrial processes. Shanghai Enterprise has reported a 50% energy savings in their paper drying process through the use of microwave heating instead of conventional heating because of reduced drying time (Theury, 1992). Companies employing the use of microwaves in the printing industry report a 30% cost savings compared to conventional heating for the task of drying the ink in printed materials. An added benefit of this technology in the drying process for certain products, such as paper, is that the risk of fire is eliminated since the use of open-flame heaters has been discontinued. Drying rates are increased while the product temperature only reaches 80° F instead of 200°-300° F as with conventional heating. Glued products can be dried much more quickly, and leather products can be dried in 30%-50% less time after tanning and with less shrinkage using microwaves. Because of the penetrating effects of microwaves, large poured molds used in the foundry industry can be dried faster and with improved product quality. In the case of large foundry molds, the low thermal conductivity of the material and high thermal

gradients present in drying creates significant complications such as cracking when conventional heating methods are employed. In the plastics industry, where solvents must be removed from the product, microwave heating is highly effective because the solvents are heated more readily than the material. The selective heating of the solvents results in less distortion and damage to the final product.

One of the earliest industrial applications for microwave heating continues to be a major user of the technology to this day. Vulcanization of rubber is the primary task for microwave processing of elastomers. It is an area where many of the same benefits gained by microwave heating in drying applications can be realized. Vulcanization is a process in which the long monomer chains in the material become cross-linked, which results in parts that retain their shape and elastic properties to a much higher degree than do untreated parts (Theury, 1992). Microwaves are also quite instrumental in the devulcanization process that is essential in recycling of many rubber products such as automobile tires.

Still more industrial processes benefit greatly from the use of microwave heating and some would not be possible using only conventional heating methods. These include thermosetting of polyester and epoxy resins, dewaxing of casting molds, soil defrosting, asphalt road repair, and accelerating the setting of concrete (Theury, 1992). They can be used to form emulsions of certain immiscible liquids, aid in the magnetic purification of coal by removing sulfurous compounds, and can solidify droplets of radioactive waste material to aid in waste disposal. One of the most interesting industrial applications involves the use of microwaves to generate extreme internal stresses in rock and concrete to "crush" the material for removal or disposal. One industrial application that results in superior material quality with microwave heating is the sintering of ferrite and ceramic materials. Sintering involves applying pressure and heat to a mold filled with granular or powdered material to cause the grains to fuse together into a solid part. Microwave sintering can result in superior product properties and can virtually eliminate porosity. The mechanisms of microwave sintering of ceramics are discussed further in Section 1.4.5.

Before microwave heating became a serious part of industrial applications it was employed frequently in the food service and agriculture industries. Microwave energy

couples very well with water molecules, which are present in large quantities in most food products and vegetable matter. The specifics of this interaction are discussed in detail in Section 1.4.5. It was realized early on that microwaves are useful in dehydrating, cooking, thawing, freeze drying, and the destruction of fungus, yeast, bacteria, mildew, and pests from many food products. The spoiling of certain fruit and vegetable products can be reduced or delayed through enzymatic inactivation by microwaves (Theury, 1992). Microwaves can be used to kill unwanted seeds and pests in agricultural situations as an environmentally friendly alternative to herbicides. On the other hand, microwaves have shown promise in experimental situations in protecting crops from frost damage. If employed on a large scale, this new technology could save millions of dollars annually in the prevention of crop damage. Because microwave heating can be controlled to a greater degree than conventional heating, it is frequently used in the fermentation of wine. The ideal enzymatic reaction temperature in such a process is 30° C, and microwave heating allows the product to be produced in a third of the time and with a greater quality compared to traditional fermentation methods.

Microwaves are a relatively new technology in the medical field and have been shown to aid in the treatment of diseases such as cancer (Theury, 1992). Irradiating the brain with moderate levels of microwave energy has been shown to increase the permeability of the blood-brain barrier (BBB) to chemotherapy agents. This is an important development in the treatment of brain tumors, as the BBB is relatively impermeable to most chemotherapy drugs. Because the drugs are not effective, surgical removal of the tumors is the only viable treatment to date even though it is a highly dangerous operation. Direct application of microwave energy has shown promise in treating cancers in other parts of the body as well. The microwaves are used to cause "hyperthermia" where the tumor and surrounding tissues are heated to 40° C. This increases the blood flow to the surrounding healthy tissue by a factor of four to six and actually decreases the blood flow to the tumor. Like the effects on the BBB permeability, the local application of microwaves causes the cell membranes of the tumor to be more permeable to the chemotherapy agents. The combination of these effects has been shown to have a significant impact on the success of cancer treatment. While there are medical benefits to specific microwave exposure in certain instances, careless exposure to

microwave fields can lead to health problems. Extremely low levels of exposure are unavoidable today, as microwaves are used for a variety of signal broadcasting and navigational beacons. However, low-level exposure has not been shown to be harmful. In fact, during the cold war era from 1953 to 1976, the US embassy in Moscow was continuously irradiated with low-level RF energy with no apparent adverse effects on the inhabitants. Direct exposure to microwaves of significant intensity for various periods of time has been shown to produce cataracts, testicular degeneration, necrosing coagulations in the brain with behavioral consequences, and other neurological damage. Experiments on bacterial and yeast cells have shown that microwave irradiation at non-thermal levels can disturb the process of cellular division, inhibit certain metabolic processes, and slow the overall growth rate. Microwave irradiation can also alter the composition of chemicals, proteins, and other components in the blood. While irradiation can depress certain immune system functions, some studies have shown that specific schedules of irradiation can actually increase the viral-fighting capabilities in laboratory animals and can increase the production of lymphocytes by a factor of two. Such uses of microwaves, however, are still a long way from providing feasible medical breakthroughs for humans.

#### **1.4.4 Microwave Basics**

The term "nuking" became a popular synonym for cooking food with microwaves at some indistinguishable point in the last 25 years, perhaps after the incident at Three Mile Island. This term leads some people to the mistaken belief that there is some radioactive material such as uranium or plutonium inside the oven and that their ovens could be harmful to them by leaking radiation. The radiation emitted by radioactive isotopes is in the gamma radiation band, at frequencies much higher than those used in microwave devices. This type of radiation is dangerous because it is "ionizing" radiation that is capable of changing molecular configurations and causing cellular damage and mutation. While microwave energy is indeed a form of radiation, it is not the high-energy penetrating radiation such as produced by the spontaneous decomposition of heavy isotopes used in nuclear reactors. Microwaves can cause physical damage if proper

safety is not observed in the presence of strong microwave fields not contained in a shielded device. However, this damage would most likely be in the form of burns or hyperthermia instead of molecular damage, and low levels are not harmful due to the low penetration ability of weak fields. We are constantly in the presence of microwave fields, as they are used quite extensively today for many kinds of communication signals. What is loosely referred to as "radiation" is really electromagnetic waves of various frequencies. The term "radiation" comes from the means by which energy is transported by the force fields of electromagnetic waves; they can "radiate" through a perfect vacuum and do not need any physical medium to transfer energy from one object to another. Electromagnetic energy has many different names associated with it, but it is all the same phenomenon. X-rays, gamma rays, solar radiation, ultraviolet rays, visible light, thermal radiation (including infrared), microwaves and radio waves are all forms of electromagnetic waves with different wavelengths and frequencies. Figure 1.1 below shows the electromagnetic spectrum that is made up by these familiar types of radiation.

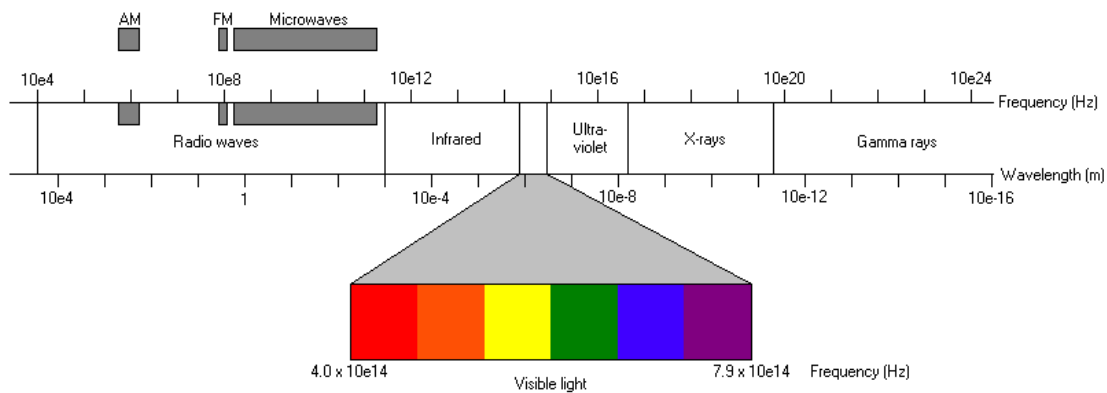


**Figure 1.1:** The electromagnetic spectrum

Two fundamental characteristics of any periodic wave phenomenon are the frequency and the wavelength. For electromagnetic waves, these properties are related by

$$c = f\lambda, \quad (1.1)$$

where  $c$  is the speed of light in the medium,  $f$  is the frequency of the wave, and  $\lambda$  is the wavelength (or spatial repetition) of the wave.

Low frequency electromagnetic waves with long wavelengths are called "radio waves" and are used primarily for broadcasting various types of communications systems within the atmosphere. Microwaves are a subset of radio waves and fall into the frequency range from 300 MHz to 30 GHz, as shown in figure 1.1. It is interesting to note that modern personal computers now have processor clock speeds that are rising into the low end of the microwave frequencies. As clock speeds have increased, the need for adequate electromagnetic interference (EMI) shielding on these devices has become more noticeable. A computer operating at a clock speed between 88 MHz and 108 MHz (the FM frequency band) without sufficient EMI shielding would create substantial interference with nearby radio equipment.

The term "electromagnetic" justifiably implies the involvement of electric and magnetic components in an electromagnetic wave. As postulated by Maxwell in 1873, such waves are indeed composed of electric and magnetic field components aligned at right angles to one another. The components are in phase and vary in time and space as they propagate. The orientation obeys the familiar "right-hand-rule" where the index finger indicates the direction of propagation, the extended thumb indicates the alignment of the  $\vec{E}$  field, and the palm indicates the alignment of the  $\vec{H}$  field component. Figure 1.2 depicts a continuous propagating electromagnetic wave at one instant in time that is emitted along the x-axis from the origin.

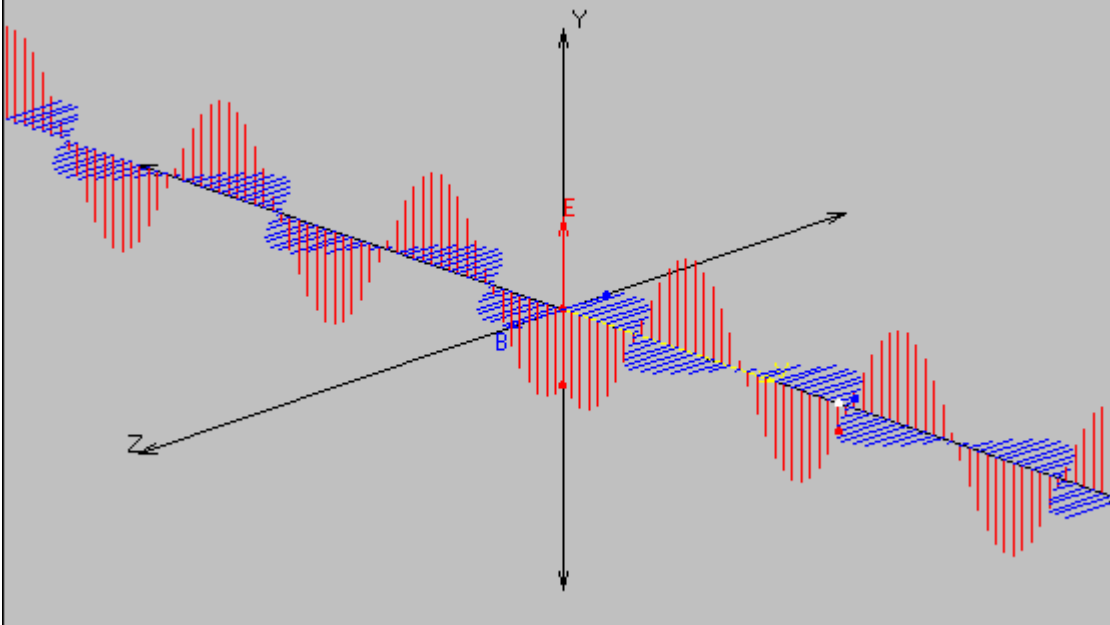


**Figure 1.2:** A propagating electromagnetic wave

At a later instant in time, the location of the peaks in the field components would be shifted in the direction of propagation along the x-axis. In the figure, the electric field, denoted as  $E$ , is aligned with the y-axis and the magnetic field, denoted as  $B$ , is aligned with the z-axis. The orientation of either of the fields may be in any direction about the axis of propagation but the two field components are always constrained to be perpendicular to one another. Electromagnetic waves, like other types of wave phenomena, can exhibit reflection, refraction, polarization, and constructive and destructive interference, as was shown by Hertz in the late nineteenth century.

In principle, electromagnetic waves are generated by the acceleration or deceleration of electrically charged particles, such as electrons. As mentioned previously, the first such devices used to intentionally generate electromagnetic waves were simple electronic oscillators. The most rudimentary of such devices could consist of a voltage source, such as a battery, and a loop of wire to complete the circuit. When the circuit is closed and the positive and negative terminals are connected by the wire, there is an initial period where the free electrons in the wire are accelerated by the electrical potential difference of the battery. Likewise, when the circuit is opened, no electrical potential drives the flow of electrons in the wire and they decelerate to rest. Due to the acceleration of charged particles, opening and closing the circuit causes the

production of a pulse of electromagnetic energy to leave the wire in the form of an electromagnetic wave. When the flow of current does not vary in time, no electromagnetic wave is produced; static fields can exist independently. A stationary permanent magnet, such as in a stereo speaker, produces a magnetic field in its vicinity with no accompanying electric field. In a fully charged parallel-plate capacitor, a net negative charge collects on one plate and a net positive charge on the other which results in an electric field surrounding the plates with no magnetic field. However, an electric or magnetic field that varies in time produces a field of the other type. This is the principle of induction. A meter designed to measure AC electric current flow in a wire indirectly by detecting the induced magnetic field will not work on a wire carrying only DC current because no magnetic field is induced. In an electromagnetic wave, both components are varying in time and space, so of course both components must exist, as they are coupled phenomena.

Certainly, the means to produce electromagnetic waves has become much more sophisticated in the last 120 years. Modern devices rely on a variety of ways to accelerate and decelerate electrons to achieve continuous output of electromagnetic energy instead of the brief pulses created by the electric oscillators described above, and at much higher frequencies. While acceleration of charged particles creates electromagnetic waves, electromagnetic waves can cause the acceleration of charged particles. This duality is the fundamental principle in modern devices to produce electromagnetic waves, including microwave generators. Figure 1.3 outlines the development of the most important microwave generators since 1920.

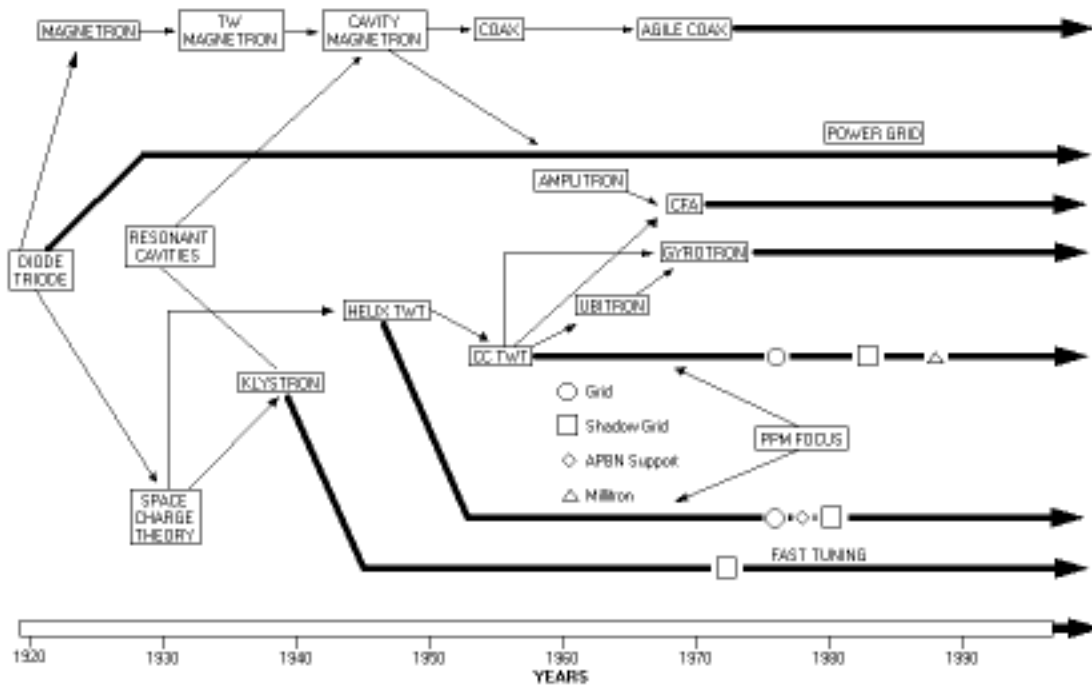


**Figure 1.3:** Historical development of microwave generators and amplifiers (National Research Council, 1994)

The invention of the diode early in the twentieth century made it possible to generate electromagnetic waves at higher frequencies than before with electric oscillators due to its high-speed switching ability. Still, the real advances in microwave generators did not come about until the invention of the magnetron, which is discussed in more detail later in this section. It was a huge advance in that it was the first device to use the interrelation between the acceleration of electrons and a time-varying electromagnetic field to produce microwave energy. Early magnetron units generated pulses of electromagnetic energy output but later units were capable of continuous output. The development of the magnetron was followed by the other major microwave generators, the klystron, the traveling wave tube (TWT) and the gyrotron. Each successive device became more sophisticated and more costly. The different designs can be constructed to operate with specific power and frequency capabilities, as is shown in figure 1.4. While most microwave generators can only operate at one frequency to which the resonant

properties of the structure have been designed, the TWT amplifiers do not rely on a resonance and are capable of variable frequency output.

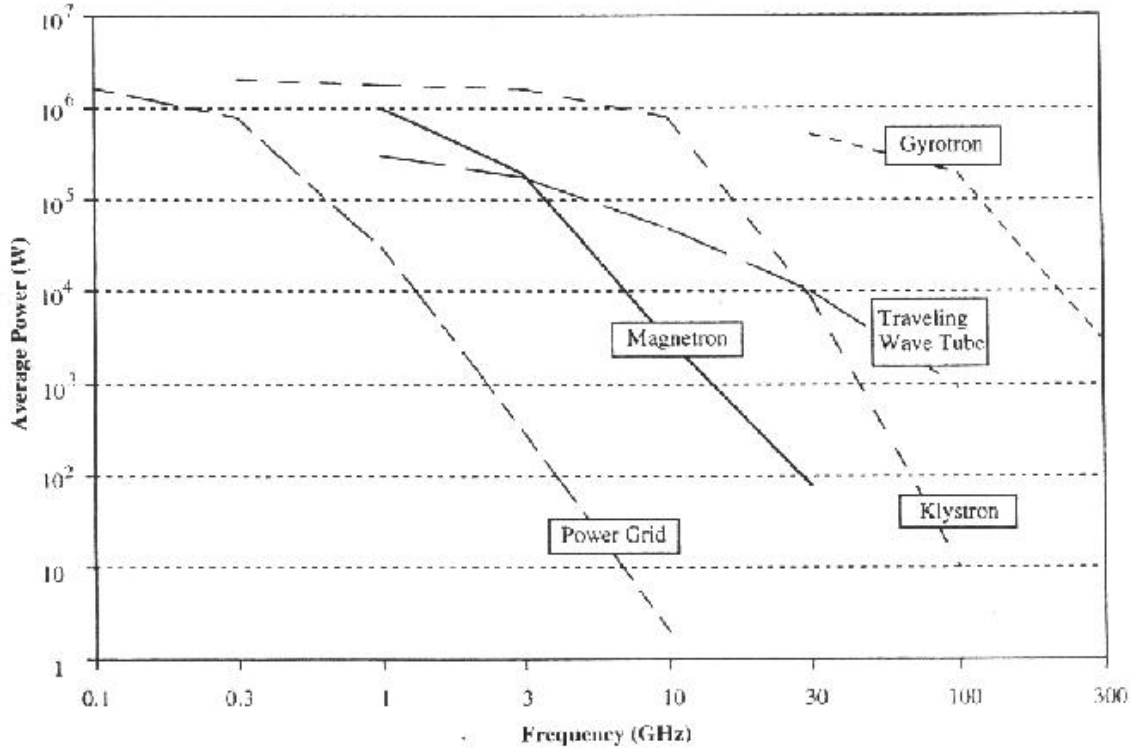


**Figure 1.4:** Power-frequency output limits of various microwave generators (National Research Council, 1994)

The operating principle of the magnetron microwave source was the brainchild of Albert Wallace Hull in the year 1921. The device was later prototyped and developed independently by researchers in Czechoslovakia, Britain, France, Germany, Japan, and the United States (Thuery, 1992). The magnetron is the most common and widely used microwave generator as it is the heart of every modern household microwave oven. Typical home ovens have an output of about 700-800 W with efficiencies approaching 65%, but units exist capable of several thousand W or more. The essential components of the magnetron source are shown in figure 1.5.

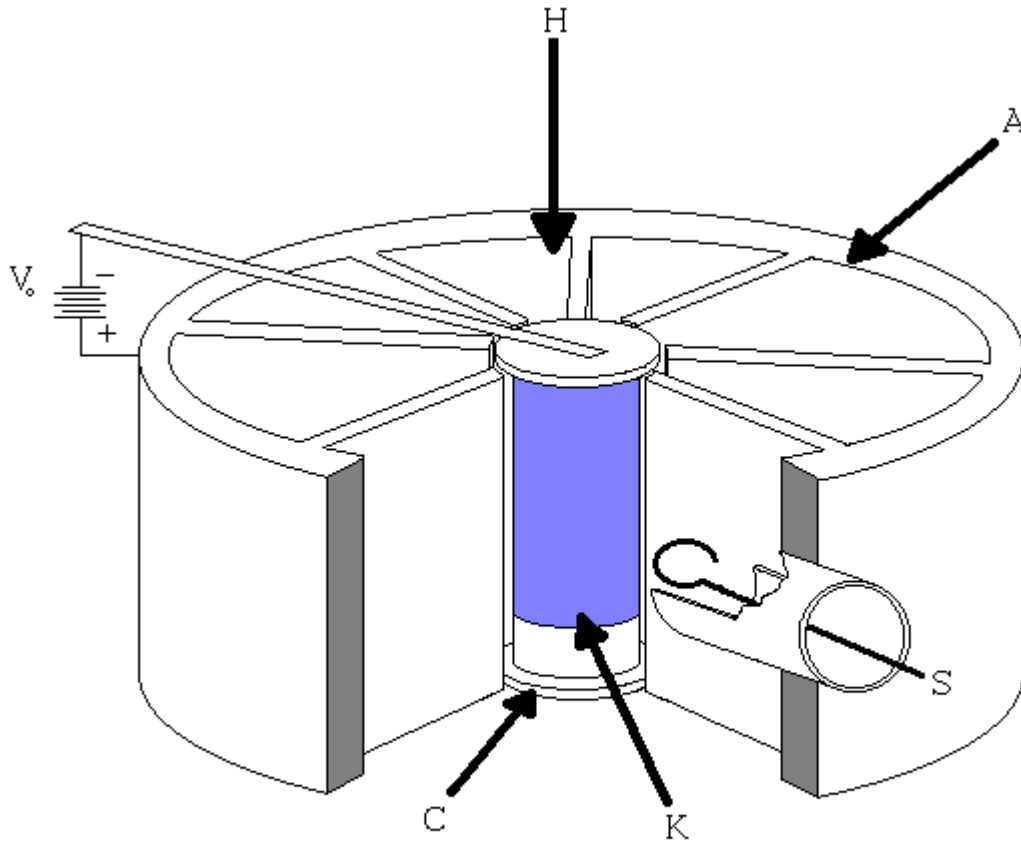


**Figure 1.5:** Schematic of a magnetron microwave generator

The magnetron is a complete unit in and of itself, unlike many of the other resonant microwave generators that operate by amplifying the low-power microwave signal from an external circuit (Thuery, 1992). The magnetron is quite simple in construction, but the operating principles involved are rather sophisticated. The two major components are the metallic resonant enclosure that acts as the anode (labeled A) and the high-temperature cathode (labeled C) located at the "hub" of the wheel-shaped anode. The pie-shaped cavities arranged around the circumference of the enclosure act as resonant structures in their interaction with the electrons that generate the microwave output. The electrons do not travel into these cavities. Instead, they are confined to the small radial gap between the cathode and the spokes of the anode structure by the effects of the electric potential between the cathode and the anode. This steady DC potential

must be very large, on the order of several thousand volts. The cathode must be maintained at a high temperature during operation and is usually made of tungsten (labeled K). The high potential difference and the heated cathode are necessary to maintain an adequate rate of electron flux from the cathode. A strong magnetic field (labeled H), generated either by permanent magnets or by electromagnets, is aligned such that the magnetic flux lines are parallel to the orientation of the cathode and the electron interaction gap. The presence of this magnetic field interacts with the charge on the electrons and causes them to rotate about the cathode as they travel towards the anode surface. The combination of the electric potential and the magnetic field causes the electrons to travel in a nearly cycloidal path. As they travel outward from and rotate about the cathode, the proximity of the electrons to the anode changes due to the periodic spacing of the spokes and cavities. Because of this periodic structure, the instantaneous location of the electron emitted from the cathode relative to the position of the anode determines the degree of radial acceleration the electron experiences at any given instant. The acceleration of the individual electrons is therefore influenced by their position. This periodic acceleration of the electrons in the proximity of the resonant cavities between the spokes of the anode induces a periodic radio frequency (RF) field in the cavity region. The induced field also extends into the gap between the cathode and anode. Note that the frequency of a microwave field is a subset of the radio frequency band. The formation of this resonant field is dependent on the design of the structure of the anode. It necessarily occurs at the output frequency of the device. The induced periodic field, once established (a process that happens within a few milliseconds from when the voltage potential is established), further influences the electrons in the interaction gap. The local fields induced in the cavities alternate in polarity at a given instant from one cavity to the next. Electrons rotating clockwise about the cathode may experience a further tangential (in addition to the influence of the uniform magnetic field) acceleration or a deceleration depending on the polarity of the induced field in the vicinity of a particular resonant cavity. Figure 1.6 indicates the direction of the local RF field polarity at a given instant with fine arrows and the direction of the electron rotation with dark arrows. The shaded portion indicates the areas where the electrons concentrate as they move to the anode.

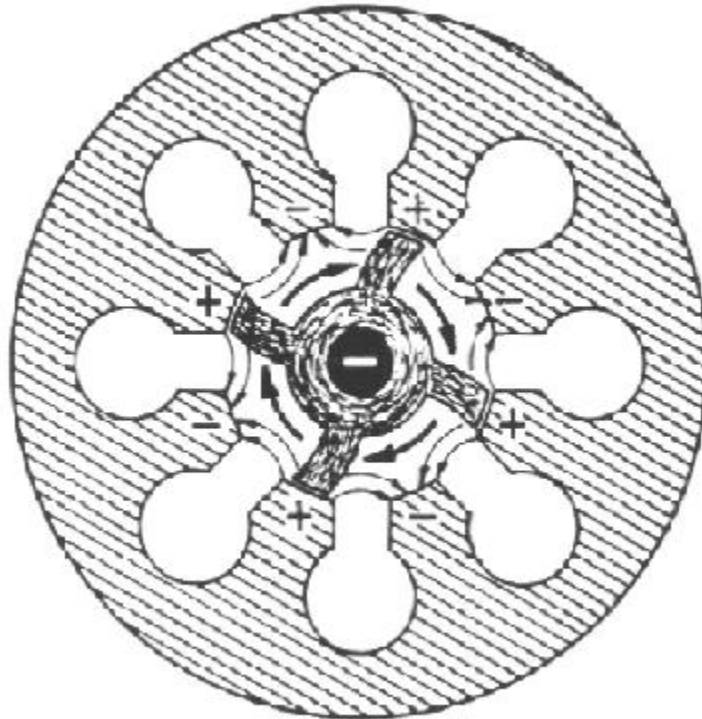


**Figure 1.6:** The distribution of electrons in the magnetron interaction space (Veley, 1987)

Depending on the polarity of the local RF field, an electron may gain energy from the RF field, in which case it experiences tangential acceleration in the direction of rotation as well as radial acceleration back to the cathode. In the event that the electron returns to the cathode, it carries more energy than when it was emitted due to the acceleration by the RF field. This excess energy goes to heat the cathode and cause more electrons to be emitted. The alternative fate is that the accelerated electron may be influenced again by the local RF field before it reaches the cathode and may resume its travel towards the anode. An electron may also give up energy to the local RF field, in which case it experiences a tangential deceleration and "falls" to the anode as a result. The combination of tangential accelerations in some electrons and decelerations in others results in the radial "bunching" of electrons in the interaction gap as shown in figure 1.6. The net input of electrical energy to the device results in electrical energy being transferred to the RF field via the electron interactions, more than is needed to sustain the influence on the electrons. The excess RF energy is taken from one of the pie-shaped

resonant gaps via an induction loop (label S in fig. 1.5). The RF field induces a current in the loop and transmits the energy to some type of load, usually a radiating antenna.

The klystron is similar to the magnetron in that it utilizes the effects of a RF field in a resonant cavity to transfer energy from electrons to the RF field through electron modulation. However, there are two fundamental differences between the devices. The most obvious is that the klystron is arranged in a linear configuration rather than a radial one, as can be seen in figure 1.7 (Smith and Phillips, 1995).

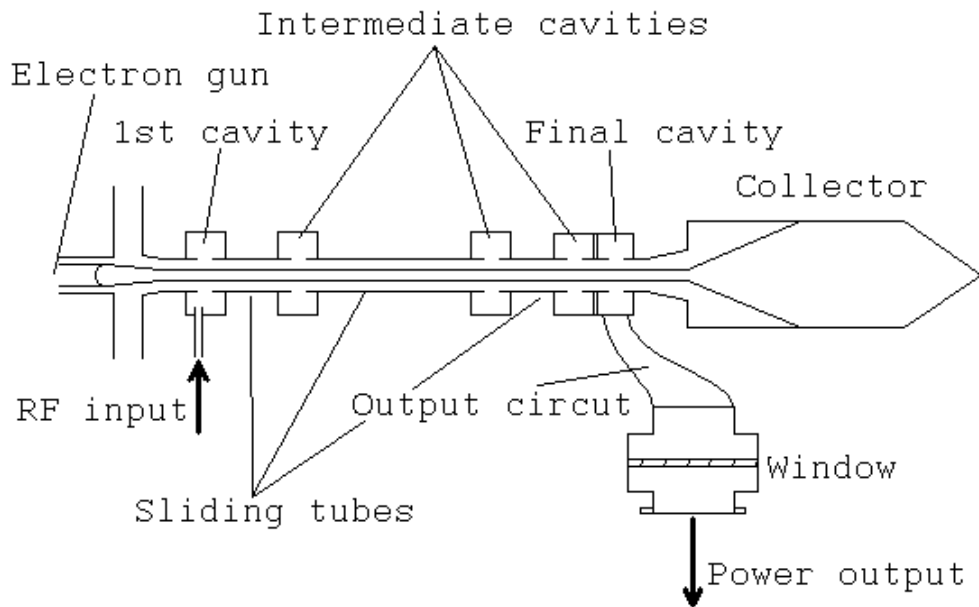


**Figure 1.7:** Schematic of a 4-cavity klystron microwave amplifier

The less-obvious difference is that the klystron amplifies the RF signal produced by a small, external source and the magnetron generates and amplifies its own signal. Klystron amplifiers are not constrained to have four cavities as shown; they can have fewer but most have at least two. The reflex klystron is an exception to this, having only one cavity. The electrons to be modulated (bunched-up) are produced at one end of a long metal tube by an electron gun. The electron gun uses a strong electromagnet and cathode to produce a constant stream of electrons. Due to the repulsive force between the electrons, the beam must be focused with a ring-shaped electrode to prevent excessive divergence of the electron stream. The focused stream of electrons enters the tube and

travels a short distance to where the first resonant cavity is located. The cavity is a metal enclosure that is coupled to the tube through a small opening. A RF input signal is fed into this cavity, usually with an induction loop similar to the type used to extract energy from the magnetron. The RF field in the cavity extends into the tube and influences the stream of electrons as they travel past the opening. Depending on the polarity and strength of the field in the opening at the time they pass, the electrons in the vicinity will experience varying degrees of acceleration or deceleration. The electron stream now has electrons traveling with different velocities as the beam continues down the tube towards the next cavity. The length of the tube between the first and second cavities is adjusted so that the modulation of the beam is at a relative maximum as it passes the second cavity. That is, the decelerated electrons will have bunched up with the electrons not influenced at the first cavity, and the accelerated electrons will have caught up with them. The result is that instead of a constant, uniform stream of electrons passing the opening to the second cavity, the electrons are traveling in loose bunches at regular intervals (the same frequency as the RF input). The bunches of electrons passing the cavity opening induces a RF field in the cavity. Like the resonant cavities in the magnetron, the design of the cavities is such that the phase delay between the modulated electron stream and the induced RF field in the cavity results in the field further modulating the beam. That is to say that the loosely bunched electrons are acted upon such that they are bunched tighter when they reach the next cavity along the tube. This process continues as the electrons pass successive cavities. The modulation of the beam does have a practical limit, so the number of cavities used seldom exceeds four. The final cavity has a RF probe similar to the one used to excite the field in the first cavity, except this one is used to remove energy from the device. The field induced in the final cavity is at the same frequency as the input signal but, due to the energy transfer from the electron stream, at a much greater strength, hence the device is an amplifier. The modulated stream of electrons is collected after the RF energy has been extracted so that the excess power can be safely dissipated. Since klystron amplifiers are capable of high-power continuous-wave output, they are typically used in such areas as aircraft radar, linear particle accelerators, and radiation therapy for cancer patients (NMAB, 1994).

The traveling wave tube (TWT) is similar to the klystron in its linear configuration and the amplification due to electron beam modulation, but it differs fundamentally in the fact that it is not a resonant device. This feature gives the TWT one of its greatest advantages; because it is not constrained to operate at a single frequency due to resonant considerations, the TWT can amplify RF signals over a range of frequencies. However, TWT amplifiers are considerably more expensive than magnetron sources and are usually only found in applications where the variable frequency output is critical. Typically, the size of this frequency range is dictated by the power output of the device which may be tens to a few hundred W (Gilmour, 1994) for most devices. The trade-off for a high-power device, which may be capable of  $10^6$  W of power output, is that the frequency range of the output is limited compared to a low-power device, perhaps as little as 10%-20%. For a device with a moderate power output, the output may be varied over as much as two decades in frequency. Again, it must be emphasized that the TWT, like the klystron, amplifies an external signal and is not capable of producing microwaves or other RF signals on its own. A typical TWT can boost the input signal by as much as 40 dB. The schematic representation of the TWT, shown in figure 1.8, demonstrates the linear configuration of the device.

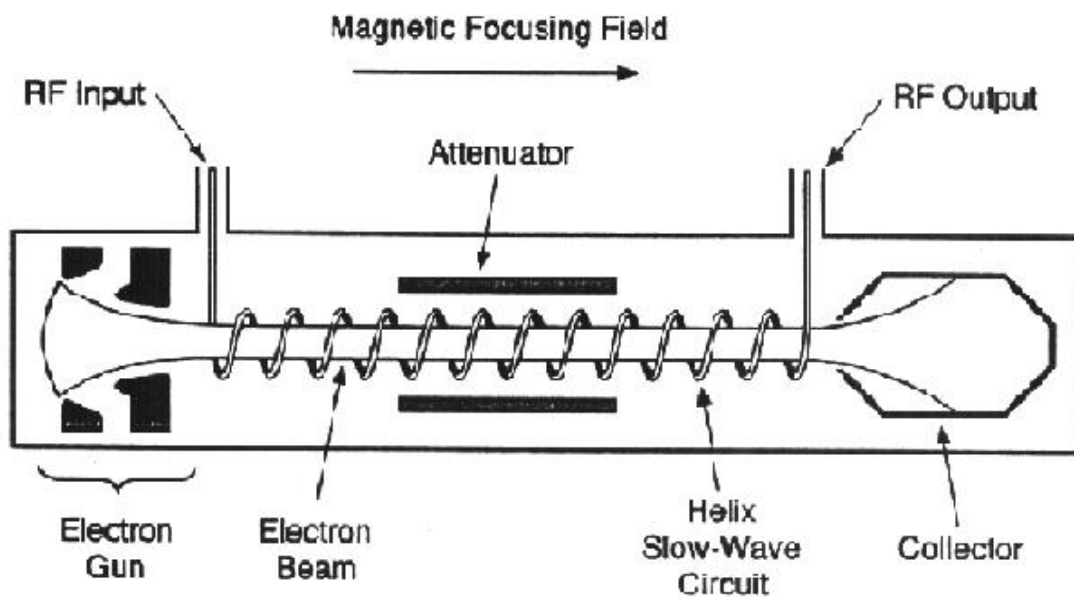


**Figure 1.8:** Schematic of a helix Traveling Wave Tube (TWT) microwave generator (Gilmour, 1994)

The TWT is also similar to the klystron in that it produces a focused, constant stream of electrons at one end with an electron gun and collects the modulated beam at the other end after the amplification is achieved. The modulation of the electron beam is also achieved through the interaction with a RF field. One major difference between the TWT and other microwave amplifiers is that the electromagnetic field responsible for modulating the electron stream is due to electric current flow in a wire. Other devices rely on a resonant cavity of a specific geometry to support the electromagnetic field. The speed of a RF signal, traveling in a conductor, approaches that of light, but the speed of the electrons emitted from the gun is much slower. The electron stream velocity is lower because the electrons are traveling through air instead of a conductor, so the velocity depends on the electric potential at the cathode. The propagation of the RF signal along the axis of the TWT must be slowed down to match the speed of the electron stream in order to maximize the coupling between the field and the electrons. In order to do this the conductor carrying the signal is coiled into a helix, similar to the threads on a screw, as is shown in figure 1.8. The signal then travels through the conductor at speeds approaching that of light, while traveling axially at a lower speed due to the "pitch" of the helix. Because the RF signal receives energy from the electron stream, the average velocity of the electrons decreases as they travel along the axis of the helix. For this reason, the pitch of the helix is usually decreased along the length of the interaction space to maintain a high degree of coupling between the RF field and the electron stream by continuously matching the axial speed. Figure 1.9 shows the orientation of the electric field patterns and the polarity of the RF charge in a helix at an instant in time.

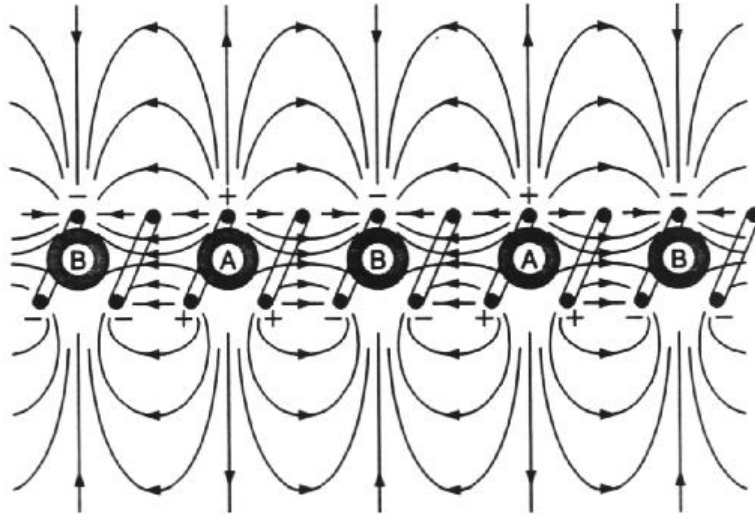


**Figure 1.9:** RF charge and electric field patterns for a helix (Gilmour, 1994)

Like in the devices described previously, the field surrounding the helix causes a modulation of the electron beam by accelerating some electrons and slowing others. The modulated beam in turn affects the field resulting in a net transfer of energy to the field. The output frequency of the TWT is determined by the input frequency of the signal fed into the helix. The helix design optimizes the amplification ability at the center of the possible frequency range, and the efficiency of the amplification falls off as the input frequency diverges from the optimum. The effective range of frequency is thus determined by the range of frequency where the amplification achieved can be justified versus the power consumption of the device.

The gyrotron is the most powerful of the modern microwave generators. It was developed independently and simultaneously in the US and the USSR in the 1970's. It is capable of high-energy output in the 100+ GHz frequency range and is only used in the most specialized of applications because it is very large, heavy, and extremely expensive. Its design requires the use of large cooling systems, high-vacuum chambers, and powerful magnetic fields. Despite its drawbacks, the gyrotron is capable of feats that no other class of microwave device can match. One of its primary uses is in the field of nuclear fusion research for the task of plasma heating (NMAB, 1994). Like the klystron and the TWT, the gyrotron is an amplifier, not a generator, and relies on an external source to provide the microwave frequency input. Like all of the devices mentioned, it

achieves amplification through the interaction between electromagnetic fields and electrons via the modulation of an electron stream. Like the klystron and the TWT, it utilizes an electron gun and collector to produce and collect the electron stream. It is similar to the TWT in that it does not rely on resonant structures to achieve amplification. Instead, the interaction occurs in a large chamber that is evacuated to an extremely low pressure. Hence, the power output of the device is not limited by the size of the interaction space as in resonant devices (Veley, 1987). It is similar to the magnetron in that it uses radial modulation rather than linear modulation of the electrons, such as in the klystron and TWT amplifiers. Inside the gyrotron, the electrons travel in a helical path from the electron gun to the collector. This is due to the influence of an extremely powerful magnetic field in the interaction region. A periodic electric field, from an external source, is introduced into the region with a cyclic frequency equal to the rotational frequency of the electrons orbiting the center of the region. The interaction with the field causes some of the electrons to either accelerate or decelerate (in rotation, not axial velocity) and travel in modulated groups. Unlike the electron streams in the other devices, the electrons in this device are approaching the speed of light due to the extreme voltage potential driving them and the influence of the strong EM field in the interaction region. This is the reason for the large difference in power output of the gyrotron compared to other microwave amplifiers. In accordance with the theory of relativity for matter traveling near the speed of light, the electrons gain mass as they accelerate and lose mass as they decelerate. This relativistic effect increases the amount of energy that the electrons give up and adds to the amplification effect on the EM field. Due to the size, expense, and power demands, there are a limited number of these devices in use today.

More microwave generators than those discussed here are available. Power-grid tubes, such as the triode and tetrode, among others, operate at the low-frequency end of the microwave band and have a low cost due to their extensive use in the radio and television broadcasting industry (NMAB, 1994). Some of the other devices include the reflex klystron tube (Veley, 1987), backward-wave oscillator, and crossed-field amplifier. These devices are not discussed here, as they have limited use in the field of microwave heating of industrial materials.

## 1.4.5 Microwave/Material Interaction

In order for a given material to be heated with microwaves, some of the energy carried in the electromagnetic field must be transferred to the material. Two fundamental properties of a material govern its interaction with electromagnetic fields in the area of microwave heating. The first of these is the dielectric constant,  $\epsilon'$ , also known as the real permittivity of the material. This property is a characterization of the ability for electromagnetic energy to penetrate the material. For most materials, this value can realistically be treated as a constant with minimal variation due to the temperature of the material and the frequency of the electromagnetic radiation. The second fundamental material property is the dielectric loss factor,  $\epsilon''$ , also known as the dielectric loss or imaginary permittivity. It is essentially a measure of the ability of the material to store electromagnetic energy. A material with a high dielectric loss does not store the energy effectively, and a significant portion of the energy is converted ("lost") to thermal energy within the material. All of the various mechanisms that result in electromagnetic energy being dissipated in a material are included in the dielectric loss factor (Tinga, 1993). The two permittivity values are often lumped together into a single parameter called the complex permittivity,  $\epsilon_c$ , comprised of the real and imaginary permittivity such that

$$\epsilon_c = \epsilon_0(\epsilon' - j\epsilon'') \text{ (F/m)}. \quad (1.2)$$

Of the two dielectric properties, the loss factor is the primary indicator of how well a given material can be heated with microwave energy. A low-loss material, with a low value of  $\epsilon''$ , is able to store electromagnetic energy well and does not absorb much of the stored energy. In these cases, the material may be said to have a permittivity,  $\epsilon$ , which is essentially just the real part of the complex permittivity because the imaginary part is so small as to be negligible. A lossy material, with a high value of  $\epsilon''$ , absorbs a larger portion of the electromagnetic energy instead of storing it all. The absorbed energy is converted into thermal energy within the material through several dissipation mechanisms. Since these materials absorb a larger portion of any incident electromagnetic energy, they are heated more readily than a low-loss material. Lossy

materials are often characterized by a quantity known as the loss tangent,  $\tan \delta$ , which is defined as

$$\tan \delta = \frac{\epsilon''}{\epsilon'} \quad (1.3).$$

The materials that heat most readily by microwave energy must possess sufficient penetration for the energy to reach deep into the material, and a high loss to transform as much of the penetrating energy into heat as possible (NMAB, 1994). The power dissipated in the form of heat into a finite-sized element of material can be described by the relationship

$$dP_d = 2\pi f \epsilon_0 \epsilon'' |E|^2 dV \text{ (W)} \quad (1.4),$$

where  $f$  = the source frequency (Hz),  $\epsilon_0$  = the permittivity of free space =  $8.854 \times 10^{-9}$  (F/m),  $|E|$  = the RMS magnitude of the electric field (V/m), and  $dV$  = the volume of the element ( $m^3$ ).

The means by which the material absorbs the stored energy is related to the cyclic influence of the electric field component of the electromagnetic radiation (Theury, 1992). The electric field component exerts a force on the charged particles on an atomic scale within the material. This force is resisted within the material by the atomic and molecular bonds of the molecules. The resulting intermolecular friction dissipates some of the electric field energy within the material as heat. This is the same principle that causes a piece of wire to get hot when it is bent back and forth repeatedly except the source of the work is electrical instead of mechanical. Four primary modes of energy dissipation exist in lossy dielectric materials, each dominating different frequencies of excitation that may or may not lie in the microwave frequency range.

The first mode is called space charge polarization and it occurs at low excitation frequencies. This mode requires that the material have some free electrons in order to occur. The electric field causes the free electrons to move through the material until a grain boundary or similar obstacle is reached where the electrons will accumulate. This results in localized regions of the material becoming electrically polarized in a manner similar to the principles used in semiconductor electronic devices.

The second mode is called dipole alignment and occurs with high-frequency excitation. This is the fundamental mode of energy transfer in microwave heating. All

molecules are made up of elements, many of which have a net electrical charge. Some monoatomic elements, such as hydrogen, have a net negative charge, and others, such as oxygen, have a net positive charge. When these elements combine to form a molecule, the like charges of each of the elements repel one another so that the elements have a specific relative position that results in a stable molecule. The water molecule,  $H_2O$ , is a good example for illustration of this principle and is shown in figure 1.10(a).

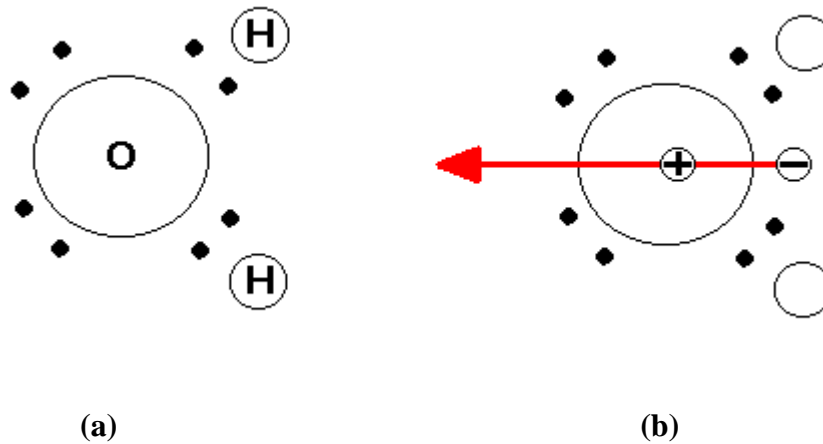


**Figure 1.10:** The atomic structure and dipole moment of the water molecule

The oxygen atom has six valence electrons and a +2 charge, and each of the hydrogen atoms has a single valence electron and a -1 charge. The valence electrons in figure 1.10 are represented by black dots. By sharing valence electrons, the three atoms form a stable molecule that is not ionic, meaning that it has no net electric charge. Because each of the valence electrons carries the same negative charge, the stable molecular configuration is "bent" as shown in the figure by the repulsive force between the valence electron pairs. This results in the centers of positive and negative charge, caused by the individual charges carried by the protons and electrons in the atoms, to occur in different locations as shown in figure 1.10(b). The arrow represents the permanent dipole moment that occurs when the centers of positive and negative charge do not coincide. Having a dipole moment means that the force exerted on the molecule by an external electric field will tend to rotate the molecule and align the centers of charge with the direction of the field. Molecules with highly regular structures tend to have low molecular polarity and therefore have almost no dielectric loss (Theury, 1992). Examples of low-loss molecules

include polypropylene, polytetrafluoroethylene (PTFE), argon, carbon tetrafluoride, methane, carbon tetrachloride, and propane (Metaxas and Meredith, 1983). These molecules have positive and negative charge centers that are nearly coincident such that they have almost no dipole moment. Polyethylene is a long, symmetric chain monomer and has no theoretical dipole moment. Examples of polar molecules include water, urea, acetone, polyvinyl acetate, and certain proteins like gelatin and hemoglobin. Dipole alignment is the fundamental mechanism for microwave heating of most materials. The microwave energy irradiating an object contains a cyclic electric field component. As stated above, the electric field exerts a rotational force on the polar moment of the molecules in the material. The polarity, or direction, of the electric field component reverses at every half-cycle of the radiation frequency and results in a corresponding reversal in the direction of the exerted rotational force on the molecules. Many materials exhibit a frequency dependence for this loss mechanism in particular, depending on the structure and composition of the molecules. In aqueous solutions and liquids, the molecules may be free to rotate with the exerted forces and the friction between the rotating molecules results in heating. In solids, the molecules are bound together and the force on individual molecules causes them to exert a force on the bonds that hold adjacent molecules together. The cyclic reversal of the force exerted on these bonds converts some of the energy from the field to heat by the "hysteresis damping" effect of the intermolecular bond.

The third mode of energy dissipation in dielectric materials is called ionic polarization and occurs when materials are excited at infrared frequencies. The mechanism of this type of energy transfer is "the separation of positive and negative ions in the molecule" (Theury, 1992). Irradiation by infrared frequencies will result in the heating of any material. The domain of radiation heat transfer deals primarily with electromagnetic radiation in this frequency range.

The fourth and final mode of energy dissipation is called electronic polarization and it dominates only at very high frequencies at the near-ultraviolet range. This is similar to the effect of dipole alignment but it occurs on the atomic scale rather than the molecular scale. The center of an atom has a positive charge because it is made up of protons and neutrons. The cloud of electrons orbiting the nucleus has a negative charge.

The influence of an alternating electric field of sufficiently high frequency does not act for a sufficiently long period of time to cause a dipole alignment in a molecule due to the relative mass of the molecule. In comparison, the mass of the electron cloud surrounding a nucleus has a vastly smaller mass than the nucleus of the atom. This mass is even smaller when compared to the overall mass of an entire molecule. Therefore, frequencies that are too high to act on the molecule can still effect the electron clouds surrounding a nucleus within a molecule. The alternating polarity of the electric field acts on the negative charge of the electron cloud and causes the relative position of the cloud to "vibrate" about the nucleus. Since the electron cloud is bound to the nucleus by an electric attraction force, the energy from the electric field is converted to heat in the atom by a hysteresis damping effect that is analogous to the heat conversion in dipole alignment in solids.

One of the difficult aspects of controlling the microwave heating process is that the dielectric loss factor of certain materials has a significant dependence on the source frequency or the material temperature or both. This makes the application of Eq. (1.4) nonlinear in most real world situations. Certain materials have an extremely low dielectric loss at ambient temperatures, but the loss factor grows exponentially as the temperature increases. Many metal oxides and ceramics fall into this category. One such material, zirconia, exhibits these characteristics, as can be seen in the plot of dielectric loss versus temperature in figure 1.11.

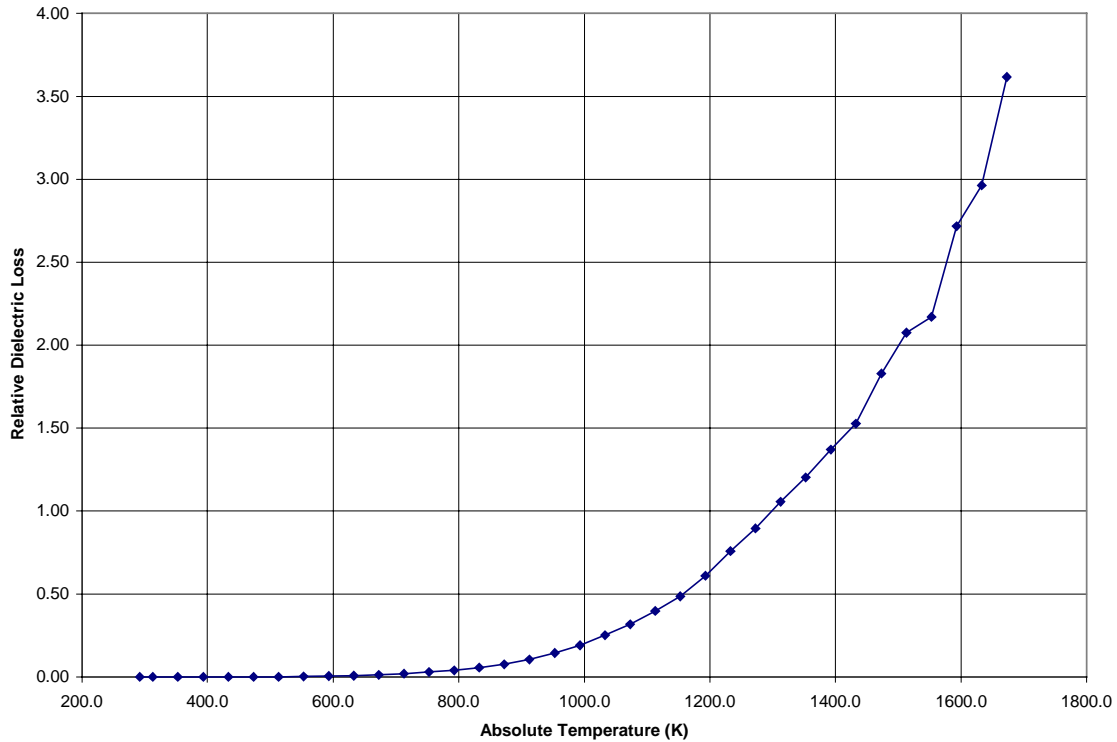


**Figure 1.11:** The temperature dependence of  $\epsilon''$  in zirconia

These are called thermal runaway materials because the energy absorbed by the material may increase in an uncontrolled fashion as the material temperature increases. This may lead to cracking or melting of the material or other destructive phenomena. The physical mechanism that causes this behavior occurs when the temperature of the material becomes sufficiently high that large numbers of electrons are freed from their molecular bonds (Kenkre et al.). Because they couple well with the microwave energy, these free electrons cause a large increase in the dielectric loss factor with a small increase in temperature. The problem of thermal runaway has been rigorously investigated and the primary solution appears to be incorporating feedback into the power control system of the microwave applicator. By reducing the supplied microwave power as the temperature and dielectric loss of the material increases, stable heating scenarios at elevated temperatures are possible for thermal runaway materials.

Other means exist for controlling the dielectric loss characteristics of materials to be heated with microwaves. In the case of low-loss materials, such as alumina and silica ceramics, impurities with different dielectric properties may be added to the parent

material. These impurities act as catalysts that reduce the energy required to free electrons and increase the dielectric loss at the expense of reducing the penetration depth of the microwave energy (Tinga, 1988).

Another factor that can influence the dielectric loss factor in certain materials is sintering, as mentioned in Section 1.4.3. As the material is sintered, it may experience several changes in its crystalline structure, density, and grain size that may cause the material to have different values of dielectric loss. In alumina, the sample may begin as a powder consisting of boehmite ( $\text{AlOOH}$ ) (Freim et al.). At 450 °C, the boehmite undergoes the first phase transformation to the close-packed cubic structure of the  $\gamma$ -alumina polymorph. At 800 °C, the next transformation to  $\delta$ -alumina occurs. This is followed by the transformation at 1000 °C to the  $\theta$ -alumina polymorph. Finally, the phase transformation to  $\alpha$ -alumina, a hexagonal close-packed corundum polymorph, occurs at 1200 °C. Once a sample has been sintered and transformed into  $\alpha$ -alumina, it remains as such. However, the dielectric loss is strongly dependent on the degree to which the sample has been sintered. Sintering increases the density of a ceramic material by reducing the density of the pores within the material and causes the individual grains of material to become larger as the crystals grow (Tinga, 1988). A given increase in material density due to sintering may cause a corresponding increase in the dielectric loss such that  $\epsilon'' \propto (\rho)^3$  (Thomas, 1999). Sintering a material at higher temperatures achieves a greater increase in the percentage of theoretical density (%THD) than sintering at a lower temperature for a given amount of time. The plot shown in figure 1.12 demonstrates this phenomenon for mullite, another thermal runaway ceramic material.

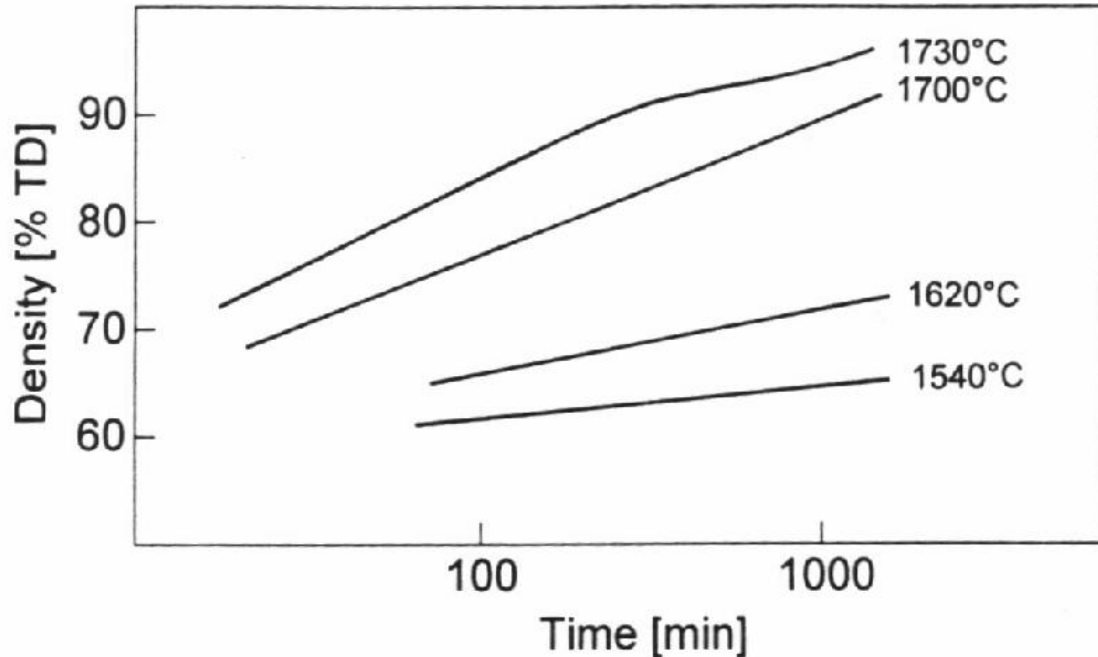


**Figure 1.12:** %TD versus sintering temperature and duration for mullite (Schneider et al., 1994)

One of the benefits of microwave sintering is that the volumetric heat generation allows the material to be sintered to a desired %THD more quickly and with smaller temperature gradients (Tinga, 1988). This has added effects on the grain distribution in the sintered product including smaller grain size and increased grain size uniformity. Both of these are considered superior qualities in a sintered ceramic because they lead to superior mechanical properties. Grain size plays an important role in the dielectric loss factor as well. This is due to the fact that grain boundaries have a higher affinity for absorbing microwave energy than other parts of the microstructure (Tinga, 1993). This further complicates the task of predicting heating rates in these materials because there can be unpredictable variation in the dielectric loss. These variations cannot be predicted by density because two samples with the same density may have different average grain sizes and pore densities.

## 1.4.6 Waveguides and Resonators

The two fundamental classes of microwave applicators are single-mode and multi-mode. Multi-mode applicators are familiar to most people because the microwave ovens found in the kitchen fall into this category. A "mode" is a propagating electromagnetic wave of a given frequency. A microwave source may generate a single frequency, but the output wave may reflect inside and interact with the applicator before the wave reaches the material to be heated. This results in microwave energy of different orientations being present inside the applicator. Each orientation present in the applicator is called a mode. In a multi-mode device, the geometry of the heating cavity is such that all of the modes are free to exist and reflect about the enclosure. To draw an analogy to the behavior of fluids, one could describe the radiation patterns inside a multi-mode enclosure as being turbulent. The radiation inside the enclosure when averaged over a span of time is somewhat isotropic. Like microwave ovens, some multi-mode devices use what is called a "mode-stirrer" to increase the isotropic nature of the energy field. It consists of a rotating metal paddle wheel similar to a fan that is placed in the path of the output beam from the source. The microwaves from the source reflect from the mode-stirrer in many directions. The mode-stirrer also causes multiple modes to be generated from the source beam. This helps to distribute the radiation throughout the cavity and reduces the occurrence of "dead spots" and "hot spots" in the cavity where the fields are weaker or stronger, respectively. Anyone who has used a microwave oven to reheat a plate of leftover food knows that these problems can cause one tater-tot to be burning hot while the one next to it is stone cold. In industrial applications, multi-mode applicators are primarily used for heating parts that are large and/or have a complex geometry. This is due to the ability of the multi-mode enclosure to effectively fill a heating cavity of large size with a uniform radiation field. The shape of the enclosure can be designed to partially, or completely, shield certain areas of the part from the microwave energy to tailor the heating as desired.

The focus of this work, as specified previously, involves the use and modeling of a single-mode resonator cavity. The information presented in this section is intended to be a brief overview of the principles and terms relating to such devices. More details concerning specific aspects of electromagnetic propagation in the applicator used in this

work are introduced in Section 2.3 as they are needed to present a clear discussion of the field modeling in the study. A single-mode device is one where only a single structure of microwave radiation is used for heating. Other modes may exist at certain locations within a single-mode device, but those modes typically do not propagate very far or represent significant levels of the overall microwave energy present. Single-mode devices cannot fill a large space with a uniform radiation field. Instead, they possess the ability to concentrate large amounts of microwave energy into a small space. This makes them ideal for heating parts of small size or cross-section, such as thin rods (Metaxas and Meredith, 1983). The single-mode devices can be single- or multiple-pass applicators. In a single-pass applicator, the object to be heated is located in the path of a wave propagating from the source. All but a small percentage of the microwave energy penetrates into the object, and the rest is reflected from the surface of the object. Usually, this type of device is used to heat objects that are thicker than the penetration depth of the microwaves so that all of the energy that penetrates into the object is absorbed. If the object does not absorb or intercept all of the radiation coming from the source, the excess energy is not absorbed and continues past the object where it must be dissipated by other means, such as a microwave trap (Metaxas and Meredith, 1983). A good example of a single-pass application is in the hyperthermia treatment of cancerous tumors. The microwave energy from the source is focused on the area to be treated and has one chance at being absorbed.

The other class of single-mode device is the multiple-pass applicator. This means that any energy not absorbed by the target material on the first pass is reflected back to the target one or more times for another chance at being absorbed. This type of device usually takes the form of a resonant cavity. A resonant cavity is very similar to the enclosures used in multi-mode devices, essentially an enclosed space surrounded by metal walls, but the dimensions of the enclosure are designed via analytical formulations for a specific interaction with the microwaves. The height and width of the enclosure are sized to allow one specific mode to propagate. The length of the enclosure must be an integer multiple of half the wavelength of the fundamental mode that is to exist in the cavity. This ensures that the waves reflecting from the far walls along the axis of propagation will interfere constructively with the waves traveling in the opposite

direction to create a standing wave in the cavity. This is the principle of constructive interference as was first demonstrated by von Helmholtz in the nineteenth century. If the dimensions of the enclosure were large, several modes could propagate successfully and it would then be considered a multi-mode cavity. The interference between modes would make a sustained standing wave impossible to achieve. A cavity that is sized to support a standing wave pattern while no object is present in the enclosure will usually not support a standing wave pattern when a dielectric object is added. The dielectric object interacts with the electromagnetic field and changes the wavelength of the propagating microwaves in the dielectric part of the cavity. In order to support the standing wave pattern, the cavity must be "tuned" to account for this wavelength shift. This can be accomplished by shifting the frequency of the microwave energy being added to the cavity, but this approach requires a variable-frequency source such as a TWT amplifier. Since most industrial microwave generators are single-frequency sources, such as the affordable magnetron, a different approach is usually used. One of the walls along the axis of propagation, called the "short", is movable so that the length of the cavity can be altered. By moving the short into or out of the enclosure, the geometry of the cavity is altered so that the standing wave is supported again at the resonant frequency. A small change in the power input to the cavity will cause a change in the temperature of the dielectric object inside. Since the dielectric properties of the object may depend on temperature, this change will affect the interaction of the object with the field, and the cavity will again need to be tuned.

Three principal methods are used to couple microwave energy into the cavity. One method is an induction probe as is used to insert and extract microwave energy in the resonant cavities in magnetrons and klystrons. It is simply a length of wire that connects to the microwave source at one end and forms a loop inside the cavity. The loop must be placed at a point in the cavity where the magnetic field is at a maximum to optimize the power transfer into the cavity. The oscillating current in the loop couples energy into the cavity by adding it to the magnetic field component. A second method to add power to a cavity is a stub antenna. Placed in free space, the stub antenna would act like a miniature radio antenna and could broadcast a signal. Like the induction loop, it is a length of wire that connects to the microwave source. The difference between them is that the stub

antenna is straight at the other end and sticks into the cavity at a location where the electric field is at a maximum. The oscillating current in the stub couples energy into the cavity by adding it to the electric field component. The third method to add energy to the cavity is by use of an aperture. An aperture is simply a small hole in the enclosure wall opposite the short that connects to a waveguide. A waveguide is very similar to a cavity except that it is usually longer and is open on both ends. In a sense, the cavity is a specialized type of waveguide that is closed on both ends. One end of the waveguide usually connects to the microwave source and the other end connects to the cavity. Its purpose is to channel the energy from the source to wherever it is needed. Like the cavity, the cross-section of the waveguide is carefully chosen to support the fundamental mode that is being carried. Usually, both the cavity and the waveguide have the same cross-section. The wall of the cavity that contains the aperture is usually made of a thin metal plate with a hole in it called an iris. The iris is securely held in place between the waveguide and the cavity. The iris allows the energy carried in the waveguide to enter the cavity. Some of the microwave energy that travels down the waveguide reflects off of the iris instead of passing through the aperture into the cavity. In order to prevent damage, this reflected energy must not be allowed to return to the source.

To prevent the energy from reaching the source, a device called a "circulator" is usually placed between the source and the waveguide sections. The circulator is housed in a tee-shaped waveguide section and has a piece of ferro-magnetic material that is positioned between the source and the waveguide. The material allows the energy from the source to pass through to the waveguide but diverts the reflected energy to a "dummy load" and prevents it from reaching the source. The dummy load may consist of a stream of cool water or a large container of graphited sand that absorbs and dissipates all of the reflected energy.

The ability to measure the energy in the waveguide and cavity is essential for performing experimentation and for monitoring industrial heating operations. Devices that accomplish this create either a digital or analog electric signal from transducers that are connected to the applicator. Small probes, like those that can be used to add energy to the cavity, connect to the transducers which detect the level of energy excited in the probe and create the corresponding electric signal to be measured. A device called a

directional coupler is built into a short section of waveguide. When this device is attached to the waveguide section coming from the circulator, it allows measurements to be taken of the microwave energy coming in one direction from the source and reflecting from the iris in the other direction. Another probe can be attached to the cavity at a location coincident with a peak in the standing wave pattern. This probe senses the power flowing into it from the field in the cavity, and one is able to deduce the strength of the electric field at the probe from the power flux measurement.

These components are the primary parts used in many single-mode devices, but many other components not mentioned exist for use in specific applications. The device studied in this work is essentially the same as that described with a few differences as discussed in Section 2.3.

# Chapter 2

## Historical Review

### 2.1 Literature Review

Microwave applicators for various industrial processes have benefited from numerous advances in the past three decades. The tasks involved may include drying, sintering, joining, and curing, to list but a few of the many uses where the selective heating, penetration effects, and decreased processing times provided by microwaves proves to be advantageous over conventional heating sources. Simulation is a cost-effective means to perform parameter studies of the numerous controllable aspects in the design of these microwave applicators. A few common styles of numerical model have been developed to accomplish this task as an aid in the design of microwave heating devices. In this section, the various simulation methods developed by researchers in the past are discussed with the advantages and drawbacks of each type being addressed. The need for continued research into the field of numerical modeling and experimental verification for microwave applicators is developed, which is therefore the basis for this research. As the primary focus of this work concerns the heating of cylindrical dielectric elements in stationary and continuous processing using microwave applicators, this section also reviews several current theoretical and experimental endeavors that are relevant to the focus.

### **2.1.1 Challenges in Modeling**

The task of modeling the microwave heating process is by no means a simple endeavor. Highly accurate predictions of the electric field and temperature distributions are difficult to obtain theoretically because of the nonlinear nature of the problem and the coupling of thermal and electromagnetic effects (Tinga, 1993). Analytical solution methods are useful in solving very small aspects of the problem, such as the Q-factor of a resonant cavity or the cutoff frequency. Otherwise, these methods must impose drastic oversimplification of the overall problem to obtain a result. Some of the properties of the material being modeled, such as material density, are in most cases rather insensitive to temperature or source frequency. Other properties such as thermal conductivity and specific heat, may be moderately dependent on one of these parameters. Some of the properties, such as dielectric loss in thermal runaway materials, are highly sensitive to temperature or frequency. In order to handle all aspects of the nonlinear problem, numerical methods must be employed. Since property values are crucial to the accuracy of results obtained in numerical simulations of this type, it is essential to utilize the best available temperature- and frequency-dependent property data available (Arai et. al, 1993; NMAB, 1994; Tinga, 1988). Many researchers working on the development of microwave heating simulations agree that the available database on these properties needs to be improved and expanded (Iskander, 1991). In addition, means to validate numerical models against experimental results need to be expanded and standardized to facilitate comparisons (Iskander, 1993). In order for the formulation of a microwave heating simulation to be truly complete, it must include models of both the electric field distribution and the heat transfer process in a coupled fashion. Many simulations that have been developed so far either focus on one aspect or the other instead of on both of them together.

### **2.1.2 Electromagnetic Field Models**

Several fundamental numerical methods exist for use in modeling the electromagnetic fields inside microwave applicators and the interaction of the field with the process material. The most common are differential formulations, such as the finite

difference time domain (FDTD) method, which solve Maxwell's curl equations in time and space (Iskander, 1993). In this type of formulation, the interaction space, including the process material, is partitioned into small cells. Differential equations are used to describe the field in each cell and the interactions with adjacent cells based on the properties of the space that the cell occupies. It is a popular formulation because it facilitates modeling of complex volumes by using locally conforming Cartesian, spherical, or cylindrical coordinate "meshes" (Grotjohn and Asmussen, 1996). The meshes must overlap to allow the regions to be connected through interpolation functions. The solution of models using the FDTD method must be accomplished through multiple iterations at each time step to converge the solution (Iskander, 1991). This method of modeling the electromagnetic field is ideal for coupling the results to a FDTD heat transfer model because of the similar partitioning of the process material. However, the FDTD electromagnetic model is most practical for solutions in finite enclosures. If the solution method were to be applied to a very large region, artificial boundaries would have to be applied in order to constrain the solution domain. These artificial boundaries introduce error into the formulation of the problem and the solution is inexact. In solving for field distributions in a small enclosed space, such as in microwave applicators, the metal walls of the system provide a natural boundary for the solution regime. The interactions at the conducting walls are readily accounted for in the boundary conditions of the differential formulation.

Integral formulations are another class of numerical solution techniques for electromagnetic field distributions. Whereas the FDTD methods use differential equations to describe the problem, these use integral equations. These models frequently employ dyadic Green's functions to represent the required field quantities (Iskander, 1991). Certain expansion and weighting functions must be used in the formulation, and the accuracy of the solution may be improved by choosing complicated or higher-order functions. However, increased accuracy comes at the expense of longer run times and use of more computational resources. As in the FDTD methods, these methods are capable of treating the scattering and absorption effects due to a three-dimensional inhomogeneous dielectric object in the solution region.

Another field simulation method utilizes spherical wave expansions to describe the field patterns inside and outside of objects being heated (Iskander, 1991). Point-matching procedures are used to find unknown expansion coefficients. The basis functions developed in this fashion are considered complete and result in improved computational efficiency. This method is generally not applicable in cases where the process material has an irregular cross-section and, compared to the other two formulations, has not been used extensively by researchers.

One can find detailed descriptions in the current literature of many models that simulate just the electromagnetic field distribution in microwave applicators. While they are not able to predict the temperature distributions within the process material, most such simulations are suitable for describing the effects of frequency, applicator dimensions, and material interactions for a known temperature distribution on the field distribution. The model developed by Chapman et al. (1992) is a three-dimensional FDTD formulation that is capable of calculating the resonant frequency and Q factors in a cavity, and the specific absorption ratio (SAR) distribution in the sample. It accounts for parameters such as sample geometry and coupling iris dimensions for loaded and unloaded cavities. The results of this model were validated by comparison to values obtained through the method of perturbational analysis. The three-dimensional FDTD model developed by Grotjohn and Asmussen (1996) stands out because it is capable of modeling complicated applicator and process material shapes. As described previously, it utilizes a system of locally conforming meshes that overlap in order to describe the complex geometries as a collection of simpler shapes. Their work was also verified against specific analytical cases, but no experimental comparisons were drawn. A three-dimensional FDTD field model developed by Smith et al. (1992) for multimode rectangular cavities was verified by comparison to experimental results. The energy density distribution in an actual cavity of similar dimensions was measured by placing a LCD (liquid crystal display) sheet in the cavity for a short period of irradiation. The energy distribution was compared to the distribution predicted by the simulation, and parameters of the simulation were adjusted to achieve a good qualitative correlation. The magnitudes were not adjusted to match the measured values as the model is intended for use in identifying trends due to parameter variations. An electromagnetic field model

was developed by Tranquilla et al. (1996). The authors of that work claim that "It is believed that the developed simulations, which can provide precise quantitative data on absorbed power, scattering parameters, eigenmodes, quality factors, and energy density patterns, taking into account the finite conductivity and thickness of waveguide walls is the most accurate available to date." However, they fail to provide any evidence to support their claim. One could assume that they did some verification, but it is not stated whether this was done by comparison to analytical solutions or experimental data. An interesting field simulation, developed by Hile and Kriegsmann (1996), uses a hybrid asymptotic/numerical method. The focus of their work was in the modeling of the fields in a  $TE_{10n}$  single-mode cavity. Their assumption was that the higher-order modes excited by the field interactions with the iris were local and that they did not propagate to interact with the load or the short. Essentially, this means that the complete field solution is due to two independent problems, the "iris" problem and the "cavity" problem. Using scattering matrix theory, the iris is "mathematically removed" from the rest of the solution region. The effects of the iris on the cavity fields are solved independently one time and the results are used thereafter in the solution for the cavity fields. This greatly reduces the computational effort required over the traditional FDTD methods that must solve for the iris interactions iteratively at every time step. However, the article does not indicate that the resulting model was verified by any specific means. The article by Iskander (1993) does not describe any one specific field model in detail, but discusses the pros and cons of the FDTD method in general. It stresses the importance of validating numerical models against experimental results instead of just analytical cases.

Although this work is discussed in detail in Section 2.3, the model developed by Terril (1998) must be mentioned here. Based on the recommendations of another Virginia Tech graduate student, Terril developed a detailed model to predict the electric field distribution in an iris-coupled rectangular single-mode resonant cavity. The model utilized a mode matching approach. It was able to account for the influence of a nonhomogeneous dielectric cylinder located in the cavity at a resonant peak in the standing wave. Although not coupled to a heat transfer model, the distribution of the dielectric properties along the sample could be specified or assumed uniform. However, the model was developed with the ultimate purpose of being incorporated into a heat

transfer model in the future (the current work is the realization of that goal). The influence of iris geometry was the primary parameter of interest in this particular model. The model was verified against analytical solutions but not against experimental data.

### **2.1.3 Heat Transfer Models**

The most common solution method for determining the temperature distribution in a sample is the transient FDTD method which, as mentioned previously, can also be applied to determine the electromagnetic field distribution in a microwave applicator. Unlike analytical methods for determining the temperature distribution in a solid, like Green's function representations, the FDTD methods can easily represent objects with nonuniform shapes. The FDTD methods are either explicit or implicit formulations. Several important distinctions exist between the two types. In the explicit formulations, the temperature at a given node is computed based on the temperatures of that node and adjacent nodes from the previous time step. While this method is the simpler of the two from a computational standpoint, it has the disadvantage that the time interval must be chosen to satisfy a stability criterion (Incropera and DeWitt, 1996). The value must be sufficiently small to prevent the solution from becoming divergent, clearly an undesirable circumstance. As a result, the explicit formulation often requires longer run times due to the increased number of time steps in spite of its simplicity in computational effort. The implicit formulations solve for the temperatures at a given node based on the other unknown adjacent nodal temperatures at the current time step. This results in a system of simultaneous equations that must be solved for the nodal temperatures with matrix operations such as Gauss-Seidel iteration or LU-decomposition. While this method involves a greater degree of computational effort to solve for the temperature distributions at a given time step, it has the advantage of being unconditionally stable. Any value may be used for the time interval and the solution will not diverge. Of course, better solution accuracy is obtained with smaller time intervals up to a point; one need not use a smaller time interval if doing so results in no appreciable improvement in the resulting temperatures. In the event that the thermophysical properties, dielectric properties, or heat transfer coefficients for the discretized volumetric elements are not constant (i.e. they vary with temperature), then the solution of the FDTD equations must

proceed in an iterative process. To optimize the accuracy of the solution at a particular time step, the average value of the properties during the time step at each node should be used. Without knowing the exact values of the newly calculated temperatures at the end of a time step, the solution must assume a value of the properties based on the results from the previous time step. When a new set of temperatures is computed for the new time step, the results will often indicate that the property values used in that computation were not ideal. Based on the newly calculated temperatures for that time step, the temperatures are again re-computed using the improved property values. This process proceeds iteratively until the change in calculated temperatures resulting from modifying the property values falls below some specified criterion. Having used the "correct" properties for the time step that results in the "correct" temperature distribution for the given time step, the process starts over again for the next time step. Because of the great increase in the number of calculations resulting from variable properties, some simulations treat the properties as constants and sacrifice accuracy for ease of computation. This may be acceptable for some materials in specific heating scenarios, but this assumption is certainly invalid when working with thermal runaway materials such as those considered in this work. In order to reduce the complexity and computational requirements in numerical simulations of microwave heating, some researchers choose to adopt simplified assumptions about the electric field distribution along the process material. Usually, the distributions are assumed to be uniform or of some specified distribution based on empirically simplified models or available experimental data (NMAB, 1994).

A simulation utilizing the implicit FDTD formulation for the heat transfer solution was developed by Singh et al. (1993) where the process material was a slab of lossy silicon carbide (SiC). Because the material was thick compared to the microwave wavelength and possessed a high dielectric loss, penetration depth effects could not be neglected. This is not the case in the material samples considered in this work. In their model, the attenuation of the field with increasing material depth was accounted for, but the incident field was idealized instead of being modeled. The model computed all of the dielectric and thermophysical properties, as well as the radiation and convection heat loss rates, as functions of the local material temperature. No procedures or comparisons that

may have been performed to validate the model were presented in the article. A FDTD model developed by Johnson et al. (1993) assumed that the cylindrical sample was "thin" compared to the wavelength of the electromagnetic radiation so the field could be treated as uniform across the sample cross-section. The model employs temperature dependent dielectric properties, but thermal conductivity is the only thermophysical property modeled with temperature dependence. While the authors acknowledge this to be oversimplified, the model assumes that the electric field distribution along the sample is uniform in space and time. The results obtained using the model must have been compared to either analytical solutions or some experimental data, although such is not explicitly stated; rather it is stated that the model was useful for finding trends due to parameter variation but not for predicting exact temperatures. Tian et al. (1992) developed a two-dimensional model using the explicit FDTD method. It incorporated temperature dependence into the thermophysical and dielectric properties, but assumes a uniform distribution of the electric field over the sample. Again, no reference to any experimental or analytical validation was presented.

The model developed by Brandon et al. (1992) is a three-dimensional FDTD formulation designed to investigate large-scale heating applications. Their company, EA Technology, installed a 5 kW, 2.45 GHz microwave furnace to sinter large (250 + kg) blocks of alumina without performing prior simulation studies. The results were unsatisfactory and their investment was largely wasted. Since the results of modeling small applicators are generally not applicable to large-scale applicators, they devised a simulation for the specific task. Because modeling the fields in a large cavity of complex shape is quite difficult, they modeled a simplified representation of the cavity geometry and assumed a uniform electric field distribution at the surface of the part (while recognizing this to be somewhat unrealistic). The model is capable of describing hybrid heating that combines convection and microwave heat sources. The model was validated against actual cases for convection heating only, but the microwave heating aspects were not validated.

The model developed by Kriegsmann (1994) is for studying thin ceramics in a single-mode cavity. Like several of the other models presented in this section, this model utilizes temperature dependence in the calculation of the thermophysical properties and

heat transfer coefficients. This model differs in that, although the electric field distribution is assumed, the electric field is assumed to have sinusoidal variation along the length. This is an attempt to explain why stable hot spots are measured at the middle of a sample in heating experiments while theory (possibly based on over-simplified models) predicts that a hot spot should consume the entire sample once initiated. Because this model was developed to study the parameters that influence hot spot formation and stabilization, it was not validated against any experimental data.

Although a detailed discussion is presented in Section 2.3, the works of two former Virginia Tech students must be mentioned here. A one-dimensional implicit FDTD model was developed by Duchez (1996) to study the heating of thin ceramics in a single-mode cavity. The model uses temperature dependent properties and heat loss, and allows the sample to be passed through the applicator at a specified velocity. The model uses assumed electric field distributions along the sample with an emphasis on using specific distributions to obtain a desired temperature profile. Duchez allowed that these profiles may not be attainable with existing applicators. This model was not verified against any experimental data, but the work was later expanded by Goodson (1997) with this purpose in mind. Goodson expanded the model to a two-dimensional FDTD to allow for a radial temperature variation and improved accuracy in thicker rods, and his model assumes a uniform field distribution along the sample. The model was compared to the experimental results obtained at the Los Alamos National Laboratory (LANL) in 1997 under the direction of G. Vogt. The details of the work at LANL are given in Section 2.2. The results obtained with Goodson's model shows good qualitative agreement with the experimental data, but the predicted temperatures are consistently higher than those measured experimentally. Goodson suggested that this is a result of losses in the applicator system being included in the power measurements from the experiments. If a significant portion of the power measured was dissipated in the applicator and not absorbed by the sample, the results of a simulation under the assumption that all of the power gets into the sample would obviously be erroneous. Goodson suggested that the two-dimensional FDTD heat transfer model be coupled to an electromagnetic field simulation to obtain the proper electric field distribution at the sample and to account for the power losses in the applicator.

## 2.1.4 Combined Electromagnetic/Heat Transfer Models

Even before Terril, Duchez and Goodson, students at Virginia Tech have worked on the problem of numerical simulations of microwave heating problems. An early work by May (1991) was the development of a two-dimensional FDTD model for heating in a cylindrical cavity. The model utilized the FDTD method for both the electromagnetic field solution and the temperature distribution, although the models were run independently in this case. In other words, the results of the heat transfer model were fed into the field model, then those results were returned to the heat transfer model and so on until convergence was obtained. The heat transfer and field models were each verified independently against analytical cases, but the results of the combined simulations were not validated. The following year, Mascarenhas (1992) improved May's model so that the heat transfer and electric field models ran together in one program. They still ran in succession iteratively, but did so in an automated fashion. This version also allowed for energy release from the exothermic chemical reactions involved in the curing of epoxy resins in composite materials, which adds to the volumetric heat generation term of microwave heating. As with May's model, this work was verified against only simplified analytical cases. In both cases, the authors recognized the need for verification of the models against experimental results and recommended that such work be done in the future. Mascarenhas also recommended that the models be adapted to run iteratively at each time step instead of iteratively in sequence. Another recommendation was that the losses in the applicator be modeled to improve the accuracy of the simulation. A model developed by Bringhurst et al. used a three-dimensional FDTD model with electric field and heat transfer aspects to simulate drying of samples in a multi-mode RF dryer. The model used the same mesh for both the field and heat transfer models. The heat transfer model was independently verified against results obtained with the finite-element software package ANSYS. The authors report that the combined model was then compared to experimental results obtained at an actual RF dryer at the University of Utah, but the results of the comparison were not given in the article. This seems to indicate that the degree of correlation was insufficient. A coupled field/heat transfer model, employing the FDTD method for both, was developed by Newman et al. at the Oak Ridge National Laboratory. It simulates a multi-mode cavity excited by a

microwave horn source. The model utilizes fully temperature-dependent properties and the field patterns have been validated experimentally using LCD sheets. The model has also been compared to experimental results in the heating of composite SiC rods and exhibits good qualitative results, but the accuracy falls off with increasing temperature. A model developed by Craven et al. (1996) uses a novel approach to solving for the temperature distribution and field distribution by modeling the components of the microwave applicator as equivalent transmission line components. The model is highly flexible and allows the user to select individual components for the applicator from a library rather than being constrained to a single applicator configuration. The interface is touted as being extremely user-friendly. The model is checked against several analytical solutions to verify the field modeling and the heat transfer aspects, but no experimental validation is mentioned.

### **2.1.5 Summary**

Many of the models described in the previous sections had certain strengths and shortcomings. In some cases, the model solves for the field distribution but not the temperature distribution. In others, the model assumes a highly simplified field distribution to solve for the temperature distribution. In some cases, the authors attempt to validate their results against simplified analytical solutions. In only a few of the models, the authors attempt to validate the results against tangible experimental results while most admit that such means are necessary for improving the quality of the numerical simulation results. In all cases, the need for accurate material property data is emphasized. The works outlined here, with their various strengths and weaknesses, can be used to develop an outline of what is the epitome of microwave heating simulation:

- Temperature dependence of thermophysical and dielectric properties
- Temperature dependence of radiation and convection heat transfer parameters
- Coupled electromagnetic and heat transfer models that run together at each time step
- Minimum computer resource requirements balanced with maximum accuracy
- Validation of the model against concrete experimental data

- User-friendly interface to facilitate the modeling process
- Means to account for power losses in the applicator
- Utility in aiding the design of real-world microwave applicators

The current work attempts to address all of these issues. This work, resulting from the endeavors of current and previous students and the esteemed faculty of the various engineering departments, is certainly the most advanced microwave heating simulation developed at Virginia Tech.

## **2.2 LANL Experiments**

The scientists at LANL have performed numerous experiments in the field of microwave heating in the past few years. They have heated such thermal runaway materials as zirconia, alumina, and mullite, both solid rods and fibrous tows, in a single-mode WR-284 resonator cavity. In some applications, they utilized a TWT source and a unique feedback control system to maintain the cavity at resonance while providing a specified power level to the load. Because they used a TWT microwave source, the control system was able to adjust the source frequency to maintain the resonant condition in the cavity as the dielectric properties of the sample changed. They measured and recorded several data series at one-second intervals in each experiment including the time, source frequency, forward and reflected power from the waveguide system, the power inside the cavity, and the temperature of the sample at the center of the cavity. The source frequency was measured using a signal counter attached to the generator, and the time was recorded directly from the data acquisition computer. Figure 2.1 shows several views of one of their applicator devices with accompanying annotations. The important parts and assemblies shown in the figure are itemized in table 2.1.

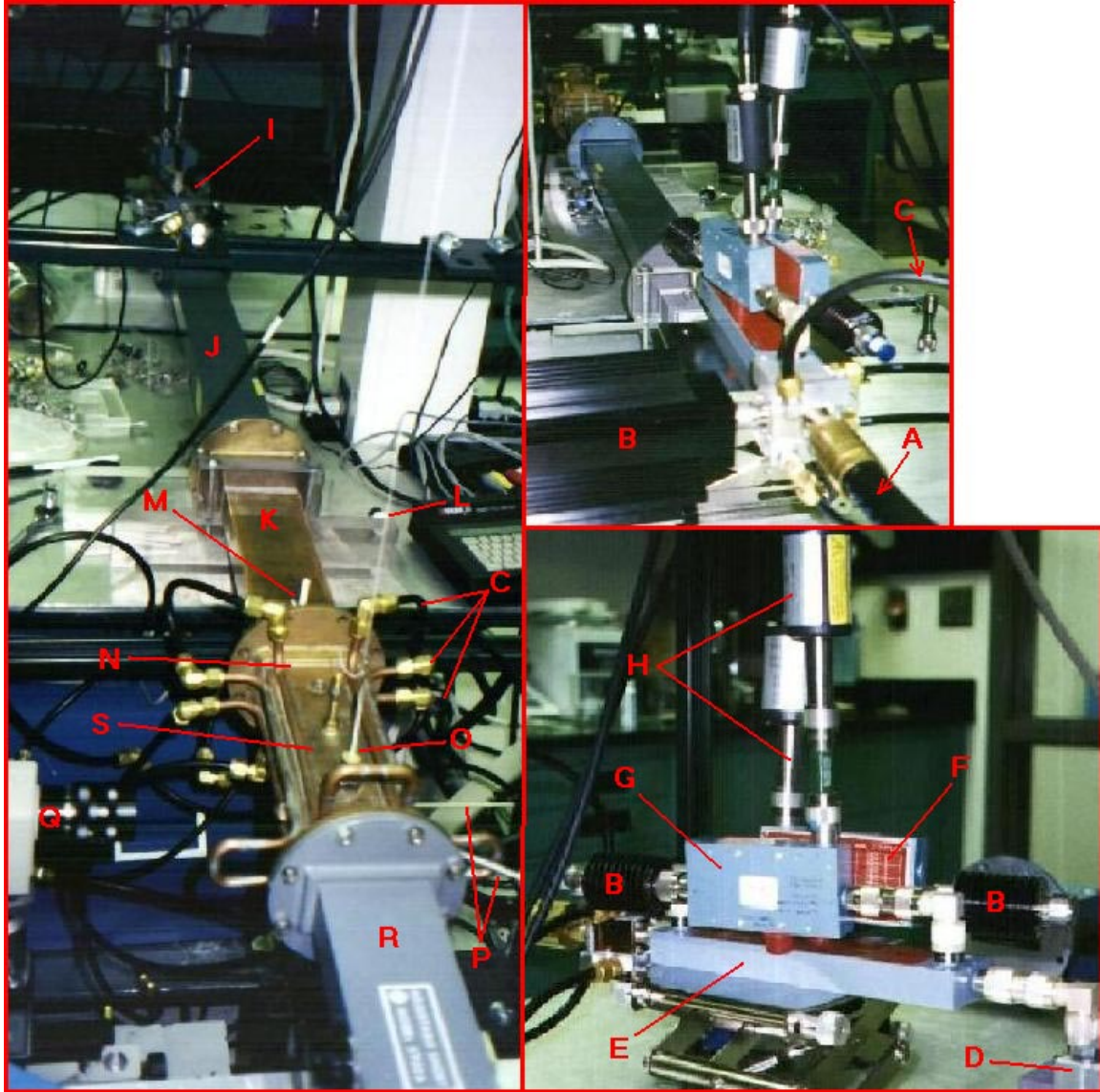


**Figure 2.1:** The LANL experimental microwave applicator

**Table 2.1:** Legend items for figure 2.1

A	microwave input coaxial cable from TWT generator	K	tapered WR284 copper waveguide section
B	dummy load for excess power	L	sample hanger from take-up spool
C	cooling water circulating pipe	M	Teflon tuning wedge
D	antenna coupling to waveguide	N	inductive/capacitive copper iris
E	bi-directional power coupler	O	sample inlet port
F	forward power attenuator	P	optical temperature probes
G	backward attenuator power	Q	video camera
H	power sensors	R	adjustable shorting plane
I	couplers, dummy loads, and input antenna	S	copper resonator cavity

The microwave power from the TWT source was fed into the applicator system through a coaxial cable, (A) in the lower right of the image. In general, coaxial cable has a higher signal attenuation than other means of transferring microwave power, on the order of 20-30 dB per 100 feet of length (Scott, 1993). In this case, the losses due to the coaxial cable are not significant or important because the length of the cable was short and the losses occur before any power measurements are made in the system. The coaxial cable delivers the microwave power to a circulator that diverts reflected power to a dummy load (B) while allowing forward power to pass through to the directional coupler (E). As the forward power passes through the directional coupler, the forward power flux is measured through the power attenuator (F) by a power sensor (H). The power attenuator reduces the strength of the signal before it reaches the power sensor to prevent damage. The reflected power returning from the applicator is measured by a separate sensor as it passes through the directional coupler in the opposite direction. The attenuation of the forward power, and likewise the reflected power, transmitted through the directional coupler is non-zero, but is small enough to be considered negligible. The forward power leaving the directional coupler is transmitted into the waveguide through a small stub antenna (D). This antenna is similar to the electric field coupling probe discussed in Chapter 1. Ideally, it would be positioned in the waveguide at a distance equal to  $1/4 \lambda_g$  from the shorting plane. This position would maximize the coupling to the electric field in the waveguide (Veley, 1987). If the probe is closer to or farther from the shorting plane, destructive interference between the field in the waveguide and the field generated by the probe will result in cancellation and power losses. Any power losses after the directional coupler are considered detrimental, as they are included in the total power measurements attributed to the applicator system but are not contributing to the heating of the process material. The system at LANL was designed to operate at a range of frequencies from 2 to 15 GHz (Vogt, 1999), so the positioning of the excitation probe was not done with one particular frequency in mind. The experiments performed in 1997, the data from which are used in this work, were at a nominal frequency of 2.93 GHz, so it is likely that some small degree of loss resulted from the positioning of the excitation probe.

The power radiated into the waveguide is contained within the waveguide and channeled through it to the load. The waveguide used was a WR-284 section with copper walls. The WR-284 has the properties listed in table 2.2.

**Table 2.2:** Section properties of a WR-284 waveguide

Outer Dimensions (in.)	3.000 x 1.500
Wall Thickness (in.)	0.080
Inner Dimensions (mm)	72 x 34
Theoretical Attenuation (dB/100 ft.)*	1.102 - 0.752
Theoretical Power Rating (MW)*	2.2 - 3.2
Frequency Range (GHz) for dominant TE <sub>10</sub> mode	2.60 - 3.95

\* Range is for lowest to highest frequency supporting dominant TE<sub>10</sub> mode

Clearly, the attenuation of the waveguide section is a small fraction of the power attenuation in a given length of coaxial line. For this reason, the power loss due to the plain waveguide sections can effectively be neglected. The losses that do occur in the waveguide sections are primarily due to Joule heating by the current flowing in the conducting walls (Metaxas and Meredith, 1983), or because of irregularities in the joints between waveguide sections. The waveguide section containing the excitation probe is bolted to a longer section of waveguide (J). Care must be taken to ensure that the connection joint is of the highest possible quality because "any irregularities in the joints cause reflection effects, create standing waves, and increase the attenuation" (Veley, 1987).

The far end of the long ( $\cong$  30 in.) waveguide section is bolted to a short waveguide section that contains a device known as a "beyond-cutoff" variable coupler. The coupler serves several purposes. First, it allows the operator "...to externally reduce the operating loaded Q of the cavity...and to critically couple microwave power from the source into the cavity. This flexible system makes it possible to fully couple any power level into the cavity and thus achieve any microwave electric field up to, and including, breakdown in dry nitrogen" (Vogt and Unruh, 1992). In addition, the coupler allows the operator a means to fine-tune the electric field strength in the cavity through small

adjustments of the coupler position. However, this feature was not the primary means of cavity tuning at LANL because the power control was affected by the source power as modulated by the feedback control system. The coupler is more useful in cases where the applicator is used without a feedback control system. Finally, the device improves the impedance match between the source and the resonator cavity. This is beneficial in that it results in a more efficient transfer of power into the cavity. However, this benefit is tempered by the fact that the component makes analysis of the applicator system more difficult. The reason for this complication stems from the layout of the parts within the coupler, as shown in figure 2.2.

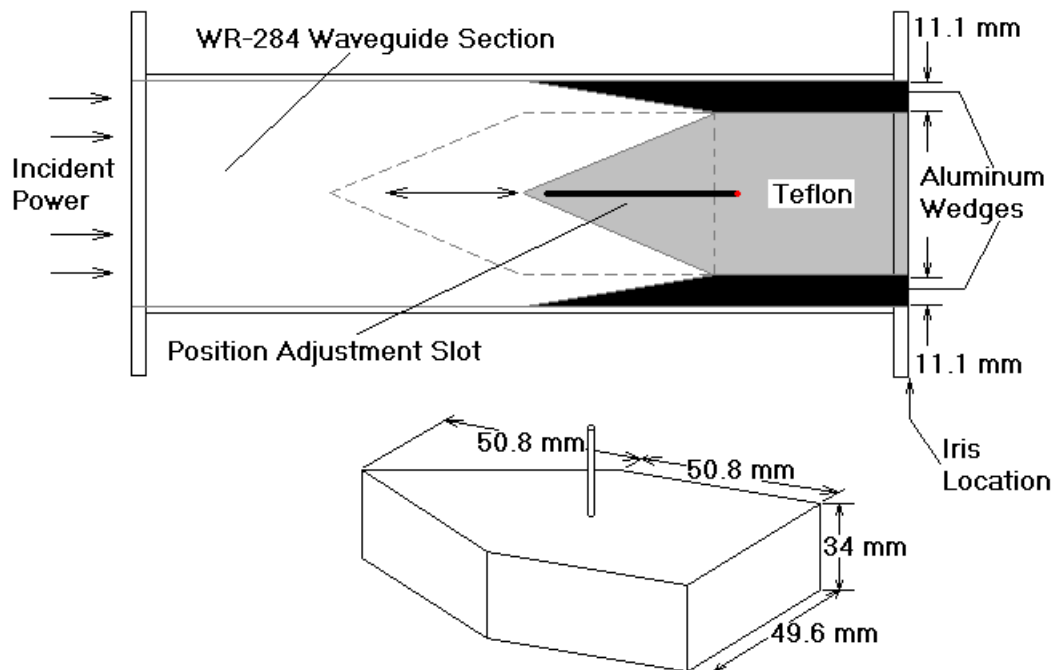


**Figure 2.2:** Schematic layout of the "beyond-cutoff" variable coupler

The device consists of three primary parts, a wedge-shaped block of Teflon (polytetrafluoroethylene, PTFE), and two wedge-shaped aluminum pieces that are fixed to the inside walls of the waveguide section as shown. According to Veley (1987), "any sudden change in the size, shape, or direction of the waveguide system will result in the introduction of reflection effects and an increase in the standing wave ratio (SWR)."

Thus, the introduction of the variable coupler to the waveguide system is a sudden discontinuity and the reflection effects cause destructive interference with the incident field. This results in a significant amount of the forward power being dissipated and lost as the energy propagates through the variable coupler. If the reduction in the interior wide dimension of the waveguide due to the aluminum wedges had been less abrupt, the losses would have been reduced (Veley, 1987). Ideally, changes in waveguide dimensions should occur gradually over a minimum distance of  $2\lambda_g$ , where  $\lambda_g$  is the guide wavelength. Unfortunately, the two scientists responsible for the development of this variable coupler, W. Unruh and D. Christiansen, are no longer available to provide additional information about the exact nature of the device. It was later determined, through experimental analysis of the variable coupler in the labs at Virginia Tech, that the largest percentage of the loss in the coupler was due to reflection effects from the aluminum wedges. The loss due to the propagation through the Teflon wedge was relatively small. This is explained by the long chain structure of the PTFE molecule (Sillars, 1973) and the resulting low relative dielectric loss, on the order of  $\epsilon'' = 0.00015$  (Marcuvitz, 1986), which makes the material almost transparent to the microwave energy. This observation was made by measuring the exterior surface temperature of the waveguide near the variable coupler and inside the core of the Teflon wedge during power delivery to the cavity. In one instance, the temperature in the Teflon was only 32.7 °C while the temperature of the waveguide surface adjacent to the aluminum wedge was in excess of 50 °C. The higher temperature in this area indicates that, when compared to the Teflon wedge, a greater amount of the electrical power was being converted to heat energy. The side of the Teflon block facing the incident field is tapered, apparently to improve the level of crosspolarisation (Oliver, 1994). The waveguide cutoff frequency is normally increased when the wide dimension of the waveguide section is reduced, such as in the variable coupler. However, this effect is offset by the decreased propagation velocity of the microwaves as they enter the Teflon. The net result is that the waveguide cutoff frequency is not impacted significantly by the variable coupler. The relative effects of these two parameters are changed based on the position of the Teflon wedge in the variable coupler as it is moved along the axis of the waveguide. The wedge can be adjusted through a maximum distance of 58.7 mm and

can be positioned directly against the metal cavity iris. The variable coupler is very complicated in terms of its effects on the fields in the waveguide and their interaction with the iris and cavity. Explaining it completely is beyond the scope of this work and is left for future researchers to explore. For the purpose of this work, it is sufficient to recognize two important points; the device enables a degree of fine-tuning of the field strength in the resonant cavity, and it improves the impedance match at the expense of significant power losses. These losses make the determination of the power absorbed by the process material more difficult, as is explained further in Section 2.3.

Beyond the variable coupler, the resonator cavity (S) (refer to figure 2.1) is separated from the rest of the system by a thin copper iris (N). The iris has both inductive and capacitive properties based on the dimensions and location of the aperture, or hole, and allows the power to pass into the cavity. The iris acts as an additional impedance matching device and can be treated in equivalent transmission line concepts as a band-pass filter. The forward power that does not enter the cavity through the aperture, due to dissimilar impedances, is reflected from the metal surface of the iris back up the waveguide. The cavity region is where the high-intensity standing wave is established to heat the process material. In the experiments relevant to the current work, mullite rods with diameters from 1 mm to 4.67 mm were passed into the cavity at a location where the electric field intensity in the standing wave is at a maximum. An adjustable short (R) is located at the end of the cavity opposite the iris to provide gross tuning of the cavity. The fine-tuning of the LANL cavity, to maintain resonance as the process material temperature changed, is achieved by affecting variations in the source frequency. A third power sensor is attached to the cavity with a small electric probe to measure the "power" in the cavity. This is a rather ambiguous measurement because it is not representative of the power being absorbed and lost by the cavity, nor is it a measure of the power absorbed by the sample. Rather, it is proportional to the electric field strength at the peak of the standing wave, but the actual computation of the field strength was not made at the time.

The power control system is not able to specifically control the power absorbed by the process material, as was the original intention (Vogt et al., 1996), but is able to control the power absorbed by the entire applicator. This included the power lost through

waveguide joints, excitation probes, Joule heating of the metal enclosure, the losses in the variable coupler and adjustable short, and the power actually absorbed by the process material. Of these sources, the losses due to the excitation probe, waveguide joints, and Joule heating outside of the cavity are quite small compared to the total power delivered to the applicator. Therefore, the primary loads on the power supply are the variable coupler, Joule heating losses in the cavity, iris, and short, and the power absorbed by the process material. The other losses are considered negligible. Although the power absorbed by the process material was not controlled directly in the LANL experiments, it was controlled indirectly by monitoring the power absorbed in the applicator. By adjusting the forward power, the difference between the forward and reflected power readings could be maintained at a desired level. It was known that the power losses would be constant in steady-state heating conditions, so by maintaining a constant power to the applicator they effectively maintained a constant (but unknown) power absorption in the process material. Since the goal of the experiments at LANL was to explore power control to prevent thermal runaway, this result was sufficient. However, as is explained in Chapter 4, the process of reproducing the experimental data through numerical simulation is significantly complicated by the fact that the researchers did not directly determine the power absorption by the rod.

Two Accufiber optical pyrometers were inserted into the cavity with dual-wavelength light pipes to take noncontact temperature measurements of a small area of the process material at the center of the cavity. Each device is capable of reading radiation intensities from the sample at wavelengths of 0.8  $\mu\text{m}$  and 0.95  $\mu\text{m}$ . The two readings could be used together, assuming an emissivity value of unity, to provide an accurate temperature reading of a target with unknown emissivity. However, the system response was such that the dual-wavelength "ratio temperature" could only be used reliably when the temperature of the target was relatively stable. This means that for most of the experiment, when the temperature was changing due to varying amounts of microwave power, the temperature at a single-wavelength was the measured quantity. Since the material emissivity is less than unity, the single-wavelength temperatures were consistently too low. By measuring the change in the recorded temperatures when the sensor switched to dual-wavelength mode, a linear interpolation scheme was developed at

Virginia Tech that allowed the proper temperatures to be deduced from the readings in single-wavelength mode. Further details of the interpolation are discussed in Chapter 4.

The data obtained from the experiments at LANL included the heating of rods of several diameters. All but one of the data sets recorded were for experiments where the process material was being passed through the cavity at a specified velocity. Although the simulation presented in this work has the capability to model processes of this nature, the data obtained at LANL are not adequate for a proper comparison to be made between the experimental and simulated results. This is because the temperature sensor was positioned to measure the temperature of the sample only at the center of the cavity. When the sample is being moved through the cavity while heating, the location of the highest temperature in the rod moves towards the end of the cavity where the material is leaving. For this reason, Goodson chose to base the comparisons of his simulation of the LANL experiments on the one available case where the rod was kept stationary in the cavity. In that particular experiment, the location where the temperature was recorded coincided with the location of the peak surface temperature in the material (a 4.67 mm diameter mullite rod). This is the quantity of interest in many real-world industrial applications such as sintering or joining. The comparisons of this work to the LANL experiments, presented later in Section 4.1, are based on the same case for the same reasons.

## **2.3 Prior Work at Virginia Tech**

This section is intended to provide an overview of the projects developed at Virginia Tech that pertain to the current work. Details that are more specific are given in Chapter 3 on the topics that have significant relevance to the current simulation.

In the past decade, several M.S. theses have been developed by students in the mechanical and electrical engineering departments of Virginia Tech that pertain to simulations and experimental analysis of microwave heating applicators. In the past four years, the works of four particular graduate students have had a significant influence on the direction of the work presented here. In 1996, W. Duchez developed a one-

dimensional FDTD model to simulate the heating of a thin, cylindrical dielectric load in a single-mode resonant microwave cavity. The model assumed symmetry in the circumferential direction and no radial temperature gradients in the sample. For this assumption to be valid, the heated sample must have a suitably small diameter. The model allowed the sample to move through the microwave cavity at a specified velocity to model industrial continuous delivery heating scenarios in addition to stationary cases. It did not simulate the electric field; rather it was used to explore various field distributions in order to obtain a specified temperature distribution in the sample.

In 1997, C. Goodson presented a model that was inspired by the earlier efforts of Duchez. His model was expanded to two-dimensional to allow for a radial temperature distribution in the sample so that cylinders of larger diameters can be modeled without the error induced by a simplified one-dimensional model. It also allows for continuous delivery of a sample as well as stationary samples. The primary material used in his investigation was a thermal runaway ceramic mixture of alumina,  $\text{Al}_2\text{O}_3$ , and silica,  $\text{SiO}_2$ . This mixture is known as mullite. The material is a crystalline solid with an octahedral lattice structure (Schneider et al., 1994) with a typical molar composition of approximately 60% alumina. The material is characterized as having low thermal expansion, low thermal conductivity, excellent creep resistance, high-temperature strength, and good chemical stability. Its high melting temperature,  $\sim 1828^\circ\text{C}$ , makes this material suitable for uses including refractory components, thermocouple and burner tubes, high-temperature heat exchangers, exhaust ducting, brake lining, and fibrous insulation. The reason this material was selected for study was the availability of experimental data from LANL that could be used to verify the heat transfer model. In the models properties of mullite, such as thermal conductivity, specific heat, dielectric constant, and dielectric loss are allowed to vary with temperature according to available data. The details of this temperature dependence are discussed in detail in Section 3.1.1 of this work. The convection heat transfer coefficient of the individual surface nodes is allowed to vary with temperature and was modeled analytically. Likewise, a coefficient for the radiation heat removal rate from individual surface nodes is varied with temperature according to the variation of the material emissivity (total, hemispherical) with temperature. However, Goodson was unable to obtain reliable emissivity data for

mullite. As an alternative, the emissivity of alumina was used due to the high molar content of alumina in mullite. A range of values for the temperature-dependent emissivity of alumina was available (Touloukian, 1972), and a median value was selected at each temperature to model the emissivity of mullite. While selecting higher or lower values within the range had an appreciable effect on the results of the simulation, Goodson had no basis for using one value over another. Rather than modeling the electric field distribution within the cavity, the model assumes that the field intensity is uniform along the length of the sample. Goodson recognized this assumption to be a significant simplification of the system and recommended that the model be improved to provide a more realistic representation of the field distribution along the sample.

The accuracy criteria of Goodson's model can be adjusted with three parameters to balance the accuracy of the temperature distribution against the required computer resources. The model utilizes the implicit formulation of the finite-difference equations; any time step can be selected as a parameter with unconditional stability but varying degrees of accuracy. While this allows for larger time steps, hence fewer overall calculations, the temperature distribution has to be determined simultaneously at each time step. Therefore, an efficient means of solving the simultaneous equations is implemented. Rather than use the tried-and-true method of Gaussian elimination, Goodson selected the line-by-line method because it requires less computer resources and computational time. Since the thermophysical properties and heat transfer coefficients are temperature-dependent, the solution for the temperature distribution is solved iteratively at each time step. A convergence criterion associated with the temperature convergence at a given time step allows control of the amount of computation spent at each time step. Specifying a larger value for the convergence criterion means that less iteration is required at each time step at the expense of overall accuracy. A convergence criterion is built in for determining when steady-state conditions have been achieved. Like the criterion for convergence at a given time step, specifying a larger value means that the simulation finished sooner, but again accuracy was the trade-off.

When the predicted temperatures from Goodson's simulation were compared to the measured temperature values from the experimental simulation at LANL, the predicted temperatures were consistently higher than the measured values. However, the

correlation, qualitatively speaking, was considered very good. The discrepancy was attributed to one or more of the following four primary causes:

- 1) The exact point on the sample where the temperature was measured experimentally may not have been the point of comparison in the simulated model.
- 2) The true emissivity of mullite was not known and, therefore, could not be properly modeled. Since the emissivity is multiplied by  $T^4$ , the influence of radiation heat loss could be significant.
- 3) The actual distribution of the electric field along the sample was known to be non-uniform due to the local distortion of the field by its interaction with the non-homogeneous dielectric rod. The assumption of a uniform distribution was clearly a source of error, although its influence could not be determined with the cited model.
- 4) The power delivered to the load in the experiments included all of the losses in the system as well as the power delivered to the sample. The model operated by specifying the power delivered only to the sample. By including the loss power in the power specification in the model, the predicted temperatures would necessarily be larger than the measured temperatures.

The fourth case was identified as the likely cause for most of the discrepancy in temperatures. The recommendations for future work in Goodson's thesis (Goodson, 1997) include suggestions that the last three of these issues be addressed to improve the accuracy of the simulation.

In 1998, an electrical engineering graduate student, N. Terril (1998), developed a numerical simulation to address the issue of the field distribution along the length of the dielectric sample in the resonant cavity. He developed his model to represent the WR-284 cavity dimensions and coupling iris that were used in the LANL experiments Goodson used for comparison. His model considers the effects of the dielectric properties of the sample when determining the electric field distribution. Since the dielectric properties of mullite, and many other ceramics and polymers, are dependent on the local material temperature, the model allows the distribution of the dielectric properties along the sample to be non-homogeneous. However, the electric field

simulation does not model the dielectric distribution itself; the distribution has to be specified as an input parameter. The model differs from most electric field simulations in that it does not use the FDTD differential method to determine the field distribution. Terril's model utilizes a unique mode-matching technique with an integral formulation to determine the field distribution along the fiber. The model assumes an isotropic field incident on the metal iris of unit amplitude. Since the effects of the incident field result in linear changes in the resulting field distribution, the calculated field distribution in the cavity can be scaled linearly to account for more intense incident fields. The model uses a dyadic series Green's function to represent the magnetic current present in the aperture. The higher-order modes represented in the aperture solution are dependent on the number of modes included in the series representation, and using more modes in the aperture results in increased accuracy in the resulting field distribution in the cavity. The complete solution would incorporate an infinite number of modes, but computational limitations demand that the number of modes be truncated at a finite value. Terril performed a parameter study on the model and compared the results to analytical solutions to determine guidelines for the minimum number of modes to be included that produce acceptable results.

The solution scheme decomposes the cavity into three separate solution regimes: the aperture, the sample, and the short regions. The solutions for the aperture and sample regions include unknown coefficients for the forward and backward travelling modes, while the short region has a single set of coefficients for the standing wave modes between the sample and the shorting plane. The model develops partitioned matrices for each solution regime, uses constraint equations to relate the equations in adjacent regimes, and then solves for the unknown coefficients by solving a set of simultaneous equations. The result yields the shape of the tangential electric field component along the heated sample. The model treats the heated sample as a line current source to account for the influence of the dielectric properties of the rod on the electric field distribution. The dielectric effectively distorts the electric field in the immediate vicinity of the rod to a degree that is dependent on the local material temperature. The resulting field distribution is not uniform unless the sample is at a uniform temperature. Terril was able to compare the results of the model to specific analytical solutions to verify the

performance of the model. His model was developed with the intent that it would later be coupled with Goodson's heat transfer model to provide a more complete solution to the microwave heating problem.

One shortcoming of the model developed by Terril was the fact that the variable coupler section used at LANL was not considered. In fact, this difference was never formally recognized in the presentation of the model. The primary impact of this simplification is that the assumed isotropic  $TE_{10}$  field incident on the aperture is invalid. The true incident field may be greatly effected by the variable coupler. It will not be isotropic, and it will likely contain many higher-order modes than the assumed dominant mode. This difference should be considered in validating the accuracy of simulating the experiments at LANL where the variable coupler was included. The only way to determine the true impact of the variable coupler on the cavity field distribution would be to expand the electromagnetic field model to include the effects of the additional hardware.

In 1999, J. Curtis performed experimental research on microwave heating of thermal runaway ceramics and polymers. One challenge he faced in his experimental work was heating thermal runaway materials to stable high temperatures without an automated power feedback control system. The other goal of his work was to investigate the losses associated with the resonator cavity so that the power absorption by the process material could be quantified to a reasonable degree of accuracy. His work utilized a system similar to the applicator employed at LANL but with some appreciable differences. The greatest difference between the two was the microwave source. At LANL, the TWT source operated at a nominal frequency of 2.93 GHz, but the frequency could be varied to maintain the resonance condition in the loaded cavity as the sample heated. The source employed in the experimental work at Virginia Tech was a magnetron source operating at a nominal frequency of 2.45 GHz and a variable power output up to 3 kW. This source is not able to produce a variable frequency, and cavity resonance was controlled by adjusting the position of the shorting plane. While the WR-284 waveguide section has a nominal cutoff frequency of approximately 2.08 GHz, the reported minimum frequency for ideal support of the dominant  $TE_{10}$  mode is 2.60 GHz, hence the efficiency of the waveguide may be acceptable but not ideal with this source

(Metaxas and Meredith, 1983). One of the difficult aspects of achieving stable heating rates with this system is the lack of feedback control. The cavity has to be tuned manually which is a tedious task. The system did not utilize the variable coupler device, making the cavity system more compatible with the electromagnetic field model developed by Terril. Instead, a directional coupler was placed adjacent to the cavity iris to measure forward and reflected power. This meant that the difference power measured would be attributed to the cavity, shorting plane, iris, and process material. Because the variable coupler was not used and the power levels were measured much closer to the cavity, the approximation of system losses was simplified in comparison to the LANL applicator. A power meter attached to the resonator cavity, at a peak in the standing wave, measured a power flux proportional to the field strength in the cavity, just as in the LANL applicator. However, Curtis was able to utilize an algorithm to convert the measured power flux to the sensor, in W, to the corresponding field strength, in volts/meter.

The losses in the cavity, mainly Joule heating due to the electric current flux through the finite resistance of the cavity walls, are proportional to the field strength in the cavity. Curtis was able to design a series of experiments to determine the losses in the cavity based on a specified forward source power and field strength in the cavity. The applicator at LANL maintained the cavity at peak resonance and varied the forward power to control the heating rate of the sample. In Curtis' experiments, the forward power was maintained at a fixed level and the power absorption in the sample was controlled by intentionally detuning the cavity to reduce the field strength. This allowed for effective temperature control in the sample without requiring a change in the forward power from the source. Maintaining a fixed forward power was necessary due to the means by which Curtis had characterized the cavity losses.

During a heating experiment, the difference between the forward and reflected power readings (at the directional coupler in front of the resonant cavity) can be attributed to the power absorption by the cavity walls and the process material. The losses in the cavity depend on the electric field strength in the cavity and are independent of the inclusion of a process material. The cavity losses are characterized by measuring the load power (forward – reflected power in front of the iris) and the field strength in the

empty cavity. The load power for the empty cavity represents the power loss to the iris, cavity walls, and shorting plane. To characterize the cavity loss, the load power was recorded as the field strength in the cavity is reduced to zero from the maximum value. With this information, the portion of the load power due to the cavity losses could be determined based on the forward power and field strength measurements when a load is in the cavity. By subtracting the power loss from the total load power, Curtis was able to deduce the power absorbed by the rod in the applicator.

Once the means for accounting for the power losses had been completed, Curtis was able to use the adjustable shorting plane to produce several heating scenarios for a variety of materials. His data include cases where the following parameters were held constant: power absorption by the load (cavity + sample), power absorption by the sample, and electric field strength in the cavity. Similar measurements were taken for alumina rods, mullite rods, and a fibrous nylon tow. Due to the fixed temperature range of the optical pyrometer used, the maximum temperature was approximately 700 °C. This limited the experiments to low power levels. For comparison, the pyrometers used in the LANL experiments could measure temperatures above the melting point of mullite at 1824 °C.

# Chapter 3

## Method of Investigation

### 3.1 Heat Transfer Model

A great deal of credit for the heat transfer modeling used in this work must go to Goodson (1997), the original author of most of the computer code. His code was originally written as one large program in FORTRAN 77 but was subsequently converted to FORTRAN 90 for the work reported in this thesis. The code was also decomposed into individual subroutines and functions, each with its own specific purpose. This transformation makes the code more easily utilized for future additions and modifications, and facilitates debugging as a part of good code structuring procedure. Although the fundamental aspects of the heat transfer code are outlined in this section, additional details may be found in Chapter 5 of Goodson's thesis (Goodson, 1997).

A fundamental principle governing the heat transfer in any system is the conservation of energy. For a given volume of material, the relationship can be simply stated as

$$\dot{E}_{in} + \dot{E}_{gen} - \dot{E}_{out} - \dot{E}_{stored} = 0, \quad (3.1)$$

where  $\dot{E}_{in}$  and  $\dot{E}_{out}$  are the energy rates conducted and transported in and out,  $\dot{E}_{gen}$  is the rate of energy generation within, and  $\dot{E}_{stored}$  is the rate of energy storage. This relationship applies to systems of any size, shape, or material. For this work, the materials treated are assumed to be of cylindrical cross-section, and "thin" in diameter as

compared to the penetration depth of the microwave field. It is assumed that there is circumferential symmetry of temperatures within the material, so a two-dimensional representation is used to describe the temperature distribution within the three-dimensional part. This symmetry results in an assumed adiabatic boundary along the axial centerline of the cylindrical sample, and the temperature distribution varies axially and radially. In order to use the FDTD method to model the heat transfer in the cylindrical sample, the volume must be subdivided into smaller volumes within which the properties are assumed constant. The FDTD method of treating properties differs from a finite element (FE) representation of a three-dimensional solid. In both cases, the part being considered is divided into regular volumes. In a FE model, the "nodes" are placed along the boundaries of the volume, and each node is assigned all of the values and properties being considered within the model. The property values within the volume are derived from weighted averages of the nodal values along the boundaries of the element. In a finite-difference (FD) model, the nodes are placed at the center of each volume element. The properties of the entire element are represented by the properties of the single point that represents the node. The temperature accuracy and property gradient representation in a FD model approaches those in a FE model (and the "real" solution, assuming the model is valid) as the mesh of the part is refined. Meshing refers to the scheme by which the part is sub-divided into individual volume elements. A compromise must be made between resolution in the temperature distribution and computational resource requirements as the part is subdivided. Utilizing more volume elements (a finer mesh) results in better resolution in the property of interest and higher accuracy, but fewer volume elements (a coarser mesh) results in a faster solution. Again, it must be emphasized that mesh refinement only improves the accuracy of the solution if the physics of the model are a realistic representation of the actual part. If the workings of the model are wrong, it does no good to expend more resources only to converge to the "wrong" solution. The meshing used in the heat transfer model is selected based on knowledge of the size of the parts to be modeled. As stated previously, the meshing choice is a compromise between resolution/accuracy and computational time. Since the model assumes that the diameter is sufficiently small to allow the penetration depth effects to be negligible, the maximum diameter for which this model may be used is

already limited. The size of the samples used in the LANL and Virginia Tech experiments, which are to be used for validation purposes, did not exceed 4.67 mm in diameter. Therefore, the radial mesh in the model uses eight volumetric divisions, or nine radial nodes with one at the center, one at the surface, and the rest positioned concentrically with equal radial spacing. This scheme of radial meshing is most easily implemented in a computational sense, but it results in a higher mesh density, relative to element volume (in a three-dimensional sense), at the center of the sample. A scheme in which the radial spacing of the nodes decreases at locations further from the center of the sample would be able to provide a constant node-to-volume ratio, but would be more difficult to implement. Ideally, the model should use the highest mesh density in regions where the gradient in the quantity of interest, temperature in this case, are greatest. This would dictate a meshing scheme where the highest mesh density occurs midway between the center and surface where the temperature gradient is at a maximum. The detrimental effects of utilizing a nonuniform meshing scheme can be justified in two ways. First, the uniform mesh spacing is easier to implement, and second, the overall mesh density can be increased to improve the resolution. The axial meshing of this model is such that the 34-mm length within the WR-284 cavity is divided into 40 axial nodes, again with equal spacing. As with the radial spacing, the axial positioning of the nodes would be optimized in a case where the highest nodal density coincided with areas with the largest gradient in temperature. However, the axial case is complicated by the additional factor of axial sample velocity. If the sample were always stationary, it would be a simple matter to determine the location of the greatest temperature gradient in the sample and construct the mesh accordingly. When the rod is moving through the cavity, the temperature gradients in the sample are no longer symmetrical about the center of the cavity. The greatest temperature gradient then occurs near the side of the cavity where the material is exiting. Since the material may be raised or lowered through the cavity, the side where this occurs is not always the same. The speed at which the sample moves through the cavity, and the power level applied, will influence the location and severity of the resulting temperature gradient. Due to these complications, the evenly spaced axial meshing scheme provides the best overall solution.

The aspects that govern the heat transfer between these elements and their environment must be represented as a series of simultaneous mathematical equations in order to solve for the temperature distribution using the FD method. The resulting meshed representation of the process sample contains three distinct types of volume elements and/or nodes. The first of these are the center nodes. They are distinguished as having one adiabatic boundary, at the center of the three-dimensional solid, due to the circumferential symmetry assumption. These nodes experience heat transfer phenomena governed by the rod axial velocity and the local nodal properties. The first of these is the axial transport term, due to the axial velocity of the material. This simulates the effects of having material move through the cavity by incorporating an equivalent axial heat flux into or from the element. The second effect is axial conduction, where conduction heat transfer occurs to or from adjacent axial elements. The third effect is conduction to or from the adjacent radially positioned interior elements. Due to the adiabatic symmetry boundary, they only experience radial heat conduction with one radially adjacent element. The final effect is volumetric heat generation. In this model, volumetric heat generation is due to the influence of the microwave field. Other models may also consider other volumetric heat generation sources, such as the spontaneous decay of radioactive materials or chemical reactions such as the curing of epoxy resins. The second class of volumetric elements includes the interior elements. The interior elements experience all of the modes of heat transfer listed for the center elements except they experience conduction at both radial boundaries. This is because they are not adjacent to the adiabatic symmetry boundary. The third class of elements includes the surface nodes. Compared to the core nodes and interior elements, the surface nodes have the additional heat transfer considerations of convection and radiation heat transfer. These effects are readily accommodated into the FD equations.

When the implicit FDTD method is applied to the particular meshing scheme in the cylindrical part, it results in a set of  $n$  simultaneous equations where  $n$  is the total number of nodes in the model. The equation based on each node accounts for the allowed modes of heat transport and generation within the local nodes. Each node has a specific temperature at any given time step. According to those nodal temperatures, the volume surrounding any particular node is assigned specific properties, such as thermal

conductivity, specific heat, dielectric loss, and dielectric constant. The equations for the surface nodes include terms for the convection and radiation heat transfer from the respective elements based on the local material temperature, sample geometry, and the sample surroundings. These properties, convection rates, and radiation rates are computed based on functions that depend on the temperature and/or geometry of the local element area. The rate of heat conduction between elements is primarily governed by the local temperature gradients and thermal conductivity. Since a temperature is assigned to each nodal point, the effective thermal conductivity between the nodes is computed based on the volume and temperature of the adjacent elements. The energy storage term for each element is dependent on the local value of heat capacity. The volumetric heat generation rate of the material is dependent on the local value of the dielectric loss factor by the relationship shown in Eq. 1.4. In this model, the materials used are such that the density does not vary significantly with temperature, based on available data. Therefore, the density of the materials used is treated as a constant within the simulation. Hence, for the most part, the equations that represent the heat flux, generation, and storage at a particular volumetric element are highly dependent on the local values of the material properties, convection, and radiation heat transfer rates. The finite-difference representation of the various nodes is given as (Goodson, 1997):

**Surface Nodes:**

$$\begin{aligned}
& \left[ k\Delta x \left( \frac{1}{\Delta r} - \frac{1}{2r} \right) \right] T_{m,n-1}^{(p+1)} + \left[ \left( \Delta r - \frac{\Delta r^2}{4R} \right) \left( \frac{k}{2\Delta x} + \rho C_p \frac{v}{4} \right) \right] T_{m-1,n}^{(p+1)} + \\
& \left[ -k\Delta x \left( \frac{1}{\Delta r} - \frac{1}{2R} \right) - \frac{k}{\Delta x} \left( \Delta r - \frac{\Delta r^2}{4R} \right) - h_c \Delta x - h_r \Delta x - \rho C_p \frac{\Delta x}{2\Delta t} \left( \Delta r - \frac{\Delta r^2}{4R} \right) \right] T_{m,n}^{(p+1)} + \\
& \left[ \left( \Delta r - \frac{\Delta r^2}{4R} \right) \left( k \frac{1}{2\Delta x} - \rho C_p \frac{v}{4} \right) \right] T_{m+1,n}^{(p+1)} = -h_c \Delta x T_\infty - h_r \Delta x T_{wall} - \\
& \left( \Delta r - \frac{\Delta r^2}{4R} \right) \dot{q} \frac{\Delta x}{2} - \left[ \rho C_p \left( \Delta r - \frac{\Delta r^2}{4R} \right) \frac{\Delta x}{2\Delta t} \right] T_{m,n}^p
\end{aligned} \tag{3.2}$$

**Interior Nodes:**

$$\begin{aligned}
 & \left[ k\Delta x \left( \frac{1}{\Delta r} - \frac{1}{2r} \right) \right] T_{m,n-1}^{(p+1)} + \left[ \frac{k^- \Delta r}{\Delta x} + \frac{\rho v C_p^- \Delta r}{2} \right] T_{m-1,n}^{(p+1)} + \\
 & \left[ -\frac{k^- \Delta r}{\Delta x} - \frac{k^+ \Delta r}{\Delta x} - 2\frac{k\Delta x}{\Delta r} - \frac{\rho C_p \Delta x \Delta r}{\Delta t} \right] T_{m,n}^{(p+1)} + \left[ k\Delta x \left( \frac{1}{\Delta r} + \frac{1}{2r} \right) \right] T_{m,n+1}^{(p+1)} + \\
 & \left[ \frac{k^+ \Delta r}{\Delta x} - \frac{\rho v C_p \Delta r}{2} \right] T_{m+1,n}^{(p+1)} = -\dot{q}\Delta x \Delta r - \left[ \frac{\rho v C_p \Delta r}{\Delta t} \right] T_{m,n}^{(p)}
 \end{aligned} \tag{3.3}$$

**Center Nodes:**

$$\begin{aligned}
 & \left[ k \frac{\Delta r}{\Delta x} + \rho C_p v \frac{\Delta r}{2} \right] T_{m-1,n}^{(p+1)} + \\
 & \left[ -4k \frac{\Delta x}{\Delta r} - k \frac{\Delta r}{\Delta x} - \rho C_p \frac{\Delta x \Delta r}{\Delta t} \right] T_{m,n}^{(p+1)} + \left[ 4k \frac{\Delta x}{\Delta r} \right] T_{m,n+1}^{(p+1)} + \\
 & \left[ k \frac{\Delta r}{\Delta x} - \rho C_p v \frac{\Delta r}{2} \right] T_{m+1,n}^{(p+1)} = -\dot{q}\Delta x \Delta r - \left[ \rho C_p \frac{\Delta x \Delta r}{\Delta t} \right] T_{m,n}^{(p)}
 \end{aligned} \tag{3.4}$$

where

$T_{m,n-1}^{(p+1)}$  = Temperature at  $(-\Delta r)$  step from the point of evaluation at time  $t + \Delta t$ ,

$T_{m-1,n}^{(p+1)}$  = Temperature at  $(-\Delta x)$  step from the point of evaluation at time  $t + \Delta t$ ,

$T_{m,n}^{(p+1)}$  = Temperature at the point of evaluation at time  $t + \Delta t$ ,

$T_{m,n+1}^{(p+1)}$  = Temperature at  $(+\Delta r)$  step from the point of evaluation at time  $t + \Delta t$ ,

$T_{m+1,n}^{(p+1)}$  = Temperature at  $(+\Delta x)$  step from the point of evaluation at time  $t + \Delta t$ , and

$T_{m,n}^{(p)}$  = Temperature at the point of evaluation at time  $t$ .

These equations are subject to the boundary conditions described in table 3.1 corresponding to the locations shown in figure 3.1.

**Table 3.1:** Boundary and initial conditions for nodal finite-difference equations

$T(x,r,t) = T_\infty$	@ $x = 0$
$T(x,r,t) = T_\infty$	@ $x = L$
$-k \frac{\partial t}{\partial r} = 0$	@ $r = 0$
$-k \frac{\partial t}{\partial r} = h_c(T - T_\infty) + h_r(T - T_{wall})$	@ $r = R$
$T(x,r,t) = T_\infty$	@ $t = 0$

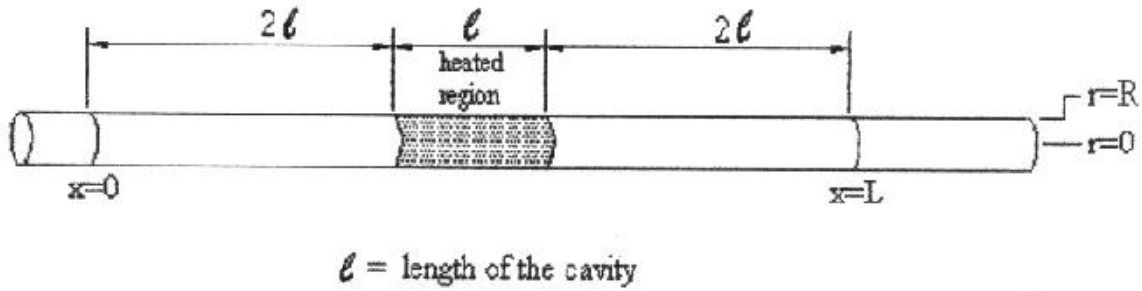


**Figure 3.1:** Schematic representation of the process material for applying boundary conditions (Goodson, 1997)

Once the heat transfer relationships between the material elements have been developed, the resulting set of simultaneous equations must be solved for the new nodal temperature distributions. Solution methods such as Gaussian elimination require storage and calculations of many zero-valued matrix elements. This leads to slow solutions and inefficient use of computational resources. Therefore, this heat transfer model uses the line-by-line method, also known as the Alternating Direction Implicit (ADI) solver (Goodson, 1997). In a one-dimensional FDTD model, the solution matrix has only three terms on the diagonal, making the set of equations suitable for a tridiagonal solution technique. However, in the two-dimensional formulation used in this simulation, five terms are on the diagonal. This prevents the use of standard tridiagonal solvers, which are desirable due to their computational efficiency. The line-by-line method solution works well for diagonally dominant matrices as an iterative implementation of the tridiagonal solver. It sweeps in the axial and radial directions in successive iterations. Subsequent pairs of iterations are performed until the solution for the temperature distribution is converged. As mentioned in Chapter 2, the inclusion of temperature-

dependent properties requires that this iterative solution scheme be performed iteratively within the time step to properly converge the material properties for the correct temperature distribution.

The model requires that certain parameters be specified by the user in order to operate. The temperature dependence of most of the thermophysical and dielectric properties, discussed in Section 3.1.1, is built into the model. The user must specify such details as the material, sample diameter, convergence criteria, and either the power to be absorbed by the rod or the constant electric field strength of the source. The input parameters required for the electric field model are addressed in the next section. The solution scheme employed in the heat transfer simulation is outlined in figure 3.2. Three convergence criteria must be given by the user specify the accuracy of the sample absorbed power, time step temperature convergence, and steady-state temperature convergence, respectively.

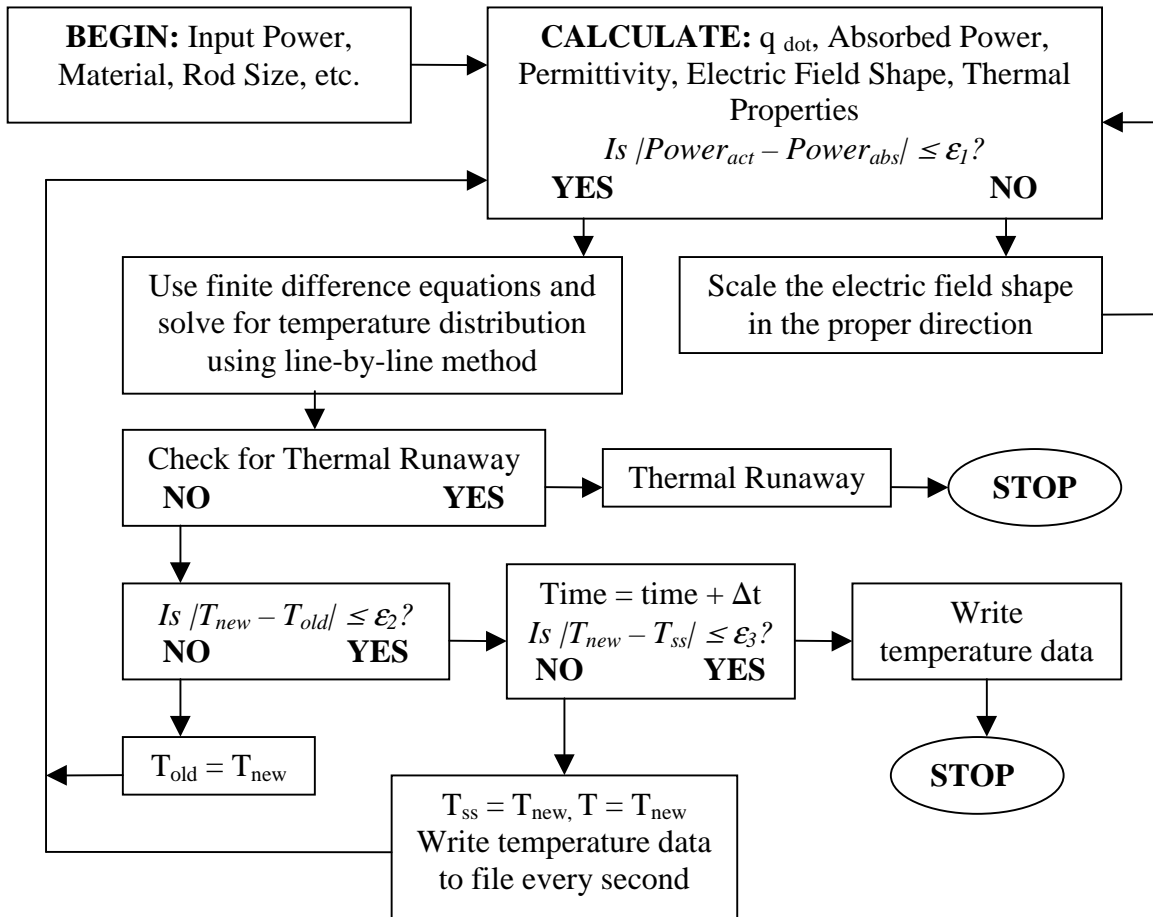


**Figure 3.2:** Outline of the computations performed by the heat transfer model

The computer code that implements this solution method is included as Appendix A.

### **3.1.1 Thermophysical Properties**

Certain thermophysical properties used in the heat transfer model are allowed to vary with local element temperature. The primary material studied in this work was mullite. The motivation for selecting this material remains unchanged from prior works at Virginia Tech; the material was available for further lab study and existing experimental data would allow for validation of the model. The density of mullite is quite constant with variation in temperature below the melting temperature (Goodson, 1997), so the material density is modeled with a constant value of  $2600 \text{ kg/m}^3$ . This value is the reported material density from the supplier, Bolt Technical Ceramics, Inc. of Conroe, Texas. The earlier model by Goodson (1997) uses a value of  $2500 \text{ kg/m}^3$ , which is reportedly derived from measurements. The specific heat of mullite is modeled using a logarithmic curve fit to published data from Russel et al. (1987) and Schneider (1994). The two publications provide the specific heat over two overlapping temperature ranges. Good agreement between the values in the overlapping temperature range allowed both sets of data to be fit with a single curve. The thermal conductivity data used in the model are derived from thermal diffusivity data published by Russel et al. (1987). The model uses a linear interpolation between data points and extrapolation based on the last two points to determine the material thermal conductivity within and above the temperature range covered by the published data. The emissivity of mullite is modeled by a polynomial fit to the published data from Bauer and Steinhardt (1990). Goodson's (1997) model does not use emissivity data that is specific to mullite. Since mullite has a large molar fraction of alumina, an average value from a range of measured values of alumina emissivity is used in the previously mentioned model. The difference between the two emissivity curves is considerable, as can be seen in figure 3.3.

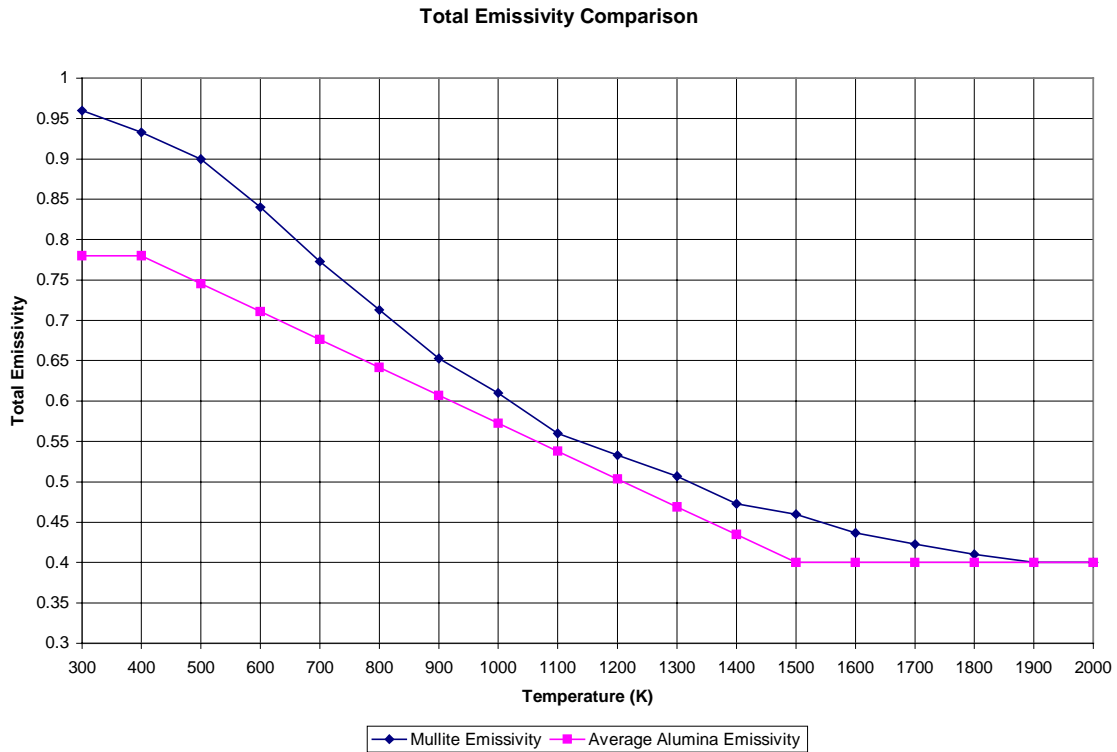


**Figure 3.3:** Emissivity of alumina (Touloukian, 1972) and mullite (Bauer and Steinhardt, 1990)

The uncertainty in the emissivity values was previously noted (Goodson, 1997) as a possible source of error in Goodson’s model. Incorporating the more accurate emissivity values into the uniform field heat transfer model (Goodson, 1997) resulted in lower temperature predictions, but the improvement was not sufficient to completely eliminate the difference between predicted temperatures and measured experimental values. However, including the new emissivity data in the current model rules out one possible source of error. The dielectric properties of mullite are discussed in Section 3.2.1. The convection heat transfer coefficient for each local surface element is determined by analytical methods based on the length of the rod in the cavity, local surface temperature, and the surrounding air temperature. This representation is taken from the earlier work of Goodson (1997).

## 3.2 Electromagnetic Field Model

The electromagnetic field model incorporated into the current simulation is largely unchanged from the version developed by Terril (1998). Two primary changes have been made in order to implement the model within the combined simulation. The first change centers on making the stand-alone model into a subroutine. The original code operated through a combination of a user interface, where the user was prompted for inputs, and a data file, where information on the material permittivity distribution was stored. The modified code had to operate as a subroutine where all of the required information was passed into it with the CALL statement. This was effected by removing all aspects of the user interface and passing in data in array form rather than using data files. Likewise, the code was modified so that the results were returned to the main program in an array rather than being written to a data file. Terril (1998) had actually written two programs designed to be used together. The first code acts as a "solver" and writes raw data to an output file. The second program acts as a "post-processor", reading in the file from the "solver". It then generates yet another file to be used by Matlab for plotting the results. In the present work, all of these separate programs are combined into a single subroutine so that the desired results, which are the distribution of the tangential component of the electric field along the sample, are returned to the main program for subsequent use. The user interface in Terril's code allows the user to choose between solving a "fiber problem", "aperture problem", or the "combined problem". Since the current simulation uses the information developed through the solution of only the combined problem, all other aspects of Terril's code used only for the other two solution types was removed. The other fundamental modification was in matching the mesh size along the sample to the mesh size used in the heat transfer model. Terril's code decomposed the 34 mm length of the sample in the cavity into 34 sections, each 1 mm in length. The relative magnitude of the electric field at each of these sections was computed. In the heat transfer model, the sample in the cavity was decomposed into 40 axial segments. In order for the models to work together, the number of segments in the field model was increased to 40 to match the divisions in the heat transfer code. A

secondary modification to the original field simulation code was the addition of comments to describe the variables, subroutines, and improve the readability of the code.

The basis for the field simulation is the solution of Maxwell's curl relations, which govern the behavior of the electromagnetic waves within the waveguide and its components. Maxwell's curl relations, in vector differential form, are given as

$$\nabla \times \vec{E} = -j\omega\mu\vec{H} \quad (3.5a)$$

and

$$\nabla \times \vec{H} = j\omega\epsilon\vec{E}, \quad (3.5b)$$

where  $\vec{E}$  and  $\vec{H}$  are the local electric and magnetic field vectors, respectively. In the field model, auxiliary potential functions are used to uncouple the two equations. These equations apply to all points in space within the waveguide and resonator cavity, but for the analysis, the space has been divided into three separate solution regions. A schematic side-view of the cavity, depicting the solution regions and components of interest, is shown in figure 3.4.

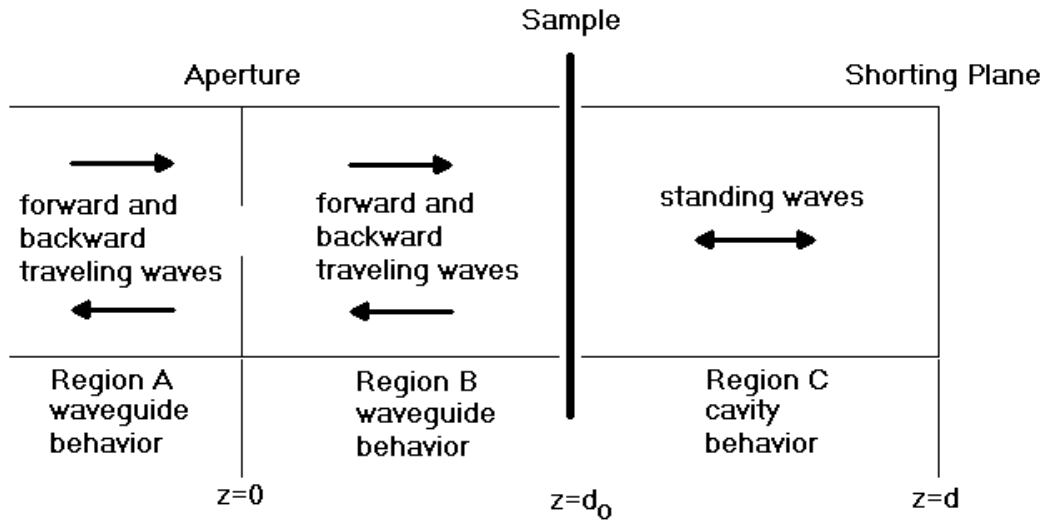


**Figure 3.4:** A schematic representation of the electromagnetic solution regions

In each solution region, a set of amplitude coefficients is used to describe the local electromagnetic field components. Regions A and B have two sets, one for the

forward and backward traveling components, while region C has a single set. Region C has only a single set because it is assumed that there is no loss caused by the reflection from the shorting plane. If two sets of amplitude coefficients were used in this region, they would be identical due to this assumption, so only one set is used. If losses were assumed in the shorting plane, two sets of coefficients would be needed since the losses would cause a reduction in the amplitudes of the reflected coefficients. A complete set of coefficients has an amplitude value for each of the  $TE_{mn}$  modes. The subscripts  $m$  and  $n$  are integers used to designate the mode of propagation. The total number of coefficients included is  $(m \times n)$  for each set of amplitude coefficients. When the model is initiated to solve for the electric field distribution along the sample, the coefficients for the forward traveling wave in region A are known and the rest of the coefficients are unknown. The forward region A coefficients are known because the incident wave from the source is assumed to be a pure  $TE_{10}$  mode, where all of the  $TE_{mn}$  coefficients are zero except the  $TE_{10}$  coefficient which is assumed to have a value of unity. In cases where the variable coupler is not included directly prior to the metal aperture, this assumption is realistic. Any higher-order ( $m > 1, n > 0$ ) modes would not propagate through the long waveguide section and only the dominant ( $TE_{10}$ ) mode would reach the aperture. The magnitudes of the higher-order coefficients would be so small that neglecting them does not affect the solution. However, when the variable coupler is placed in the waveguide system before the aperture, the interaction of the  $TE_{10}$  incident field with the coupler will cause the higher-order modes to be excited. Therefore, the assumption of the pure  $TE_{10}$  incident field at the aperture is inaccurate for modeling experiments where the variable coupler is included. The error introduced into the solution cannot be determined with the current model and is worthy of future investigation. The nature of a  $TE_{10}$  field can be visualized with the aid of figure 3.5, which shows the assumed field patterns incident on the aperture in the electromagnetic field model.

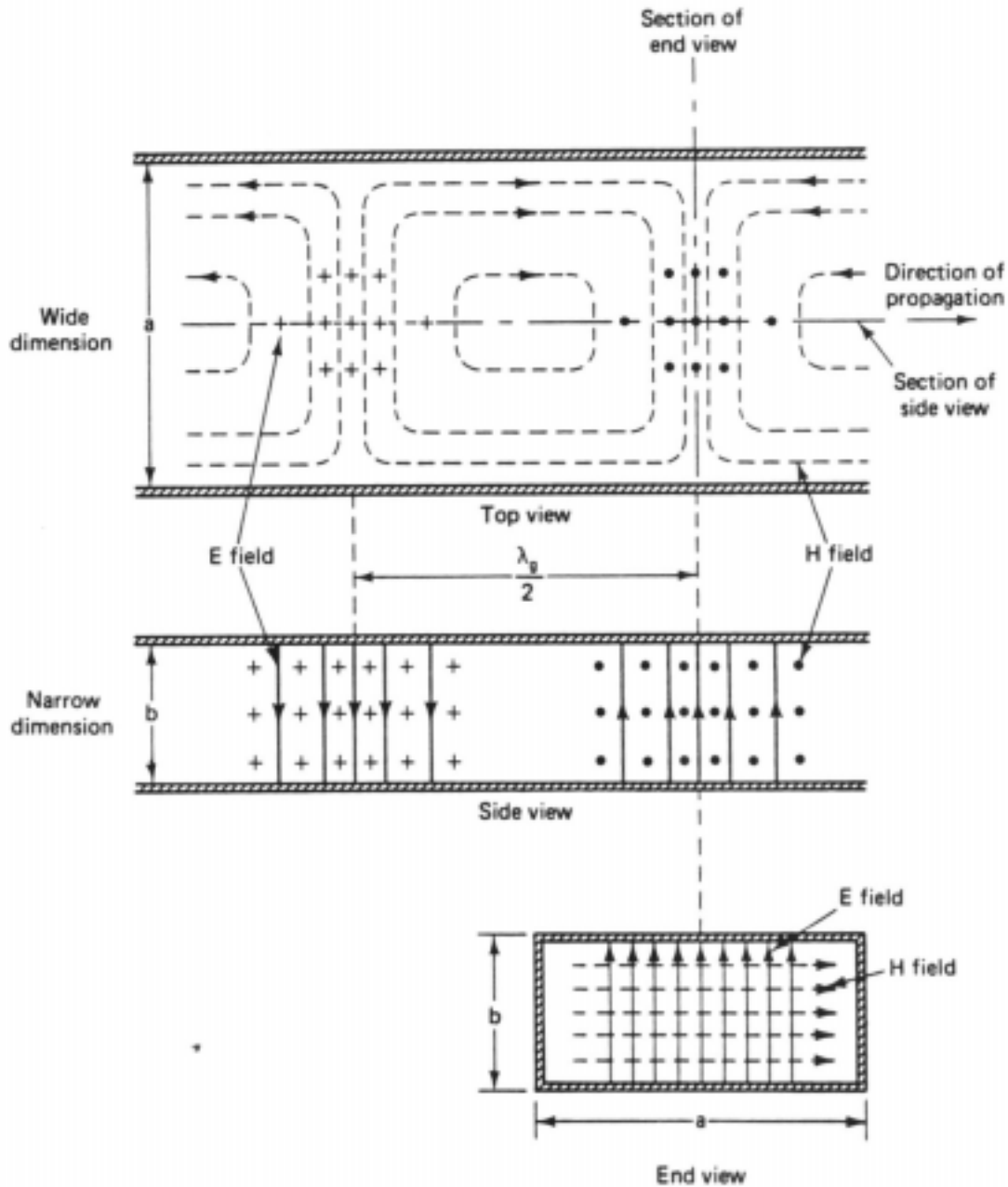


**Figure 3.5:** Distribution of the electric and magnetic field components in a TE<sub>10</sub> mode (Veley, 1987)

While the incident amplitude coefficients are assumed, four sets of coefficients still must be found. If the metal aperture and the dielectric sample in the cavity did not interact with the incident field, the solution of the problem would be trivial. The fact that a complicated series of interactions takes place at both the aperture and the sample

complicates the analysis considerably. When the incident field in region A reaches the aperture, a portion of the energy is "scattered" and reflects from the aperture while the rest is transmitted through the aperture into region B. This assumes that there is no loss due to the interaction with the aperture. Likewise, the backward traveling wave in region B has some of the energy reflected from the back side of the aperture and the rest is transmitted through into region A. At the sample, the field interaction with the dielectric material also results in some incident energy scattering and some being transmitted to the adjacent region. All of these effects are accounted for in the field model.

The solution of the problem is constrained by particular boundary conditions at the four longitudinal metal walls, the metal shorting plane, the metal iris, and the dielectric sample. For the purposes of this model, the boundary conditions are applied assuming that the metal surfaces are perfect electrical conductors (PEC). At a PEC boundary condition, the tangential (relative to the surface) component of the electric field must be zero. This can be seen in figure 3.5 where the E field lines can exist normal to a metal surface, but must not have a tangential component. At a PEC boundary, the magnetic field H is continuous. At the metal iris, assumed to have zero thickness (idealized), both the electric and magnetic fields are continuous across the iris. At the metal surfaces, the E field is continuous and zero across the iris. At the aperture opening, the E field is continuous but non-zero. The electric field in the aperture is known to be continuous, but the exact distribution within the aperture opening must be solved for in the model. The magnetic field is continuous and zero in the opening. The PEC boundary condition at the shorting plane is similar, except the E field is zero everywhere at the short.

The boundary condition enforced at the transverse plane where the sample is located is different. The sample is treated as a non-homogeneous line source of current to account for the interaction of the fields with the material and to match the coefficients between regions B and C at the sample interface. This implies that the sample is treated as a one-dimensional object with no diameter, similar to the treatment of the thickness of the metal iris. This is a suitable assumption that results from the relatively small diameter of the sample compared to the penetration depth of the microwaves used. If the sample were large, such that there was significant attenuation of the field quantities within the

sample, this assumption would not be valid. Since the sample is a dielectric material and not a PEC, the E and H fields must be continuous at the sample, but neither of the components is forced to zero.

The ultimate goal of the model is to determine the distribution of the electric field along the sample in the cavity. To accomplish this, the fields at all locations in the cavity must be determined. This involves finding the two electric field vectors,  $\vec{E}^h$  and  $\vec{E}^e$ , and two magnetic field vectors,  $\vec{H}^h$  and  $\vec{H}^e$ , that describe the field distributions in the cavity. These four quantities are developed from the electric vector potential function,  $\vec{F}$ , and the magnetic vector potential function,  $\vec{A}$ , and describe the field distribution completely for a single TE<sub>mn</sub> mode. Hence, they must be found for each mode included in the model. These respective vector functions describe the distributions of the electric and magnetic fields in the transverse plane as functions of longitudinal position in the cavity. Each of the vector potential functions can be formed from the product of two individual scalar potential functions that describe the distributions in only one direction to provide the field descriptions in the transverse plane. In this sense, the electric vector potential is found with the scalar potential functions

$$\psi^h(\vec{\rho}) \quad (3.6a)$$

and

$$\phi^h(k_z z) \quad (3.6b),$$

where  $\vec{\rho}$  is the transverse coordinate variable,  $z$  is the axial coordinate variable, and  $k_z$  is the mode propagation constant. The magnetic vector potential is found with similar scalar potential functions

$$\psi^e(\vec{\rho}) \quad (3.7a)$$

and

$$\phi^e(k_z z) \quad (3.7b).$$

The particular forms of these functions must be chosen so that the resulting vector potential functions satisfy the prescribed boundary conditions that govern the solution domain (Terril, 1998, p. 14). The complete transverse electric and magnetic field components for the waveguide regions of the system, regions A and B, can be described by (Terril, 1998):

$$\begin{aligned}\vec{E}_t^{(\pm)} &= \sum_v \left[ \hat{z} \times \nabla_t \psi_v^h E_v^{h(\pm)} \mp Z_v^e \nabla_t \psi_v^e E_v^{e(\pm)} \right] \phi_w^{(\mp)} \\ \vec{H}_t^{(\pm)} &= \sum_v \left[ -\hat{z} \times \nabla_t \psi_v^e E_v^{e(\pm)} \mp \frac{1}{Z_v^e} \nabla_t \psi_v^h E_v^{h(\pm)} \right] \phi_w^{(\mp)}, \quad (3.8a)\end{aligned}$$

where  $v$  denotes a particular (mn) mode,  $Z^e$  is the wave impedance, and  $E_v^{h(\pm)}$  and  $E_v^{e(\pm)}$  are the unknown mode amplitudes. For the cavity region, region C, the field components are described by (Terril, 1998):

$$\begin{aligned}\vec{E}_t &= \sum_v \left[ \hat{z} \times \nabla_t \psi_v^h E_v^{h(\pm)} + j Z_v^e \nabla_t \psi_v^e E_v^e \right] \phi_c^h \\ \vec{H}_t &= \sum_v \left[ -\hat{z} \times \nabla_t \psi_v^e E_v^e - j \frac{1}{Z_v^e} \nabla_t \psi_v^h E_v^h \right] \phi_c^e, \quad (3.8b)\end{aligned}$$

Solving for the six vectors described in (3.8a,b), from the summation over a truncated set of infinite mode combinations, is sufficient to completely describe the fields in the areas of interest. To accomplish this, the amplitudes for each mode in the summation must be determined.

The determination of the unknown mode amplitude coefficients is accomplished via a mode-matching technique. This is done by enforcing boundary conditions at an interface between two solution regions to relate the mode coefficients in adjacent regions. At the iris separating regions A and B, the three primary boundary conditions are as described previously: the electric field is continuous and zero at the metal surface, the electric field is continuous and non-zero at the opening, and the magnetic field is continuous and zero in the opening. Two additional boundary conditions are used at the iris: the discontinuity in the magnetic field on the metal surface must equal the electric surface current in the metal iris, and  $\hat{z} \times \vec{E}^A$  must equal the magnetic surface current in the opening. The mode-matching solution employed in the model solves for the magnetic current in the opening to find the coefficients of the transmitted modes in terms of the coefficients of the incident modes. The method of moments solution technique is used to solve for the magnetic current. It accomplishes this by developing a series type dyadic (of two parts) Green's function to express the magnetic current in the aperture. This is an integral formulation where the independent sets of basis and weighting functions are truncated (from an infinite set) and the forms of the functions are appropriately chosen to

result in proper convergence to the desired solution. In both cases, harmonic functions are utilized. In a general sense, the Green's function is determined by enforcing the specified boundary conditions at the iris and aperture. The basis and weighting functions are integrated in the aperture region, and the resulting set of matrix equations is solved to determine the unknown mode coefficients of the forward and backward traveling waves in region B, and the backward traveling waves in region A. The matrix equations are solved with a LU decomposition technique. The results from the aperture interface solution are used to match the mode amplitudes at the sample interface by enforcing the continuity of the tangential electric field component at the interface. What has been presented here on the field model is intended to provide a general overview of the solution methods employed. For more details, refer to Terril (1998), and the FORTRAN code included in Appendix B. A good understanding of the implementation of the solution can be gained from the comments that have been added to and included in the FORTRAN code.

### **3.2.1 Dielectric Properties**

The electromagnetic field simulation requires knowledge of the dielectric constant and the dielectric loss distributions along the sample. The dielectric loss is a critical property value because it also appears explicitly in the element volumetric heat generation terms of the heat transfer model, as shown by Eq. (1.4). Two available sources of mullite dielectric property measurements are that of Jackson (1997) and Xi and Tinga (1991), shown in figure 3.6.

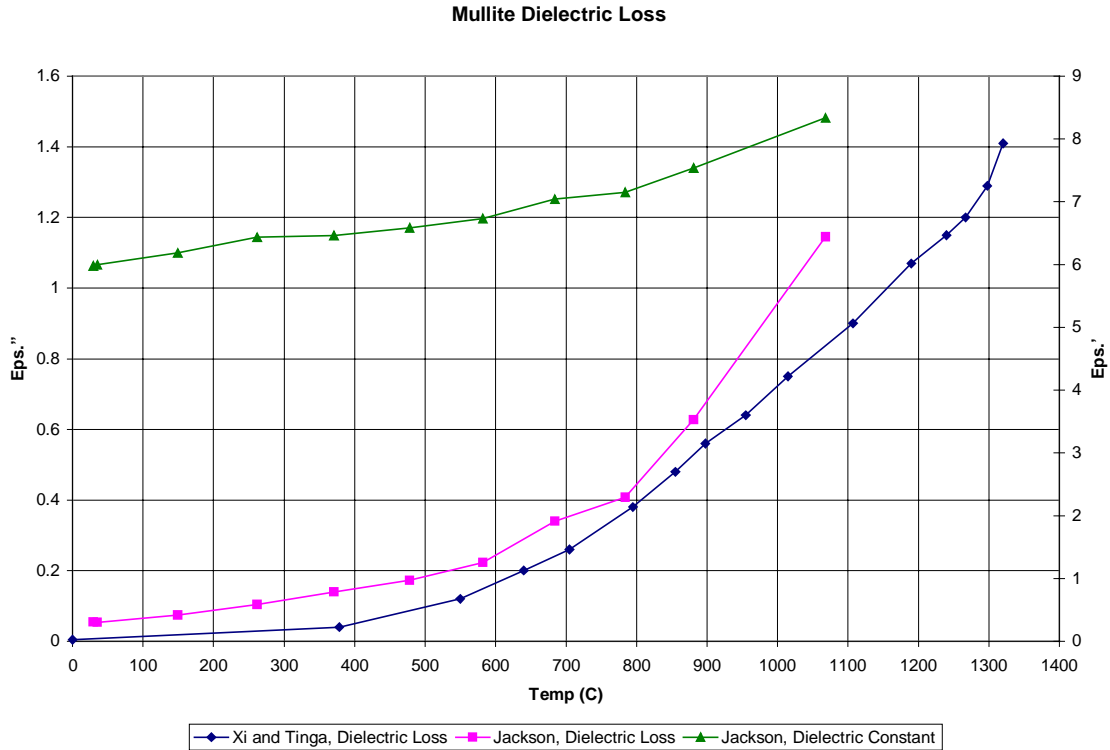


**Figure 3.6:** Dielectric constant and dielectric loss of mullite

The data obtained from Jackson (1997) is used in the model because the property measurements were made on samples of mullite from the same supplier as the samples used in both the LANL and Virginia Tech experiments. The model uses linear interpolation between the data points and a linear extrapolation based on the last two points for property values at temperatures above the measured points. This method of modeling the dielectric loss raises certain questions, especially in the extrapolation at high temperatures. Thermal runaway materials, such as alumina and zirconia (see figure 1.11), are typified by an exponential increase in the dielectric loss with increasing temperature. Modeling the loss at high temperatures with a linear extrapolation from the highest two data points results in a linear increase in loss with temperature, while the trend exhibited by the measured data suggests that an exponential increase may be more appropriate. The justification of one assumption over another can only be validated if experimental dielectric loss measurements at higher temperatures become available in the future. Further aspects of the dielectric loss modeling are discussed in chapter 4.

### 3.3 Interface Development

Both the heat transfer simulation developed by Goodson and the electric field simulation developed by Terril are based on standard FORTRAN computer code. The models are similar in that both are designed to run from the inputs in a separate file, and both send their results to another output file. The inputs and outputs are composed entirely of alphanumeric characters, and must be viewed and edited with a text editor program. If graphical visualization is to be created from the data files, it must be done with yet another software package. Unfortunately, this method of data handling has been "standard engineering practice" for decades when dealing with most numerical simulations. The past ten years has seen an explosion in the prevalence of graphical user interface (GUI) software packages for the simple fact that most people find the GUI systems easier to work with. With this in mind, a new interface system was developed to make the combined heat transfer and electric field simulation more flexible and easier to use. The new program runs from any Microsoft Windows platform in a manner that is familiar to most computer users. This was implemented using Microsoft Visual Basic (VB) 5.0. The numerical solution is still done with the powerful FORTRAN computer language, but the user no longer has to waste time with separate software packages to create, view, and plot information in data files. The user enters the input parameters through the VB interface and selects a path and file name to save the simulation data. To aid the user in making selections for the input parameters, default values can automatically be loaded. On-screen help is available to explain the functions and parameters involved in the simulation process. The FORTRAN code is called automatically by the VB program when directed by the user. It runs "behind the scenes" but can be viewed to inform the user of the status and progress of the simulation. The VB interface informs the user when the simulation has finished and a new simulation can be initiated. Several simulations can be run simultaneously in order to utilize a greater portion of the available computer memory that is managed by the Windows platform. The VB interface also allows immediate graphical representation of the simulation results without having to use intermediate software packages. The program can animate both the surface temperature distribution and the electric field distribution in a real-time graphical

plot, and lists the numerical temperature data for the centerline and surface of the specimen. The graphics section displays other important information in the window to relate the input parameters, average field strength, and peak core and surface temperatures at a glance while the animation is in progress. The animation can be paused, restarted, or reset easily while running. The new software and interface are quite robust. The VB interface is designed to predict common user errors, such as leaving a critical input parameter blank, and prompts the user for proper usage instead of crashing. A veteran user may not see this feature often, but it certainly aids novice users. A complete listing of the Visual Basic 5.0 code used to create the VB interface program is included as Appendix C in this document.

### **3.4 Data Collection**

The methods and parameters from the experimental work at LANL in 1997 were discussed in detail in Chapter 2, so the focus in this section is on the parameters used in the numerical simulations. The data obtained by the simulations is presented and discussed in Chapter 4.

Some of the simulation parameters were invariant between the models of the LANL and Virginia Tech experiments. These include the following: ambient and cavity wall temperatures were set to 25 °C, but it was found through sensitivity studies that moderate changes in these values had very little effect on the steady-state temperatures predicted by the simulation. The time step interval was set to 0.05 for obtaining steady-state conditions at various power levels. With this time step, and the additional convergence criteria discussed in this section, typical simulations represented between 350 and 400 seconds of heating. For all cases, the criterion for convergence of the absorbed power level was set to +/- 0.001 Watt. This means that for a specified power level, the simulation would adjust the scaling of the electric field distribution until the resulting power absorption was within the specified tolerance. The criterion for temperature convergence at each time step was set to 0.05%. This caused the temperature dependent properties to undergo continuous improvement from previous

iterations within a time step until the change in predicted temperatures was less than 0.05%. Likewise, the criterion for the steady-state convergence was set to 0.05%. This forced the simulation to continue through successive time steps until the largest temperature change from the preceding time step was less than 0.05%. However, convergence to steady-state was checked at five-second intervals, as opposed to every time step, to reduce the overall number of calculations. The number of aperture and cavity modes included for the electric field simulation was set to 10 in X and 5 in Y for both sets of modes. The electric field distribution was recalculated whenever the temperature at one of the nodes had changed by 10 °C. This criterion was selected based on the results of a sensitivity study and was shown to have a negligible effect on the resulting temperature distributions. However, it had the positive effect of yielding substantial savings of computer time compared to solving for the field distribution in every time step.

The parameters for the numerical simulations performed for this work can be divided into two classes. In each case, the simulation parameters were chosen to match the conditions used in each experimental situation. The first class includes the simulations where the parameters were selected to match the conditions of the experimental procedures at LANL. The frequency selected was 2.93 GHz based on the nominal source frequency used in the experimental work. This value was reported by observers present at the experiment and was confirmed from the data file recorded by a signal counter. The diameter of the mullite rods used at LANL ranged from 1 mm to 4.67 mm, but only the largest size (4.67 mm) was used in the simulation. This is due to the fact that only one of the experimental procedures was performed on a stationary rod, as discussed in chapter 2. A sample of the rod was measured with a dial micrometer (0.0001-inch resolution) to confirm the diameter. When the simulation was used to model the 4.67 mm stationary mullite rod experiment, the time step was increased from 0.05 seconds to 0.1 seconds. This was done to accommodate the extended duration of the simulation run (over an hour of heating). While this increase has a negative effect on the temperature accuracy, a sensitivity study was performed to show that the degree of adverse change is minimal and acceptable. The simulation operates by specifying the power absorption into the sample, and the losses in the system must be accounted for

apriori to specify the correct simulation power level. It is important to reemphasize that the field simulation used in this model assumes an isotropic incident  $TE_{10}$  field on the iris. This is not a valid assumption for the experimental apparatus used at LANL because of the variable coupler effects. The incident field is, therefore, no longer isotropic and will contain higher-order modes. The impact of this complication cannot be determined with the current model and there are no parameters that can be adjusted to account for the difference.

The simulation parameters for modeling the experiments performed at Virginia Tech differ from those used for modeling the LANL experiments. A magnetron microwave source was used instead of a TWT amplifier, so the Virginia Tech simulations use a nominal input frequency of 2.45 GHz. Another simulation parameter that differed was the rod diameter. The rods used at Virginia Tech were also measured with a dial micrometer and were found to have a nominal diameter of 4.5 mm. The remaining input parameters for simulating the Virginia Tech experiments were similar to those discussed previously.

# Chapter 4

## Interpretation of the Data

### 4.1 Comparison of Simulation to LANL Data

#### 4.1.1 Microwave Power Losses

In order to make a valid comparison between the results of the LANL experiments and the numerical simulations, the losses included in the power measurements at LANL must be estimated. This fact was recognized by Goodson (1997) based on earlier simulation comparisons to the LANL data, as discussed in Sections 2.1.3 and 2.2. Certain components in the waveguide system used at LANL induce negligible losses in the power measurement, including the coaxial fittings and the uniform waveguide section. Other components, such as the radiating antenna probe, variable coupler, and applicator cavity, cause losses in the power measurement that are not negligible. Therefore, the assumption that the entire difference between the forward and reflected power measurements in the LANL system represents only power absorbed by the process material is not valid. The challenge lies in estimating the portion of the difference power (forward power - reflected power) that is due to the non-trivial losses so that more realistic power inputs can be used in simulating the experiments. A fundamental problem in using experimental procedures with the Virginia Tech equipment to estimate the significant losses in the LANL data is the difference in the source frequencies. The losses measured experimentally at 2.45 GHz with the Virginia Tech

magnetron source can only be assumed to be representative of the losses that result from using the same components at 2.93 GHz. The difference may or may not be significant, but quantifying the difference is not possible at this time.

Two of the fundamental system losses were investigated by Curtis (1999). A radiating antenna probe was used to transmit microwave power into the waveguide from the directional coupler in the LANL apparatus. It can be seen in figure 2.1 as the component labeled D. As discussed previously, the axial position of the probe relative to the shorting wall at the end of the waveguide determines the degree of coupling between the probe and the waveguide. If the probe is located at a distance from the end of the waveguide equal to  $1/4$  of the guide wavelength for the given input frequency, the energy transfer efficiency is maximized and the resulting losses are minimal. However, since the component was designed for use over a wide range of frequencies, with both 2.93 GHz and 2.45 GHz being on the low end of the range (Vogt, 1999), the probe positioning was not at the ideal location for either frequency. Consequently, negative wave interference results in cancellation and losses in the energy transmission from the probe to the waveguide. Therefore, the losses due to the coupling antenna used at LANL are not negligible. In the early experimental work by Curtis (1999), the radiating antenna probe was investigated as a means for coupling a magnetron microwave generator to the waveguide system at Virginia Tech. This system, as well as later revisions in the Virginia Tech system, consisted mainly of components on loan from LANL. Most of the components were used in the original LANL experiments. One of the operations performed by Curtis was a characterization of the radiating antenna section. The insertion loss due to this component was found to be approximately 15% of the forward power level at a nominal frequency of 2.45 GHz (Curtis, 1999).

Another power loss in the LANL and Virginia Tech systems is attributed to the resonant cavity. Because it is a resonant structure, the cavity can be tuned such that the field intensity inside is much higher than the field in the waveguide sections connecting the cavity to the microwave source. In any metallic enclosure, the interaction between the electromagnetic fields and the metal enclosure walls results in electric currents flowing in the metal surface. Because the metal is not a perfect electrical conductor, although this is assumed in the boundary conditions of the electromagnetic field model,

the waveguide and cavity walls have finite electrical resistance. Therefore, the resistance to the current flowing in the metal walls results in Joule heating losses such that

$$P_{loss} \text{ (Watts)} = I^2 R, \quad (4.1)$$

where  $P_{loss}$  is the loss power,  $I^2$  is the square of the current flowing in the conductor, and  $R$  is the electrical resistance of the metal. These losses are negligible in the uniform waveguide section connected to the resonant cavity, as seen in table 2.2; the maximum attenuation in a three-foot section of WR-284 waveguide is 0.01102 dB. However, because the intensity of the fields in the resonant cavity is much greater than in the waveguide, the currents flowing in the metal surfaces of the enclosure are also greater. This implies that the losses due to Joule heating are not negligible in the resonant cavity. Radiant heat transfer from a hot sample in the cavity tends to heat the cavity walls, but this effect is countered by a water cooling jacket which maintains the walls at ambient temperature. Therefore, the electrical resistance of the cavity structures can be assumed to remain constant. By Eq. (4.1), the losses in the cavity due to Joule heating are proportional to the current in the walls, which is in turn proportional to the field strength in the cavity. Curtis (1999) determined that the losses in the cavity were dependent on the field strength in the cavity regardless of the presence of a dielectric sample in the cavity. For a specified forward power level, Curtis was able to measure the field strength in the empty cavity while also recording the incident and reflected power at the coupling iris. The control of the field strength was effected by manually detuning the resonant cavity through adjustment of the shorting plane at the end of the cavity. Curtis stated that the difference between the incident and reflected power readings was due to the losses in the empty cavity, and that similar losses would result in a loaded cavity at the same field strength and incident power. Thus, for a known incident power and cavity field strength, the losses caused by the cavity can be accurately estimated. A typical cavity characterization curve is shown in figure 4.1.

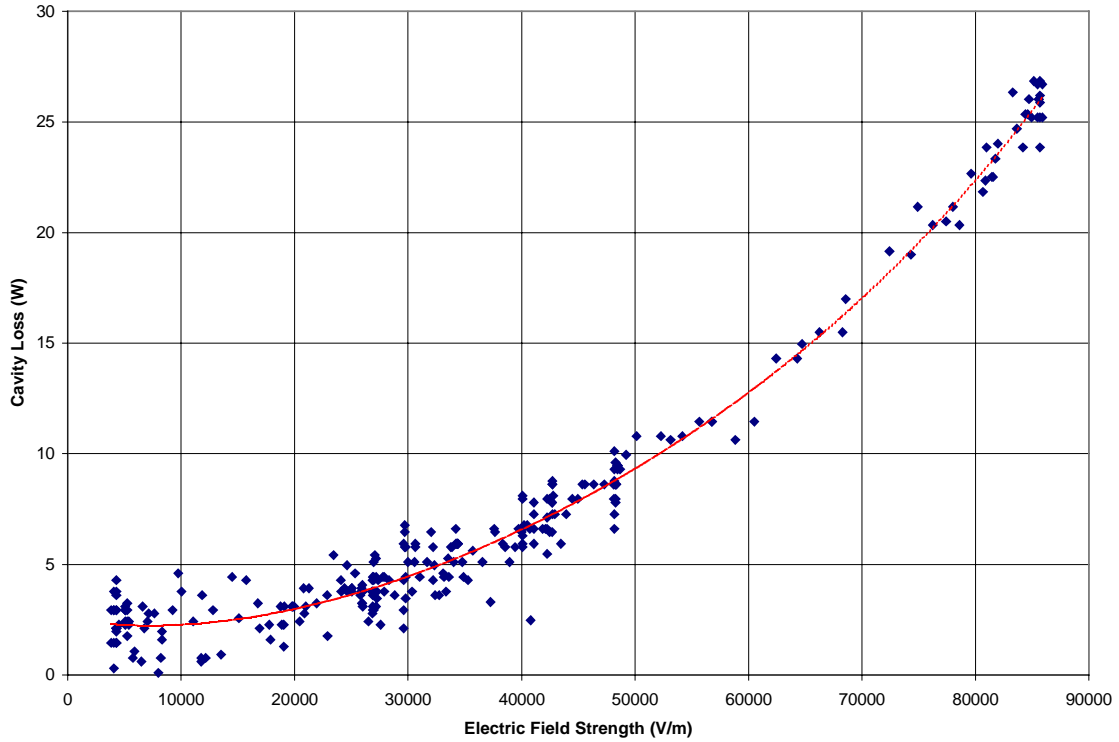


**Figure 4.1:** A cavity characterization curve for 190 W forward power

The cavity losses were found greatest at the beginning of a heating experiment when the field strengths needed to achieve a desired heating rate are highest and the dielectric loss of the material is at a minimum. As the material temperature and dielectric loss increases, the field strength required to maintain a desired heating rate and the resulting cavity losses decrease. However, there is a complication in applying these findings to the experimental data from LANL. The sensor used by Curtis (1999) to measure the electric field strength in the resonant cavity provided information on the power flux into the sensor through a small probe in the cavity. This power measurement, in W, had to be processed using known information about the attenuation and calibration of the specific probe and sensor used. Only after this information had been processed by the data acquisition computer could the field strength in the cavity be determined. The actual cavity field strength, in Volts/meter, resulted in a power flux to the meter, which was the measured quantity. The field strength cannot be measured directly and can only be determined if all of the required information is available. The data collected at the LANL experiments includes measurements of the power flux, in W, to the cavity power

sensor. However, essential information such as the attenuation and calibration of the power sensor, was not recorded and cannot be determined at this time. This means that, although the power sensor readings were recorded, the electric field strength in the cavity during the LANL experiments cannot be determined. Consequently, the power losses due to the cavity in the LANL experiments must be inferred from available data taken at Virginia Tech at a different source frequency.

The final source of significant power loss in the LANL experiments is the variable coupler, presumably used for its desirable attributes as described in Section 2.2. While its components are relatively basic in construction, this component is the most difficult to characterize. The position of the Teflon tuning block within the component has a significant effect on the amount of loss it induces in the system. Unfortunately, the position of the tuning block during the LANL experiments was variable and was not recorded. These complications are in addition to the fact that its behavior is likely to vary with the source frequency due to resonance considerations. The loss induced by the variable coupler was characterized experimentally using the available equipment at Virginia Tech. The configuration of the apparatus used to characterize the loss was identical to the one utilized by Curtis (1999) except that the variable coupler was inserted between the directional coupler and the metal coupling iris on the cavity. To minimize the inclusion of cavity effects in the characterization of the variable coupler, the shorting plane was moved as far into the cavity as possible to completely detune the resonant cavity. Therefore, only a negligible amount of power was transmitted into the cavity structure. This method of characterization includes some Joule heating due to energy reflection from the front surface of the coupling iris. However, the relatively low field strengths in the waveguide, compared to the cavity, imply that this effect is not significant. Also, the specific geometry and positioning of the aluminum tapers in the variable coupler (see figure 2.2) effectively block 30.8% of the iris surface from incident microwave energy, reducing the area in which Joule heating occurs on the front side of the iris. This is only worthy of note because the cavity characterization scheme used by Curtis (1999) also includes this Joule heating loss on the front side of the iris. Since the cavity characterization methods cannot be directly applied to the LANL data (the cavity field strengths are not known), this small effect is negligible. Experiments were

performed during which the incident and reflected power were measured before the variable coupler section at several forward powers. During each experiment, the forward power was left constant (with a minor degree of drift) and the tuning block was moved towards the iris from its outermost position. While the block was moved, the reflected power was recorded. The change in the reflected power indicates that the losses induced by the variable coupler are dependent on the tuning block position. Figure 4.2 shows the results of the variable coupler characterization.

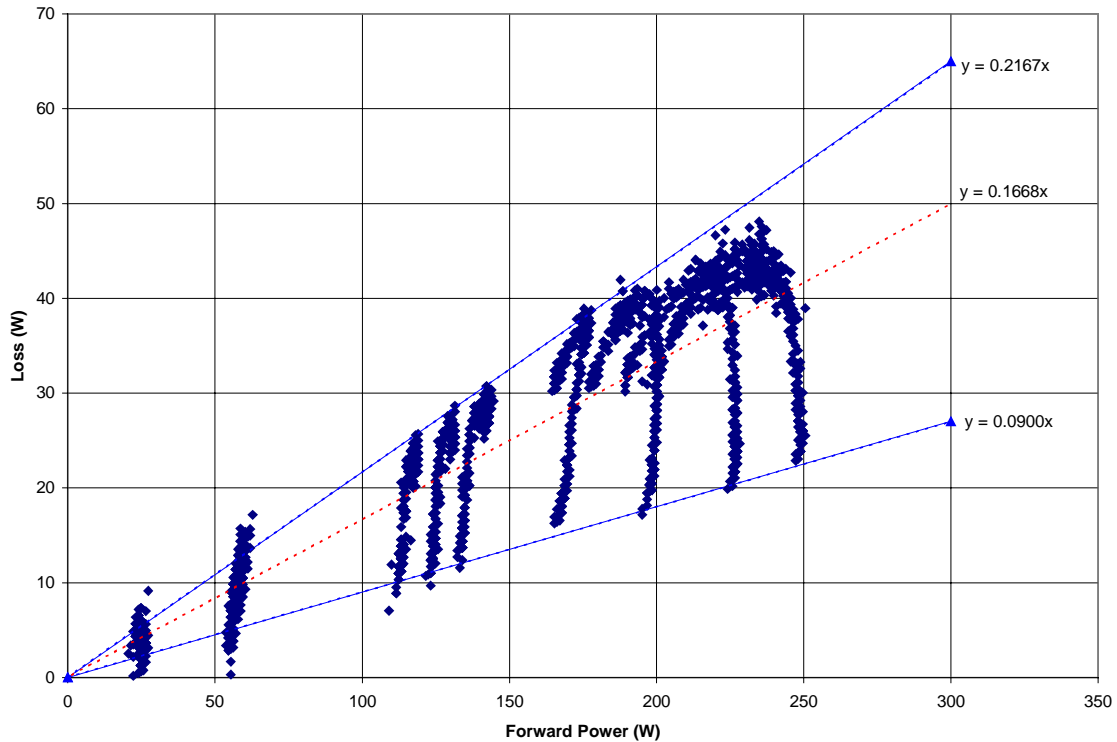


**Figure 4.2:** Loss versus tuning block position and forward power in the variable coupler

The dashed line is a linear least-squares fit to the data points, indicating the average loss at a given forward power level. The solid lines represent upper and lower bounds to the loss at a given forward power. The data shown in the figure indicates that the loss due to the variable coupler ranges from 9% to 21.67% of the forward power, with a mean value of 16.68%. Since the exact position of the tuning block was not recorded during the LANL experiments, the variable coupler losses can only be bound by the upper and lower

values in the figure, assuming that the variation due to the difference in source frequency is not significant.

In order to provide an accurate estimation of the power absorbed by the process material in the LANL experiments, the effects of the three major sources of power losses in the system must be combined in an appropriate fashion. Only then can the material power absorption be derived by subtracting the total losses from the recorded load power. Since the radiating antenna was characterized as having a 15% insertion loss, the actual power delivered to the waveguide must be considered as being 15% less than the forward power recorded at the directional coupler. Likewise, the reflected power returning to the radiating antenna must be considered as being 15% greater than the recorded value. Due to the losses in the variable coupler, the power delivered to the cavity must be less than the power delivered to the waveguide. If the amount of attenuation is consistent with the average results from the coupler characterization, the power delivered to the cavity can be assumed to be nearly 17% less than the power delivered to the waveguide. Combining this effect with the insertion loss of the radiating antenna, the power delivered to the cavity is assumed to be 71% of the recorded forward power at the directional coupler. These losses are somewhat straightforward in their application compared to the more formidable task of estimating the LANL cavity losses. The steady-state temperatures recorded in experiment vt305a at LANL, the stationary 4.67 mm mullite rod case, varied from approximately 700 °C to 1300 °C. Since the actual cavity field intensity to produce such temperatures cannot be determined from the recorded data, the field intensities must be estimated via alternate means. According to previous experimental work (Curtis, 1999, figure 4.11b), steady temperatures approaching 700 °C can be achieved with a field strength of 22.5 kV/m at 2.45 GHz. The simulation results from the current work indicate that similar temperatures are achieved with a higher field strength (30.5 kV/m at 2.45 GHz and 27.9 kV/m at 2.93 GHz). The difference in the required field strengths at different source frequencies indicates that a given material temperature can be achieved with lower cavity field strength by using higher frequencies. Based on the temperature dependence of the dielectric loss of mullite, and trends indicated by the current numerical simulation, it can be shown that temperatures from 700 °C to 1300 °C are obtainable with decreasing electric field intensities in the cavity (i.e.  $\bar{E}_f(700^\circ) < \bar{E}_f(1300^\circ)$ ). The

forward power recorded at LANL for this temperature range varied from 56 W to 204 W with an average of 130 W. Over the range of field strengths from 22.5 kV/m to 27.9 kV/m, the experimental cavity characterization curve at 130 W forward power and 2.45 GHz indicates that a cavity loss of approximately 4 W is an appropriate estimate. This value is 3% of the nominal forward power in the experimental cavity characterization at 130 W forward power. The value of the cavity loss at LANL varied with field strength and resulting material temperature, and the experimental results at 2.45 GHz are not exactly representative of an experiment at 2.93 GHz. However, approximating the cavity losses as 3% of the incident power at the cavity in the LANL experiments is justifiable. It is clear that the cavity losses are small relative to the coupler and antenna losses. Consequently, small variations in the actual cavity loss do not dominate the overall loss approximation. Subtracting 3% from the power incident on the cavity (71% of the forward power recorded at the directional coupler) results in 69% of the measured forward power actually being left to heat the sample. From this amount, 115% of the recorded reflected power at the directional coupler must be subtracted to account for the reflected power not absorbed by the process material. In summary, the power absorbed by the rod in LANL experiment vt305a can best be approximated by

$$P_{rod} (\text{Watts}) = (0.6864 \times P_{forward}) - (1.15 \times P_{reflected}), \quad (4.2)$$

where  $P_{rod}$  is the estimated power absorbed by the rod,  $P_{forward}$  is the measured forward power, and  $P_{reflected}$  is the measured reflected power.

## 4.1.2 VT305A Simulation Results

When the formulation shown in Eq. (4.2) is applied to the recorded values of forward and reflected power from the LANL experiment (vt305a), the resulting rod power can be used as the specified absorbed power input to the numerical simulation. The absorbed power levels are read into the simulation at one-second intervals of simulated time. This interval corresponds to the frequency at which data was recorded in the LANL experiment. Figure 4.3 shows the load (forward - reflected) power from the LANL experiment and the computed estimation of the power absorbed by the rod in the

cavity. The results reported by Goodson (1997) specified that the load power represented the power absorbed by the rod in the cavity. In contrast, the current work uses a lower estimate based on the probable losses in the experimental system to specify the power absorbed by the process material.

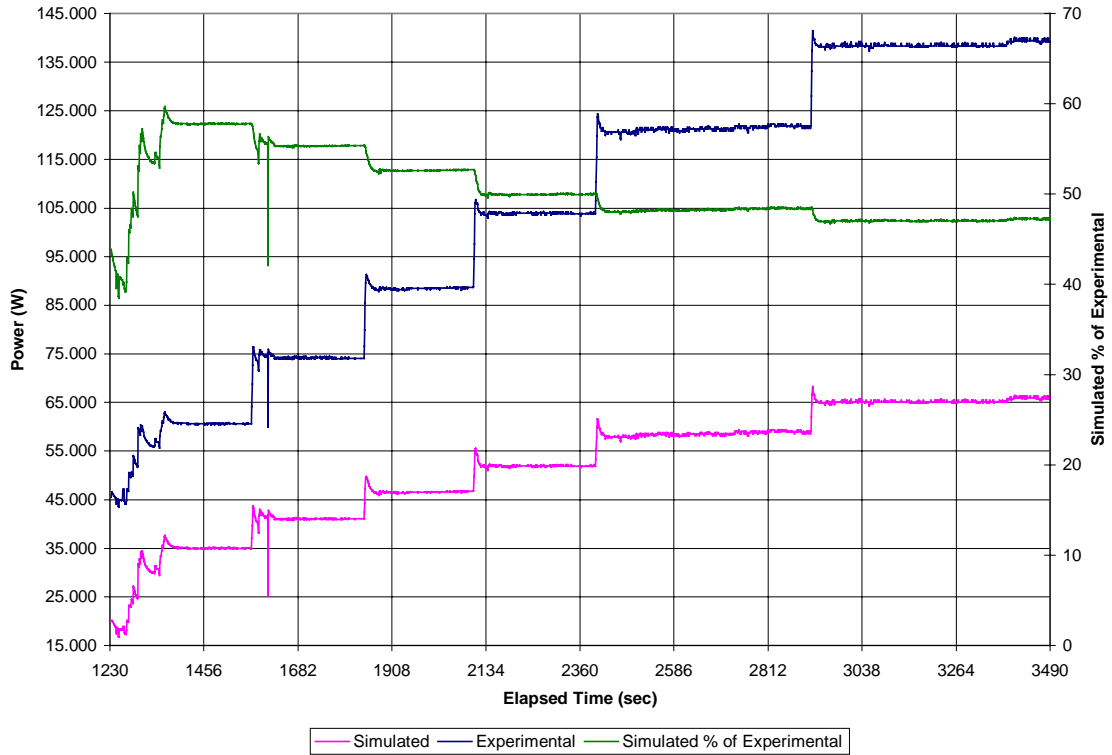


**Figure 4.3:** Experimental load power versus simulation rod power for LANL vt305a

Figure 4.4 shows a comparison between the experimental temperature measurements (corrected based on the single and dual wavelength pyrometer readings) and the simulation temperature predictions based on the estimated rod power absorption. The figure does not include the entire simulation because of the minimum temperature capacity of the LANL optical pyrometer. The device reported a minimum temperature of 550 °C, so the figure shows the results beginning at the first temperature excursion above 550 °C. The figure displays the results up until the power to the cavity was cut off in the LANL experiments. The average temperature discrepancy between the experimental and simulation results is 1.79% (absolute) for the range shown in the figure.

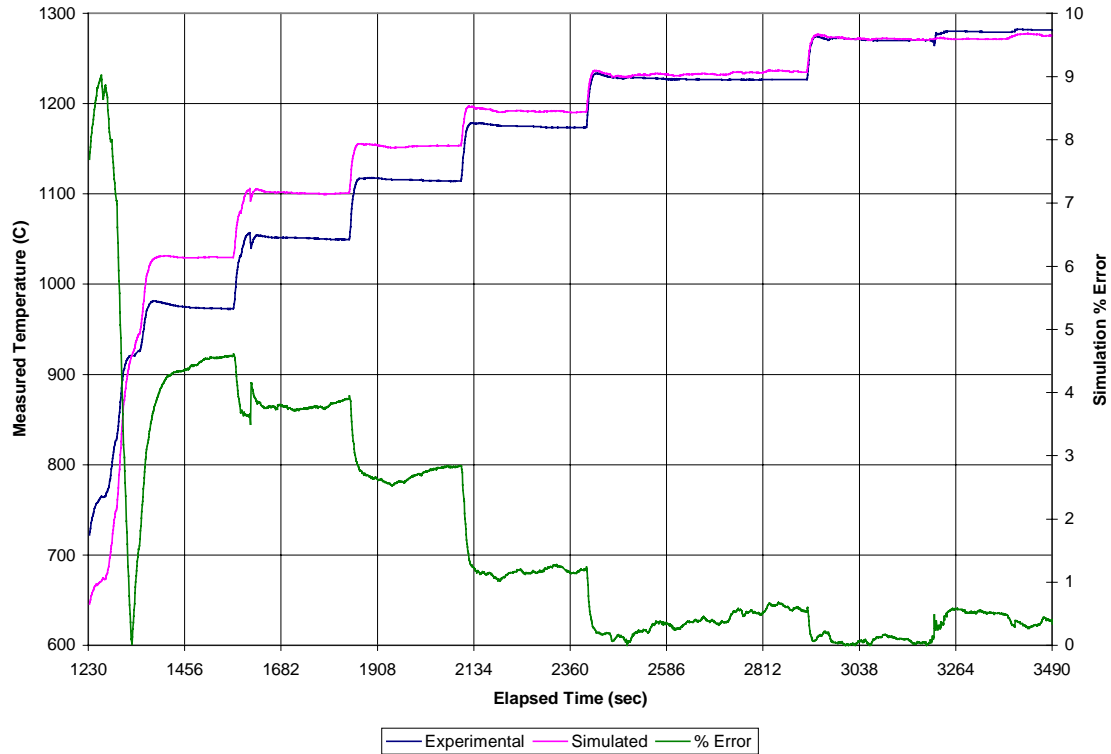


**Figure 4.4:** Experimental versus simulated temperatures and % error for LANL vt305a

### 4.1.3 Additional Simulations Based On LANL Parameters

In order to explore the capabilities of the numerical simulation more completely, it was used to predict the temperature and electric field distribution in a 4.5 mm mullite rod over a specified range of absorbed power levels. However, similar data was not recorded at LANL. The source frequency was selected to match the output from the TWT source used in the LANL experiments. Other aspects of the simulation input parameters used to produce the results in this section are given in Section 3.4. Figure 4.5 shows the steady-state surface temperatures at the midpoint of the rod in the cavity as predicted by the simulation at various levels of constant rod power absorption.

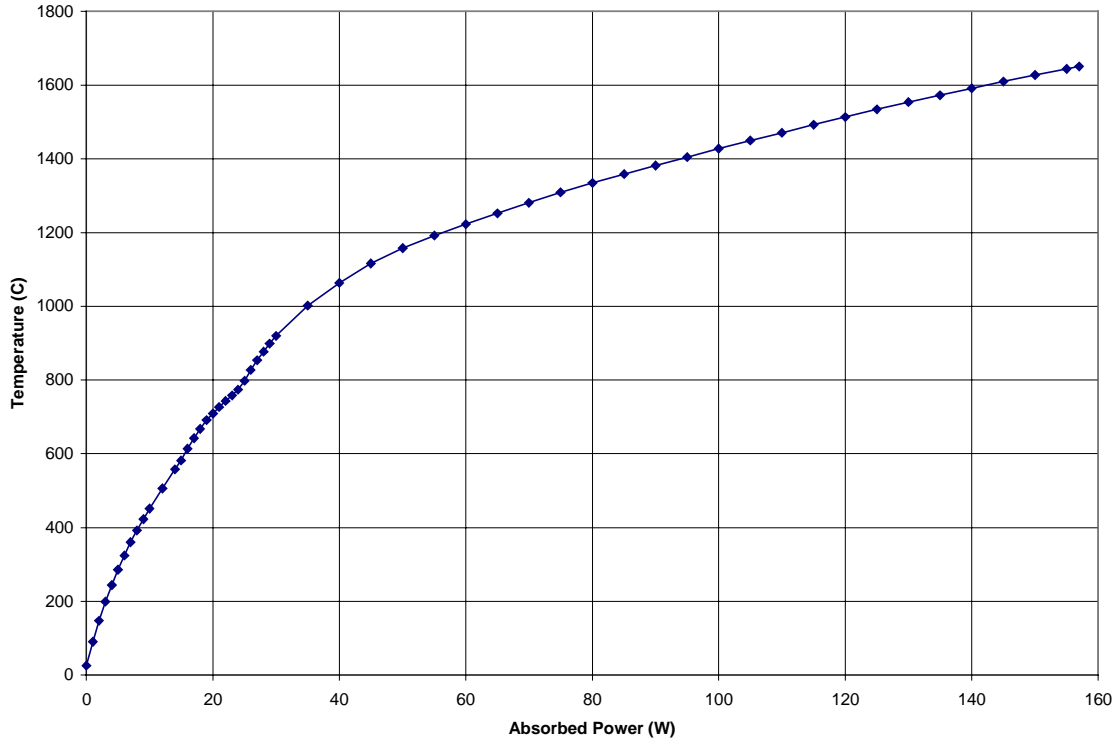


**Figure 4.5:** Midpoint steady-state surface temperatures versus absorbed power as predicted for a 4.5 mm mullite rod

The resulting power/temperature curve is quite smooth except for two small "dents" occurring at 14 W and 24 W. Referring to figure 3.6, the temperatures produced between 14 W and 24 W of absorbed power correspond to the "hump" in the otherwise smooth dielectric loss curve. The irregularity in the loss curve is due to the data points at 582 °C, 684 °C, and 784 °C. These points are actual property measurements taken at the Oak Ridge National Laboratory (Jackson, 1997) from the samples used at LANL and later at Virginia Tech. While the loss increases over this temperature range, the gradient in the loss curve is not smooth. The effect of this irregular behavior in the dielectric loss curve can be seen more clearly when the steady-state surface temperature is plotted against the steady-state average electric field strength along the rod. Such a plot is shown for a 4.5 mm mullite rod at 2.93 GHz in figure 4.6.

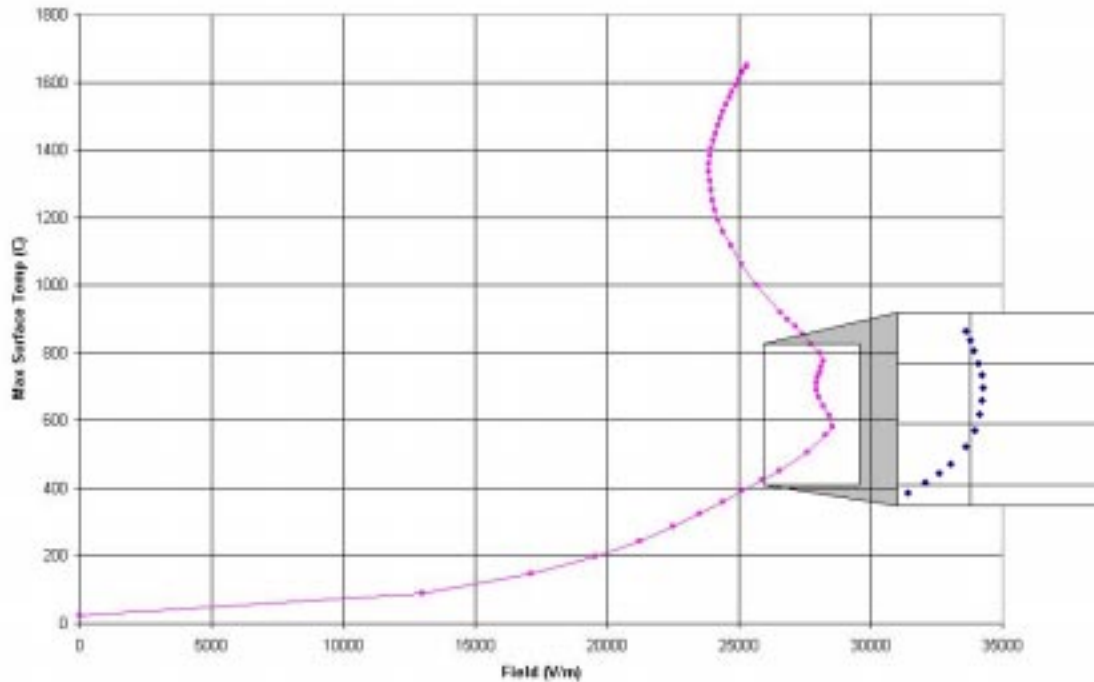


**Figure 4.6:** Midpoint steady-state surface temperatures versus average electric field strength as predicted for a 4.5 mm mullite rod

The field/temperature curve is a smooth S-shaped curve with the exception being the "dented" region corresponding to temperatures between 582 °C and 773 °C. Again, this disturbed region corresponds exactly with the "irregular" region in the dielectric loss curve. The exploded section in the figure represents the field/temperature curve that results when the dielectric loss curve (see figure 3.6) is modeled with a smooth exponential curve fit instead of a piecewise linear interpolation to the actual data points. This indicates that the "dents" in both the temperature/power curve and the field/temperature curve are simply artifacts of the dielectric data interpolation scheme employed in the numerical simulation, not true characteristics of the applicator/material combination. To emphasize this fact, figure 4.7 shows the field/temperature curve for an alumina sphere (NMAB, 1994). While this figure was developed from numerical simulation of a material other than mullite, it exhibits the characteristics expected for the mullite rod.

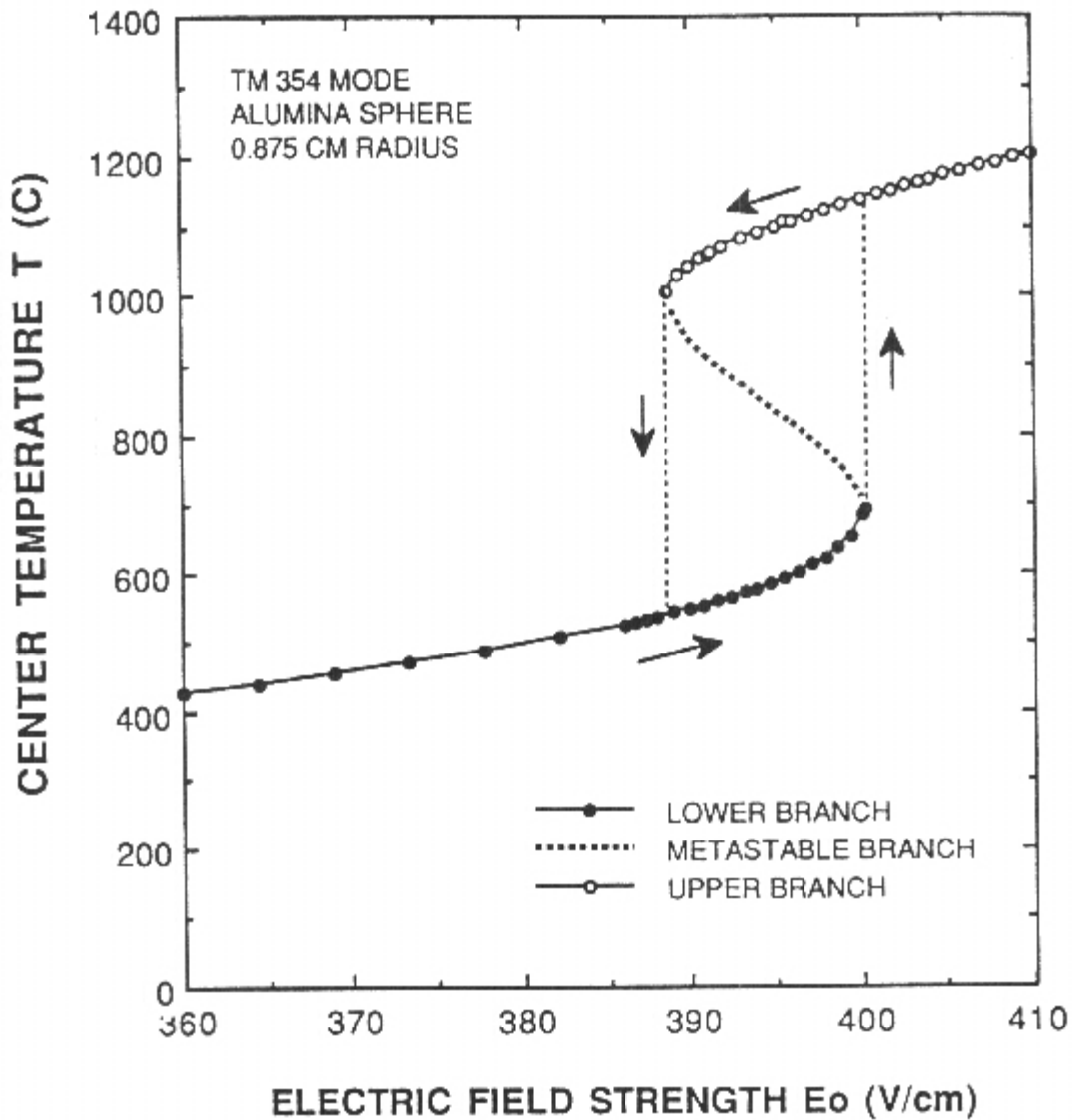


**Figure 4.7:** Predicted power-temperature response curve for an alumina sphere (NMAB, p. 37, 1994)

The data in figures 4.5 and 4.6 do not contain points at temperatures approaching 1824 °C (the melting temperature of mullite) for two reasons. The first reason is due to the volumetric nature of the heat generation; the temperatures at the center of the rod are significantly higher than the temperatures at the surface. This is evident in figure 4.8, which shows the radial temperature distribution of a 4.5 mm mullite rod absorbing 150 W at steady-state from a 2.93 GHz source.

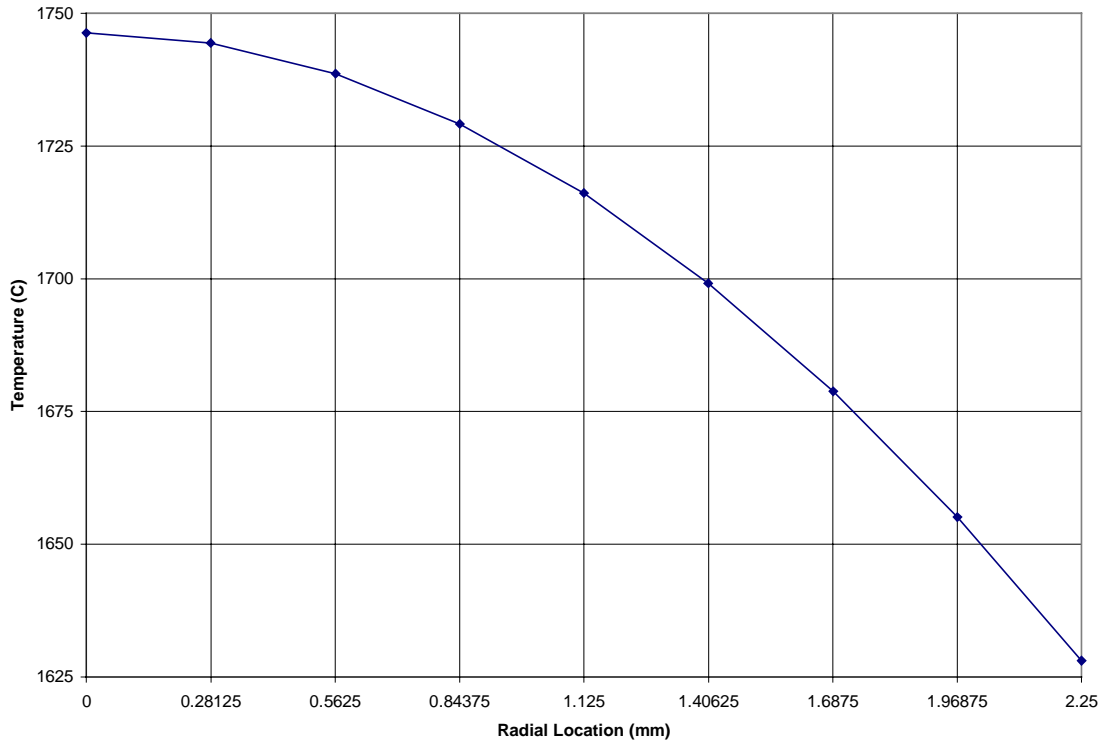


**Figure 4.8:** Radial temperature distribution at steady-state, 150 W

With a significant radial temperature gradient, the material at the center of the rod would experience melting well before the measured surface temperature exceeded the melting temperature. The second reason for figures 4.5 and 4.6 stopping short of the melting temperature is due to the transient heating response of a rod absorbing a fixed amount of power. The material initially heats at a rapid rate, with a substantial gradient in the temperature from the cavity entrance to the point midway between the cavity entrance and exit. After the initial rapid heating occurs and the surface temperature at the midpoint peaks, the material nearer to the entrance and exit slowly continue to heat while the temperatures at the midpoint actually decrease slightly. This trend continues at ever-slower rates until steady-state is reached. Figure 4.9 shows the transient temperature history of the surface element midway between the cavity entrance and exit for a 4.5 mm mullite rod absorbing a steady 150 W from a 2.93 GHz source.

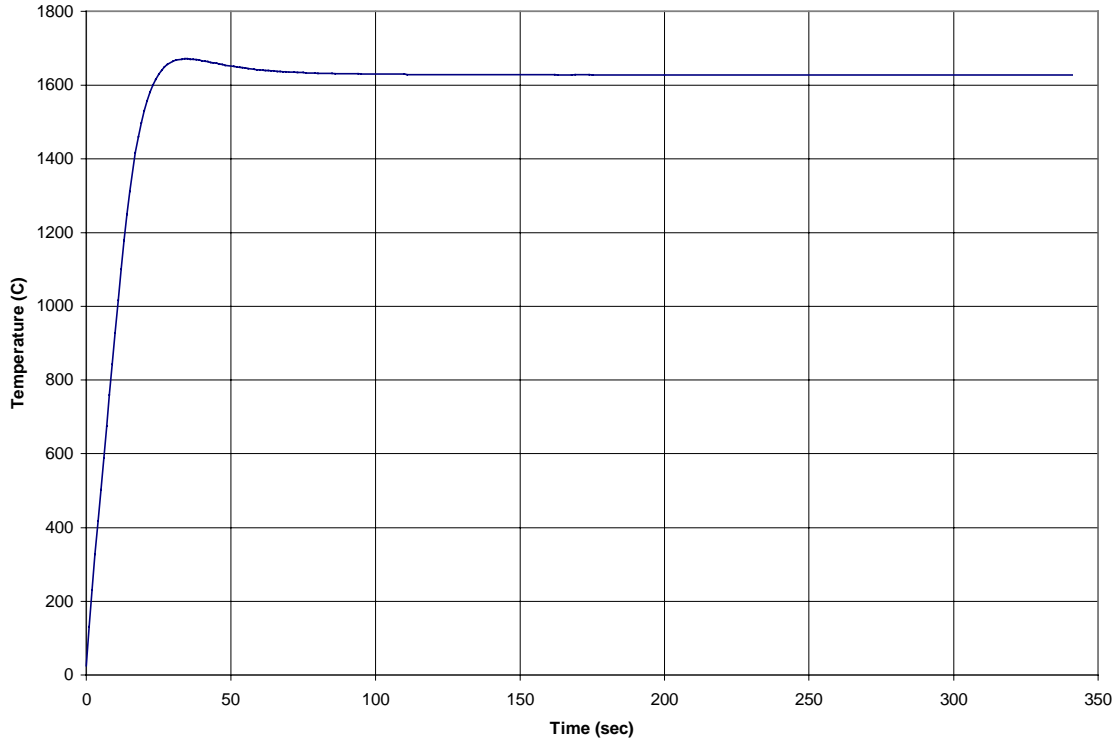


**Figure 4.9:** Midpoint transient surface temperature at 150 W absorbed power

Based on the information in figure 4.9, it would appear that steady-state is reached within the first 150 seconds. However, a comparison of the axial surface temperature distribution at various times reveals that the axial temperature distribution is still becoming slightly more uniform at longer time periods. Figure 4.10 shows the axial temperature variation with time for the same conditions as used for figure 4.9. The definition of "steady-state" is subject to the criteria used. In a true sense, steady-state is defined by a condition where no properties of the sample are changing with time. Because of the finite computer resources available, steady-state in this case is defined by a condition in which the temperature of the material elements changes less than a specified amount in a single time step. In this sense, the steady-state criterion could be selected so that the sample reaches "steady-state" after any finite time interval, be it short or long in duration.

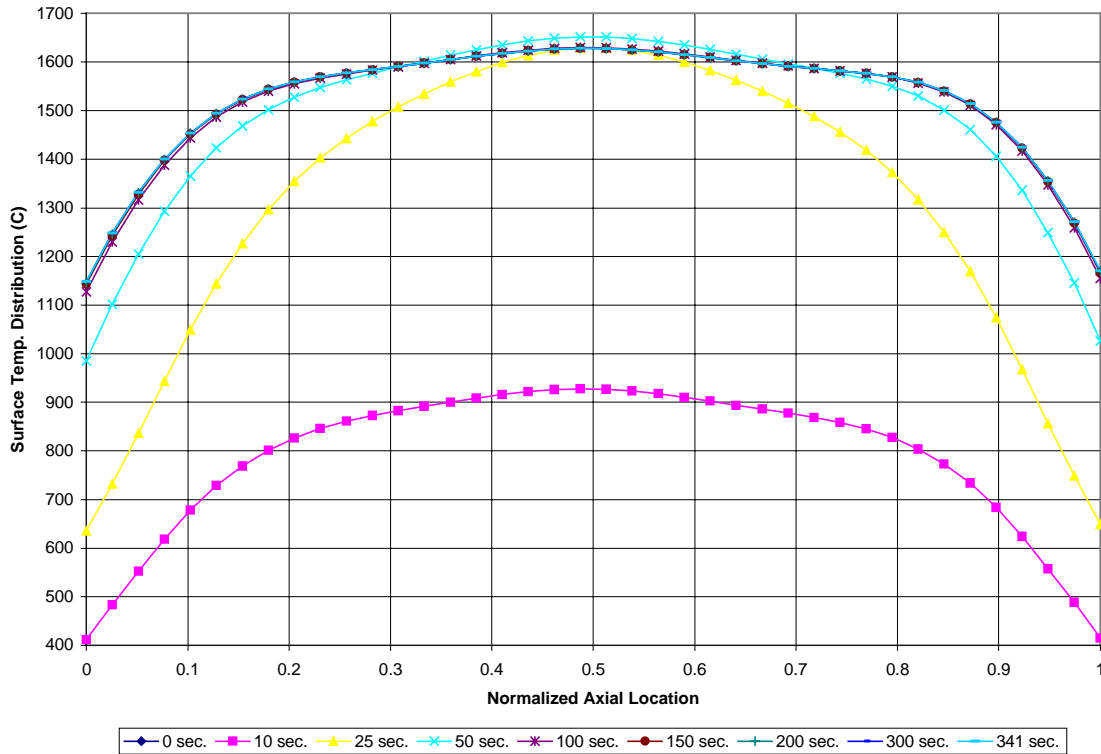


**Figure 4.10:** Transient axial temperature distribution at 150 W absorbed power

## 4.2 Comparison of Simulation to Virginia Tech

### Data

The temperatures recorded during the Virginia Tech experiments were measured by one of two optical pyrometers. The first pyrometer detects radiation in the 8-14  $\mu\text{m}$  wavelength band, and is capable of reading temperatures from 0  $^{\circ}\text{C}$  to 500  $^{\circ}\text{C}$  when set to an emissivity of 1.0. Since most real substances do not exhibit ideal blackbody emission, the readings from the pyrometer must be modified based on known emissivity data for the material being measured. This calibration procedure assumes that the substance can be realistically modeled as having gray emission characteristics. The procedure is described in detail in the work by Curtis (1999, Appendix C). With the calibration procedure completed for the mullite samples, the low temperature pyrometer is capable of displaying temperature measurements up to 700  $^{\circ}\text{C}$ . The second pyrometer, used for

high temperature measurements, detects radiation in the 2.0-2.7  $\mu\text{m}$  wavelength band and is capable of reading temperatures from 300 °C to 2200 °C. This pyrometer was calibrated using the previously mentioned technique while set to an emissivity of 0.6. The calibration of the low temperature pyrometer was checked by measuring the temperatures of ice water at 0 °C and boiling water at 100 °C, but the remainder of the sensor temperature range was not validated. Ideally, a variable blackbody emitter of known temperature should be used to validate the operation of both optical pyrometers. However, such a device was not available at the time of these experiments. For the material presented in Section 4.2, it is sufficient for the reader to be aware that two different pyrometers were used in the experiments.

In addition to the pyrometer used, a second fundamental parameter of the Virginia Tech experiments is the inclusion of the variable coupler section in the waveguide system. The variable coupler, designed and manufactured at LANL, was generally used only for experiments where higher power absorption by the process material was desired. For low power experiments, where the low temperature pyrometer was used, sufficient power could be coupled into the resonant cavity regardless of the impedance mismatch between the waveguide and resonant cavity. In order to couple higher power levels into the cavity, the variable coupler was necessary to improve the impedance match between the waveguide and cavity. This was the case for experiments where the extended range of the high temperature pyrometer was required. For the results presented in this section, the reader must be aware of a) which pyrometer was used, and b) whether or not the variable coupler was used. The implications of these parameters are discussed fully in Section 4.3.

### **4.2.1 Transient Heating Comparison**

Experimental transient heating data collection was limited to low power levels where the low temperature pyrometer was used and the variable coupler was not included. The variable coupler was not included because the power absorption control in the rod was performed by manually tuning the cavity. To maintain the rod power absorption at a steady level throughout the transient heating experiment, the position of

the short is frequently adjusted to control the field strength, and thus the power absorption by the rod. This in itself is a complicated task to perform. The variable coupler was not included in the experimental setup because it further complicates the tuning of the microwave cavity. While it does offer a degree of fine-tuning while the cavity is operating at near-steady-state conditions, it was impossible to coordinate the positions of both the short and the variable coupler to control the rod power absorption manually. The fact that the variable coupler was not used explains why the transient heating experiments were limited to low power levels using the low temperature pyrometer. This is because at higher power levels, approaching 30 W, the ability to couple such a large amount of power into a cold rod breaks down without the inclusion of the variable coupler in the waveguide system. It is only possible to couple such large amounts of power into the rod at a steady rate without the variable coupler after the rod has heated to well above room temperature. Thus, the conundrum is exposed; it is possible to couple higher power levels into the cool rod with the variable coupler, but precise control of the power with the coupler in a transient situation is too difficult to achieve.

As is shown in Section 4.2.2, the simulation steady-state temperatures and the experimental results (without the variable coupler, using the low temperature pyrometer) have a high degree of agreement in the rod power absorption range of 3-5 W. Figure 4.11 shows a comparison of the experimental transient heating temperatures and the corresponding simulation temperatures for an experiment where the rod power was within this range. Since a small degree of fluctuation in the rod absorption power is inevitable, due to sensor precision and human control of the short, the input power used in the simulation is an average of the values recorded in the experimental procedure. The nominal power input for the simulation was 5.15 W.

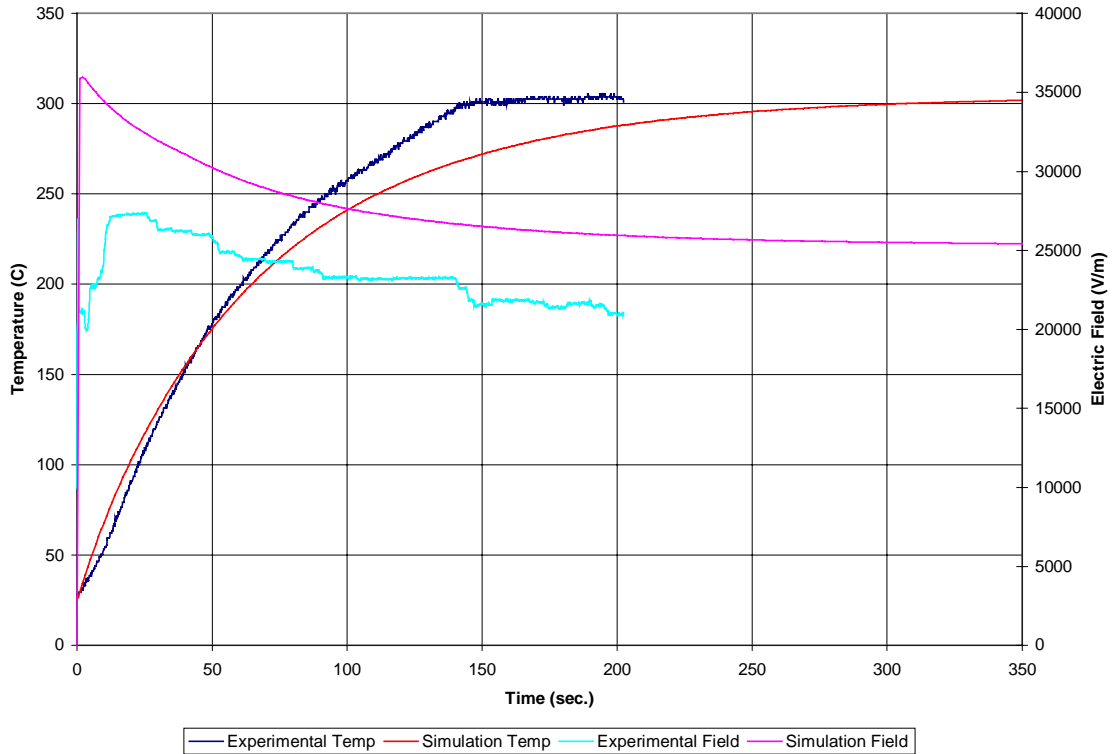


**Figure 4.11:** Transient heating at 5 W, simulated and experimental results

The steady-state temperatures reached both experimentally and with the simulation, for this power level, are nearly identical at 302 °C. The experimental measurements show that the material reached steady-state in the first 150 seconds, while the simulation required twice the amount of time to reach steady-state. The qualitative agreement in the electric fields required shows a high degree of correlation, but the magnitudes of the simulated field are greater by a nearly constant offset. Possible explanations for this are given in Section 4.3.

## 4.2.2 Steady-State Heating Comparison

The steady-state heating experiments performed fall into two categories. The first set utilized the low temperature pyrometer without the variable coupler section. Figure 4.12 compares the simulated steady-state mid-surface temperatures to the values measured experimentally for such cases.

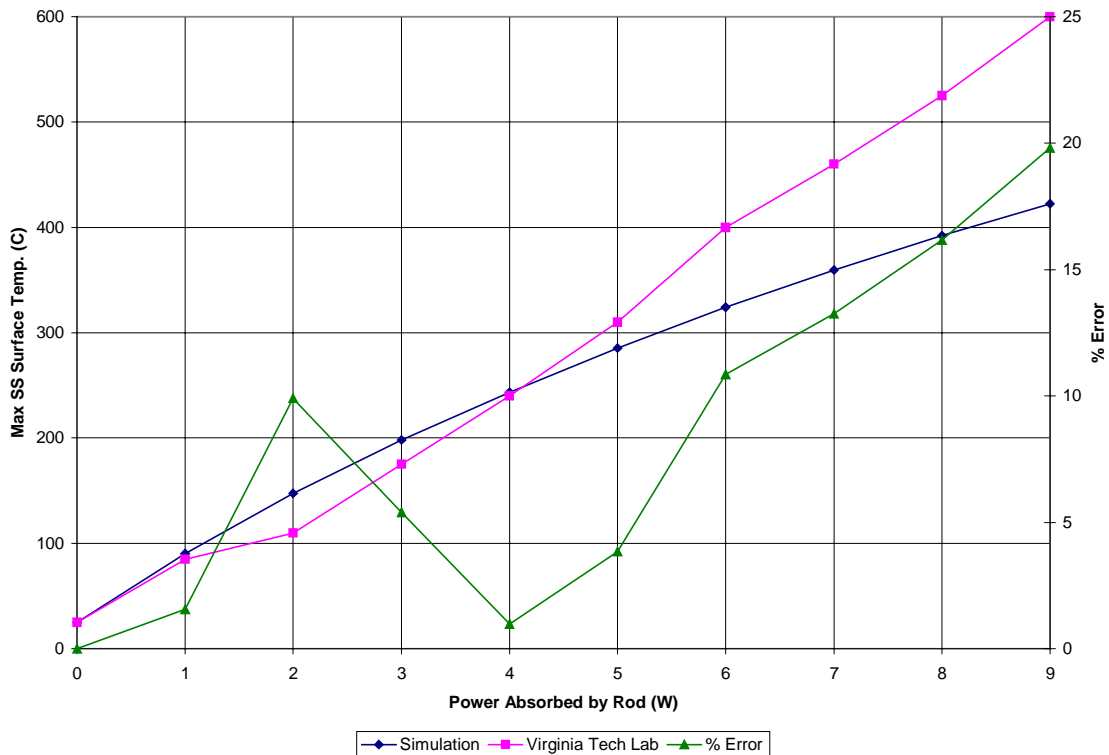


**Figure 4.12:** Comparison of simulated and measured temperatures at low levels of absorbed power (low temperature pyrometer used)

As mentioned in the previous section, the results coincided to within a few percent at 4 W of power absorption by the rod. The general trend seen from the figure is that the slope of the temperature/power curve is greater for the experimental results when compared to the curve for the simulation results. While one would hope to see an exact correlation or a uniform offset difference, the differences here appear to be linear in behavior. The exact nature and justification of these differences are given in Section 4.3.

The comparisons utilizing the low temperature pyrometer were limited to absorbed powers of 9 W or less by the maximum temperature value of the low temperature optical pyrometer. The power absorbed by the rod in the experimental procedure was determined using the data from the cavity characterization technique as described in Section 4.1.1. Figure 4.13 shows a comparison between the measured and simulated electric field intensities corresponding to the temperatures shown in the above figure. The trend exhibited in this plot is similar to the trend in the transient heating

comparison discussed in the previous section. The field strengths reported from the experiments are consistently below the value required in the simulation for a given rod power absorption.

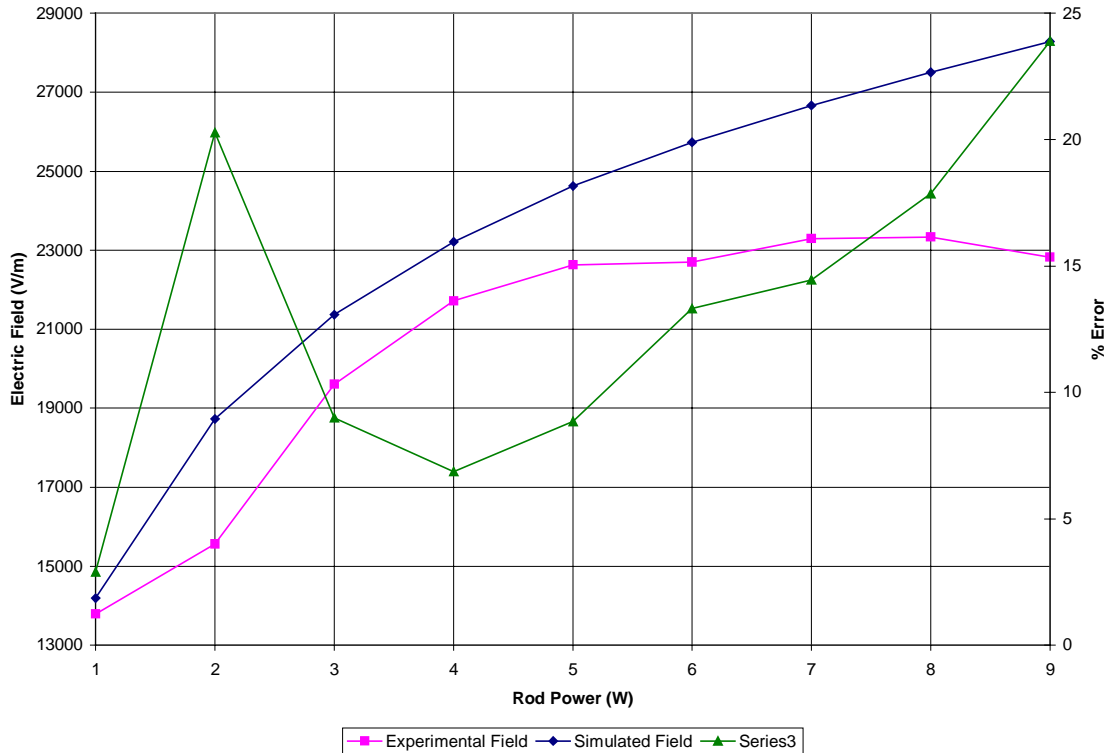


**Figure 4.13:** Comparison of simulation and experimental electric field intensities at low levels of absorbed power

The experiments performed to utilize the extended temperature range of the high temperature pyrometer required the use of the variable coupler. Without the variable coupler, the 4.5 mm mullite rod could not be heated to temperatures much greater than 1000 °C, even with large amounts of forward power. This effect was due to the impedance mismatch between the cavity and the waveguide. Even when forward powers in excess of 800 W were incident on the iris, most of the power was reflected from the iris without the variable coupler in place and did not couple to the resonant cavity or the rod. When the variable coupler was used to improve the impedance match, temperatures approaching 1300 °C were achieved using the same amount of forward power. In these experiments, the power absorbed by the rod was determined from the measurements in a

three-step process. First, the power dissipated in the variable coupler with the cavity detuned was recorded. Then, the power dissipated in the cavity was calculated from the field strength and forward power. Finally, these two losses were subtracted from the measured load power when the rod reached steady-state. This technique was used to produce the experimental results for a 4.5 mm mullite rod, shown in figure 4.14. The figure also displays the midpoint temperatures predicted by the simulation over the same absorbed power range and the calculated percent error between simulated and experimental temperatures.

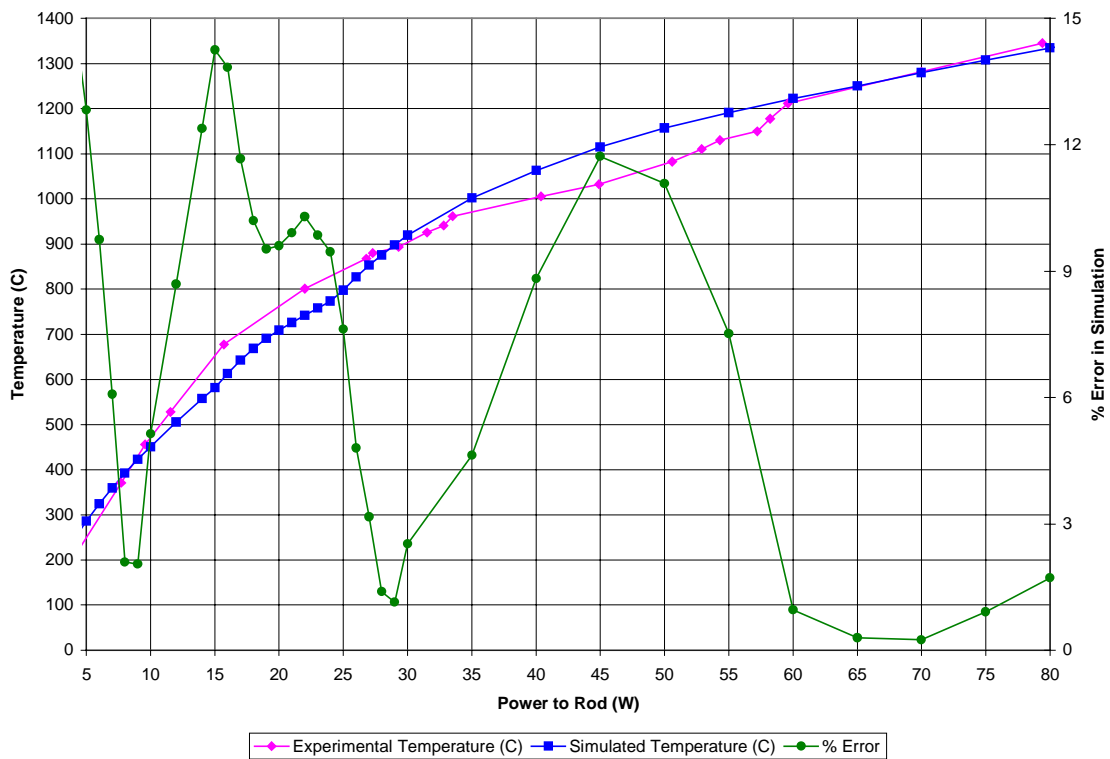


**Figure 4.14:** Comparison of simulation and experimental temperatures at high levels of absorbed power (high temperature pyrometer used)

It is clear that the temperatures measured experimentally with the high temperature pyrometer exhibit a much higher degree of correlation with the simulation results than do the temperatures measured with the low temperature pyrometer, as seen in figure 4.12. This inequity between the errors in comparing the simulation to the two different

pyrometers emphasizes the need for some means of validating the temperature readings from both pyrometers.

Figure 4.15 compares the electric field strength measured in the cavity during the high temperature experiments to the average electric field strength predicted by the simulation for similar amounts of absorbed power. The trend exhibited in this set of data corresponds to a similar trend seen in the field strength comparison for low levels of absorbed power in figure 4.13. While the values compare well qualitatively, the measured experimental field strengths are generally lower than the corresponding simulated values at a given level of absorbed power in both cases. Again, the trend shows a nearly constant offset between the two readings.

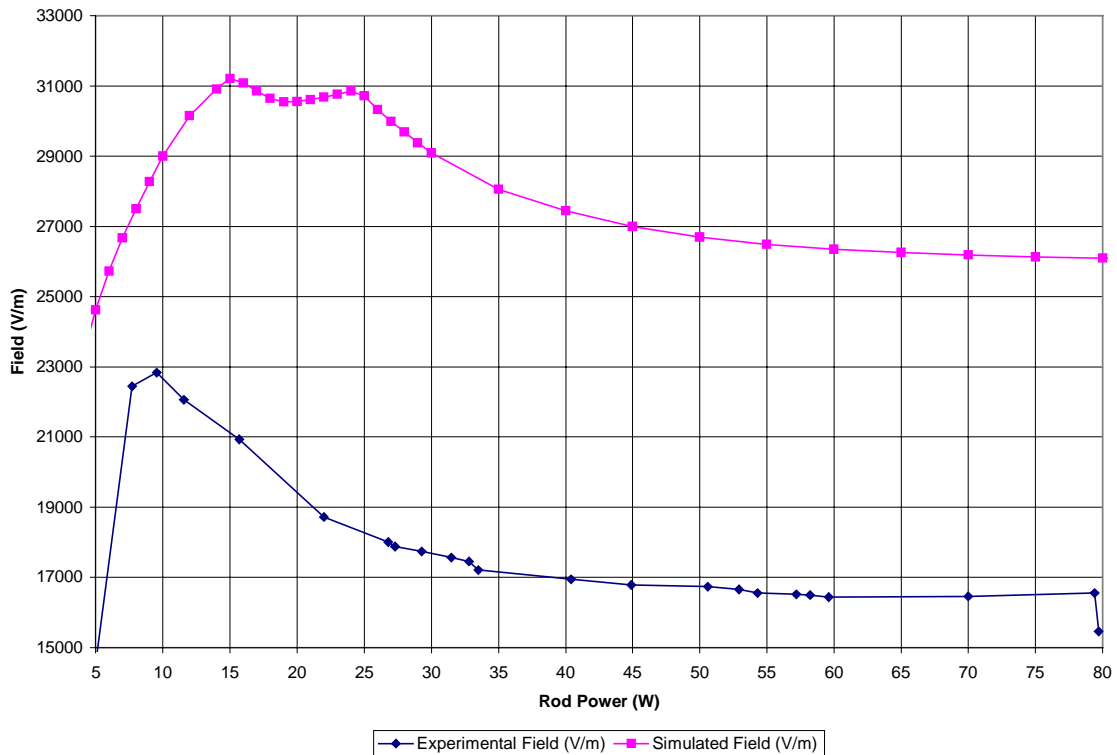


**Figure 4.15:** Comparison of simulation and experimental electric field intensities at high levels of absorbed power

It should be noted that the "dent" in the simulated field strength, as seen in the figure, is an artifact of the linear interpolation between dielectric loss data points used in the numerical simulation. This is identical to the effect discussed in Section 4.1.3 for the

simulations at 2.93 GHz; the same interpolation function is used to determine the dielectric loss in both cases. If more sample points were available for the mullite dielectric loss to provide a smoother loss/temperature curve, the calculated field/rod power curve would also be smooth and have higher magnitudes than those shown in the range between 15 and 25 W of absorbed power.

The current numerical simulation, with the enhanced electric field modeling capability, produces lower steady-state midpoint temperatures for a given absorbed power when compared to the results of a simulation using a uniform electric field distribution. The current model is capable of incorporating either field distribution assumption into the heat transfer model. Figure 4.16 compares the steady-state midpoint temperatures and average electric field intensities for simulations of 4.5 mm mullite rods using both the enhanced and uniform field models.

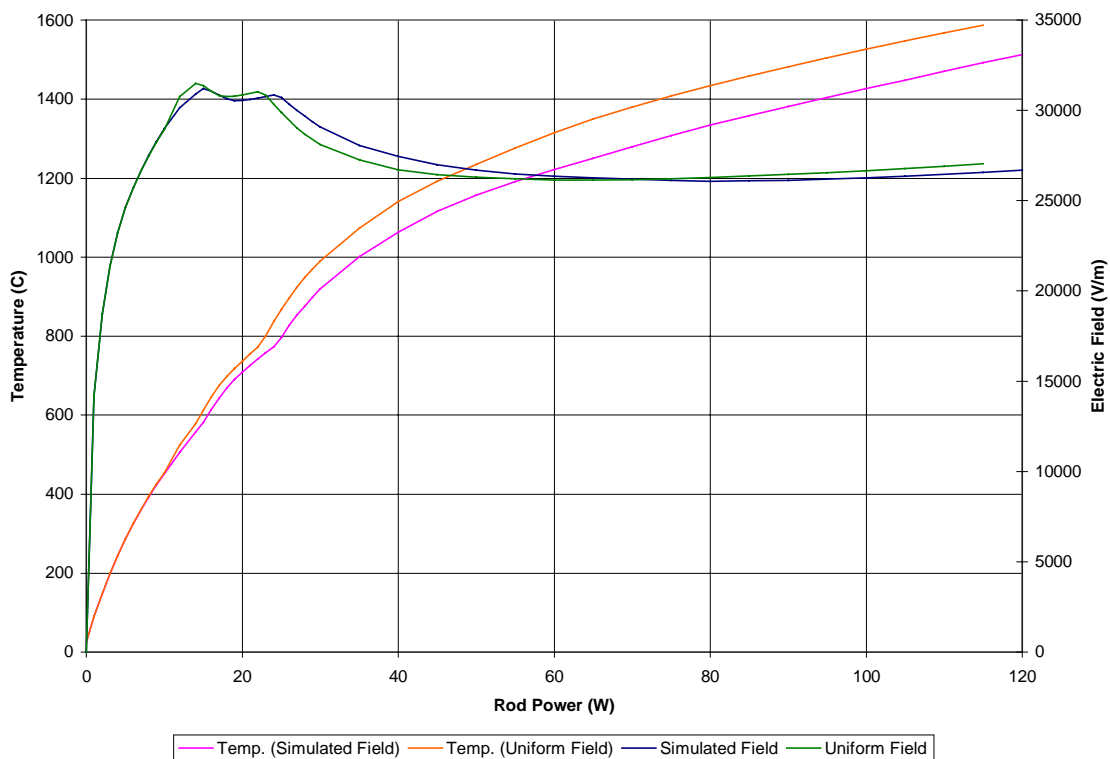


**Figure 4.16:** Comparison of steady-state midpoint temperatures and average electric field intensity between enhanced and uniform field simulations

The figure shows that there is an excellent qualitative agreement between the results produced with the two electric field models. However, the enhanced field simulation produces lower midpoint temperatures than the uniform field model for a given level of power absorption in the rod. In addition, the magnitude of the average axial field strength required by the enhanced field model and the magnitude of the uniform field strength in the uniform field model have excellent agreement both qualitatively and quantitatively.

The results shown in the figure for the uniform field model are not identical to those produced with the original version of Goodson's (1997) model. The original code assumed an emissivity of mullite based on average values in published literature for alumina. The results in the figure differ in that they were developed using emissivity data specific to mullite. The difference in steady-state temperatures resulting from the change in emissivity is slight, but the effect is that the current reported temperatures are lower than those produced with the alumina-based emissivity values. The difference in the emissivity values can be seen in figure 3.3.

The effect of including the enhanced field simulation into the heat transfer model is not limited to changes in the peak material temperature. The axial temperature distribution is effected along the entire rod length, and the temperature gradients are altered. Figure 4.17 shows the difference in the axial distributions of temperature and electric field for simulations using both field models at 115 W absorbed power in a 4.5 mm mullite rod. It can be seen that the enhanced field distribution produces a temperature distribution that has less axial variation and a higher degree of uniformity. This result is due to the non-uniform electric field intensity modeled along the axial length of the rod in the cavity. The enhanced field model predicts higher fields adjacent to the walls of the cavity and lower field intensity in the middle than does the uniform field model. The smaller axial temperature gradients resulting from this variation in the field distribution are a consequence of this difference in the field intensities. This difference primarily results from the fact that the enhanced field model is capable of accounting for the influence of the dielectric properties of the heated rod on the nearby electric field.

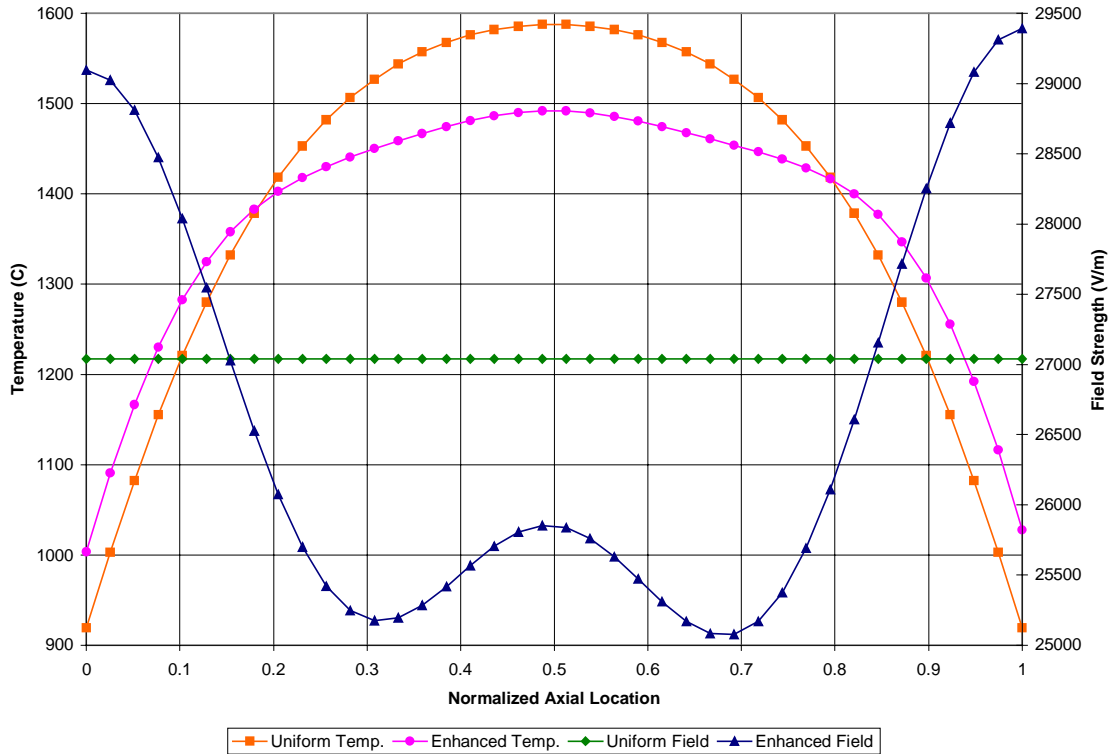


**Figure 4.17:** Axial temperature and field comparison, uniform and enhanced field models

One aspect of the results shown in figure 4.17 is particularly intriguing. Although the temperatures plotted for the uniform field case appear to be perfectly symmetric about the midpoint of the cavity, there is a minute degree of asymmetry. When the numerical values of the temperature distribution are displayed, rounded to two decimal places, a varying number of points with locations symmetric about the midpoint of the cavity differ in temperature. Usually, this is only seen in the last reported significant figure as a  $\pm 0.01$  degree variation. Because the temperatures displayed are computed in double precision (16 significant figures) and rounded to two decimal places (no more than 6 significant figures) for display purposes, a variation of  $0.001\text{ }^{\circ}\text{C}$  could be displayed as a difference of  $0.01\text{ }^{\circ}\text{C}$  (i.e.  $1495.014$  rounds to  $1495.01$  while  $1495.015$  rounds to  $1495.02$ ). However, the asymmetry in the temperatures reported for the enhanced field model results in nearly  $24\text{ }^{\circ}\text{C}$  difference between the cavity entrance and exit. The asymmetry in the uniform field temperatures is much smaller. The cause for this difference between the asymmetry in the two models is due to the effects of material

temperature on the local dielectric properties. At  $t = 0$ , the temperature and electric field distributions for both models are identical and uniform. Once the material begins to heat, the local material temperature alters the distribution of the dielectric properties in the enhanced field model. The resulting distribution of the dielectric properties along the axis of the rod affects the calculated electric field distribution because of the field interactions with the dielectric material. Any small perturbations in temperature symmetry resulting from the calculations in the heat transfer model is amplified by the resulting change in dielectric property symmetry. The thermal perturbations seen in the temperature distribution are not representative of any real physical phenomena; it is an artifact somehow generated in the numerical calculations. This has been investigated and the cause lies somewhere within the heat transfer code. This is evident because the asymmetry exists when the uniform field assumption is used in the model. It could be a result of finite computational precision, rounding error, or some possible defect in the solution algorithm. The impact of these phantom thermal perturbations is discussed in the next section.

## **4.3 Justification of Results**

### **4.3.1 LANL Comparison**

In figure 4.4, the experimental and simulated temperature readings for experiment vt305a are shown along with the relative error between simulated and experimental temperatures. It is clear that, compared to the experimental temperature readings, the simulation exhibits excellent qualitative results. It is highly probable that the measured experimental temperatures shown in the figure correspond closely to the actual material temperatures during the experiment. This assertion is based on the nature of the dual-wavelength measurements provided by the Accufiber optical fiber thermometers used at LANL. When the emissive characteristics of the target are known with a high degree certainty, single-wavelength temperature measurements are less susceptible to induced error (Utah Vacuum Symposium, 1993). However, if the emissive characteristics of the

material are unknown, dual-wavelength measurements are superior in that the computed temperatures are indicative of the true material temperature. This was the case in the experimental work performed at LANL. With the emissivity set to unity on the optical thermometer, a specific amount of error results in measuring an object with a different emissivity at a fixed temperature and wavelength. If the emissivity of the object is equal at the pyrometer wavelengths of  $0.8\ \mu\text{m}$  and  $0.95\ \mu\text{m}$ , the temperature error induced by the unknown emissivity at both wavelengths will cancel and the proper material temperature can be found. If the spectral emissivity of the material is significantly different at the two measurement wavelengths, the errors in the temperature measurements at each wavelength will not completely cancel and some degree of error is seen in the computed material temperature. The induced error will increase at higher material temperatures, with measurements at higher wavelengths, and with the gradient in spectral emissivity between measurement wavelengths. This type of error can also be induced if the spectral transmission characteristics of the optics or deposits on the lightpipe cause a differential attenuation in the measured emissive power between the two measurement wavelengths. While the specific transmission characteristics are not known for the sapphire lightpipes used at LANL, available data on the spectral emissivity of mullite (Bauer and Steinhardt, 1990) suggests little or no variation between the optical measurement wavelengths of  $0.8\ \mu\text{m}$  and  $0.95\ \mu\text{m}$ . This increases the probability that the measured temperatures are valid.

As mentioned previously, the raw experimental temperature data recorded at LANL contained intervals where the temperature was measured at a single wavelength using a unity value of material emissivity. The dual-wavelength algorithm is only stable when the material temperature is not changing rapidly, so most of the data was taken at a single wavelength. The optical thermometer system was measuring the temperature at the lower of the two possible wavelengths during this period. This is because the error induced in the measurements because of unknown emissivity is minimized by using lower wavelengths in the measurement. When material temperatures reported in single-wavelength mode had become stable, the optical thermometer recorded the temperature for a brief interval in dual-wavelength mode. During this interval, the unknown material emissivity was factored out to yield an accurate measurement of the true material

temperature. As would be expected, the dual-wavelength temperatures were higher than the corresponding single-wavelength temperatures (where the emissivity is assumed = 1.0) at a given material temperature. The percent changes in temperature at each interval where the readings switched from single- to dual-wavelength mode and back again were used to approximate the true material temperatures recorded in single-wavelength mode. This was accomplished by using a linear interpolation between dual-wavelength readings to adjust the single-wavelength temperatures by a percentage of the reading. This allowed for a seamless transition between single- and dual-wavelength temperature readings. This interpolation scheme assumes that the material emissivity variation can be approximated as linear over moderate (~100 °C) changes in temperature. Confidence in this interpolation scheme is high, based on the available emissivity data (see figure 4.17), so it is unlikely that this is a source of discrepancy between the simulated and experimental temperature readings.

A possible source of error in the simulation results is the available dielectric properties. These are critical values in the numerical modeling because they directly effect the volumetric heat generation (see Eq. (1.4)). The dielectric loss appears directly as  $\epsilon''$  in the equation, and indirectly through the  $|E|^2$  term by the dielectric influence on the local electric field intensity. The dielectric properties of the LANL samples were measured experimentally, but the reported values only extend to a maximum temperature of 1068 °C. The majority of the experimental temperature values used in the comparison between LANL and simulated scenarios are greater than the highest measured value of the dielectric properties. Therefore, the exact behavior of the dielectric properties used in the simulation for a considerable portion of the comparison is based on extrapolated information. Clearly, using dielectric properties that are confirmed experimentally for the entire temperature range investigated would be more appropriate if such data were available. If indeed the increase in mullite's dielectric loss were exponential with increasing temperature, the simulation would produce higher temperatures at elevated power levels than those reported. This would reduce the apparent accuracy of the simulation, but such speculation cannot be justified until more complete dielectric loss data is available.

As discussed in Section 4.1.1, the degree of power loss incorporated into the simulation was approximated based on the results of experiments with the waveguide components. It is probable that the approximation is not an exact representation of the true losses in the LANL experiments. The only means to develop improved estimations of the system losses in the LANL device would entail experimental characterization with the TWT source used in the vt305a experiment. With this source of uncertainty, the discrepancy between the current vt305a simulation and experimental temperatures (see figure 4.14) is acceptable. Clearly, the results are an improvement over previous simulation efforts (Goodson, 1997) shown in figure 4.18.

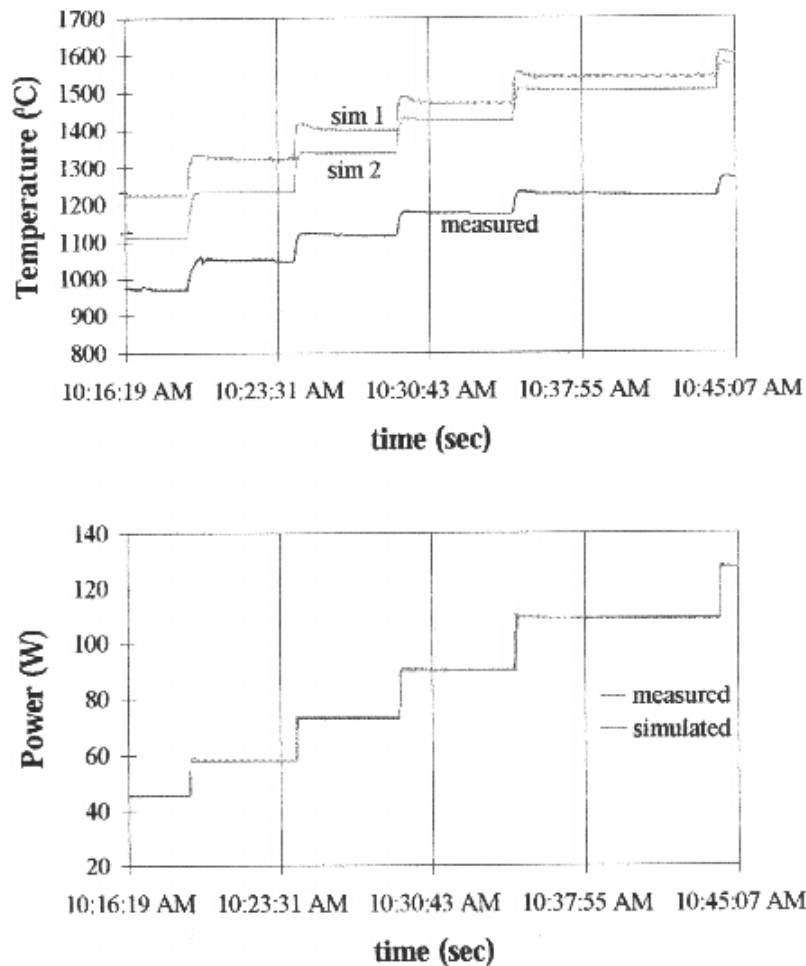


**Figure 4.18:** Power absorption and temperature predictions of Goodson's model (Goodson, 1997)

The effects of the variable coupler on the fields incident on the cavity were mentioned in Section 2.3. It was stated that the incident field assumed in the electromagnetic field model was not indicative of the actual incident field when the variable coupler is used due to the field interactions with the device. Since the error in the vt305a simulation results is minor, the impact of the simplified assumption in the field model may not be significant. Although the current evidence does not indicate that the assumption is highly detrimental to the simulation accuracy, this theory can only be validated with additional research.

It is not possible to compare the field strengths utilized by the simulation to the actual values in the vt305a experiment because such data was not explicitly recorded at LANL. Figure 4.6 shows the average electric field strength along the 4.5 mm mullite rod versus steady-state temperature for the power/temperature curve in figure 4.5. The profile of the curve in figure 4.6 is quite similar to the curve shown in figure 4.7 for an alumina sphere. This indicates that the model is generally capable of predicting the correct qualitative behavior of a thermal runaway ceramic material in response to various electric field strengths.

### **4.3.2 Virginia Tech Comparison**

In all cases where the simulation results are compared directly with the experimental data in the Virginia Tech experiments, the simulation consistently predicts higher electric field strengths being required for a given level of power absorption by the rod. This is clearly seen in figure 4.13 for the low power experiments and in figure 4.15 for the high power experiments. Figure 4.11, the transient heating comparison at 5 W of absorbed power, shows that the difference in average simulated field strength and experimentally measured values is nearly constant. This effect is also seen in figure 4.15 for the high temperature steady-state comparison, but the difference in figure 4.13 appears to diverge slightly as the power absorption increases. A simple explanation for this consistent difference between the simulation and experimental fields would be incorrect positioning of the field sensor relative to the rod. If the field sensor and rod were at distances from the iris such that the rod was positioned at a standing wave peak in

the cavity and the sensor was not, the sensor would consistently read a field strength lower than what was actually incident on the rod. Figure 4.19 shows the distribution of the standing wave pattern in the cavity at two source frequencies as predicted by analytical calculations.

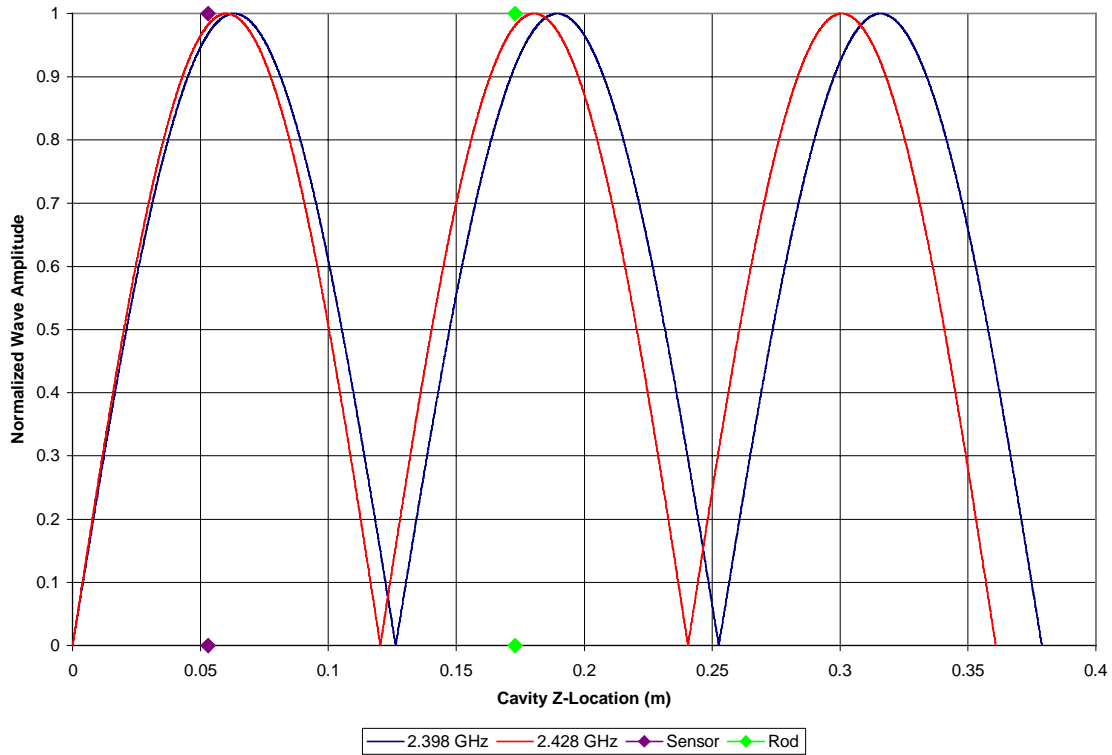


**Figure 4.19:** Standing wave patterns in a WR-284 cavity at two source frequencies

The lower frequency corresponds to the Virginia Tech magnetron output at lower power output levels, consistent with the low power experiments. Likewise, the higher frequency corresponds to the high power experiments. The difference in output frequency at various power levels is a characteristic of the source (refer to Curtis, 1999, figure 3.4). At high power levels, the standing wave patterns indicate that the sensor should read a field strength that is nearly identical to the field strength at the rod. At low power levels, there is a difference, but the effect is that the probe will read field strengths *higher* than those at the rod. If sensor/rod positioning were to explain the difference seen between the experimental and simulation results, the probe would have to read field strengths *lower* than those experienced by the rod. Therefore, the sensor/rod positioning is not an

obvious justification of the observed discrepancy. It is possible that the method of power control used in the experimental procedures could complicate the analysis of sensor/rod positioning. The analytical methods assume a perfectly tuned resonant cavity in the determination of the standing wave patterns. Power control in the experiments was achieved by manually detuning the cavity to control the field strength at the rod. Although this is said not to have a considerable effect on the standing wave pattern (Davis, 1999), the exact nature of this difference has not been quantified. Regardless, other means for justifying the electric field discrepancy must be investigated.

A likely cause for the discrepancy between the electric fields estimated by the simulation and those measured experimentally is the dielectric property data used in the simulation. If the actual dielectric loss of the material is greater than the value used in the simulation, Eq. (4.1) dictates that a higher value of  $|E|^2$  would be required for a given power absorption to compensate for the lower value of  $\epsilon''$  in the simulation. Figure 3.6 shows the dielectric loss of mullite measured by Jackson (1997) and the data measured by Xi and Tinga (1991). The data measured by Jackson was used in the numerical simulation, with linear interpolation for values between measured data points and linear extrapolation for values above the measured temperature range. The basis for using this data instead of the values measured by Xi and Tinga was the fact that Jackson's measurements were performed on a mullite sample used at LANL, so the material composition was known to match the samples used in the heating experiments. Clearly, the values measured by Jackson are uniformly greater than the dielectric loss values measured by Xi and Tinga. Although the dielectric loss data compares well in a qualitative sense, the average difference between the two is 103%. Such a difference raises suspicion as to variation of the dielectric properties among individual samples of mullite. The measurements were performed at Microwave Materials Technologies (Knoxville, TN) using modern cavity perturbation techniques (Thomas et al., 1997). The discrepancy between the simulated fields and experimental values would be justified if the model used the lower loss values reported by Xi and Tinga while the experimental samples had the higher loss values reported by Jackson. However, since this was not the case, the discrepancy could only be explained if Jackson's measurements somehow *underestimated* the dielectric loss of the sample. The variation between the dielectric loss

values reported by Jackson and Xi and Tinga suggests that this could be a possibility. In addition to dielectric loss variation among samples, the heating history of a given sample can effect the dielectric properties of a given sample. As reported in chapter 1, a given increase in material density due to sintering may cause a corresponding increase in the dielectric loss such that  $\epsilon'' \propto (\rho)^3$  (Thomas, 1999). Figure 1.12 shows that sintering mullite at high temperatures for extended periods can result in a significant increase in the density of the sample. Since the mullite rods used the LANL and Virginia Tech experiments had experienced varying degrees of sintering, this effect may have altered the dielectric properties of the sample by an amount that could justify the discrepancy between simulation and experimental field strengths. While a number of new mullite rods were obtained for use in some of the Virginia Tech experiments, the new rods were from a different batch than the original rods and the composition may not have been the same. It is also possible that the field discrepancy could be due to error in the experimental measurement techniques.

In addition to the differences in field strengths between the experimental and simulated data, the figures in Section 4.2 show discrepancies in the temperature data. One possible source for the temperature differences is the temperature dependent thermophysical properties used in both the numerical simulation and the calibration of the optical pyrometers. The emissivity data (see figure 4.17) used in the simulation was obtained from a source (Bauer and Steinhardt, 1990) for which the mullite contained 70%  $[\text{Al}_2\text{O}_3 + \text{TiO}_2]$ . This is known to be different from the actual mullite samples used in the LANL experiments. Based on the technical data provided from the supplier (Bolt Technical Ceramics, Conroe Texas), it is known that the LANL material contained 60%  $\text{Al}_2\text{O}_3$ . No information on the rest of the molar composition is available. Because the emissive heat loss is proportional to  $T^4$ , small variations in the true material emissivity have an increased effect on the material temperature as the temperature increases. Therefore, if the emissivity values used in the model differ from the actual behavior of the rod in the experiments, the resulting discrepancy in emissive heat loss will result in an error in the modeled temperatures. As reported in 3.1.1, changing the values used in the simulation to model the mullite emissivity from Goodson's (1997) values to those reported in Bauer and Steinhardt (1990) resulted in changes in the simulation results,

although they were relatively minor. Of greater concern is the effect of material emissivity on the temperature readings from the optical pyrometers used at Virginia Tech. This is because the temperature difference due to a small error in emissivity is much greater in the temperature measurements than in the simulation results. Figure 4.20 shows the error induced in an optical temperature measurement resulting from various percentages of error in the material emissivity at two pyrometer wavelengths.

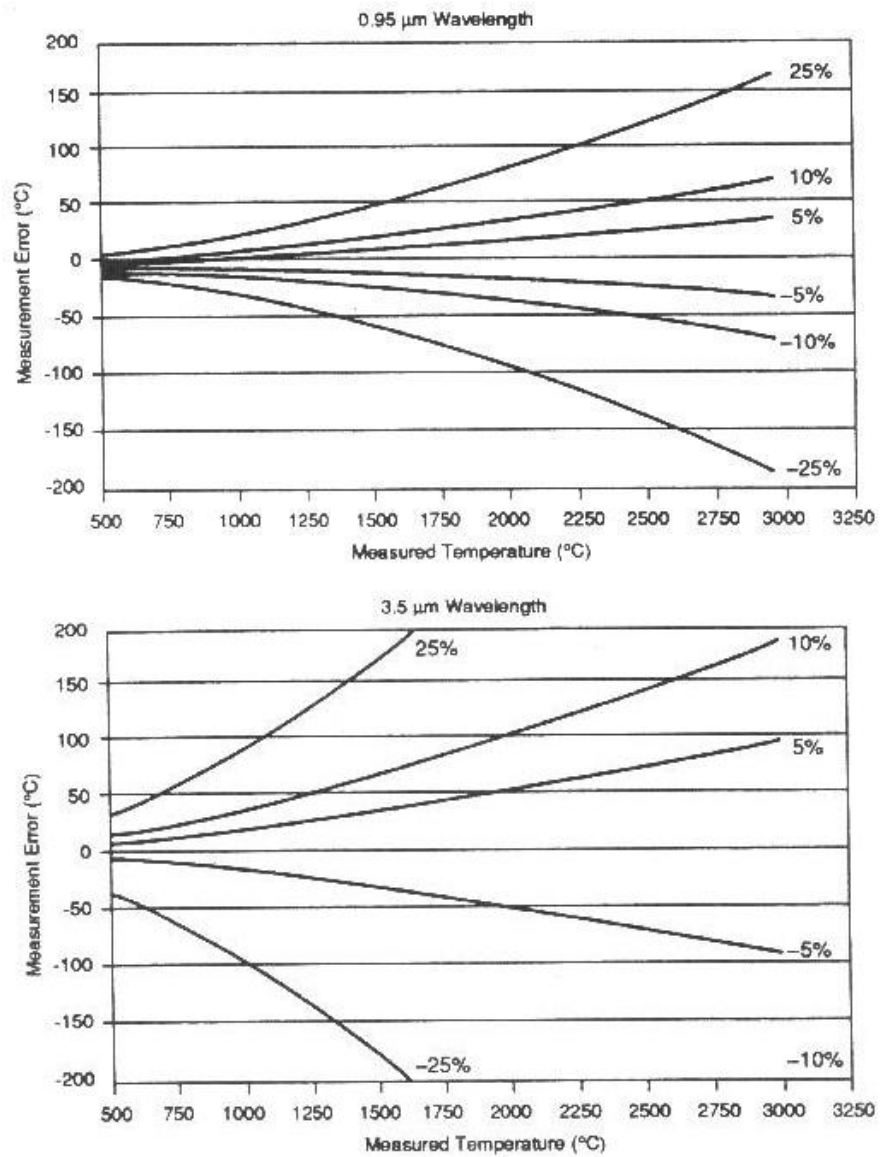


**Figure 4.20:** Temperature measurement error as a function of temperature, wavelength, and emissivity error (NMAB, 1994)

The figure clearly shows that the measurement error increases with emissivity error, material temperature, and measurement wavelength.

The emissivity data used in the pyrometer calibration (Bauer and Steinhardt, 1990) is the total emissivity of the material, meaning that it "integrates out" the material behavior over any particular wavelength band. Thus, at a given temperature, there are likely to be differences between the total emissivity over all wavelengths and the emissivity within a particular wavelength band. Figure 4.20 shows that pyrometers reading at lower wavelengths exhibit a substantially lower measurement error than those reading at higher wavelengths for a given material temperature and percent error in emissivity. This is a likely explanation for the difference in agreement between the simulation and experimental results for the low and high power comparisons. Figure 4.12 shows that, in the low power experiments, the simulation and experimental steady-state temperatures tend to diverge as the power and temperature increase. The pyrometer used for measuring these experimental temperatures operates by reading the emissive power in the wavelength interval between 8  $\mu\text{m}$  and 14  $\mu\text{m}$ . If the trend exhibited in figure 4.20 between 1  $\mu\text{m}$  and 3.5  $\mu\text{m}$  is extrapolated to this wavelength band, small differences between the emissivity of the material and the emissivity used to calibrate the pyrometer will result in large temperature errors. This effect is the likely cause for the majority of the temperature discrepancy seen in figure 4.12 between the simulation and experimental steady-state temperatures.

In the high power experiments, the pyrometer used to measure the mullite temperature operated in the 2.0  $\mu\text{m}$  to 2.7  $\mu\text{m}$  wavelength band. The lower measurement wavelength implies that the readings are far less susceptible to error due to differences between the actual emissivity and the data used in the pyrometer calibration. This tends to validate the results shown in figure 4.14, the comparison between simulation and experimental steady-state temperatures at high power levels. Over the experimental temperature range from 300  $^{\circ}\text{C}$  to 600  $^{\circ}\text{C}$ , the same divergent trend seen in the low power experiments is repeated in the high power experiments; the experimental temperatures increase at a greater rate than the simulation temperatures with increasing rod power. However, figure 4.14 shows that this trend does not continue throughout the measured

temperature range above 700 °C. That the simulation results are not uniformly too high or too low compared to the experimental data suggests that no single parameter can be explicitly shown to cause the temperature discrepancy. As is suggested for the low power experiments, emissivity calibration error in the pyrometer measurements could account for the discrepancy between the simulation and experimental temperatures. The calibration values used could be higher or lower than the actual material values in the given wavelength band at different temperatures. Such variation could easily cause the "waviness" in the measured experimental temperature curve. In an overall sense, the comparison between the simulation predictions and the high power experimental temperatures indicates an excellent correlation, with an average of less than 1.4% error over the power range shown in figure 4.14.

# Chapter 5

## Conclusions and Recommendations

### 5.1 Conclusions

Based on the work presented and discussed in the previous sections, the following conclusions can be drawn:

- 1) The incorporation of the electromagnetic field model into the heat transfer model produces significant changes in the axial temperature distribution of the heated rod. The temperature distributions resulting from the enhanced field model, compared to those from a uniform field assumption, have a greater uniformity along the sample with smaller temperature gradients. This condition is favorable in many industrial heating applications
- 2) As suggested by Goodson (1997), the power losses included in the LANL experimental data are significant, on the order of 50% of the total load power. The power loss characterization allowed the power absorption by the heated samples in the experiments to be estimated with acceptable accuracy. The loss characterization experiments were based on methods developed by Curtis (1999).
- 3) The enhanced numerical simulation was validated against the available experimental data obtained at LANL. The agreement between the LANL vt305a experimental data and the corresponding simulated temperatures were within an average of 1.79%. This is a notable improvement over the original simulation, which was recognized as having several deficiencies. The temperature error in Goodson's (1997) simulation

approached 30% in the same experimental comparison. This was due to an inability to quantify the power losses, an assumed uniform field distribution, and inaccurate emissivity data. All three of these deficiencies have been corrected in the development of the simulation presented in this work.

- 4) The simulation has been validated against experimental data from Virginia Tech. The comparisons at low power levels (9 W or less absorbed by the rod), where the temperatures were recorded by a low-temperature pyrometer (0-700 °C), are shown to have an average correlation within 7.98% of the simulation predictions.
- 5) The comparisons at high power levels (5-80 W absorbed by the rod), where the temperatures were recorded by a high-temperature pyrometer (300-2200 °C), are shown to have an average correlation within 3.77% of the simulation predictions.
- 6) The primary cause of the difference in accuracy between comparisons at low power and high power is the error in the optical pyrometers. The error is most likely due to differences between the actual material emissivity and the published values used to calibrate the pyrometers. The high-temperature pyrometer is less susceptible to error because it operates at a lower wavelength band than the low-temperature pyrometer.

## 5.2 Recommendations

It is certain that the dielectric and thermophysical properties used in the numerical simulation are incomplete and for incorrect material composition, respectively. The dielectric properties of the mullite samples used in the study have not been measured at high temperatures, so the behavior must be extrapolated from the available property data. The validity of the extrapolated data cannot be determined unless accurate property values in the high temperature range are measured for comparison. If Virginia Tech is to continue to make advances in the field of experimental microwave processing of materials, additional effort must be put forth to obtain the most comprehensive compilation of material properties possible for the materials being investigated. Since there is variation in material composition between batches and suppliers, it would be

most beneficial for Virginia Tech to develop relations with organizations willing to assist in the measurement of the various properties. Alternatively, the ability to measure the required material properties in-house would be ideal. Most specifically, properties such as dielectric constant, dielectric loss, and emissivity, all of which experience variation with material temperature must be obtained for the specific samples used. This is because dielectric loss and emissivity have a large influence on the heating rate of the sample, especially at higher temperatures. Data for all of the properties should be specific to the particular composition of the materials being used, and the values should cover as much of the temperature range under investigation as possible. It would be ideal if additional properties, such as specific heat, thermal conductivity, and density, could be measured experimentally for the specific samples under study. Alternatively, these properties should be modeled from the most complete and reliable published data. These properties, while still highly important to accurate numerical simulations, are less dependent on the material temperature and do not appear directly in the volumetric heat generation equation (see Eq. (1.4)).

The variable coupler should be investigated in the future through additional experimental characterization and specific modeling efforts. An accurate numerical model of the coupler could be used to investigate the validity of the uniform  $TE_{10}$  field that is assumed to be incident on the cavity iris in the current electromagnetic model. If the results of such a study indicate that the uniform incident field assumption is not valid when the variable coupler is included in the waveguide system, the combined heat transfer/electromagnetic simulation should be modified to include the modeling of the variable coupler. Such a model of the coupler could be developed to compute the losses induced by the component for comparison to the available experimental characterization data. Indeed, the results of the experimental loss characterizations for all of the microwave components used at Virginia Tech and LANL suggest that a rigorous effort to model the losses in the various components numerically may be worthwhile.

A troubling aspect of the heat transfer code was identified in this work and needs to be investigated. Regardless of which field model is used, the temperature predictions for a stationary rod tend to be asymmetric about the middle of the cavity. There is no obvious justification for this artifact. The effects of the temperature asymmetry are

exacerbated when the enhanced field simulation is used because the local dielectric properties of the material are temperature dependent and effect the local electric field strength. A small temperature perturbation can develop into a large temperature asymmetry as the local elevation in temperature increases the materials' affinity for power absorption (see figure 4.17). The modeling of the dielectric loss of the material has a profound effect on this problem. When the high-temperature dielectric loss of mullite (above the values measured by Jackson (1997)) is modeled by a linear extrapolation from the highest two data points, the temperature asymmetry is somewhat constrained and the difference between surface temperatures at opposite ends of the cavity do not exceed 30 °C at power levels not resulting in melting. However, if the high-temperature dielectric loss is modeled with an exponential curve fit to Jackson's (1997) data, the small temperature perturbation continues to grow and the peak temperature moves well away from the center of the cavity. Figure 5.1 shows the temperature and field distributions for a simulation at 75 W of absorbed power in a 4.5 mm mullite rod using an exponential model of the material dielectric loss.

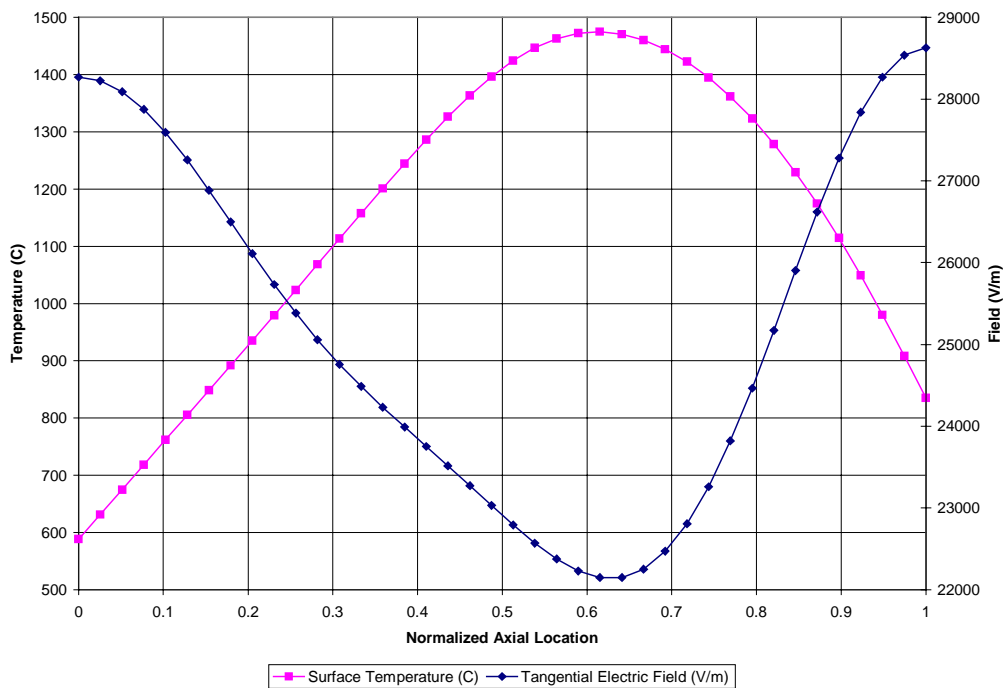


**Figure 5.1:** Temperature and field asymmetry

This phenomenon is possible if there is a valid cause for the temperature perturbation and the material indeed exhibits an exponential increase in dielectric loss with increasing temperature. However, the thermal perturbation that initiates this is an artifact of the heat transfer model. The cause for this temperature asymmetry must be investigated.

It would be beneficial if some means were developed in the future to enable temperature measurement at multiple locations on the heated sample. The current hardware only allows the temperature to be measured at the midpoint of the sample. This ability would be beneficial in heating experiments where the process material is passing through the cavity at a given velocity. Being able to measure the peak material temperature, which does not occur in the center of the cavity in such conditions, would improve the usefulness of the data obtained in the experiment. It is this limitation that allows the numerical simulation results to be compared to just one of the many heating experiments performed at LANL; vt305a is the only data set where the rod was stationary and the peak temperatures coincided with the measurement position.

One final consideration that must be investigated is the calibration of the two optical pyrometers used in the Virginia Tech experiments. While the low-temperature pyrometer was calibrated at 0 °C and 100 °C, most of the useful temperature range was not validated. Since the measurement error increases with sample temperature when the calibration is incorrect, validating the performance at higher temperatures is important. The calibration would require a device capable of reaching high temperatures at a known emissivity and temperature. This would necessitate an independently verified indication of the object temperature, such as a thermocouple. The device should be such that the temperature could be varied to validate the pyrometer readings over their entire range. Ideally, the device should be capable of reaching temperatures at 2200 °C, the extreme range of the high-temperature optical pyrometer. Such a device is not currently available at Virginia Tech. Confidence in the data measured by the optical pyrometers is dependent on such a calibration procedure being completed in the future.

There are a few aspects of the Virginia Tech experimental apparatus that could use improvement, as time and funding permit. The scientists at LANL enjoyed an automated power control system that could automatically tune the cavity and control the

level of power output. While this capability was largely due to their expensive TWT microwave source, modifications to the existing system at Virginia Tech could serve the same purpose. It would be quite possible to modify the adjustable short for control by an electromechanical device instead of manual control. Such a device could be controlled via an interface with the data acquisition computer through the parallel port. A similar device could be used to control the position of the variable coupler if it is included in the waveguide system. Likewise, the forward power could be controlled by an electromechanical drive on the source adjustment knob. Having these devices on automated control would enable greater precision in the control of rod heating, and the positions of the tuning elements could be recorded. That these positions were not recorded in the LANL experiments made estimation of the power losses more difficult. Control of the forward power could eliminate the "drift" that normally occurs in experimental situations. Development of such a control apparatus and computer interfacing would be a suitable task for future study. At the very least, the knob that controls the power output of the microwave source should be replaced with a much larger one. This would enable the level of forward power to be adjusted with greater precision. It is currently quite difficult to make accurate, small changes to the forward power.

# Bibliography

Adams, F., and Laughlin, G., "The Five Ages of the Universe," pp. 18, New York: The Free Press, 1999.

Arai, M., Binner, J., Carr, G., and Cross, T., "High Temperature Dielectric Property Measurements of Engineering Ceramics," in: *Ceramic Transactions - Microwaves: Theory and Application in Materials Processing II*, eds. D. Clark, W. Tinga, and J. J.R. Laia, Vol. 36, pp. 483-492, ACS, 1993.

Bauer, W., and Steinhardt, R., "Emissivity of Refractories," *Gas Warne International*, Vol. 39, pp. 388-391, 1990.

Brandon, J., Samuels, J., and Hodgkins, W., "Microwave Sintering of Oxide Ceramics," in: *Microwave Processing of Materials III*, eds. R. Beatty, W. Sutton, and M. Iskander, Vol. 269, pp. 237-243, MRS, Pittsburgh, 1992.

Bringhurst, M., White, M., and Iskander, M., "Numerical Simulation and Experimental Validation of RF Drying," in: *Microwave Processing of Materials V*, eds. M. Iskander, J. J.O. Kiggans, and J. Bolomey, Vol. 430, pp. 339-344, MRS, Pittsburgh, 1996.

Chapman, B., Iskander, M., Smith, R., and Andrade, O., "Simulation of Sintering Experiments in Single-Mode Cavities," in: *Microwave Processing of Materials III*, eds. R. Beatty, W. Sutton, and M. Iskander, Vol. 269, pp. 53-59, MRS, Pittsburgh, 1992.

Craven, M., Cross, T., and Binner, J., "Enhanced Computer Modeling for High Temperature Microwave Processing of Ceramic Materials," in: *Microwave Processing of*

*Materials V*, eds. M. Iskander, J. J.O. Kiggans, and J. Bolomey, Vol. 430, pp. 351-356, MRS, Pittsburgh, 1996.

Curtis, J., Private Communication, November 1999.

Curtis, J., "Experimental Verification for Microwave Processing of Materials in a Single Mode Rectangular Resonant Cavity," M.S. Thesis, Virginia Polytechnic Institute and State University, 1999.

Davis, W., Private Communication, 1999

Duchez, W., "Role of Electric Field Profiles in Continuous Microwave Processing of Thermal Runaway Materials," M.S. Thesis, Virginia Polytechnic Institute and State University, 1996.

Freim, J., McKittrick, J., Katz, J., and Sickafus, K., "Phase Transformation and Densification Behavior of Microwave Sintered  $\gamma$ -Al<sub>2</sub>O<sub>3</sub>," in: *Microwave Processing of Materials IV*, eds. M. Iskander, R. Lauf, and W. Sutton, Vol. 347, pp. 525-530, MRS, Pittsburgh, 1996.

Gilmour, A. Jr., "Principles of Traveling Wave Tubes," London, UK: Artech House, 1994.

Goodson, C., "Simulation of Microwave Heating of Mullite Rods," M.S. Thesis, Virginia Polytechnic Institute and State University, 1997.

Grotjohn, T., and Asmussen, J., "Numerical Simulation of Resonant Cavity Microwave Systems for Materials Processing," in: *Microwave Processing of Materials V*, eds. M. Iskander, J. J.O. Kiggans, and J. Bolomey, Vol. 430, pp. 357-362, MRS, Pittsburgh, 1996.

Hile, C. and Kriegsmann, G., "A Hybrid Numerical Method for Modeling Microwave Sintering Experiments," in: *Microwave Processing of Materials V*, eds. M. Iskander, J. J.O. Kiggans, and J. Bolomey, Vol. 430, pp. 319-331, MRS, Pittsburgh, 1996.

Incropera, F., and DeWitt, P., "Fundamentals of Heat and Mass Transfer," New York: John Wiley & Sons, 1996.

Iskander, M., "Computer Modeling and Numerical Techniques for Quantifying Microwave Interactions With Materials," in: *Microwave Processing of Materials II*, eds. W. Snyder, W. Hutton, M. Iskander, and D. Johnson, Vol. 189, pp. 149-171, MRS, Pittsburgh, 1991.

Iskander, M., "Modeling the Microwave Process - Challenges and New Directions," in: *Ceramic Transactions - Microwaves: Theory and Application in Materials Processing II*, eds. D. Clark, W. Tinga, and J. J.R. Laia, Vol. 36, pp. 167-187, ACS, 1993.

Jackson, M., Private Communication, May 1997.

Johnson, D., Skasmer, D., and Spatz, M., "Temperature Gradients in Microwave Processing: Boon and Bane," in: *Ceramic Transactions - Microwaves: Theory and Application in Materials Processing II*, eds. D. Clark, W. Tinga, and J. J.R. Laia, Vol. 36, pp. 133-146, ACS, 1993.

Kenkre, V., Skala, L., Weiser, M., and Katz, J., "Theory of Microwave Effects on Atomic Diffusion in Sintering: Basic Considerations of the Phenomenon of Thermal Runaway," in: *Microwave Processing of Materials II*, eds. W. Snyder, W. Hutton, M. Iskander, and D. Johnson, Vol. 189, pp. 179-184, MRS, Pittsburgh, 1991.

Kriegsmann, G., "Growth and Stabilization of Hot Spots in Microwave Heated Ceramic Fibers," in: *Microwave Processing of Materials IV*, eds. M. Iskander, R. Lauf, and W. Sutton, Vol. 347, pp. 473-478, MRS, Pittsburgh, 1996.

Marcuvitz, N., "Waveguide Handbook," London, UK: Peter Peregrinus Ltd., 1986.

Mascarenhas, W., "An Improved Finite-Element Model for Simulating Microwave Processing of Polymers and Polymer-Composites in a Cylindrical Resonant Cavity," M.S. Thesis, Virginia Polytechnic Institute and State University, 1992.

May, E., "A Coupled Electromagnetic and Heat Transfer Finite-Element Model for Simulating Microwave Processing of Composite Materials in a Cylindrical Resonant Cavity," M.S. Thesis, Virginia Polytechnic Institute and State University, 1991.

Metaxas, A., and Meredith, R., "Industrial Microwave Heating," London, UK: Peter Peregrinus LTD., 1983.

National Materials Advisory Board Commission on Engineering and Technical Systems, "Microwave Processing of Materials," Washington, D.C.: National Academy Press, 1994.

Newman, J., Walsh, R., Tholen, T., Andrade, O., Iskander, M., Bunch, K., and Kimrey, H., "Experimental Validation of Numerical Simulations of the Microwave Sintering Process," in: *Ceramic Transactions - Microwaves: Theory and Application in Materials Processing II*, eds. D. Clark, W. Tinga, and J. J.R. Laia, Vol. 36, pp. 229-237, ACS, 1993.

Oliver, A., Clarricoats, P., Kisk, A., and Shafai, L., "Microwave Horns and Feeds," New York: IEEE Press, 1994.

Rolev, A., Private Communication, 1999.

Russell, L., Johnson, L., and Hasselman, D., "Thermal Conductivity/Diffusivity of Silicon Carbide Whisker Reinforced Mullite," *Journal of American Ceramic Society*, Vol. 70, pp. C226-C229, 1987.

Schneider, H., Okada, K., and Pask, J., "Mullite and Mullite Ceramics," Chichester, UK: John Wiley & Sons, 1994.

Scott, A., "Understanding Microwaves," New York: John Wiley & Sons, 1993.

Sillars, R., "Electrical Insulating Materials and Their Application," London, UK: Peter Peregrinus Ltd., 1973.

Singh, R., Viatella, J., Fathi, Z., and Clark, D., "Thermal Analysis of Microwave Processing of Ceramics," in: *Ceramic Transactions - Microwaves: Theory and Application in Materials Processing II*, eds. D. Clark, W. Tinga, and J. J.R. Laia, Vol. 36, pp. 247-255, ACS, 1993.

Smith, M., and Phillips, G., "Power Klystrons Today," New York: John Wiley & Sons, 1995.

Smith, R., Iskander, M., Andrade, O., and Kimrey, H., "Finite-Difference Time-Domain (FDTD) Simulation of Microwave Sintering in Multimode Cavities," in: *Microwave Processing of Materials III*, eds. R. Beatty, W. Sutton, and M. Iskander, Vol. 269, pp. 47-52, MRS, Pittsburgh, 1992.

Terril, N., "Field Simulation for the Microwave Heating of Thin Ceramic Fibers," M.S. Thesis, Virginia Polytechnic Institute and State University, 1998.

Theury, J., "Microwaves: Industrial, Scientific, and Medical Applications," Norwood, UK: Artech House, Inc., 1992.

Thomas, J.R. Jr., Private Communication, 1999.

Thomas, J.R. Jr, Goodson, C., Stern, C., Jackson, M., and Vogt, G., "Microwave Sintering of Ceramic Rods: Experiments and Models," Correspondence: Mechanical Engineering Department, Virginia Polytechnic Institute and State University, p. 3, 1997.

Tian, Y., Feng, J., Sun, L., and Tu, C., "Computer Modeling of Two Dimensional Temperature Distributions in Microwave Heated Ceramics," in: *Microwave Processing of Materials III*, eds. R. Beatty, W. Sutton, and M. Iskander, Vol. 269, pp. 41-46, MRS, Pittsburgh, 1992.

Tinga, W., "Fundamentals of Microwave-Material Interactions and Sintering," in: *Microwave Processing of Materials*, eds. W. Sutton, M. Brooks, and I. Chabinsky, Vol. 124, pp. 33-43, MRS, Pittsburgh, 1988.

Tinga, W., "Microwave Material Interactions and Process Design," in: *Ceramic Transactions - Microwaves: Theory and Application in Materials Processing II*, eds. D. Clark, W. Tinga, and J. J.R. Laia, Vol. 36, pp. 483-492, ACS, 1993.

Touloukian, Y., "Thermal Radiative Properties," Vol. 8, Perdue University, New York-Washington, p. 142, 1972.

Tranquilla, J., Al-Rizzo, H., and Clark, K., "An Overview of Electromagnetic Modeling of Single- and Multi-Mode Applicators at EMR Microwave Technology Corporation," in: *Microwave Processing of Materials V*, eds. M. Iskander, J. J.O. Kiggans, and J. Bolomey, Vol. 430, pp. 309-317, MRS, Pittsburgh, 1996.

Unknown Author(s), "Optical Temperature Measurements in Vacuum Environments with Single and Dual Wavelength Measurement Techniques," provided by Luxtron Corporation, Utah Vacuum Symposium, 1993

Veley, V., "Modern Microwave Technology," Englewood Cliffs: Prentice-Hall, 1987.

Vogt, G., Private Communication, October 1999.

Vogt, G., Regan, A., Rohlev, A., and Curtin, M., "Microwave Process Control Through a Traveling Wave Tube Source," in: *Microwave Processing of Materials V*, eds. M. Iskander, J. J.O. Kiggans, and J. Bolomey, Vol. 430, pp. 513-518, MRS, Pittsburgh, 1996.

Vogt, G., and Unruh, W., "Processing Aerosols and Filaments in a  $TM_{010}$  Microwave Cavity at 2.45 GHz," in: *Microwave Processing of Materials III*, eds. R. Beatty, W. Sutton, and M. Iskander, Vol. 269, pp. 245-250, MRS, Pittsburgh, 1992.

Xi, W., and Tinga, W., "A High Temperature Microwave Dielectrometer," *Ceramic Transactions*, Vol. 21, pp. 215-224, 1991

# Appendix A

## Heat Transfer Simulation Code

---

### HTMain.f90:

```
!-----!  
! Brian McConnell 7/7/99 Absoft Pro Fortran Compiler  
! Program Name: HTMain.f90 Fortran 90 language  
!  
! This is a re-structured version of the original heat transfer model  
! written by Craig C. Goodson for his Masters Thesis. The section  
! dealing with the electric field distribution is a modified version  
! of the code written by Nathan Terril for his Master's Thesis. Both  
! codes were changed to work together, increase their performance, and  
! use a consistent programming style. The Goodson program was written  
! in Fortran 77 and has been modified to incorporate the latest  
! features of the Fortran 90 programming language. This code is  
! designed to utilize the Visual Basic interface program written by  
! McConnell although it is not essential if another means of generating  
! the required input file should be needed.  
!  
! Purpose: The purpose of this program is to simulate the heating of  
! thin ceramic rods in a single-mode microwave resonator cavity. The  
! program allows for temperature dependent properties of each material  
! element such as thermal conductivity, specific heat, emissivity, and  
! dielectric permeability. It uses a finite difference scheme to solve  
! for the temperature distribution at each time step. The inclusion of  
! the electric field model developed by Terril allows an accurate  
! simulation of the field distribution along the rod instead of the  
! previously assumed uniform distribution. The code has been changed  
! to allow the use of a power/velocity input file that enables the user  
! to model the exact input parameters used in the LANL experiments.  
!  
! Variables:  
! T(I,J) = temperature ( i = x-component j = r-component)  
! TP(I,J) newly calculated temprature to compare to old temp TOLD(I,J)  
! QMV = volumetric heat source (W/m3)  
! HC4 = convection heat transfer coeff. (W/m2K)  
! HR4 = radiation heat transfer coeff.  
! CP(I,J) = specific heat (J/kgK)
```

```

! CO(I,J) = thermal conductivity (W/mK)
! RR = radius to point of evaluation (m)
! AA(I,J) = number that goes with T m,n-1
! BB(I,J) = number that goes with T m-1,n
! CC(I,J) = number that goes with Tm,n
! DD(I,J) = number that goes with T m,n+1
! EE(I,J) = number that goes with Tm+1,n
! ZZ(I,J) = constants or knowns in the finite diff eqn
! POW = absorbed power criteria (W)
! E = Electric Field Strength (V/m)
! LENG = length of microwave applicator in m(length of rod in applictr)
! LENT = Entry length (length of rod outside cavity to where the temp
! of rod is equal to ambient temp.) in meters
! LEXT = Exit length (same as LENT, but on other side of cavity)
! DIAM = rod diameter (m)
! R = radius (m) = DIAM/2
! DR = finite difference length along radius (m)
! DT = change in time (sec)
! DX = finite difference length along length (m)
! MN = # of x-direction finite differences on rod outside of entry end of cavity
! N = # of x-direction finite differences on rod in cavity
! M = MN except on exit end of cavity
! MR = # of finite differences in r direction (only in r, not in diameter)
! NUMBR = total # of elements in x-direction of entire rod
! NUM2 = total # of elements in r-direction of rod
! TINF = ambient Temperature (K)
! TAIR = same (not used)
! TTUB = Temperature of cavity (tube) wall (K)
! V = velocity of rod (m/s)
! DIFF = criteria for convergence to find temp at a given time
! SIGMA = Boltz. constant
! TIME = time (sec)
! NAC = counter to write temperature every NAC centi-seconds
! ITIME = counter to check S.S. convergence every NTIME centi-seconds
! DIFFSS = criteria for convergence to find steady state temp
! LSTOP = counter to check thermal runaway
! RO = density (kg/m3)
! Nss = flag to run to steady state
! INFILE = file path and name to use for LANL inputs
! INFLAG = flag if LANL inputs are used or not
!
!-----!
PROGRAM HTMain
IMPLICIT DOUBLE PRECISION(A-H,O-Z)
CHARACTER*8 MATERL,SOURCE
CHARACTER*40 PATHNAME,INFILE

```

```

DOUBLE PRECISION LENG,LEXT,LENT,MAXSURF,MAXELEM
PARAMETER(L = 201, LL = 9)
DIMENSION T(L,LL),TP(L,LL),AA(L,LL),BB(L,LL),CC(L,LL),DD(L,LL),&
    EE(L,LL),ZZ(L,LL),A(L),B(L),C(L),D(L),TOLD(L,LL),TT(L),&
    CO(L,LL),CPOS(L,LL),CNEG(L,LL),CP(L,LL),CPPOS(L,LL),&
    CPNEG(L,LL),QMV(L,LL),TSS(L,LL),BETA(L),GAMMA(L),&
    PERM(2,201,9),field(40),field2(40),EFIELD(40),EFIELD2(40),&
    TTEST(L,LL)
COMPLEX*16 TRANS,REFL
!-----!
! "Initial" opens the input file and reads in the input data. It then
! opens the output file and writes the input data and header to the
! output file. It then uses the input to calculate new values, and
! gives initial values to certain variables. It finally writes the
! initial condition data to the output file for time = 0.
Call Initial(Nss,mtot,ntot,Iptot,Iqtot,c2a,v2b,t2a,loss,Iftype,&
    SOURCE,POW,d2lg,freq,V,MATERL,LENG,DIAM,aaa,bbb,E,TINF,&
    TTUB,DT,POWCHECK,DIFF,DIFFSS,PATHNAME,INFLAG,INFILE,&
    scaling,LENT,LEXT,R,DR,DX,M,N,MN,MR,NUMBR,NUM2,TAIR,&
    SIGMA,TIME,NAC,ITIME,NTIME,LSTOP,ITCOUNT,MAXELEM,&
    MAXSURF,POWLOST,POWABS,EBAR,T,TOLD,TP,QMV,TSS,ITSTEP,&
    INEW,TTEST,TLIMIT)

! "Density" returns the temperature-independent density of the material
! being used.
Call Density(MATERL,RO)

! The subroutine "Aperture" solves for the reflection and transmission
! coefficients of the iris so that the iris analysis can be skipped in
! subsequent calls to "combined" to solve for the field distribution
! along the fiber.
! CALL Aperture(c2a,v2b,t2a,freq,d2lg,aaa,bbb,loss,TRANS,REFL)

!***** MAIN PROGRAM LOOP STARTS HERE *****!
! The only way to exit the loop is
!     1) Steady state is reached
!     2) End of input file is reached
!     3) Material melts
!     4) Thermal runaway occurs

DO

! "ReLoop" resets certain values before each loop iteration.
13 CALL
ReLoop(X,MAXSURF,MAXELEM,AA,BB,CC,DD,EE,ZZ,NUM2,NUMBR,TINF)

```

```

! "SeePee" finds the material element specific heats.
  CALL SeePee(MATERL,CP,CPPOS,CPNEG,TOLD,NUMBR,NUM2)

! "ThCond" finds the material element thermal conductivities.
  CALL ThCond(MATERL,CO,CPOS,CNEG,TOLD,NUMBR,NUM2)

! "TOTPERM" finds the material element complex permittivity
  CALL TOTPERM(T,MATERL,NUM2,PERM)

! "GetField" is called to solve for the electric field shape in the
! case when uniform field is not being used. The no-loss field shape
! is returned in the "field" array, and the loss-included shape is
! returned in the "field2" array only if loss is being considered.
! Check the value of "INEW" to determine if the field shapes need to
! be computed at this time. If it is calculated and the user does not
! want it found at every time step, reset the flag "INEW" to zero.
IF (INEW .EQ. 1) THEN
  CALL GetField(mtot,ntot,Iptot,Iqtot,c2a,v2b,t2a,freq,d2lg,aaa,&
    bbb,PERM,M,N,loss,Iftype,field,field2)
  IF (TLIMIT .NE. 0.0) THEN
    INEW = 0
  ENDIF
ENDIF

! "ScaleE" is used to scale the tangential electric field distribution
! so that the proper absorbed power level is achieved.
  CALL ScaleE(Iftype,EFIELD,EFIELD2,loss,E,MN,N,NUM2,DX,DR,freq,&
    PERM,POWLOST,EBAR,scaling,POW,field,field2,&
    POWCHECK,SOURCE,POWABS,T,QMV)

! "BuildMat" uses the rod geometry and property data to build the
! matrices for the finite difference equations.
  CALL
BuildMat(MATERL,NUMBR,NUM2,TTUB,TOLD,LENG,TINF,SIGMA,CO,&
  RO,CP,CPPOS,CPNEG,CPOS,CNEG,QMV,DR,DX,DT,T,V,R,&
  MR,AA,BB,CC,DD,EE,ZZ)

! "SolveMat" uses a tri-diagonal solver to solve the set of linear
! finite difference equations and returns the values for TP(L,LL),
! the new temperature distribution.
  CALL SolveMat(AA,BB,CC,DD,EE,ZZ,TP,NUM2,NUMBR)

! "DataChek" checks the newly found temperatures to see if the the
! program has converged for the given time step. It checks to see how
! many times the program has looped for the current time step. If it

```

```

! loops too many times without converging, "Thermal Runaway" is
! reported.
  CALL DataChk(MATERL,LSTOP,TOLD,TP,NUM2,NUMBR,ITSTEP,DIFF,&
    INEW,TTEST,TLIMIT)

! If the temperatures have converged for the time step, go on. If not,
! then go back to the start of the main program loop and find new
! material properties.
  IF (ITSTEP .EQ. 0) THEN
    GOTO 13
  ENDIF

! Once the temperatures have converged for the current time step, the
! material temperatures must be checked to make sure the melting
! temperature of the solid has not been exceeded. If melting occurs,
! the program reports this condition and terminates.
  CALL
MeltChk(MATERL,TP,NUM2,NUMBR,MAXSURF,MAXELEM,TINF,TIME,&
  DT)

! "SSChk" compares the temperature distribution from the current time
! step to the values from the previous time step to see if steady state
! has been reached. If steady state, exit the main loop.
  CALL
SSChk(TIME,LSTOP,NAC,ITIME,NTIME,TSS,TP,NUMBR,NUM2,INFLAG,&
  DIFFSS,IAMSS)
  IF (IAMSS.EQ.1) THEN
    GOTO 999
  ENDIF

! "DataOut" writes the data to the output file at the end of each
! one second interval and reads in the new power and velocity if the
! input file option is being used. If the end of the input file is
! reached, exit the main loop.
  CALL
DataOut(ITCOUNT,TIME,EBAR,POWABS,POWLOST,MAXSURF,MAXELEM,&
  MN,N,TP,EFIELD,EFIELD2,loss,INFLAG,POW,V,T,&
  IAMDONE,DT,NUMBR,NUM2)
  IF (IAMDONE.EQ.1) THEN
    GOTO 999
  ENDIF

ENDDO
! End of the main program loop.

! "LastOut" writes the final pieces of information to the output file.

```

```
999 CALL
LastOut(loss,ITCOUNT,EBAR,POWABS,POWLOST,MAXSURF,MAXELEM,MN,&
        N,INFLAG,TP,EFIELD,EFIELD2)
```

```
STOP
END
```

---

### Initial.f90:

```
!-----!
! Brian McConnell   7/7/99  Absoft Pro Fortran Compiler
!
! Purpose: This subroutine opens the input file created by the Visual
! Basic interface program and reads in the input data. It opens the
! output file and writes the input parameters and header to the output
! file. It initializes certain variables with the values needed to
! begin the computation in the main program. It returns certain values
! to the main program for use later.
!
! Variables:
! scaling = The value to multiply the electric field distribution
!           values by to achieve the proper magnitudes for the desired
!           absorbed power level.
! QMV = volumetric heat source (W/m3)
!-----!
SUBROUTINE Initial(Nss,mtot,ntot,Iptot,Iqtot,c2a,v2b,t2a,loss,Iftype,&
    SOURCE,POW,d2lg,freq,V,MATERL,LENG,DIAM,aaa,bbb,E,TINF,&
    TTUB,DT,POWCHECK,DIFF,DIFFSS,PATHNAME,INFLAG,INFILE,&
    scaling,LENT,LEXT,R,DR,DX,M,N,MN,MR,NUMBR,NUM2,TAIR,&
    SIGMA,TIME,NAC,ITIME,NTIME,LSTOP,ITCOUNT,MAXELEM,&
    MAXSURF,POWLOST,POWABS,EBAR,T,TOLD,TP,QMV,TSS,ITSTEP,&
    INEW,TTEST,TLIMIT)
IMPLICIT DOUBLE PRECISION(A-H,O-Z)
PARAMETER(L = 201, LL = 9)
CHARACTER*8 MATERL,SOURCE
CHARACTER*40 PATHNAME,INFILE
DOUBLE PRECISION LENG,LEXT,LENT,MAXSURF,MAXELEM
DIMENSION T(L,LL),TP(L,LL),TOLD(L,LL),QMV(L,LL),TSS(L,LL),TTEST(L,LL)
!-----!

! Open the input file and read in the input parameters. Then close the
! input file.
OPEN (8,FILE='interout.dat')
READ(8,*) Nss,TLIMIT
READ(8,*) mtot
READ(8,*) ntot
READ(8,*) Iptot
```

```

READ(8,*) Iqtot
READ(8,*) c2a
READ(8,*) v2b
READ(8,*) t2a
READ(8,*) loss      !1 = include loss, 0 = neglect loss
READ(8,*) Iftype   !1 = enhanced field, 0 = uniform field
READ(8,*) SOURCE
READ(8,*) POW
READ(8,*) d2lg
READ(8,*) freq
READ(8,*) V
READ(8,*) MATERL
READ(8,*) LENG
READ(8,*) DIAM
READ(8,*) aaa
READ(8,*) bbb
READ(8,*) E
READ(8,*) TINF
READ(8,*) TTUB
READ(8,*) DT, POWCHECK
READ(8,*) DIFF
READ(8,*) DIFFSS
READ(8,*) PATHNAME
READ(8,*) INFLAG, INFILE
CLOSE(8)

```

! Open the output file and write the input parameters to the data file.

```

OPEN(9,FILE=PATHNAME)
IF (INFLAG .NE. 1) THEN
  WRITE(9,*) 'For use with Visual Basic interface'
END IF
WRITE(9,*) Nss,TLIMIT
WRITE(9,*) mtot
WRITE(9,*) ntot
WRITE(9,*) Iptot
WRITE(9,*) Iqtot
WRITE(9,*) c2a
WRITE(9,*) v2b
WRITE(9,*) t2a
WRITE(9,*) loss
WRITE(9,*) Iftype
WRITE(9,*) SOURCE
WRITE(9,*) POW
WRITE(9,*) d2lg
WRITE(9,*) freq
WRITE(9,*) V

```

```

WRITE(9,*) MATERL
WRITE(9,*) LENG
WRITE(9,*) DIAM
WRITE(9,*) aaa
WRITE(9,*) bbb
WRITE(9,*) E
WRITE(9,*) TINF
WRITE(9,*) TTUB
WRITE(9,*) DT, POWCHECK
WRITE(9,*) DIFF
WRITE(9,*) DIFFSS
WRITE(9,*) PATHNAME
WRITE(9,*)

```

```

! If the Input File was selected (INFLAG = 1) then open the input file
! to be used and read in the power and velocity data for the first
! second of the simulation. All lines of data in the input file
! contain first the power level in W and then the velocity in
! mm/sec. Velocity sign convention is + down, - up.

```

```

IF (INFLAG .EQ. 1) THEN
  OPEN(7,FILE=INFILE)
  READ(7,*) POW, V
ENDIF

```

```

! Now use the input parameters to compute other values and initialize
! certain variables.

```

```

INEW = 1
scaling = 1.0d0
LENT = 2.0D0 * LENG
LEXT = 2.0D0 * LENG
R = DIAM/2.0D0
DR = R/8.0D0
DX = (LENT+LENG+LEXT)/200.0D0
M = LEXT/DX
N = LENG/DX
MN = LENT/DX
MR = R/DR
NUMBR = M+N+MN+1
NUM2 = MR + 1
TAIR = TINF
SIGMA = 5.6697D-8
TIME = 0.0D0
NAC = 0
ITIME = 0
NTIME = 100

```

```

LSTOP = 0
ITCOUNT = 0
MAXELEM = TINF
MAXSURF = TINF
POWLOST = 0.0D0
POWABS = 0.0D0
EBAR = 0.0D0
ITSTEP = 0

DO I=1,NUMBR
  DO J=1,NUM2
    T(I,J) = TINF
    TOLD(I,J) = TINF
    TP(I,J) = TINF
    QMV(I,J) = 0.0D0
    TSS(I,J) = TINF
    TTEST(I,J) = TINF
  ENDDO
ENDDO

! Write the first data set to the output file for the initial condition
! i.e. for time = 0 seconds.
WRITE(*,100) TIME
WRITE(9,101) ITCOUNT,EBAR,POWABS,POWLOST,MAXSURF,MAXELEM
DO I=MN+1,MN+N
  IF (INFLAG .NE. 1) THEN
    WRITE(9,102) EBAR,TP(I,1),TP(I,2),TP(I,3),TP(I,4),TP(I,6),&
      TP(I,7),TP(I,8),TP(I,9)
  ELSE
    WRITE(9,103) EBAR,TP(I,9)
  END IF
ENDDO
ITCOUNT = ITCOUNT + 1
100 FORMAT(F9.3)
101 FORMAT(I5,1X,F9.2,1X,F6.2,1X,F8.6,1X,F7.2,1X,F7.2)
102 FORMAT(F8.1,1X,F7.2,1X,F7.2,1X,F7.2,1X,F7.2,1X,F7.2,1X,F7.2,1X,&
  F7.2,1X,F7.2,1X,F7.2)
103 FORMAT(F8.1,1X,F7.2)
WRITE(9,*)

RETURN
END

```

---

**Density.f90:**

```

!-----!
! Brian McConnell   7/7/99  Absoft Pro Fortran Compiler

```

```

!
! Purpose: This subroutine is designed to return the value of the
! density of the material being used. It is assumed that any material
! used in this subroutine should experience negligible variation in
! density in the temperature range being used to allow a constant value
! to be used. It is assumed that no phase change will occur in the
! simulation without the program reporting an error.
!
! Variables:
! RO = The material density (kg/m^3)
!-----!
Subroutine Density(MATERL,RO)
Double Precision RO
Character*8 MATERL
!-----!
Select Case (MATERL)
Case ("ALUMINA")
  RO = 3850.0D0 / 2.0D0
Case ("ZIRCONIA")
  RO = 2780.0D0
Case ("MULLITE")
  RO = 2600.0D0
! Source = material property specifications from the manufacturer,
! Bolt Technical Ceramics, Conroe, TX
! RO = 3150.0D0
! Source = "Keith Ceramic Material LTD." data sheet
Case ("NYLON")
  RO = 1070.0D0
! Source = "The physical and thermodynamic Properties of Nylon 6-10" by
! William A. Haug, VPI library call # LD 5655 v.855 1964 H383
End Select

Return
End

```

---

**ReLoop.f90:**

```

!-----!
! Brian McConnell 7/7/99 Absoft Pro Fortran Compiler
!
! Purpose: This subroutine is called at the start of the main program
! loop. The first time through the loop, the values will already have
! been initialized to the proper values. However, on subsequent
! iterations, these values need to be reset.
!-----!
SUBROUTINE
ReLoop(X,MAXSURF,MAXELEM,AA,BB,CC,DD,EE,ZZ,NUM2,NUMBR,TINF)

```

```

IMPLICIT DOUBLE PRECISION(A-H,O-Z)
DOUBLE PRECISION MAXELEM,MAXSURF
PARAMETER(L = 201, LL = 9)
DIMENSION AA(L,LL),BB(L,LL),CC(L,LL),DD(L,LL),EE(L,LL),ZZ(L,LL)
!-----!
X = 0.0D0
MAXSURF = TINF
MAXELEM = TINF

! Initialize the proper FD matrix elements
DO J=1,NUM2
  AA(1,J) = 0.0D0
  BB(1,J) = 0.0D0
  CC(1,J) = 1.0D0
  DD(1,J) = 0.0D0
  EE(1,J) = 0.0D0
  ZZ(1,J) = TINF
  AA(NUMBR,J) = 0.0D0
  BB(NUMBR,J) = 0.0D0
  CC(NUMBR,J) = 1.0D0
  DD(NUMBR,J) = 0.0D0
  EE(NUMBR,J) = 0.0D0
  ZZ(NUMBR,J) = TINF
ENDDO

RETURN
END

```

---

**SeePee.f90:**

```

!-----!
! Brian McConnell   7/7/99  Absoft Pro Fortran Compiler
!
! Purpose: This routine uses the appropriate function calls to find the
! specific heat of each material element.
!-----!
SUBROUTINE SeePee(MATERL,CP,CPPOS,CPNEG,TOLD,NUMBR,NUM2)
IMPLICIT DOUBLE PRECISION(A-H,O-Z)
PARAMETER(L = 201, LL = 9)
DIMENSION TOLD(L,LL),CPNEG(L,LL),CPPOS(L,LL),CP(L,LL)
CHARACTER*8 MATERL
!-----!
SELECT CASE (MATERL)
CASE ("ALUMINA")
  DO I=1,NUMBR
    CP(I,1) = CAP1(TOLD(I,1))
    CP(I,NUM2) = CAP1(TOLD(I,NUM2))

```

```

DO J=2,NUM2-1
  CP(I,J) = CAP1(TOLD(I,J))
  CPPOS(I,J) = CAP1((TOLD(I,J)+TOLD(I+1,J))/2.0D0)
  CPNEG(I,J) = CAP1((TOLD(I,J)+TOLD(I-1,J))/2.0D0)
ENDDO
ENDDO
CASE ("ZIRCONIA")
DO I=1,NUMBR
  CP(I,1) = CAP2(TOLD(I,1))
  CP(I,NUM2) = CAP2(TOLD(I,NUM2))
  DO J=2,NUM2-1
    CP(I,J) = CAP2(TOLD(I,J))
    CPPOS(I,J) = CAP2((TOLD(I,J)+TOLD(I+1,J))/2.0D0)
    CPNEG(I,J) = CAP2((TOLD(I,J)+TOLD(I-1,J))/2.0D0)
  ENDDO
ENDDO
CASE ("MULLITE")
DO I=1,NUMBR
  CP(I,1) = CAP3(TOLD(I,1))
  CP(I,NUM2) = CAP3(TOLD(I,NUM2))
  DO J=2,NUM2-1
    CP(I,J) = CAP3(TOLD(I,J))
    CPPOS(I,J) = CAP3((TOLD(I,J)+TOLD(I+1,J))/2.0D0)
    CPNEG(I,J) = CAP3((TOLD(I,J)+TOLD(I-1,J))/2.0D0)
  ENDDO
ENDDO
CASE ("NYLON")
DO I=1,NUMBR
  CP(I,1) = CAP4(TOLD(I,1))
  CP(I,NUM2) = CAP4(TOLD(I,NUM2))
  DO J=2,NUM2-1
    CP(I,J) = CAP4(TOLD(I,J))
    CPPOS(I,J) = CAP4((TOLD(I,J)+TOLD(I+1,J))/2.0D0)
    CPNEG(I,J) = CAP4((TOLD(I,J)+TOLD(I-1,J))/2.0D0)
  ENDDO
ENDDO
END SELECT

RETURN
END

```

---

**ThCond.f90:**

```

!-----!
! Brian McConnell   7/7/99  Absoft Pro Fortran Compiler
!
! Purpose: This routine uses the appropriate function calls to find the

```

```

! thermal conductivity of each material element.
!-----!
SUBROUTINE ThCond(MATERL,CO,CPOS,CNEG,TOLD,NUMBR,NUM2)
IMPLICIT DOUBLE PRECISION(A-H,O-Z)
PARAMETER(L = 201, LL = 9)
DIMENSION TOLD(L,LL),CNEG(L,LL),CPOS(L,LL),CO(L,LL)
CHARACTER*8 MATERL
!-----!
SELECT CASE (MATERL)
CASE ("ALUMINA")
  DO I=1,NUMBR
    CO(I,1) = CAL(TOLD(I,1))
    CO(I,NUM2) = CAL(TOLD(I,NUM2))
    DO J=2,NUM2-1
      CO(I,J) = CAL(TOLD(I,J))
      CNEG(I,J) = CAL((TOLD(I,J)+TOLD(I-1,J))/2.0D0)
      CPOS(I,J) = CAL((TOLD(I,J)+TOLD(I+1,J))/2.0D0)
    ENDDO
  ENDDO
CASE ("ZIRCONIA")
  DO I=1,NUMBR
    CO(I,1) = CZR(TOLD(I,1))
    CO(I,NUM2) = CZR(TOLD(I,NUM2))
    DO J=2,NUM2-1
      CO(I,J) = CZR(TOLD(I,J))
      CNEG(I,J) = CZR((TOLD(I,J)+TOLD(I-1,J))/2.0D0)
      CPOS(I,J) = CZR((TOLD(I,J)+TOLD(I+1,J))/2.0D0)
    ENDDO
  ENDDO
CASE ("MULLITE")
  DO I=1,NUMBR
    CO(I,1) = CMU(TOLD(I,1))
    CO(I,NUM2) = CMU(TOLD(I,NUM2))
    DO J=2,NUM2-1
      CO(I,J) = CMU(TOLD(I,J))
      CNEG(I,J) = CMU((TOLD(I,J)+TOLD(I-1,J))/2.0D0)
      CPOS(I,J) = CMU((TOLD(I,J)+TOLD(I+1,J))/2.0D0)
    ENDDO
  ENDDO
CASE ("NYLON")
  DO I=1,NUMBR
    CO(I,1) = CNY(TOLD(I,1))
    CO(I,NUM2) = CNY(TOLD(I,NUM2))
    DO J=2,NUM2-1
      CO(I,J) = CNY(TOLD(I,J))
      CNEG(I,J) = CNY((TOLD(I,J)+TOLD(I-1,J))/2.0D0)

```

```

        CPOS(I,J) = CNY((TOLD(I,J)+TOLD(I+1,J))/2.0D0)
    ENDDO
ENDDO
END SELECT

RETURN
END

```

---

**TOTPERM.f90:**

```

!-----!
! Purpose: Calculates the total permittivity distribution for the
! surface elements given the temperature distribution in Kelvin.
!-----!
SUBROUTINE TOTPERM(T,MATERL,NUM2,PERM)
IMPLICIT DOUBLE PRECISION(A-H,O-Z)
PARAMETER(L=201, LL=9)
DIMENSION T(L,LL),PERM(2,L,LL),REPERM(L,LL),PERMIM(L,LL)
CHARACTER*8 MATERL
!-----!
DO I=1,201
  DO J=1,NUM2
    IF (MATERL.EQ.'MULLITE') THEN
      REPERM(I,J) = EPMU3(T(I,J))
      PERMIM(I,J) = eppmu3(T(I,J))
    ELSEIF (MATERL.EQ.'ALUMINA') THEN
      REPERM(I,J) = EPA(T(I,J))
      PERMIM(I,J) = eppa(T(I,J))
    ELSEIF (MATERL.EQ.'ZIRCONIA') THEN
      REPERM(I,J) = EPZR(T(I,J))
      PERMIM(I,J) = eppzr(T(I,J))
    ELSEIF (MATERL.EQ.'NYLON') THEN
      REPERM(I,J) = epn(T(I,J))
      PERMIM(I,J) = eppn(T(I,J))
    ENDIF
    PERM(1,I,J) = REPERM(I,J)
    PERM(2,I,J) = PERMIM(I,J)
  ENDDO
ENDDO

RETURN
END

```

---

**GetField.f90:**

```

!-----!
! Brian McConnell   7/7/99  Absoft Pro Fortran Compiler
!

```

```

! Purpose: This subroutine calls "combined" as needed for the electric
! field shape or shapes (in the case of loss-included).
!-----!
SUBROUTINE GetField(mtot,ntot,Iptot,Iqtot,c2a,v2b,t2a,freq,d2lg,aaa,&
    bbb,PERM,M,N,loss,Iftype,field,field2)
IMPLICIT DOUBLE PRECISION(A-H,O-Z)
DIMENSION PERM(2,201,9),field(40),field2(40)
!-----!
! Iftype = 1 when the uniform field is NOT used, 0 when it IS used.
IF (Iftype .EQ. 1) THEN
    call combined(mtot,ntot,Iptot,Iqtot,c2a,v2b,t2a,0,freq,d2lg,&
        aaa,bbb,field,PERM,M,N)
! loss = 1 when losses are to be included.
IF (loss .EQ. 1) THEN
    call combined(mtot,ntot,Iptot,Iqtot,c2a,v2b,t2a,1,freq,d2lg,&
        aaa,bbb,field2,PERM,M,N)
ENDIF
! field is the no-loss distribution, field2 includes cavity loss.
ENDIF

RETURN
END

```

### ScaleE.f90:

```

!-----!
! Brian McConnell   7/12/99       Absoft Pro Fortran Compiler
!
! Purpose: This routine takes the field shape(s) returned from the
! field simulation and scales the amplitude so that the desired power
! absorption takes place.  If losses are being used, the routine finds
! the scaling parameter with the loss-free shape and then applies that
! scaling value to the loss-included field shape.
!-----!
SUBROUTINE ScaleE(Iftype,EFIELD,EFIELD2,loss,E,MN,N,NUM2,DX,DR,freq,&
    PERM,POWLOST,EBAR,scaling,POW,field,field2,&
    POWCHECK,SOURCE,POWABS,T,QMV)
IMPLICIT DOUBLE PRECISION(A-H,O-Z)
PARAMETER(L=201,LL=9)
CHARACTER*8 SOURCE
DIMENSION EFIELD(40),EFIELD2(40),field(40),field2(40),QMV(L,LL),&
    PERM(2,L,LL),T(L,LL)
!-----!
100 POW2=0.0D0
EBARSUM = 0.0D0
IF (Iftype .EQ. 1) THEN
! If using the enhanced field with or without loss,

```

```

! fill EFIELD with the proper scaled values of NO LOSS
! field shape...
  DO I = 1,40
    EFIELD(I) = scaling*field(I)
! If using the enhanced field WITH loss,
    IF (loss .EQ. 1) THEN
      EFIELD2(I) = scaling*field2(I)
      EBARSUM = EBARSUM + EFIELD2(I)
    ELSE
      EBARSUM = EBARSUM + EFIELD(I)
    ENDIF
  ENDDO
ELSE
! If using the uniform field option,
! fill EFIELD with the uniform field value...
  DO I = 1,40
    EFIELD(I) = E
    EBARSUM = EBARSUM + E
  ENDDO

ENDIF

! Calculate the average electric field strength along the fiber.
EBAR = EBARSUM/40

DO I=MN+1,MN+N
  INUM = I-MN
  DO J=1,NUM2
    QMV(I,J)=Q(T(I,J),EFIELD(INUM),freq,PERM(2,I,J))
    IF (J.EQ.1) THEN
      ADD = 3.14159275D0*QMV(I,J)*DX*(J*DR-DR/2.0D0)**2
    ELSEIF (J.EQ.NUM2) THEN
      ADD = 3.14159275D0*QMV(I,J)*DX*&
        (((J-1)*DR)**2-((J-1)*DR-DR/2.0D0)**2)
    ELSE
      ADD = 3.14159275D0*QMV(I,J)*DX*&
        ((J*DR-DR/2.0D0)**2-((J-1)*DR-DR/2.0D0)**2)
    ENDIF
    POW2 = POW2 + ADD
    POWABS = POW2
    POWLOST = 0
! POW2 is the absorbed power for uniform field and no-loss scenarios.
  ENDDO
ENDDO

DPOW = ABS(POW-POW2)

```

```

IF (DPOW.GE.POWCHECK.AND.SOURCE.EQ.'POWER') THEN
  IF (Iftype .EQ. 1) THEN
    scaling = scaling*SQRT(POW/POW2)
  ELSE
    E = E*SQRT(POW/POW2)
  ENDIF
  GOTO 100
ENDIF

```

! The next section finds the volumetric generation when losses are  
! considered. The power actually absorbed by the rod is not what  
! is held constant, the power to the load is (losses and into rod).  
! By using the preceding loop to find the scaling value, and then  
! using that scaling value on the "loss included" field shape,  
! we can hold the "load power" constant and subtract the "loss power"  
! from that which is absorbed in the material like was done at LANL  
! in the real experiments...

```

IF (Iftype .EQ. 1) THEN
  IF (loss .EQ. 1) THEN
    POW3 = 0
    DO I=MN+1,MN+N
      INUM = I-MN
      DO J = 1,NUM2
        QMV(I,J)=Q(T(I,J),EFIELD2(INUM),freq,PERM(2,I,J))
        IF (J .EQ. 1) THEN
          ADD2 = 3.14159275D0*QMV(I,J)*DX*(J*DR-DR/2.0D0)**2
        ELSEIF (J.EQ.NUM2) THEN
          ADD2 = 3.14159275D0*QMV(I,J)*DX*&
            (((J-1)*DR)**2-((J-1)*DR-DR/2.0D0)**2)
        ELSE
          ADD2 = 3.14159275D0*QMV(I,J)*DX*&
            ((J*DR-DR/2.0D0)**2-((J-1)*DR-DR/2.0D0)**2)
        ENDIF
        POW3 = POW3 + ADD2
      POWABS = POW3
    ENDDO
  ENDDO
  ! POWLOST is the wattage lost into the cavity walls due to the fact
  ! that the walls are not "perfect" conductors
  POWLOST = POW2 - POW3
ENDIF
ENDIF

RETURN
END

```

## BuildMat.f90:

```
!-----!  
! Brian McConnell   7/9/99  Absoft Pro Fortran Compiler  
!  
! Purpose: This routine builds the finite difference matrix to be  
! solved in a subsequent routine via the tridiagonal matrix solver.  
!  
! Variables:  
! AA,BB,SS,DD,EE,ZZ = Finite difference element terms.  
! MATERL = The type of material used.  
! NUMBR,NUM2 = The number of finite difference elements in the axial  
!               and radial directions, respectively.  
! TTUB,TINF = The cavity wall and air temperatures, respectively.  
! LENG = The length of the rod inside the microwave cavity.  
! RO = The material density.  
! CO = The material thermal conductivity for each element.  
! CP = The material specific heats for each element.  
!-----!  
SUBROUTINE  
BuildMat(MATERL,NUMBR,NUM2,TTUB,TOLD,LENG,TINF,SIGMA,CO,&  
         RO,CP,CPPOS,CPNEG,CPOS,CNEG,QMV,DR,DX,DT,T,V,R,&  
         MR,AA,BB,CC,DD,EE,ZZ)  
IMPLICIT DOUBLE PRECISION(A-H,O-Z)  
PARAMETER(L=201,LL=9)  
CHARACTER*8 MATERL  
DIMENSION T(L,LL),QMV(L,LL),AA(L,LL),BB(L,LL),CC(L,LL),DD(L,LL),&  
         EE(L,LL),ZZ(L,LL),CO(L,LL),CPOS(L,LL),CNEG(L,LL),CP(L,LL),&  
         CPPOS(L,LL),CPNEG(L,LL),TOLD(L,LL)  
!-----!  
DO I=2,NUMBR-1  
! The first section computes the radiation and convection coefficients  
! to be used in filling the finite difference matrix.  
  IF (MATERL.EQ.'ALUMINA') THEN  
    HR4=SIGMA*EMISS(TOLD(I,NUM2))*(TTUB**3+TOLD(I,NUM2)*&  
      TTUB**2+TTUB*TOLD(I,NUM2)**2+TOLD(I,NUM2)**3)  
  ELSEIF (MATERL.EQ.'ZIRCONIA') THEN  
    HR4=SIGMA*EMISSZ(TOLD(I,NUM2))*(TTUB**3+TOLD(I,NUM2)*&  
      TTUB**2+TTUB*TOLD(I,NUM2)**2+TOLD(I,NUM2)**3)  
  ELSEIF (MATERL.EQ.'MULLITE') THEN  
    HR4=SIGMA*EMISSM(TOLD(I,NUM2))*(TTUB**3+TOLD(I,NUM2)*&  
      TTUB**2+TTUB*TOLD(I,NUM2)**2+TOLD(I,NUM2)**3)  
  ELSEIF (MATERL.EQ.'NYLON') THEN  
    HR4=SIGMA*EMISSNY(TOLD(I,NUM2))*(TTUB**3+TOLD(I,NUM2)*&  
      TTUB**2+TTUB*TOLD(I,NUM2)**2+TOLD(I,NUM2)**3)  
  ENDIF
```

HC4 = HC2(TOLD(I,NUM2),LENG,TINF)

! The next section builds the matrix elements using  
! the finite difference fomulae.

```
AA(I,1) = 0.0D0
BB(I,1) = CO(I,1)*DR/DX + RO*CP(I,1)*V*DR/2.0D0
CC(I,1) = -4.0D0*CO(I,1)*DX/DR - CO(I,1)*DR/DX&
          -CO(I,1)*DR/DX-RO*CP(I,1)*DX*DR/DT
DD(I,1) = 4.0D0*CO(I,1)*DX/DR
EE(I,1) = CO(I,1)*DR/DX - RO*CP(I,1)*V*DR/2.0D0
ZZ(I,1) = -QMV(I,1)*DX*DR-RO*CP(I,1)*DX*DR/DT*T(I,1)

AA(I,NUM2) = CO(I,NUM2)*DX*(1.0D0/DR-1.0D0/2.0D0/R)
BB(I,NUM2) = CO(I,NUM2)* (DR-DR**2/4.0D0/R )/2.0D0/DX&
          +RO*CP(I,NUM2)*V*(DR-DR**2/4.0D0/R)/4.0D0
CC(I,NUM2) = -CO(I,NUM2)*DX*(1.0D0/DR-1.0D0/2.0D0/R) -&
          CO(I,NUM2)*(DR-DR**2/4.0D0/R)/DX&
          - (HC4+HR4)*DX&
          -RO*CP(I,NUM2)*(DR-DR**2/4.0D0/R)*DX/2.0D0/DT
DD(I,NUM2) = 0.0D0
EE(I,NUM2) = CO(I,NUM2)* (DR-DR**2/4.0D0/R )/2.0D0/DX-&
          RO*CP(I,NUM2)*V*(DR-DR**2/4.0D0/R)/4.0D0
ZZ(I,NUM2) = -HC4*DX*TINF - HR4*DX*TTUB - QMV(I,NUM2)*&
          (DR-DR**2/4.0D0/R) *DX/2.0D0 - RO*CP(I,NUM2)*&
          (DR-DR**2/4.0D0/R)*DX/2.0D0/DT*T(I,NUM2)
DO J = 2,NUM2-1
  RR=(J-1)*(R/MR)
  AA(I,J) = CO(I,J)*DX*(1.0D0/DR-1.0D0/2.0D0/RR)
  BB(I,J) = CNEG(I,J)*DR/DX+RO*V*CPNEG(I,J)*DR/2.0D0
  CC(I,J) = -CPOS(I,J)*DR/DX -CNEG(I,J)*DR/DX-&
          2.0D0*CO(I,J)*DX/DR&
          -RO*CP(I,J)*DX*DR/DT
  DD(I,J) = CO(I,J)*DX*(1.0D0/DR+1.0D0/2.0D0/RR)
  EE(I,J) = CPOS(I,J)*DR/DX-RO*V*CPPOS(I,J)*DR/2.0D0
  ZZ(I,J) = -QMV(I,J)*DX*DR-T(I,J)*RO*CP(I,J)*DX*DR/DT
ENDDO
ENDDO

RETURN
END
```

---

**SolveMat.f90:**

```
!-----!
! Brian McConnell   7/9/99  Absoft Pro Fortran Compiler
!
! Purpose: Uses a tri-diagonal matrix solver routine to solve the set
```

```

! of simultaneous linear finite difference equations ([A][x] = [B]) for
! the new temperature distribution, TP(L,LL).
!-----!
SUBROUTINE SolveMat(AA,BB,CC,DD,EE,ZZ,TP,NUM2,NUMBR)
IMPLICIT DOUBLE PRECISION(A-H,O-Z)
PARAMETER(L=201,LL=9)
DIMENSION AA(L,LL),BB(L,LL),CC(L,LL),DD(L,LL),EE(L,LL),ZZ(L,LL),&
          A(L),B(L),C(L),D(L),TP(L,LL),TT(L),BETA(L),GAMMA(L)
!-----!
DO JJ=1,NUM2
  DO II=1,NUMBR
    A(II) = BB(II,JJ)
    B(II) = CC(II,JJ)
    C(II) = EE(II,JJ)
    IF (JJ.EQ.1) THEN
      D(II) = ZZ(II,1)-TP(II,2)*DD(II,1)
    ELSEIF (JJ.EQ.NUM2) THEN
      D(II) = ZZ(II,NUM2)-TP(II,NUM2-1)*AA(II,NUM2)
    ELSE
      D(II) = ZZ(II,JJ)-TP(II,JJ-1)*AA(II,JJ)-TP(II,JJ+1)*DD(II,JJ)
    ENDIF
  ENDDO
ENDDO

!----- Tri-diagonal Solver Program (First Sweep)-----!

  IIF = 1
  LI = NUMBR
  BETA(IIF) = B(IIF)
  GAMMA(IIF) = D(IIF)/BETA(IIF)
  IFPL = IIF+1
  DO I=IFPL,LI
    BETA(I) = B(I)-A(I)*C(I-1)/BETA(I-1)
    GAMMA(I) = (D(I)-A(I)*GAMMA(I-1))/BETA(I)
  ENDDO
  TT(LI) = GAMMA(LI)
  TP(LI,JJ) = TT(LI)
  LAST = LI-IIF
  DO KK=1,LAST
    I=LI-KK
    TT(I) = GAMMA(I)-C(I)*TT(I+1)/BETA(I)
    TP(I,JJ)=TT(I)
  ENDDO
ENDDO
! End of Tri-diagonal Solver Program (First Sweep)
DO II=1,NUMBR
  DO JJ=1,NUM2

```

```

A(JJ) = AA(II,JJ)
B(JJ) = CC(II,JJ)
C(JJ) = DD(II,JJ)
IF (II.EQ.1) THEN
  D(JJ) = ZZ(1,JJ)-TP(2,JJ)*EE(1,JJ)
ELSEIF (II.EQ.NUMBR) THEN
  D(JJ) = ZZ(NUMBR,JJ)-TP(NUMBR-1,JJ)*BB(NUMBR,JJ)
ELSE
  D(JJ) = ZZ(II,JJ)-TP(II-1,JJ)*BB(II,JJ)-TP(II+1,JJ)*EE(II,JJ)
ENDIF
ENDDO

```

!----- Tri-diagonal Solver Program (Second Sweep) -----!

```

IIF = 1
LI = NUM2
BETA(IIF) = B(IIF)
GAMMA(IIF) = D(IIF)/BETA(IIF)
IFPL = IIF+1
DO I=IFPL,LI
  BETA(I) = B(I)-A(I)*C(I-1)/BETA(I-1)
  GAMMA(I) = (D(I)-A(I)*GAMMA(I-1))/BETA(I)
ENDDO
TT(LI) = GAMMA(LI)
TP(II,LI) = TT(LI)
LAST = LI-IIF
DO KK=1, LAST
  I=LI-KK
  TT(I) = GAMMA(I)-C(I)*TT(I+1)/BETA(I)
  TP(II,I) = TT(I)
ENDDO
ENDDO
! End of Tridag program (Second Sweep)

RETURN
END

```

---

**DataChek.f90:**

```

!-----!
! Brian McConnell   7/9/99  Absoft Pro Fortran Compiler
!
! Purpose: This routine checks for thermal runaway and for convergence
! of the temperature distribution for the current time step.
!-----!

```

```

SUBROUTINE
DataChek(MATERL,LSTOP,TOLD,TP,NUM2,NUMBR,ITSTEP,DIFF,&

```

```

      INEW,TTEST,TLIMIT)
IMPLICIT DOUBLE PRECISION(A-H,O-Z)
PARAMETER(L=201,LL=9)
CHARACTER*8 MATERL
DIMENSION TOLD(L,LL),TP(L,LL),TTEST(L,LL)
!-----!
LSTOP = LSTOP + 1
! Check for Thermal Runaway.
IF (LSTOP.GT.1000)THEN
  WRITE(*,*) 'THERMAL RUNAWAY'
  WRITE(9,*) 'THERMAL RUNAWAY IN ',TIME,' SECONDS'
  STOP
ENDIF
ERMAX=ABS(TP(1,1)-TOLD(1,1))/TOLD(1,1)

! Find the largest change in temperature for an element between the
! old value and the newly calculated value.
DO I=2,NUMBR
  DO J=1,NUM2
    ERROR=ABS(TP(I,J)-TOLD(I,J))/TOLD(I,J)
    IF (ERROR.GT.ERMAX) THEN
      ERMAX=ERROR
    ENDIF
  ENDDO
ENDDO

! If the temperatures have converged for this time step, set the flag
! to go on to the next time step. Otherwise, the thermal properties
! need to be modified again and the loop repeated.
IF (ERMAX.GT.DIFF) THEN
  DO I = 1,NUMBR
    DO J = 1,NUM2
      TOLD(I,J) = TP(I,J)
    ENDDO
  ENDDO
  ITSTEP = 0
ELSE
  ITSTEP = 1
ENDIF

IF (INEW .NE. 1) THEN
  DO I = 1,NUMBR
    DO J = 1,NUM2
      IF (ABS(TP(I,J)-TTEST(I,J)) .GE. TLIMIT) THEN
        INEW = 1
        DO II = 1,NUMBR

```

```

        DO JJ = 1,NUM2
          TTEST(II,JJ) = TP(II,JJ)
        ENDDO
      ENDDO
    ENDIF
    IF (INEW .EQ. 1) EXIT
  ENDDO
  IF (INEW .EQ. 1) EXIT
ENDDO
ENDIF

RETURN
END

```

---

**MeltChek.f90:**

```

!-----!
! Brian McConnell   7/9/99  Absoft Pro Fortran Compiler
!
! Purpose: This routine compares the maximum element temperature to the
! melting temperature for the appropriate material and stops the
! program if melting occurs.
!-----!
SUBROUTINE
MeltChek(MATERL,TP,NUM2,NUMBR,MAXSURF,MAXELEM,TINF,TIME,&
          DT)
  IMPLICIT DOUBLE PRECISION(A-H,O-Z)
  DOUBLE PRECISION MAXELEM,MAXSURF
  PARAMETER(L=201,LL=9)
  CHARACTER*8 MATERL
  DIMENSION TP(L,LL)
!-----!
  MAXELEM = TINF
  MAXSURF = TINF

! Find the maximum surface and element temperatures.
DO I=2,NUMBR
  DO J=1,NUM2
    IF (J .EQ. NUM2) THEN
      IF (TP(I,J) .GT. MAXSURF) THEN
        MAXSURF = TP(I,J)
      ENDIF
    ENDIF
    IF (TP(I,J) .GT. MAXELEM) THEN
      MAXELEM = TP(I,J)
    ENDIF
  ENDDO

```

ENDDO

```
! Compare the maximum element temperature to the melting temperature
! of the material. If melting occurs, terminate the program.
! MELTING DATA SOURCES:
! Alumina, Mullite = Bolt Technical Ceramics data sheet
! Zirconia = Unconfirmed --> locate a verified source!
! Nylon = Web site www.pspglobal.com - Nylon - Material Technical Data
SELECT CASE (MATERL)
  CASE ("ALUMINA")
    TMELT = 1973.15D0
  CASE ("ZIRCONIA")
    TMELT = 1773.15D0
  CASE ("MULLITE")
    TMELT = 2101.15D0
  CASE ("NYLON")
    TMELT = 523.15D0
END SELECT

IF (MAXELEM .GT. TMELT) THEN
  WRITE(*,*)'Material melting temperature has been exceeded!'
  WRITE(9,*)'Material melting temperature was exceeded in ',TIME,&
    'seconds.'
  STOP
ENDIF

TIME = TIME + DT

RETURN
END
```

---

**SSChek.f90:**

```
!-----!
! Brian McConnell   7/10/99       Absoft Pro Fortran Compiler
!
! Purpose: This routine checks to see if steady state has been reached.
! If the temperature change of any element is greater than the max
! permissible change (DIFFSS) then the program continues to iterate.
!-----!
SUBROUTINE
SSChek(TIME,LSTOP,NAC,ITIME,NTIME,TSS,TP,NUMBR,NUM2,&
      INFLAG,DIFFSS,IAMSS)
IMPLICIT DOUBLE PRECISION(A-H,O-Z)
PARAMETER(L=201,LL=9)
DIMENSION TP(L,LL),TSS(L,LL)
```

!-----!

IAMSS = 0

! Write the new time step to the screen so that the user can

! see the progress.

WRITE(\*,100) TIME

LSTOP = 0

NAC = NAC+1

ITIME = ITIME + 1

IF (ITIME.EQ.NTIME) THEN

ERSSM=(ABS(TSS(1,1)-TP(1,1)))/TP(1,1)

DO II=1,NUMBR

DO J=1,NUM2

ERSS=ABS(TSS(IL,J)-TP(IL,J))/TP(IL,J)

IF (ERSS.GT.ERSSM) THEN

ERSSM=ERSS

ENDIF

ENDDO

ENDDO

! Check to see if steady state has been reached (temperature

! change from the previous time step is within tolerance).

! If the "Input File" option is being used, skip this step

! and stop when the end of the data file is reached.

IF (INFLAG .EQ. 0) THEN

IF (ERSSM.LT.DIFFSS) THEN

IAMSS = 1

GOTO 200

ENDIF

ITIME = 0

DO II=1,NUMBR

DO J=1,NUM2

TSS(IL,J) = TP(IL,J)

ENDDO

ENDDO

ENDIF

ENDIF

100 FORMAT(F9.3)

200 RETURN

END

---

**DataOut.f90:**

!-----!

! Brian McConnell 7/10/99

Absoft Pro Fortran Compiler

```

!
! Purpose: This routine takes care of the details at the end of the
! main computer loop; it writes the data to the output file at the end
! of each 1-second time interval, checks for the end of the input file
! if that mode is being used, and it resets the stored temperatures for
! the next loop.
!-----!
SUBROUTINE
DataOut(ITCOUNT,TIME,EBAR,POWABS,POWLOST,MAXSURF,MAXELEM,&
        MN,N,TP,EFIELD,EFIELD2,loss,INFLAG,POW,V,T,&
        IAMDONE,DT,NUMBR,NUM2)
IMPLICIT DOUBLE PRECISION(A-H,O-Z)
PARAMETER(L=201,LL=9)
DIMENSION TP(L,LL),T(L,LL),EFIELD(40),EFIELD2(40)
DOUBLE PRECISION MAXELEM,MAXSURF
!-----!
DIFFT = ITCOUNT - TIME
IAMDONE = 0
IF (DIFFT .LE. DT) THEN
  WRITE(9,100) ITCOUNT,EBAR,POWABS,POWLOST,MAXSURF,MAXELEM
  DO I=MN+1,MN+N
    IF (loss .EQ. 1) THEN
      IF (INFLAG .NE. 1) THEN
        WRITE(9,101) EFIELD2(I-MN),TP(I,1),TP(I,2),TP(I,3),&
          TP(I,4),TP(I,6),TP(I,7),TP(I,8),TP(I,9)
      ELSE
        WRITE(9,102) EFIELD2(I-MN),TP(I,9)
      END IF
    ELSE
      IF (INFLAG .NE. 1) THEN
        WRITE(9,101) EFIELD(I-MN),TP(I,1),TP(I,2),TP(I,3),&
          TP(I,4),TP(I,6),TP(I,7),TP(I,8),TP(I,9)
      ELSE
        WRITE(9,102) EFIELD(I-MN),TP(I,9)
      END IF
    END IF
  ENDDO

  WRITE(9,*)
  ITCOUNT = ITCOUNT + 1

  IF (INFLAG .EQ. 1) THEN
    READ(7,*) POW, V
! The last line in the data file must have 1234567.8 as the power
! so that the FORTRAN code stops and doesn't try to read past the
! end of the data file.

```

```

      IF (POW .EQ. 1234567.8) THEN
        IAMDONE = 1
      ENDIF
    ENDIF
  ENDIF
ENDIF

! Now update the values stored in the temperature array with the
! newly found temperatures.
DO II=1,NUMBR
  DO J=1,NUM2
    T(II,J)=TP(II,J)
  ENDDO
ENDDO

100 FORMAT(I5,1X,F9.2,1X,F6.2,1X,F8.6,1X,F7.2,1X,F7.2)
101 FORMAT(F8.1,1X,F7.2,1X,F7.2,1X,F7.2,1X,F7.2,1X,F7.2,1X,&
          F7.2,1X,F7.2,1X,F7.2)
102 FORMAT(F8.1,1X,F7.2)

RETURN
END

```

---

**LastOut.f90:**

```

!-----!
! Brian McConnell   7/10/99       Absoft Pro Fortran Compiler
!
! Purpose: This routine writes the final pieces of data to the output
! file after steady state has been reached.
!-----!
SUBROUTINE
LastOut(loss,ITCOUNT,EBAR,POWABS,POWLOST,MAXSURF,MAXELEM,&
        MN,N,INFLAG,TP,EFIELD,EFIELD2)
IMPLICIT DOUBLE PRECISION(A-H,O-Z)
PARAMETER(L=201,LL=9)
DIMENSION TP(L,LL),EFIELD(40),EFIELD2(40)
DOUBLE PRECISION MAXSURF,MAXELEM
!-----!
WRITE(9,100) ITCOUNT,EBAR,POWABS,POWLOST,MAXSURF,MAXELEM
DO 780 I=MN+1,MN+N
  IF (loss .EQ. 1) THEN
    IF (INFLAG .NE. 1) THEN
      WRITE(9,101) EFIELD2(I-MN),TP(I,1),TP(I,2),TP(I,3),TP(I,4),&
        TP(I,6),TP(I,7),TP(I,8),TP(I,9)
    ELSE
      WRITE(9,102) EFIELD2(I-MN),TP(I,9)
    END IF
  END IF

```

```

ELSE
  IF (INFLAG .NE. 1) THEN
    WRITE(9,101) EFIELD(I-MN),TP(I,1),TP(I,2),TP(I,3),TP(I,4),&
      TP(I,6),TP(I,7),TP(I,8),TP(I,9)
  ELSE
    WRITE(9,102) EFIELD(I-MN),TP(I,9)
  END IF
END IF
780 CONTINUE
WRITE(9,*)
WRITE(9,*) '*****'

WRITE(9,*) ITCOUNT
CLOSE(9)

100 FORMAT(I5,1X,F9.2,1X,F6.2,1X,F8.6,1X,F7.2,1X,F7.2)
101 FORMAT(F8.1,1X,F7.2,1X,F7.2,1X,F7.2,1X,F7.2,1X,F7.2,1X,&
  F7.2,1X,F7.2,1X,F7.2)
102 FORMAT(F8.1,1X,F7.2)

RETURN
END

```

---

**Cal.f90:**

```

!-----!
! Purpose: Computes the thermal conductivity for Alumina given the
! temperature (X) in Kelvin.
!-----!
FUNCTION CAL(X)
IMPLICIT DOUBLE PRECISION(A-H,O-Z)
!-----!
CAL=0.55D0*(6.788D+3/(X-125.0D0)+(3.562D-33)*X**10)

RETURN
END

```

---

**Cap1.f90:**

```

!-----!
! Purpose: Determines the specific heat of Alumina given the
! temperature in Kelvin.
!-----!
FUNCTION CAP1(T)
IMPLICIT DOUBLE PRECISION(A-H,O-Z)
DIMENSION A(6)
DATA A/-210.672D0,5.1956D0,-7.95646D-03,6.23173D-06,&
  -2.40174D-09,3.61348D-13/

```

```

!-----!
SUMM = 0.0D0
DO I=1,5
  SUMM = T*(SUMM+A(7-I))
ENDDO
CAP1=SUMM+A(1)

RETURN
END

```

---

### Cap2.f90:

```

!-----!
! Purpose: Determines the specific heat of Zirconia given the
! temperature in Kelvin.
!-----!
FUNCTION CAP2(T)
IMPLICIT DOUBLE PRECISION(A-H,O-Z)
!-----!
CAP2=(0.1524D0+2.98D-05*(T-273.15D0)-10.633D0/T)*4.184D3

RETURN
END

```

---

### Cap3.f90

```

!-----!
! Purpose: Determines the specific heat of Mullite given the
! temperature in Kelvin.
!-----!
FUNCTION CAP3(T)
IMPLICIT DOUBLE PRECISION(A-H,O-Z)
!-----!
T1 = T-273.0D0
CAP3 = 139.01D0*LOG(T1) + 286.68D0

RETURN
END

```

---

### Cap4.f90

```

!-----!
! Purpose: Determines the specific heat of nylon (J/kg*K) given the
! temperature in degrees Kelvin.
!-----!
FUNCTION CAP4(T)
IMPLICIT DOUBLE PRECISION(A-H,O-Z)
!-----!
A = -6d-6

```

```

B = 8.9d-3
C = -5.0028d0
D = 1.2388d3
E = 1.12178d5
CAP4 = A*T**4 + B*T**3 + C*T**2 + D*T + E

```

```

RETURN
END

```

---

**Cmu.f90:**

```

!-----!
! Purpose: Determines the thermal conductivity of Mullite given the
! temperature in Kelvin.
!-----!
FUNCTION CMU(T)
IMPLICIT DOUBLE PRECISION(A-H,O-Z)
DIMENSION X(16),Y(16)
DATA X/25.0D0,100.0D0,200.0D0,300.0D0,400.0D0,500.0D0,600.0D0,&
      700.0D0,800.0D0,900.0D0,1.0D3,1.1D3,1.2D3,1.3D3,1.4D3,1.5D3/
DATA Y/5.68D0,5.21D0,4.73D0,4.26D0,4.15D0,4.0D0,3.75D0,3.55D0,&
      3.48D0,3.39D0,3.35D0,3.42D0,3.47D0,3.47D0,3.41D0,3.35D0/
!-----!
T3=T-273.0D0
N=16-1
IF (T3.GE.X(N+1)) THEN
  SLOPE = (Y(N+1)-Y(N)) / (X(N+1)-X(N))
  W = Y(N+1)-SLOPE*X(N+1)
  CMU = SLOPE*T3+W
ENDIF

IF (T3.LT.X(1)) THEN
  CMU = 5.68D0
ENDIF

DO I=1,N
  IF (T3.EQ.X(I)) THEN
    CMU = Y(I)
  ELSEIF (T3.GT.X(I).AND.T3.LT.X(I+1)) THEN
    CMU = Y(I)+(T3-X(I))*(Y(I+1)-Y(I))/(X(I+1)-X(I))
  ENDIF
ENDDO

RETURN
END

```

---

**Cny.f90:**

```

!-----!
! Purpose: Determines the thermal conductivity for Nylon given the
! temperature in Kelvin, only fits data at temperatures above 100 K.
!-----!
FUNCTION CNY(T)
IMPLICIT DOUBLE PRECISION(A-H,O-Z)
!-----!
S = 2.5d-4
B = 2.25d-1
CNY=S*T + B

RETURN
END

```

---

**Czr.f90:**

```

!-----!
! Purpose: Determines the thermal conductivity of Zirconia given the
! temperature (X) in Kelvin. Assumes a reference temperature of 273 K.
!-----!
FUNCTION CZR(X)
IMPLICIT DOUBLE PRECISION(A-H,O-Z)
!-----!
CZR=7.741D-05*(X-273.0D0)+0.13065D0

RETURN
END

```

---

**Emiss.f90:**

```

!-----!
! Purpose: This will compute the emissivity of Aluminum Oxide
! with respect to Temperature (K)
!-----!
FUNCTION EMISS(T)
IMPLICIT DOUBLE PRECISION(A-H,O-Z)
!-----!
IF (T.LT.400.0D0) THEN
    EMISS = 0.78D0
ELSEIF (T.LT.1500.0D0) THEN
    EMISS = T*(-3.45455D-4) + 9.181818D-1
ELSE
    EMISS = 0.4D0
ENDIF

RETURN
END

```

EMISSM.f90:

```
!-----!  
! Brian McConnell   7/10/99       Absoft Pro Fortran Compiler  
!  
! Purpose: This will compute the total emissivity of MULLITE with  
! respect to temperature (K). This function is based on plotted data  
! by W. Bauer and R. Steinhardt as published in Gas Wärme  
! International (a German journal), v 39 # 9 September, 1990, p 388-391  
!-----!
```

```
FUNCTION EMISSM(T)  
IMPLICIT DOUBLE PRECISION(A-H,O-Z)
```

```
!-----!  
ITEMP = NINT(T)  
SELECT CASE (ITEMP)  
CASE (:300)  
    EMISSM = 0.96  
CASE (301:400)  
    SLOPE = (0.933-0.96)*0.01  
    ADD = (ITEMP-301)*SLOPE  
    EMISSM = 0.96+ADD  
CASE (401:500)  
    SLOPE = (0.9-0.933)*0.01  
    ADD = (ITEMP-401)*SLOPE  
    EMISSM = 0.933+ADD  
CASE (501:600)  
    SLOPE = (0.84-0.9)*0.01  
    ADD = (ITEMP-501)*SLOPE  
    EMISSM = 0.9+ADD  
CASE (601:700)  
    SLOPE = (0.773-0.84)*0.01  
    ADD = (ITEMP-601)*SLOPE  
    EMISSM = 0.84+ADD  
CASE (701:800)  
    SLOPE = (0.713-0.773)*0.01  
    ADD = (ITEMP-701)*SLOPE  
    EMISSM = 0.773+ADD  
CASE (801:900)  
    SLOPE = (0.653-0.713)*0.01  
    ADD = (ITEMP-801)*SLOPE  
    EMISSM = 0.713+ADD  
CASE (901:1000)  
    SLOPE = (0.61-0.653)*0.01  
    ADD = (ITEMP-901)*SLOPE  
    EMISSM = 0.653+ADD  
CASE (1001:1100)  
    SLOPE = (0.56-0.61)*0.01
```

```

      ADD = (ITEMP-1001)*SLOPE
      EMISSM = 0.61+ADD
CASE (1101:1200)
      SLOPE = (0.533-0.56)*0.01
      ADD = (ITEMP-1101)*SLOPE
      EMISSM = 0.56+ADD
CASE (1201:1300)
      SLOPE = (0.507-0.533)*0.01
      ADD = (ITEMP-1201)*SLOPE
      EMISSM = 0.533+ADD
CASE (1301:1400)
      SLOPE = (0.473-0.507)*0.01
      ADD = (ITEMP-1301)*SLOPE
      EMISSM = 0.507+ADD
CASE (1401:1500)
      SLOPE = (0.46-0.473)*0.01
      ADD = (ITEMP-1401)*SLOPE
      EMISSM = 0.473+ADD
CASE (1501:1600)
      SLOPE = (0.437-0.46)*0.01
      ADD = (ITEMP-1501)*SLOPE
      EMISSM = 0.46+ADD
CASE (1601:1700)
      SLOPE = (0.423-0.437)*0.01
      ADD = (ITEMP-1601)*SLOPE
      EMISSM = 0.437+ADD
CASE (1701:1800)
      SLOPE = (0.41-0.423)*0.01
      ADD = (ITEMP-1701)*SLOPE
      EMISSM = 0.423+ADD
CASE (1801:1900)
      SLOPE = (0.4-0.41)*0.01
      ADD = (ITEMP-1801)*SLOPE
      EMISSM = 0.41+ADD
CASE (1901:)
      EMISSM = 0.4
END SELECT

RETURN
END

```

---

**EMISSZ.f90:**

!-----!

! Purpose: This will compute the emissivity of Zirconia with respect to

! Temperature (K).

! THIS FUNCTION IS FOR ALUMINA EMISSIVITY AND NEEDS TO BE

! REPLACED AS SOON AS A MORE SUITABLE FUNCTION IS AVAILABLE.

!-----!

FUNCTION EMISSZ(T)  
IMPLICIT DOUBLE PRECISION(A-H,O-Z)

!-----!

IF (T.LT.400.0D0) THEN  
 EMISSZ = 0.78D0  
ELSEIF (T.LT.1500.0D0) THEN  
 EMISSZ = T\*(-3.45455D-4) + 9.181818D-1  
ELSE  
 EMISSZ = 0.4D0  
ENDIF

RETURN  
END

---

**EMISSNY.f90:**

!-----!

! Purpose: This will compute the emissivity of nylon with respect to  
! Temperature (K). Data obtained through experiment on nylon tow fiber  
! from DuPont and from reference data.

!-----!

FUNCTION EMISSNY(T)  
IMPLICIT DOUBLE PRECISION(A-H,O-Z)

!-----!

IF (T.LT.433.0D0) THEN  
 EMISSNY = T\*(1.626D-3) + 2.408D-1  
ELSE  
 EMISSNY = 0.95D0  
ENDIF

RETURN  
END

---

**EPA.f90:**

!-----!

! Purpose: Determines the real portion of the complex permittivity  
! (epsilon prime, e') of Alumina given the temperature in Kelvin.  
! The function is a linear fit to data taken at LANL.

!-----!

FUNCTION EPA(T1)  
IMPLICIT DOUBLE PRECISION (A-H,O-Z)

!-----!

EPA = (2.0D-3 \* T1) + 6.3712D0

RETURN

END

---

**EPMU3.f90:**

!-----!  
! Purpose: Determines the real portion of the complex permittivity  
! (epsilon prime, e') of Mullite given the temperature in Kelvin.  
! The function is a quadratic polynomial fit to data taken at LANL.  
!-----!

FUNCTION EPMU3(T1)  
IMPLICIT DOUBLE PRECISION (A-H,O-Z)  
!-----!  
EPMU3 = (2.0D-6 \* T1\*\*2) - 5.0D-4 + 6.0638D0

RETURN  
END

---

**Epn.f90:**

!-----!  
! Purpose: Computes the dielectric constant (epsilon') for nylon given  
! the temperature in Kelvin.  
! Data of Huang, J. Mw. P. 11, 305 (1976) at 3 GHz  
!-----!

FUNCTION epn(t)  
IMPLICIT DOUBLE PRECISION(A-H,O-Z)  
DIMENSION a(4)  
DATA a/1.25891d0,3.75069d-02,-2.88218d-04,8.32581d-07/  
!-----!

x=t-273.15d0  
IF (x.LT.1.d+02) THEN  
  x=1.d+02  
ENDIF

epn=0.0d0  
DO i=1,3  
  epn=(epn+a(5-i))\*x  
ENDDO

epn=a(1)+epn

return  
end

---

**Eppa.f90:**

!-----!  
! Purpose: Computes the dielectric loss (epsilon'') for Alumina.  
! Polynomial fit to the data of Cross and Binner.

! Measurements were made on LANL samples sent summer '94

!-----!

FUNCTION EPPA(T)

IMPLICIT DOUBLE PRECISION(A-H,O-Z)

DIMENSION B(2)

DATA B/-.01400,3.3333D-04/

DATA TREF/2.73D+02/

!-----!

BASE=3.0D-02

XX=T-TREF

IF (XX.LE.6.0D+02) THEN

    EPPA=(0.06000D0-BASE)\*(XX/6.0D+02)\*\*2+BASE

    RETURN

ELSE

    EPPA=B(1)+B(2)\*XX

ENDIF

RETURN

END

---

### **Eppmu3.f90:**

!-----!

! Purpose: Determines the dielectric loss (epsilon") for Mullite

! given the temperature in Kelvin.

!-----!

FUNCTION EPPMU3(T1)

IMPLICIT DOUBLE PRECISION(A-H,O-Z)

DIMENSION X(11),Y(11)

DATA X/29.0D0,35.0D0,149.0D0,262.0D0,371.0D0,478.0D0,&  
      582.0D0,684.0D0,784.0D0,881.0D0,1068.0D0/

DATA Y/.055072D0,.053715D0,.074384D0,.10478D0,.13966D0,&  
      .17293D0,.22339D0,.34055D0,.40787D0,.62712D0,1.1451D0/

!-----!

T=T1-273.0D0

N=11-1

IF (T.GE.X(N+1)) THEN

    SLOPE = (Y(N+1)-Y(N)) / (X(N+1)-X(N))

    W = Y(N+1)-SLOPE\*X(N+1)

    EPPMU3 = SLOPE\*T+W

ENDIF

IF (T.LT.X(1)) THEN

    EPPMU3 = 0.048D0

ENDIF

DO I=1,N

```

IF (T.EQ.X(I)) THEN
  EPPMU3 = Y(I)
ELSEIF (T.GT.X(I).AND.T.LT.X(I+1)) THEN
  EPPMU3 = Y(I)+(T-X(I))*(Y(I+1)-Y(I))/(X(I+1)-X(I))
ENDIF
ENDDO

RETURN
END

```

---

**Eppn.f90:**

```

!-----!
! Purpose: Computes dielectric constant epsilon” for nylon
! Data of Huang, J. Mw. P. 11, 305 (1976) at 3 GHz
!-----!
FUNCTION eppn(t)
IMPLICIT DOUBLE PRECISION(A-H,O-Z)
DIMENSION a(5)
DATA a/0.100835d0,-6.36079d-03,1.80047d-04,-1.84848d-06,&
      7.13255d-09/
!-----!
x=t-273.15d0
IF (x.LT.45.0) THEN
  x=4.5d+01
ENDIF

eppn=0.0d0
DO i=1,4
  eppn=(eppn+a(6-i))*x
ENDDO

eppn=a(1)+eppn

RETURN
END

```

---

**Eppnzs.f90:**

```

!-----!
! Purpose: Determines the dielectric loss (epsilon”) for Zirconia
! given the temperature in Kelvin.
!-----!
FUNCTION EPPZR(T)
IMPLICIT DOUBLE PRECISION(A-H,O-Z)
DIMENSION X(16),Y(16)
DATA X/700.0D0,100.4D+1,103.0D+1,106.2D+1,109.0D+1,110.5D+1,&
      113.0D+1,113.5D+1,114.2D+1,114.5D+1,114.6D+1,115.5D+1,&

```

```

121.2D+1,124.9D+1,126.8D+1,128.0D+1/
DATA Y/0.10D0,3.05D0,3.05D0,3.05D0,3.1D0,3.15D0,3.2D0,3.45D0,&
3.75D0,4.0D0,4.75D0,5.8D0,6.4D0,6.85D0,8.9D0,14.25D0/
!-----!
T3=T-273.0D0
N=16-1
IF (T3.GE.X(N+1)) THEN
  SLOPE = (Y(N+1)-Y(N)) / (X(N+1)-X(N))
  W = Y(N+1)-SLOPE*X(N+1)
  EPPZR = SLOPE*T3+W
ENDIF

IF (T3.LT.X(1)) THEN
  EPPZR = 0.10D0
ENDIF

DO I=1,N
  IF (T3.EQ.X(I)) THEN
    EPPZR = Y(I)
  ELSEIF (T3.GT.X(I).AND.T3.LT.X(I+1)) THEN
    EPPZR = Y(I)+(T3-X(I))*(Y(I+1)-Y(I))/(X(I+1)-X(I))
  ENDIF
ENDDO

RETURN
END

```

---

**EPZR.f90:**

```

!-----!
! Purpose: Determines the dielectric constant (epsilon') for Zirconia
! given the temperature in Kelvin. The function is a fourth order
! polynomial fit to LANL data.
!-----!
FUNCTION EPZR(T1)
IMPLICIT DOUBLE PRECISION (A-H,O-Z)
!-----!
EPZR = 4.0D-12*(T1**4) - 1.0D-8*(T1**3) +&
2.0D-5*(T1**2) - 7.6D-3*(T1) + 3.0623D0

RETURN
END

```

---

**Hc2.f90:**

```

!-----!
! Purpose: Computes the convective heat transfer coefficient (hc2)

```

! for a vertical cylinder.

```
!-----!  
FUNCTION HC2(T,LENG,TINF)  
IMPLICIT DOUBLE PRECISION(A-H,O-Z)  
DOUBLE PRECISION K,NUS2,NUS2B,LENG  
!-----!  
IF (T.GT.TINF+3.0D0) THEN  
  G = 9.81D0  
  T1 = T - 273.0D0  
  TF = ((TINF-273.0D0)+T1)/2.0D0  
  PR = .71D0  
  K = 5.05D-12*TF**3.0D0 - 2.33D-8*TF**2.0D0 + 7.07D-5*TF + .0237D0  
  V = -2.81D-14*TF**3.0D0 + 1.07D-10*TF**2.0D0 + 8.8D-8*TF + 1.38D-5  
  TF = TF + 273.0D0  
  GRL = G*(1.0D0/TF)/(V**2) * LENG**3 * (T-TINF)  
  NUS2 = 0.68D0 * PR**(.5) * GRL**(.25) / (.952+PR)**(.25)  
  NUS2B = 2.0D0/(LOG(1.0D0+2.0D0/NUS2))  
  HC2 = NUS2B * K/LENG  
ELSE  
  HC2 = 5.0D0  
ENDIF  
  
RETURN  
END
```

---

**Q.f90:**

```
!-----!  
! Purpose: Determines the volumetric heat generated by the element.  
! E is the magnitude of the tangential component of the Electric field  
! at the element being processed. T it the element temperature.  
! EPS is the imaginary component of the element permittivity.  
! function returnd Q.  
!-----!  
FUNCTION Q(T,E,F,EPS)  
IMPLICIT DOUBLE PRECISION(A-H,O-Z)  
!-----!  
PI = 3.1415926D0  
EO = 8.854D-12  
! CONVERT Frequency from GHz TO Hz  
FRQ = F * 1.0d+9  
Q=(2.0D0*PI*FRQ*EO*EPS)*(E**2)  
  
RETURN  
END
```

# Appendix B

## Field Simulation Code

---

### Combined.f90:

```
!-----!  
! This code was originally created by Nathan Terril. His two programs  
! "modeprg" and "edist" have been combined and extensively modified in  
! order to incorporate them into the heat transfer model originally  
! designed by C. Goodson. Instead of working as a stand-alone  
! program, the field simulation now is a subroutine to be called from  
! within another program and no longer requires input and output files.  
! Changes to the original programs include requiring the solution of  
! the "combined" problem and removing the portions that dealt only with  
! the "aperture" or "fiber" problems. The sections of "edist" were  
! modified to only solve for the required y-line tangential electric  
! field distribution instead of the other possible distributions.  
!  
! Purpose: This subroutine is passed the required variables such as  
! source frequency, cavity and iris dimensional information, and the  
! complex permittivity distribution of the material in the cavity. The  
! output is the distribution of the tangential electric field component  
! along the material in the cavity. This information is then applied  
! in the heat transfer model.  
!  
! Variables: (commented by Nathan Terril)  
!     mtot and ntot are the number of waveguide unknowns in x and y,  
!     respectively.  
!     ptot and qtot are the number of Green's function unknowns in  
!     x and y, respectively.  
!     The solution will not converge if proper values of the above  
!     four vales are not selected.  
!     d2lg is the ratio d/lg, where d is the cavity length and lg  
!     is the guide wavelength  
!     lg2a is the ratio lg/a, where a is the width of the guide  
!     (x-direction) in meters  
!     b is the height (y-direction) of the guide in meters  
!     d0 is the location of the axis of the rod in the z-direction  
!     t2a is the ratio t/a, where t is the diameter of the rod  
!     x2a is the ratio x/a, where x is the location of the center
```

```

!      axis of the rod in the range [0,a]
!      c2a and v2b are the ratios c/a and v/b, the width and height of
!      the aperture normalized to the width and height
!      of the guide
!      Af is the cross-sectional area of the rod
!
! Additional Variables: (commented by Brian McConnell)
! ismp,isnq = The sine components of the aperture integrals.
! itmp,itnq = The cosine components of the aperture integrals.
! Mp = M+ is the first M matrix appearing in equation (2.3.76) on p.32
!   of Terril's thesis. Its elements are built from the formulae
!   in the left column of equation (2.3.77) on p.33.
! Mm = M- is the second M matrix appearing in equation (2.3.76) on p.32
!   of Terril's thesis. Its elements are built from the formulae
!   in the right column of equation (2.3.77) on p.33.
! indx = Used in the "ludcmp" subroutine called below, indx(1:n) is an
!   output vector that records the row permutation effected by the
!   partial pivoting.
! Bphe = The (Bh+ and Be+) partitioned matrix in the form shown on
!   p. 37 of Terril's thesis that stores the mode coefficients of
!   the forward traveling TE and TM modes in the waveguide region
!   between the aperture and the fiber.
! Bmhe = The (Bh- and Be-) partitioned matrix similar to Bphe as
!   described above, but for the backward traveling modes.
! fmat = The forcing vector [F] on p.39 of Terril's thesis
! Intp = The integral in y over the interval [0,b] of the quantity
!   { Y(y)*cos(t*pi*y/b)*cos(n*pi*y/b) }
!   This facilitates finding the mode coefficients for the
!   reflected modes from the fiber in terms of the incident modes.
! Y(y) = Determined from the permittivity distribution along the axis
!   of the rod.
! Che = The partitioned matrix to store the C region cavity mode
!   coefficients.
! Ey = The array to store the distribution of the tangential complex
!   electric field strength.
! PERM = The array to store the complex permittivity distribution of
!   the entire rod. Only the portion in the cavity is used for
!   the calculations.
! N = The number of elements within the cavity. This value has been
!   changed from its original value of 34 to the new value of 40 in
!   order to match the number of elements used in Goodson's model.
! M = Used to index the first of the total material elements in the
!   cavity so that the correct 40 elements of the permittivity
!   distribution are used out of a possible 201 elements.
!-----!
SUBROUTINE combined(mtot,ntot,ptot,qtot,c2a,v2b,t2a,loss,freq,d2lg,&

```

```

    a,b,field,PERM,M,N)
INTEGER mtot,ntot,ptot,qtot,mnt,pt,in,M,N,loss
INTEGER, ALLOCATABLE :: indx(:)
DOUBLE PRECISION a,b,mu,eps,pi,w,eta2,d2lg,lg2a,l2a,det,t2a,x2a,d,&
    c2a,v2b,d0,xp,zp,Af,field(40),PERM(2,201,9),freq
PARAMETER(pi=3.141592654D0,mu=1.256637D-6,eps=8.85178D-12,x2a=.5d0)
DOUBLE PRECISION, ALLOCATABLE :: ismp(:,:),itmp(:,:),isnq(:,:),&
    itnq(:,:)
COMPLEX*16, ALLOCATABLE :: Mp(:,:),Mm(:,:),Bpint(:,:),Bhe(:,:),&
    Bphe(:,:),Bmhe(:,:),zemn(:,:),Bres(:,:),&
    fmat(:,:),Intp(:,:),Che(:),Ey(:)
!-----!
! Compute the source frequency in radians per second from GHz.
w=2*pi*freq*1d9

! Subroutine "vals" computes parameters from user input
CALL vals(pi,w,mu,eps,eta2,a,b,d,d0,l2a,Af,t2a,d2lg,lg2a)
mnt=2*mtot*ntot
pt=2*ptot*qtot

! Subroutine "getzel" computes the wave impedance for each mode,
! incorporates loss into propagating mode(s)
ALLOCATE (zemn(0:mtot,0:ntot))
CALL getzel(zemn,mtot,ntot,w,eps,mu,pi,a,b,loss)

! Subroutine "getint" computes aperture integrals. The four arrays
! found (ismp, etc.) can be multiplied to create the integrands in
! equations (3.1.3)-(3.1.5) on p. 38-39 of Terril's thesis.
ALLOCATE (ismp(0:mtot,0:ptot),itmp(0:mtot,0:ptot),&
    isnq(0:ntot,0:qtot),itnq(0:ntot,0:qtot))
CALL getint(mtot,ptot,a,c2a,ismp,itmp,pi)
CALL getint(ntot,qtot,b,v2b,isnq,itnq,pi)

! Subroutine "getinty2" is called to solve the Intp array integral as
! described in the "Additional Variables" section above for
! non-uniform permittivity distributions. This is a modified version
! of Terril's "getinty" subroutine and changes were made to use the
! permittivity distribution passed in from the heat transfer model
! and to use the correct number of elements within the cavity.
ALLOCATE (intp(0:2*ntot))
CALL getinty2(ntot,Intp,w,eps,pi,b,PERM,M,N)

! Subroutine "getMs" is called to build the M+ and M- matrix
! elements in section 2.3.6 in Terril's thesis.
ALLOCATE (Mp(mnt,mnt),Mm(mnt,mnt),indx(mnt))
CALL getMs(w,eps,pi,eta2,x2a,Af,a,b,d,d0,mtot,ntot,zemn,Mp,Mm,&

```

```
      indx,mnt,Intp)
DEALLOCATE(Intp)
```

```
!-----!
```

```
! The following section, set apart by the dashed lines, is sufficiently
! different from the solution outlined in Terril's thesis that it
! is worthy of further explanation. The following comments are
! appended by Terril, the original author of the code:
```

```
!
```

```
!!!!!!!!!!!!!!!!!!!!!!!!!!!!!!!!!!!!!!!!!!!!!!!!!!!!!!!!!!!!!!!!!!!!!!!!!!!!
```

```
! The equation to be solved is  $[A][X]=[F]$  (see p.39). The coefficient
! matrix  $[A]$  is the product of two matrices. The first matrix is the
! result of the "getmatn" subroutine. The second matrix is the
! coefficient matrix  $[T]^{-1}[D]$ . Let the first matrix be called  $[Bhe]$ 
! as it is in the argument to the getmatn function.
! Eqn. (3.1.4) on p.39 is  $[Bhe][B]=[F]$ .
! The  $[B]$  on p.53 ( $[B]=[T]^{-1}[D][a]$ ) is substituted into eqn. (3.1.4).
!  $[a]$  is the set of unknowns to be solved for. The product  $[T]^{-1}[D]$ 
! is the result of "getapm".  $[Bhe]$ , the result of "getmatn", is
! multiplied by  $[B]$  to give  $[Bhe][T]^{-1}[D][a]$ , where  $[Bhe][T]^{-1}[D]=[A]$ 
! and  $[a]=[X]$  in the equation  $[A][X]=[F]$ .  $[F]$  is filled by the
! subroutine "getf". LU decomposition and backsubstitution is then
! performed to solve for the  $[X]$  or  $[a]$  coefficients.
```

```
!!!!!!!!!!!!!!!!!!!!!!!!!!!!!!!!!!!!!!!!!!!!!!!!!!!!!!!!!!!!!!!!!!!!!!!!!!!!
```

```
! Subroutine "getapm" fills the  $[D]$  matrix in equation (3.1.5) on p.39
! of Terril's thesis and returns the product  $[T]^{-1}[D]$  as described on
! p.53.
```

```
      ALLOCATE (Bpint(mnt,pt))
      CALL getapm(mtot,ntot,ptot,qtot,a,b,zemn,ismp,itmp,ismq,itnq,&
                pi,Mm,indx,mnt,pt,Bpint)
      DEALLOCATE(indx,Mm)
```

```
! Subroutine "getmatn" fills the  $[A]$  matrix in equation (3.1.5) on
! p.39 of Terril's thesis which is called  $[Bhe]$  in this code.
```

```
      ALLOCATE (Bhe(pt,mnt))
      CALL getmatn(Bhe,mtot,ntot,ptot,qtot,a,b,ismp,itmp,ismq,itnq,&
                pi,eta2,zemn)
```

```
! Subroutine "getf" fills the forcing vector  $[F]$  shown in equation
! (3.1.5) on p.39 of Terril's thesis.
```

```
      ALLOCATE (fmat(pt,1))
      CALL getf(fmat,mtot,ntot,ptot,qtot,zemn(1,0),eta2,ismp,itnq,pi,&
              a)
      DEALLOCATE(ismp,itmp,ismq,itnq)
```

! Subroutine "mult" is called to perform the matrix multiplication  
! of "Bhe" and "Bpint" to create the matrix "Bres"  
ALLOCATE (Bres(pt,pt))  
CALL mult(Bhe,Bpint,Bres,pt,mnt,pt)  
DEALLOCATE(Bhe)

! Subroutine "ridcol" is called to check the "Bres" matrix to ensure  
! any zero rows are replaced with ones before going to the  
! LU decomposition subroutine. This is in order to prevent accidental  
! "singular matrix" errors.  
CALL ridcol(Bres,pt)

! Subroutine "ludcmp", when given a matrix [a(1:n,1:n)], this routine  
! replaces it by the LU decomposition of a rowwise permutation of  
! itself. These two LU subroutines are called to solve matrix equation  
! (3.1.5) in Terril's thesis. This is to find the values of the  
! "expansion function amplitudes [ap]" in equation (3.1.3) in Terril's  
! thesis by solving the matrix equation (3.1.5) on p. 39.  
! This is in order to find the B mode coefficients.  
ALLOCATE (indx(pt))  
CALL ludcmp(Bres,pt,pt,indx,det)

! Subroutine "lubksb" solves the set of n linear equations  $AuX = B$ .  
! Here, "a" is input, not as the matrix "A" but rather as its  
! LU decomposition, determined by the routine "ludcmp".  
CALL lubksb(Bres,pt,pt,indx,fmt)  
DEALLOCATE(indx,Bres)

!-----!

! Subroutine "mult" is called to perform the matrix multiplication of  
! "Bpint" and "fmat" to create the matrix "Bphe", which contains the  
! mode coefficients for the forward traveling waves in waveguide  
! region B.  
ALLOCATE (Bphe(mnt,1))  
CALL mult(Bpint,fmat,Bphe,mnt,pt,1)  
DEALLOCATE(fmat,Bpint)

! Subroutine "mult" is called to perform the matrix multiplication of  
! "Mp" and "Bphe" to create the matrix "Bmhe", which contains the  
! mode coefficients for the backward traveling waves in waveguide  
! region B. This is expressed as equation (2.3.78) on p.53 of Terril's  
! thesis.  
ALLOCATE (Bmhe(mnt,1))  
CALL mult(Mp,Bphe,Bmhe,mnt,mnt,1)

DEALLOCATE(Mp)

!-----!  
! This would conclude the computation part of the original "modeprg"  
! program. The code used to generate an output file to be used later  
! by the "edist" program.  
! The following code sections are from the original program "edist."  
! This generates points for the magnitude of the y-component of  
! the electric field for only the "y-line" distribution.  
!-----!

! Instead of calling "getdata" we'll call a new routine "gdata"  
! This was done in order to eliminate the un-used sections in the  
! original version "getdata" which do not contribute to the current  
! problem. This subroutine finds the mode coefficients for the cavity  
! region, "C".

ALLOCATE(Che(mnt))  
CALL gdata(Bphe,Bmhe,Che,zemn,eps,w,a,d,d0,xp,zp,mtot,ntot,mnt)

! Instead of calling "getey" we'll call a new routine "gcey" which is  
! done for the same reason as using "gdata" instead of "getdata".  
! This subroutine uses the mode coefficients to solve for the  
! distribution of the tangential component of the electric field along  
! the fiber.

ALLOCATE(Ey(N))  
CALL gcey(Bphe,Bmhe,Che,Ey,zemn,eps,pi,w,a,b,d,d0,xp,yp,zp,mtot,&  
ntot,mnt,N)

! Now we call the final subroutine "fieldmag" to convert the complex  
! tangential electric field distribution into an array of real-valued  
! magnitudes to be returned to the heat transfer model.

CALL fieldmag(Ey,field,N)  
DEALLOCATE(Bphe,Bmhe,Che,zemn,Ey)

RETURN  
END

---

**Vals.f90:**

!-----!  
! Additional comments added 6/28/99 by Brian McConnell  
! Original code written by Nathan Terril.  
! Purpose: The subroutine uses the particular user input parameters  
! such as a, b, d, etc. to compute several other parameters as  
! explained below.  
! Variables:  
! eta2 = Eta squared where eta is the intrinsic impedance of the

```

!      media (air) in the waveguide. The media in this case is
!      treated as ideal.
! mu = Permiability of free space, a constant.
! eps = Permittivity of free space, a constant.
! fc = Waveguide cutoff frequency (radian) for the primary TE10
!      mode.
! k = Wave number. A real value in lossless media, a complex value
!      in a lossy propagation media.
! l2a = An intermediate step to computing lg2a.
! lg2a = The ratio of the guide wavelength to the cavity width.
!      See Cheng, p.528.
! dmd0 = guide wavelength/4.
! d = Length of the cavity, meters.
! d0 = Distance from the aperture to the rod. The computed value is
!      at 1/4th the guide wavelength which puts the rod at the peak
!      of a standing wave.
! Af = The rod cross-sectional area in meters^2.
!-----!
SUBROUTINE vals(pi,w,mu,eps,eta2,a,b,d,d0,l2a,Af,t2a,d2lg,lg2a)
DOUBLE PRECISION pi,w,mu,eps,eta2,a,b,d,d0,l2a,Af,t2a,d2lg,lg2a,&
                dmd0,k,fc
!-----!
eta2=mu/eps
fc=(pi/a)/(sqrt(mu*eps)*2*pi)
k=w*sqrt(mu*eps)
l2a=2*pi/(k*a)
lg2a=l2a/sqrt(1d0-(l2a/2d0)**2)
dmd0=1d0*lg2a*a/4d0
d=d2lg*lg2a*a
! Sets d0 at resonant peak 3/4 wavelength from the short
! i.e. at the second peak in the standing wave.
d0=d-dmd0
Af=pi*(.5*t2a*a)**2

RETURN
END

```

---

**Getzel.f90:**

```

!-----!
! Commented 6/28/99 by Brian McConnell
! Original code by Nathan Terril
!
! Purpose: This subroutine computes the values of the wave impedance
! for each of the included waveguide modes. It has the ability to
! include the effects of field losses in the longitudinal wall sections
! of the resonator cavity through a perturbational technique. This

```

```

! development can be seen on p.72 or chapter 7 in the Harrington text,
! "Time-Harmonic Electromagnetic Fields," or in greater detail on
! p.554-557 in the Rao text,"Elements of Engineering Electromagnetics."
!
! Variables:
! k2 = k^2, the square of the wave number.
! kcmn2 = kc^2, the square of the cutoff wave number for each mode,
!   designated by (mn).
! fc2f2 = The square of the ratio of the waveguide cutoff frequency
!   to the source frequency, (fc/f)^2.
! arg = Used to determine if the particular (mn) mode is evanescent
!   (non-propagating) or propagating.
! kzmn = The mode propagation constant, kz, for each (mn) mode.
! zemn = The wave impedance, z, for each TM(mn) mode. See p.152 in
!   the Harrington text mentioned above.
!-----!
SUBROUTINE getzel(zemn,mtot,ntot,w,eps,mu,pi,a,b,loss)
DOUBLE PRECISION w,eps,pi,k2,kcmn2,a,b,arg,fc2f2,mu
INTEGER mtot,ntot,loss,im,in
COMPLEX*16 kzmn,root,zemn(0:mtot,0:ntot)
!-----!
k2=(mu*eps)*w**2
do im=0,mtot
  do in=0,ntot
    kcmn2=((im/a)**2+(in/b)**2)*pi**2
    fc2f2=kcmn2/k2
    arg=k2-kcmn2
! If arg < 0, the mode is evanescent and does not propagate.
! If arg >= 0, the mode propagates.
    if (arg.lt.0) then
      kzmn=(0,-1)*sqrt(-1*arg)
    else
      kzmn=(1,0)*sqrt(arg)
    end if
! If loss = 1, include the longitudinal cavity conductor loss into
! the wave impedance for each propagating mode via an attenuation
! factor.
    if (loss.eq.1) then
      root=kzmn/sqrt(k2)
      if (real(root).ne.0d0) then
        kzmn=kzmn-(0,1)*.03*(1+2*b/a*fc2f2)/(b*sqrt(mu/eps)*&
          sqrt(1-fc2f2))
      end if
    end if
    zemn(im,in)=kzmn/(w*eps)
  enddo
enddo

```

enddo

return

end

---

**Getint.f90:**

```
!-----!  
! Comments added 6/28/99 by Brian McConnell  
! Original code written by Nathan Terril  
!  
! Purpose: To compute the "aperture integrals" and is called for either  
! the x or y directions. The arrays filled by calling this routine in  
! both directions can be multiplied to create the integrands in  
! equations (3.1.3)-(3.1.5) on p.38-39 of Terril's thesis.  
!  
! Variables:  
! mntot = mntot when "getint" is called for the x-direction and ntot  
!       when called for the y-direction. These are the number of  
!       waveguide modes in the x and y directions, respectively.  
! pqtot = ptot or qtot, the truncation order for the basis and  
!       weighting functions used to approximate the aperture surface  
!       currents.  
! ab = a or b, the cavity width and height, respectively.  
! cv2ab = c2a or v2b, the ratios of the cavity to iris dimensions.  
! cv1 = The lower limit of integration in the "aperture integral"  
!       Designates the location of the left or lower edge of the  
!       rectangular aperture opening for the x and y directions,  
!       respectively.  
! cv2 = The upper limit of integration in the "aperture integral"  
!       Designates the location of the right or upper edge of the  
!       rectangular aperture opening for the x and y directions,  
!       respectively.  
! is = The sine terms of the integrand parts.  
! it = The cosine terms of the integrand parts.  
!-----!  
SUBROUTINE getint(mntot,pqtot,ab,cv2ab,is,it,pi)  
INTEGER mntot,pqtot,imn,ipq  
DOUBLE PRECISION cv2ab,cv1,cv2,ab,pi,s,t,is(0:mntot,0:pqtot),&  
                it(0:mntot,0:pqtot)  
!-----!  
cv1=ab*(1-cv2ab)/2d0  
cv2=ab*(1+cv2ab)/2d0  
do imn=0,mntot,1  
  do ipq=0,pqtot,1  
    is(imn,ipq)=s(imn,ipq,pi,cv1,cv2,cv2ab*ab,ab)  
    it(imn,ipq)=t(imn,ipq,pi,cv1,cv2,cv2ab*ab,ab)
```

```

    enddo
enddo

return
end

```

---

**Getinty2.f90:**

```

!-----!
! Comments added 6/28/99 by Brian McConnell
! Original code written by Nathan Terril
! Purpose: This program integrates sig*cos(i)*cos(n) over [0,b]
! analytically using a dft to calculate the coefficients of an
! exponential fourier series. Signt samples at intermediate points
! along the straight line connecting two data points.
! Variables:
! ntot = The number of n's (or i's).
! N = The number of sample points.
! L is the number of coefficients in the series.
! dN = The height of the elements by which the material is partitioned.
! npts = The number of increments into which each element is divided
!       for the piece-wise integration.
! dy = The height of each increment in the integration.
! PERM = The complex permittivity distribution of the material.
! Ta = The real component of the complex permittivity of the current
!      material element.
! Tb = The imaginary component of the complex permittivity of the
!      current material element.
! Teread = The real admittance term (Y(y)) for each element. See
!          equation (2.3.66) on p. 30 of Terrils' thesis.
! Ter = The admittance for each sub-section of the elements.
! F = The Fourier coefficients to evaluate the Isig summation. See
!     equation (3.2.3) on p. 47 of Nathan's thesis.
! Isig = It's called Intp in the main program. See equation (2.3.82)
!       on pages 34 and 47. Also eqn. (3.2.6) on page 47.
!       Once this is done, the unknown mode coefficients (amplitudes)
!       for the modes reflected from the fiber can be found
!       separately (later) in terms of the incident modes.
! ecos = See the function by the same name.
!-----!
SUBROUTINE getinty2(ntot,Isig,w,eps,pi,b,PERM,M,N)
  INTEGER il,in,ip,ik,N,ntot,npts,L
  DOUBLE PRECISION pi,Ta,Tb,b,dN,dy,w,eps,PERM
  DIMENSION PERM(2,201,9)
  PARAMETER(npts=200)
  COMPLEX*16 Teread(0:N),ecos,F(N),&
    Ter(0:N*npts)

```

```

      COMPLEX*16 Isig(0:2*ntot)
!-----!
      L=N/2
      dN=b/N
      dy=b/(N*npts)

! Read in permittivity data for the sample points
      do ik=0,N
        Ta=PERM(1,M+1+ik,9)
        Tb=PERM(2,M+1+ik,9)
        Teread(ik)=(0,1)*w*eps*(Ta-(0,1)*Tb-1d0)
      enddo

      do ik=0,N-1
        Ter(ik*npts)=Teread(ik)
        do in=1,npts-1
          Ter(ik*npts+in)=in*(Teread(ik+1)-Teread(ik))/npts+Teread(ik)
        enddo
      enddo

! Calculate expansion coefficients
      do il=-L,L-1,1
        F(il+L+1)=(0d0,0d0)
        do ik=0,N*npts-1,1
          F(il+L+1)=F(il+L+1)+1d0/b*Ter(ik)*exp(-(0,1)*2*pi/b*il*ik*dy)*dy
        enddo
      enddo

! Calculate all possible integrals
      do ip=0,2*ntot-2
        Isig(ip)=(0d0,0d0)
        do il=-L,L-1,1
          Isig(ip)=Isig(ip)+F(il+L+1)*ecos(ip,il,pi,b)
        enddo
      enddo
      return
      end

```

---

**GetMs.f90:**

```

!-----!
! Comments added 6/29/99 by Brian McConnell
! Original code written by Nathen Terril
!
! Purpose: This subroutine is called to build the M+ and M- matrix
! elements in section 2.3.6 in Terril's thesis. Once the M matrices
! are built, they can be used with the forward-traveling mode

```

```

! coefficients from the "B" region of the cavity (the B+ coefficients)
! to solve matrix equation (2.3.76) for the mode coefficients for the
! back-traveling mode coefficients in the "B" region (the B-
! coefficients).
!
! Variables:
! w = The source frequency in radians per second.
! eps = The permittivity of free space, a constant.
! pi = A constant.
! eta2 = eta^2 is the intrinsic impedance of the propagation media.
! x2a = The ratio of the rod transverse position to cavity width.
! Af = The cross-sectional area of the rod, in meters^2.
! a,b = The width and height of the cavity, in meters.
! d = The length of the cavity, in meters.
! d0 = The location of the axis of the rod in the z-direction.
! mtot,ntot = The number of included waveguide modes in the x and y
!             directions, respectively.
! zemn = The wave impedance for each waveguide mode.
! Mp = M+ is the first M-matrix appearing in equation (2.3.76) on p.32
!     of Terrils' thesis. Its' elements are built from the formulae
!     in the left column of equation (2.3.77) on p.33.
! Mm = M- is the second M-matrix appearing in equation (2.3.76) on p.32
!     of Terrils' thesis. Its' elements are built from the formulae
!     in the right column of equation (2.3.77) on p.33.
! indx = Used in the "ludcmp" subroutine called below, indx(1:n) is an
!        output vector that records the row permutation effected by the
!        partial pivoting.
! mnt = 2*mtot*ntot, just used to size arrays for indexing.
! Intp = The integral in y over the interval [0,b] of the quantity
!        { Y(y)*cos(t*pi*y/b)*cos(n*pi*y/b) }
!-----!
SUBROUTINE getMs(w,eps,pi,eta2,x2a,Af,a,b,d,d0,mtot,ntot,zemn,&
               Mp,Mm,indx,mnt,Intp)
DOUBLE PRECISION w,eps,pi,eta2,x2a,Af,a,b,d,d0,det
INTEGER mtot,ntot,mnt,im,in,ii,ij,r1,r2,c1,c2,&
        indx(mnt)
COMPLEX*16 zemn(0:mtot,0:ntot),Dp,Mp(mnt,mnt),Mm(mnt,mnt),&
        Cmni,Pmnij,Inj,flag,Intp(0:2*ntot)
!-----!
do im=1,mtot
do in=0,ntot-1
do ii=1,mtot
Cmni=4/(a*b*((im*pi/a)**2+(in*pi/b)**2))*Af*(pi/a)**2&
        *sin(ii*pi*x2a)*sin(im*pi*x2a)*im*ii
if (in.eq.0) then
Cmni=Cmni/2d0

```

```

endif
do ij=0,ntot-1
  Inj=.5*(Intp(ij+in)+Intp(abs(ij-in)))
  Pmnij=Cmni*Inj
  r1=in*mtot+im
  c1=ij*mtot+ii
  r2=mtot*(in+ntot)+im
  c2=mtot*(ij+ntot)+ii
  if ((ii.eq.im).and.(ij.eq.in)) then
    Dp=1-(0,1)*cos(w*eps*zemn(im,in)*(d0-d))/sin(w*&
      eps*zemn(im,in)*(d0-d))
    flag=1
  else
    flag=0
  endif
  Mp(r1,c1)=Pmnij-flag*Dp*zemn(im,in)/eta2
  Mp(r1,c2)=Pmnij*zemn(ii,ij)*ij*a/(ii*b)
  Mp(r2,c2)=-Mp(r1,c2)*in*a/(im*b*zemn(im,in))+flag*&
    Dp/zemn(im,in)
  Mp(r2,c1)=-Pmnij*in*a/(im*b*zemn(im,in))
  Mm(r1,c1)=Mp(r1,c1)+flag*2*zemn(im,in)/eta2
  Mm(r1,c2)=-Mp(r1,c2)
  Mm(r2,c2)=-Mp(r2,c2)+flag*2/zemn(im,in)
  Mm(r2,c1)=Mp(r2,c1)
enddo
enddo
enddo
enddo

do ii=1,mtot
  do ij=0,ntot-1
    c1=ij*mtot+ii
    c2=mtot*(ij+ntot)+ii
    do im=1,2*mtot*ntot
      Mp(im,c1)=-Mp(im,c1)*exp(-(0,1)*w*eps*d0*zemn(ii,ij))
      Mp(im,c2)=-Mp(im,c2)*exp(-(0,1)*w*eps*d0*zemn(ii,ij))
    enddo
  enddo
enddo
enddo

```

! Now Mp is -M+ ready to be premultiplied by (M-)inv  
! See equation (2.3.78) on page 33 of Terrils' thesis.

```

call ludcmp(Mm,mnt,mnt,indx,det)
do im=1,mnt
  call lubksb(Mm,mnt,mnt,indx,Mp(1,im))

```

```

enddo

do im=1,mtot
  do in=0,ntot-1
    do ii=1,mtot
      do ij=0,ntot-1
        flag=0
        if ((im.eq.ii).and.(in.eq.ij)) then
          flag=1
        endif
        r1=in*mtot+im
        c1=ij*mtot+ii
        r2=mtot*(in+ntot)+im
        c2=mtot*(ij+ntot)+ii
        Mm(r1,c1)=flag+Mp(r1,c1)*exp(-(0,1)*w*eps*d0*&
          zemn(im,in))
        Mm(r1,c2)=Mp(r1,c2)*exp(-(0,1)*w*eps*d0*zemn(im,in))
        Mm(r2,c1)=Mp(r2,c1)*exp(-(0,1)*w*eps*d0*zemn(im,in))
        Mm(r2,c2)=-flag+Mp(r2,c2)*exp(-(0,1)*w*eps*d0*&
          zemn(im,in))
      enddo
    enddo
  enddo
enddo

return
end

```

---

### Getapm.f90:

```

!-----!
! Commented 6/29/99 by Brian McConnell
! Original code written by Nathan Terril
!
! Purpose: Equation (3.3.15) on p.53 of Terril's thesis is
!  $[B]=[T]^{-1}[D][a]$ . The bulk of this subroutine is filling the matrix
!  $[D]$ . The partitioned components are given in equation (3.3.3) on
! p.49 (the matrix with the integrals). The matrix passed into the Mm
! array in the subroutine is the  $[T]$  matrix. The LU decomposition
! statement essentially sets up the inversion, and the backsubstitution
! FOR loop results in the product  $[T]^{-1}[D]$  (or in terms of the
! variables,  $[Mm]^{-1}[Bpint]$ ).
!
! Variables:
! kcmn2 = The cutoff wave number squared, for each waveguide mode.
! zemn = The characteristic waveguide impedance for each mode.
!-----!

```

```

SUBROUTINE getapm(mtot,ntot,ptot,qtot,a,b,zemn,ismp,itmp,isnq,&
                itnq,pi,Mm,indx,mnt,pt,Bpint)
INTEGER mtot,ntot,ptot,qtot,im,in,ip,iq,z1,z2,z3,z4,pt,mnt,&
        indx(mnt)
DOUBLE PRECISION a,b,pi,ismp(0:mtot,0:ptot),itmp(0:mtot,0:ptot),&
                isnq(0:ntot,0:qtot),itnq(0:ntot,0:qtot),kcmn2,cmn,det
COMPLEX*16 zemn(0:mtot,0:ntot),Mm(mnt,mnt),Bpint(mnt,pt)
!-----!
do im=1,mtot
  do in=0,ntot-1
    kcmn2=(im*pi/a)**2+(in*pi/b)**2
    cmn=4/(a*b*kcmn2)
    if (in.eq.0) then
      cmn=cmn/2
    endif
    do ip=0,ptot-1
      do iq=0,qtot-1
        z1=in*mtot+im
        z2=mtot*(in+ntot)+im
        z3=ip*qtot+iq+1
        z4=qtot*(ip+ptot)+iq+1
        Bpint(z1,z3)=cmn*in*pi/b*itmp(im,ip)*isnq(in,iq)
        Bpint(z1,z4)=-cmn*im*pi/a*ismp(im,ip)*itnq(in,iq)
        if (in.eq.0) then
          Bpint(z2,z3)=0
        else
          Bpint(z2,z3)=Bpint(z1,z3)*im*b/(in*a*zemn(im,in))
        endif
        Bpint(z2,z4)=-Bpint(z1,z4)*in*a/(im*b*zemn(im,in))
      enddo
    enddo
  enddo
enddo

call ludcmp(Mm,mnt,mnt,indx,det)
do im=1,pt
  call lubksb(Mm,mnt,mnt,indx,Bpint(1,im))
enddo

return
end

```

---

**Getmatn.f90:**

!-----!

! Comments added 6/29/99 by Brian McConnell

! Original code written by Nathan Terril

```

!
! Purpose: This subroutine fills the matrix [Bhe] as used in the main
! program. [Bhe] is essentially the [A] matrix shown in equation
! (3.1.5) on p.30 of Terril's thesis. It is used to solve for the [ap]
! matrix which is needed to solve for the B mode coefficients.
!-----!
SUBROUTINE getmatn(mat,mtot,ntot,ptot,qtot,a,b,ismp,itmp,isnq,&
    itnq,pi,eta2,zemn)
INTEGER mtot,ntot,ptot,qtot,is,it,im,in,z1,z2,z3,z4
DOUBLE PRECISION a,b,pi,eta2,ismp(0:mtot,0:ptot),&
    itmp(0:mtot,0:ptot),isnq(0:ntot,0:qtot),itnq(0:ntot,0:qtot)
COMPLEX*16 zemn(0:mtot,0:ntot),mat(2*ptot*qtot,2*mtot*ntot)
!-----!
do is=0,ptot-1
  do it=0,qtot-1
    do im=1,mtot
      do in=0,ntot-1
        z1=is*qtot+it+1
        z2=is*qtot+ptot*qtot+it+1
        z3=in*2*mtot+im
        z4=in*2*mtot+mtot+im
        mat(z1,z4)=im*pi/a*itmp(im,is)*isnq(in,it)
        mat(z1,z3)=-mat(z1,z4)*in*a/(im*b)*zemn(im,in)/eta2
        mat(z2,z3)=im*pi/a*zemn(im,in)/eta2*itnq(in,it)*&
            ismp(im,is)
        mat(z2,z4)=mat(z2,z3)*in*a/(im*b)*eta2/zemn(im,in)
      enddo
    enddo
  enddo
enddo

return
end

```

---

**Getf.f90:**

```

!-----!
! Comments added 6/29/99 by Brian McConnell
! Original code written by Nathan Terril
!
! Purpose: This subroutine fills the forcing vector [F] shown in
! equation (3.1.5) on p.39 of Terril's thesis. the forcing vector is
! used to solve for the [ap] coefficients that are needed to find the
! B mode coefficients.
!-----!
SUBROUTINE getf(fmat,mtot,ntot,ptot,qtot,zemn,eta2,ismp,itnq,pi,a)
INTEGER mtot,ntot,ptot,qtot,is,it,z1,z2

```

```

DOUBLE PRECISION eta2,ismp(0:mtot,0:ptot),itnq(0:ntot,0:qtot),pi,a
COMPLEX*16 fmat(2*ptot*qtot,1),zemn
!-----!
do is=0,ptot-1
  do it=0,qtot-1
    z1=is*qtot+it+1
    z2=is*qtot+ptot*qtot+it+1
    fmat(z1,1)=(0d0,0d0)
    fmat(z2,1)=pi/a*ismp(1,is)*itnq(0,it)*zemn/eta2
  enddo
enddo

return
end

```

---

**Mult.f90:**

```

!-----!
! Comments added 6/29/99 by Brian McConnell
! Original code written by Nathan Terril
!
! Purpose: This code is used several times in the combined routine.
! It is a simple subroutine to perform matrix multiplication. The
! basic rules of matrix multiplication apply:
!   [a] = [b][c] --> # columns in [b] = # rows in [c]
!                   # rows in [a] = # rows in [b]
!                   # columns in [a] = # columns in [c]
!
! Variables:
! mat1 = A (m x n) matrix, one of the matrices to be multiplied.
! mat2 = A (n x p) matrix, one of the matrices to be multiplied.
! mat3 = A (m x p) matrix, the product matrix.
!-----!
SUBROUTINE mult(mat1,mat2,mat3,m,n,p)
INTEGER m,n,p,im,in,ip
COMPLEX*16 mat1(m,n),mat2(n,p),mat3(m,p)
!-----!
do im=1,m
  do ip=1,p
    mat3(im,ip)=(0d0,0d0)
    do in=1,n
      mat3(im,ip)=mat3(im,ip)+mat1(im,in)*mat2(in,ip)
    enddo
  enddo
enddo

return

```

end

---

**Ridcol.f90:**

```
!-----!  
! Comments added 6/29/99 by Brian McConnell  
! Original code written by Nathan Terril  
!  
! Purpose: This subroutine is used to condition the square input matrix  
! for subsequent use in the LU decomposition and back-substitution  
! subroutines. The presence of a row of zeros in the matrix would  
! cause a "singular matrix" error in the LU decomposition, so if such  
! a case happens, the row is replaced with ones.  
!  
! Variables:  
! mat = The square matrix passed into the subroutine.  
! mt = The dimension of the square input matrix.  
! im,in = Loop counter indices.  
!-----!  
SUBROUTINE ridcol(mat,mt)  
  INTEGER mt,in,im  
  DOUBLE PRECISION tst  
  COMPLEX*16 mat(mt,mt)  
!-----!  
  do in=1,mt  
    tst=0d0  
    do im=1,mt  
      tst=tst+abs(mat(im,in))  
    enddo  
    if (tst.eq.0d0) then  
      do im=1,mt  
        mat(im,in)=(1d0,0d0)  
      enddo  
    endif  
  enddo  
  
  return  
end
```

---

**Ludcmp.f90:**

```
!-----!  
! The lu-decomposition is taken from "Numerical recipes in FORTRAN"  
!  
! Largest expected n, and a small number.  
! Given a matrix a(1:n,1:n), with physical dimension np by np, this  
! routine replaces it by the LU decomposition of a rowwise  
! permutation of itself. a and n are input. a is output, arranged as
```

! in equation (2.3.14) above; indx(1:n) is an output vector that  
! records the row permutation effected by the partial pivoting; d is  
! output as (+/-) 1 depending on whether the number of row  
! interchanges was even or odd, respectively. This routine is used  
! in combination with lubksb to solve linear equations or invert  
! a matrix.

!-----!

```
SUBROUTINE ludcmp(a,n,np,indx,d)
PARAMETER (NMAX=1600,TINY=1D-20)
INTEGER n,np,indx(np),i,imax,j,k
DOUBLE PRECISION d,aamax,dum,vv(NMAX)
COMPLEX*16 a(np,np),cdum,sum
```

!-----!

! vv stores the implicit scaling of each row.

```
d=1D0
```

! No row interchanges yet.

```
do i=1,n
```

! Loop over rows to get the implicit scaling information.

```
aamax=0D0
```

```
do j=1,n
```

```
if (abs(a(i,j)).gt.aamax) aamax=abs(a(i,j))
```

```
enddo
```

```
if (aamax.eq.0.) pause 'singular matrix in ludcmp'
```

! No nonzero largest element.

```
vv(i)=1./aamax
```

! Save the scaling.

```
enddo
```

```
do j=1,n
```

! This is the loop over columns of Crout's method.

```
do i=1,j-1
```

! This is equation (2.3.12) except for  $i = j$ .

```
sum=a(i,j)
```

```
do k=1,i-1
```

```
sum=sum-a(i,k)*a(k,j)
```

```
enddo
```

```
a(i,j)=sum
```

```
enddo
```

```
aamax=0D0
```

! Initialize for the search for largest pivot element.

```
do i=j,n
```

! This is  $i = j$  of equation (2.3.12) and  $i = j + 1 \dots N$

! of equation (2.3.13).

```
sum=a(i,j)
```

```
do k=1,j-1
```

```
sum=sum-a(i,k)*a(k,j)
```

```

        enddo
        a(i,j)=sum
        dum=vv(i)*abs(sum)
! Figure of merit for the pivot.
        if (dum.ge.aamax) then
! Is it better than the best so far?
            imax=i
            aamax=dum
        endif
    enddo
    if (j.ne.imax)then
! Do we need to interchange rows?
        do k=1,n
! Yes, do so...
            cdum=a(imax,k)
            a(imax,k)=a(j,k)
            a(j,k)=cdum
        enddo
        d=-d
! ...and change the parity of d.
        vv(imax)=vv(j)
! Also interchange the scale factor.
    endif
    indx(j)=imax
    if(abs(a(j,j)).eq.0d0) a(j,j)=cmlpx(TINY)
! If the pivot element is zero the matrix is singular (at least to
! the precision of the algorithm). For some applications on singular
! matrices, it is desirable to substitute TINY for zero.
    if(j.ne.n)then
! Now, finally, divide by the pivot element.
        cdum=1./a(j,j)
        do i=j+1,n
            a(i,j)=a(i,j)*cdum
        enddo
    endif
enddo
! Go back for the next column in the reduction.

return
END

```

---

### **Lubksb.f90:**

```

!-----!
! Solves the set of n linear equations  $A \rightarrow X = B$ . Here a is input, not
! as the matrix A but rather as its LU decomposition, determined by
! the routine ludcmp. indx is input as the permutation vector

```

! returned by ludcmp. b(1:n) is input as the right-hand side vector  
 ! B, and returns with the solution vector X. a, n, np, and indx are  
 ! not modified by this routine and can be left in place for  
 ! successive calls with different right-hand sides b. This routine  
 ! takes into account the possibility that b will begin with many  
 ! zero elements, so it is efficient for use in matrix inversion.

!-----!

```
SUBROUTINE lubksb(a,n,np,indx,b)
  INTEGER n,np,indx(n),i,ii,j,ll
  COMPLEX*16 a(np,np),b(n),sum
```

!-----!

```
  ii=0
```

! When ii is set to a positive value, it will become the  
 ! index of the first nonvanishing element of b. We now do  
 ! the forward substitution, equation (2.3.6). The only  
 ! new wrinkle is to unscramble the permutation as we go.

```
  do i=1,n
    ll=indx(i)
    sum=b(ll)
    b(ll)=b(i)
    if (ii.ne.0)then
      do j=ii,i-1
        sum=sum-a(i,j)*b(j)
      enddo
    else if (abs(sum).ne.0.) then
      ii=i
```

! A nonzero element was encountered, so from now on we will  
 ! have to do the sums in the loop above.

```
  endif
  b(i)=sum
enddo
```

```
  do i=n,1,-1
```

! Now we do the backsubstitution, equation (2.3.7).

```
  sum=b(i)
  do j=i+1,n
    sum=sum-a(i,j)*b(j)
  enddo
  b(i)=sum/a(i,i)
```

! Store a component of the solution vector X.

```
  enddo
```

```
  return
  END
```

---

**Gcdata.f90:**

```

!-----!
! Comments added 6/29/99 by Brian McConnell
! Original code written by Nathan Terril
!
! Purpose: Solves for the cavity region mode coefficients, Ce and Ch.
! Like the waveguide B-region coefficients, the C mode coefficients
! are stored in a partitioned matrix to separate the TM and TE modes.
! Referring to figure 2.3 on p. 13 of Terrils' thesis, we see that
! unlike region B where there are forward and backward traveling waves
! to find coefficients for, the cavity region (C) has a standing wave
! because of the shorting plane and therefore does not need a + or -
! designation.
!
! Variables:
! Che = The partitioned matrix that stores the cavity mode
!       coefficients, Cmnh's and Cmne's.
! Bphe = The partitioned matrix that stores the mode coefficients for
!         the forward traveling waves in the waveguide region B.
! Bmhe = Like Bphe as described above, but for the backward traveling
!         waves.
! zemn = The array that stores the waveguide impedance for each mode.
! mtot,ntot = The number of waveguide modes in the x and y directions.
! eps = The permittivity of free space, a constant.
! a,d = Cavity width and length, respectively.
! d0 = The location of the rod axis in the z-direction.
!-----!
SUBROUTINE gcdata(Bphe,Bmhe,Che,zemn,eps,w,a,d,d0,xp,zp,&
                 mtot,ntot,mnt)
INTEGER mnt,mtot,ntot,im,in,r1,r2
DOUBLE PRECISION eps,w,a,d,d0,xp,zp,loc
COMPLEX*16 Bphe(mnt),Bmhe(mnt),Che(mnt),zemn(0:mtot,0:ntot),&
           sterm,eterm
!-----!
do im=1,mtot
  do in=0,ntot-1
    r1=in*mtot+im
    r2=(in+ntot)*mtot+im
    sterm=sin(zemn(im,in)*w*eps*(d0-d))
    eterm=exp(-(0,1)*zemn(im,in)*w*eps*d0)
    Che(r1)=1d0/sterm*(Bphe(r1)*eterm+Bmhe(r1))
    Che(r2)=(0,1)/sterm*(Bphe(r2)*eterm-Bmhe(r2))
  enddo
enddo

xp = 0.5d0*a
loc = 0

```

zp = d0\*(1+loc)

return  
end

---

**Gcey.f90:**

```
!-----!  
! Comments added 6/29/99 by Brian McConnell  
! Original code written by Nathan Terril  
!  
! Purpose: This subroutine uses the mode coefficients B+, B-, and C for  
! the TE and TM modes found in the previous routines and computes Ey,  
! the distribution of the tangential component of the electric field  
! along the fiber. This is the value that is used in the heat  
! generation term in the FTDT heat transfer model. The value computed  
! is a complex number and must later be converted to a real array  
! before being returned to the heat transfer model.  
!  
! Variables:  
! yp = The axial location along the fiber.  
! Ey = The array storing the complex valued tangential electric field  
! component.  
! zemn = The waveguide impedance for each mode.  
! Bphe,Bmhe = The forward and backward mode coefficient partitioned  
! matrices for the waveguide "B" region.  
! Che = The partitioned matrix for the mode coefficients in the cavity  
! "C" region.  
!-----!  
SUBROUTINE gcey(Bphe,Bmhe,Che,Ey,zemn,eps,pi,w,a,b,d,d0,xp,yp,zp,&  
    mtot,ntot,mnt,N)  
INTEGER mtot,ntot,mnt,im,in,iy,ih,ie,N  
DOUBLE PRECISION eps,pi,w,a,b,d,d0,xp,yp,zp  
COMPLEX*16 Bphe(mnt),Bmhe(mnt),Che(mnt),zemn(0:mtot,0:ntot),&  
    Ey(N),eterm1,eterm2,sterm  
CHARACTER*80 ebpath,ecpath,epath  
!-----!  
! The original version of this subroutine "getey" had a logic control  
! for the event where zp was greater than d0. Since this never happens  
! in the way we use this subroutine for the heat transfer model, the  
! superfluous logic events have been removed.  
  
do iy=1,N  
    yp=(iy-1)*b/(N-1)  
    Ey(iy)=(0d0,0d0)  
    do im=mtot,1,-1  
        do in=ntot-1,0,-1
```

```

      ih=in*mtot+im
      ie=(in+ntot)*mtot+im
      eterm1=exp(-(0,1)*zern(im,in)*w*eps*zp)
      eterm2=exp((0,1)*zern(im,in)*w*eps*(zp-d0))
      sterm=sin(im*pi*xp/a)*cos(in*pi*yp/b)
      Ey(iy)=Ey(iy)-pi*((im/a*Bphe(ih)+zern(im,in)*in/b*&
        Bphe(ie))*eterm1+(im/a*Bmhe(ih)-zern(im,in)*in/b*&
        Bmhe(ie))*eterm2)*sterm
    enddo
  enddo
enddo

return
end

```

---

### Fieldmag.f90:

```

!-----!
! Brian McConnell   6/25/99       Absoft FORTRAN 90 compiler
!
! Purpose: This subroutine is designed to take the complex tangential
! electric field distribution and turns it into an array of positive
! real numbers in order to be compatible with the heat transfer model.
!
! Variables:
! N = The number of material elements in the cavity
! I = An integer counter
! Ey(N) = Array of the tangential electric field component
! field(N) = Array of the magnitude of the absolute value of the
!           tangential electric field component
!-----!
SUBROUTINE fieldmag(Ey,field,N)
  INTEGER N,I
  COMPLEX*16 Ey(N)
  DOUBLE PRECISION field(N)
!-----!
  do I = 1,N
    field(I) = abs(Ey(I))
  enddo

  return
end

```

---

### Ecos.f90:

```

!-----!
! Commented on 6/28/99 by Brian McConnell
! Original code written by Nathan Terril

```

```

!
! Purpose: Evaluates integral(0,F)[exp(j*U*h**2*pi/b)*COS(G*PI*U/F)]dU
! This is the integral portion of equation (3.2.6) on page 47 of
! Terrils' thesis. It helps in finding the magnetic sheet current in
! the aperture.
!-----!
FUNCTION ecos(g,h,pi,f)
DOUBLE PRECISION pi,f,dif
INTEGER g,h
COMPLEX*16 ecos
!-----!
dif=ABS(g**2-4*h**2)
IF ((g.EQ.0).AND.(h.EQ.0)) THEN
  ecos=f
ELSE
  IF (dif.LT.1d-15) THEN
    ecos=.5*f
  ELSE
    ecos=(f/pi)**2*(1d0/(g**2-4*h**2))*(0,1)*h*(2*pi/f)*&
      ((-1)**g-1d0)
  ENDIF
ENDIF
RETURN
END

```

---

**S.f90:**

```

!-----!
! Comments added 6/30/99 by Brian McConnell
! Original code written by Nathan Terril
!
! Purpose: Evaluates integral
!       (F1,F2)[SIN(G*PI*U/L)*SIN(H*PI*(U-F1)/F)]dU
!
! Variables:
! f1,f2 = The limits of integration for the aperture integral, f1 the
!         lower and f2 the upper. When called in the x-direction, they
!         fix the location of the sides of the aperture. When called
!         in the y=direction, they fix the location of the top and
!         bottom of the aperture.
! f = The width of the aperture when called in the x-direction, and
!     the height of the aperture when called in the y-direction.
! g,h = The mode indexes in the x and y directions, respectively.
! l = The width of the cavity in the x-direction or the height of the
!     cavity in the y-direction.
!-----!

```

```

FUNCTION s(g,h,pi,f1,f2,f,l)
DOUBLE PRECISION s,pi,f1,f2,l,f,dif
INTEGER g,h
!-----!
dif=abs(h*l-g*f)
if ((g.eq.0).or.(h.eq.0)) then
  s=0d0
else
  if (dif.lt.1d-15) then
    s=.5*f*cos(g*pi*f1/l)
  else
    s=(f*h**2)/(pi*((g*f)**2-(l*h)**2))*((-1)**h*sin(g*pi*&
      f2/l)-sin(g*pi*f1/l))
  endif
endif
end

```

---

#### T.f90:

```

!-----!
! Comments added 6/30/99 by Brian McConnell
! Original code written by Nathan Terril
!
! Purpose: Evaluates integral
!   (F1,F2)[COS(G*PI*U/L)*COS(H*PI*(U-F1)/F)]dU
!
! Variables:
! f1,f2 = The limits of integration for the aperture integral, f1 the
!   lower and f2 the upper.  When called in the x-direction, they
!   fix the location of the sides of the aperture.  When called
!   in the y-direction, they fix the location of the top and
!   bottom of the aperture.
! f = The width of the aperture when called in the x-direction, and
!   the height of the aperture when called in the y-direction.
! g,h = The mode indexes in the x and y directions, respectively.
! l = The width of the cavity in the x-direction or the height of the
!   cavity in the y-direction.
!-----!
FUNCTION t(g,h,pi,f1,f2,f,l)
DOUBLE PRECISION t,pi,f1,f2,l,f,dif
INTEGER g,h
!-----!
dif=abs(h*l-g*f)
if ((g.eq.0).and.(h.eq.0)) then
  t=f
else

```

```

if ((g.eq.0).and.(h.gt.0)) then
  t=0d0
else
  if (dif.lt.1d-15) then
    t=.5*f*cos(g*pi*f1/l)
  else
    t=(g*l*f**2)/(pi*((g*f)**2-(l*h)**2))*((-1)**h*sin(g*pi*&
      f2/l)-sin(g*pi*f1/l))
  endif
endif
endif
end

```

# Appendix C

## User Interface Code

---

### **FrmParent:**

End of General Declaration Section

```
Private Sub MDIForm_Load()  
    Dim OutFile As String, InFile As String  
  
    frmParent.Top = 0  
    frmParent.Left = 0  
    frmParent.Width = 14000  
    frmParent.Height = 11000  
    ' When the program is initiated, show the  
    ' three children  
    frmGraphics.Show  
    frmGraphics.Width = 12720  
    frmGraphics.Height = 9030  
    frmHelp.Show  
    frmHelp.Width = 12720  
    frmHelp.Height = 8340  
    frmMain1.Show  
    frmMain1.Width = 12720  
    frmMain1.Height = 8340  
    frmIntro.Show  
    frmIntro.Top = 0  
    frmIntro.Left = 0  
  
    ' Open the Path data file and read in defaults  
    ' for the input and output file names.  
  
End Sub
```

---

### **FrmDataLoad:**

```
Private Sub cboFileType_Click()  
    'Change the Pattern of the file list box  
    'according to the File Type that the user  
    'selected.  
    Select Case cboFileType.ListIndex
```

```
Case 0
    filFiles.Pattern = "*.DAT"
Case 1
    filFiles.Pattern = "*.TXT"
Case 2
    filFiles.Pattern = "*.*"
End Select
```

```
End Sub
```

```
Private Sub Form_Load()
```

```
    frmDataLoad.Height = 5970
    frmDataLoad.Width = 6105
    txtDataFilePathAndName.Text = frmGraphics.gDataFilePathAndName
```

```
    'Fill the cboFileType combo box.
    cboFileType.AddItem "Data Files (*.DAT)"
    cboFileType.AddItem "Text Files (*.TXT)"
    cboFileType.AddItem "All Files (*.*)"
    cboFileType.ListIndex = 0
```

```
    'Update the lblDirName label with the path.
    lblDirName.Caption = dirDirectory.Path
```

```
End Sub
```

```
Private Sub drvDrive_Change()
```

```
    'The next statement may cause an error so we
    'set an error trap.
    On Error GoTo DriveError
```

```
    'Change the path of the directory list box to
    'the new drive.
    dirDirectory.Path = drvDrive.Drive
Exit Sub
```

```
DriveError:
```

```
    'An error occurred! So tell the user and
    'restore the original drive.
    MsgBox "Drive error!", vbExclamation, "Error"
    drvDrive.Drive = dirDirectory.Path
Exit Sub
```

```
End Sub
```

```

Private Sub dirDirectory_Change()
    'A directory was just selected by the user so
    'update the path of the file list box
    'accordingly
    filFiles.Path = dirDirectory.Path

    'Also update the lblDirName label.
    lblDirName.Caption = dirDirectory.Path

End Sub

Private Sub filFiles_Click()
    'Update the txtFileName text box with the file
    'name that was just selected.
    txtDataFilePathAndName.Text = filFiles.filename

End Sub

Private Sub cmdAccept_Click()

    On Error GoTo NotReady

    'If no file is selected, tell the user and
    'exit this procedure.
    If txtDataFilePathAndName.Text = "" Then
        MsgBox "You must first select a file!"
        Exit Sub
    End If

    'Make sure that the Path ends with backslash (\)
    If Right(filFiles.Path, 1) <> "\" Then
        Path = filFiles.Path + "\"
    Else
        Path = filFiles.Path
    End If

    'Extract the Path and Name of the selected file.
    If txtDataFilePathAndName.Text = filFiles.filename Then
        frmGraphics.gDataFilePathAndName = Path + filFiles.filename
    Else
        frmGraphics.gDataFilePathAndName = txtDataFilePathAndName.Text
    End If

    Unload frmDataLoad
    frmGraphics.SetFocus
    frmGraphics.txtDataFilePathAndName.Text = frmGraphics.gDataFilePathAndName

```

Exit Sub

NotReady:

MsgBox "The selected file is either in use or not available."

Exit Sub

End Sub

Private Sub filFiles\_DblClick()

'Update the txtFileName text box with the file  
'name that was just double clicked.  
'An error may result if the file is already  
'open so we set an error trap.

On Error GoTo FileBusy

txtDataFilePathAndName.Text = filFiles.filename

'Execute the cmdAccept\_Click () procedure.

cmdAccept\_Click

Exit Sub

FileBusy:

MsgBox "That file is either already in use or not available."

Exit Sub

End Sub

Private Sub cmdCancel\_Click()

Unload frmDataLoad

frmGraphics.SetFocus

frmParent.Arrange vbCascade

frmParent.Width = 14000

frmParent.Height = 11000

frmGraphics.Width = 12720

frmGraphics.Height = 9030

frmHelp.Width = 12720

frmHelp.Height = 8340

frmMain1.Width = 12720

frmMain1.Height = 8340

End Sub

---

**FrmDone:**

```

Private Sub cmdSimDone_Click()
    Unload frmDone
    frmMain1.SetFocus
    frmParent.Arrange vbCascade
    frmGraphics.Width = 12720
    frmGraphics.Height = 8340
    frmHelp.Width = 12720
    frmHelp.Height = 8340
    frmMain1.Width = 12720
    frmMain1.Height = 8340
End Sub

```

---

### **FrmGraphics:**

```

Public gCounter As Integer
Public gKeepTrack As Integer
Dim gTempLabels(0 To 4) As Integer
Dim gFieldLabels(0 To 4) As Integer
Public gDataFilePathAndName As String
Public gGoAnimate As Integer
Dim gTempScales(0 To 5) As Integer
Dim gFieldScales(0 To 5) As Long
Public gTempStep As Integer
Public gFieldStep As Long
Public gTScale As Integer
Public gFScale As Integer

Public gTimeLimit As Integer

' End of general declarations section.
' All of the sections in this form use the following
' naming convention:
' G(variable name) = a variable holding information
'     to be displayed in the graphics
'     section.
' g_(variable name) = a global variable declared in the
'     general declaration section that
'     is visible to all Subroutines in
'     the form.

```

```

Private Sub cmdPause_Click()
    If frmGraphics.gGoAnimate = 1 Then
        frmGraphics.gGoAnimate = 0
        cmdPause.Caption = "&Un-Pause"
    Else
        frmGraphics.gGoAnimate = 1
        cmdPause.Caption = "&Pause"
    End If
End Sub

```

End If

End Sub

Private Sub Form\_Load()

Dim DataFile As String

' Initialize parameters and variable initial values.

frmGraphics.gCounter = 1

frmGraphics.gKeepTrack = 0

cmdPause.Enabled = False

frmGraphics.Height = 9030

frmGraphics.Width = 12720

' TScale and FScale are used to store the current index for the

' y-axis scale for their respective plots. The plot is initialized

' to the minimum temp and max field axis scales, and the scale is

' updated as needed as the animation progresses so that the maximum

' value plotted is always less than the maximum value of the y-axis

' labels.

TScale = 0

FScale = 5

' gTempScales() holds the max axis label values for the

' various temperature ranges.

gTempScales(0) = 500

gTempScales(1) = 1000

gTempScales(2) = 1500

gTempScales(3) = 2000

gTempScales(4) = 2500

gTempScales(5) = 3000

' gFieldScales() holds the max axis label values for the

' various field strength ranges.

gFieldScales(0) = 25000

gFieldScales(1) = 50000

gFieldScales(2) = 75000

gFieldScales(3) = 100000

gFieldScales(4) = 150000

gFieldScales(5) = 200000

' Initialize the size of the elements in the table to the

' proper size.

For Counter = 0 To 1 Step 1

    grdTable.ColWidth(Counter) = 650

Next Counter

For Counter = 0 To 39 Step 1

```

    grdTable.RowHeight(Counter) = 202
Next Counter
grdTable.Width = 1376
grdTable.Height = 8930
grdTable.Top = 682
grdTable.Left = 7511

' Initialize the labels in the temperature plot area to the
' smallest scale.
lblTempAxis(4).Caption = gTempScales(gTScale)
lblTempAxis(0).Caption = 0
gTempStep = gTempScales(gTScale) / 4
For Counter = 3 To 1 Step -1
    lblTempAxis(Counter).Caption = gTempScales(gTScale) - ((4 - Counter) *
gTempStep)
Next Counter

' Initialize the labels in the field strength plot area to
' the smallest scale.
lblFieldAxis(4).Caption = gFieldScales(gFScale)
lblFieldAxis(0).Caption = 0
gFieldStep = gFieldScales(gFScale) / 4
For Counter = 3 To 1 Step -1
    lblFieldAxis(Counter).Caption = gFieldScales(gFScale) - ((4 - Counter) * gFieldStep)
Next Counter

End Sub

Private Sub cmdAnimate_Click()
    ' This section is activated when the user picks the
    ' "Start" button in the "Animation Information" frame.

    Dim Blank As String, InputString As String, ISFormatted As String

    cmdPause.Enabled = True
    If gKeepTrack = 1 Then ' The graphics are already running so stop them...
        cmdAnimate.Caption = "&Start"

        frmGraphics.gKeepTrack = 0
        frmGraphics.gGoAnimate = 0 ' Disable the timer flag.
        Close #6

    Exit Sub
Else ' The graphics are not running so start them...

```

```

cmdAnimate.Caption = "S&top"
frmGraphics.gKeepTrack = 1

If txtDataFilePathAndName.Text = "" Then
  MsgBox "Must select a data file first!"
  Exit Sub
End If

filename$ = gDataFilePathAndName
Next_File% = FreeFile
If Next_File <> 6 Then
  Open filename$ For Input As #6
End If

' Input the first line from the data file.
' If the first line indicates an improper data
' file was selected, do not continue with the subroutine.
Input #6, GHello$
If GHello$ <> "For use with Visual Basic interface" Then
  MsgBox "The data file selected is not of the correct format."
  Exit Sub
End If

' Read in the data that was originally passed to the Fortran
' program that specifies the parameters selected for the
' simulation. Write the appropriate values into the text
' boxes on the right side of the window. These values do
' not change during the animation process.
Input #6, GSSFlag%
Input #6, GMtot%
txtAnModeCX.Text = GMtot%
Input #6, GNtot%
txtAnModeCY.Text = GNtot%
Input #6, GPtot%
txtAnModeAX.Text = GPtot%
Input #6, GQtot%
txtAnModeAY.Text = GQtot%
Input #6, Gc2a#
Input #6, Gv2b#
Input #6, Gt2a#
Input #6, GLossFlag%
Input #6, GFTypeFlag%
If GLossFlag% = 0 Then
  optAnUniform.Value = True
ElseIf GFTypeFlag% = 0 Then
  optAnNoLoss.Value = True

```

```

Else
  optAnYesLoss.Value = True
End If
Input #6, GSource$
Input #6, GPower#
Input #6, GGd2lg#
Input #6, GFreq#
txtAnFreq.Text = GFreq#
Input #6, GVel#
txtAnVelocity.Text = GVel# * 1000#
Input #6, GMat$
txtAnMat.Text = GMat$
Input #6, GLeng#
Input #6, GDiam#
txtAnDiam.Text = GDiam# * 1000#
Input #6, Gaaa#
Input #6, Gbbb#
Input #6, GE#
Input #6, GTinf#
txtAnAirTemp.Text = GTinf#
Input #6, GTTub#
txtAnWallTemp.Text = GTTub#
Input #6, GDTStep#
txtAnTimeStep.Text = GDTStep#
Input #6, GDiff#
txtAnDiff.Text = GDiff#
Input #6, GDiffSS#
txtAnDiffSS.Text = GDiffSS#
Input #6, Blank
Input #6, Blank

' The next task will be to parse through the data file to
' find the integer value for the time of the last set of
' data. Once this is done, the data file must be reset to
' where it is now i.e. at the start of the animation data.
FoundItFlag% = 0
LoopCounter% = 0
Do While FoundItFlag = 0
  Input #6, InputString
  ISFormatted = LTrim(InputString)
  If ISFormatted = "*****" Then
    FoundItFlag = 1
  Else
    If LoopCounter = 1000 Then
      MsgBox "Could not find the Time length of the data file!"
      Exit Sub
    End If
  End If
Loop

```

```

    End If
  End If
Loop
' The data file is now poised before the line that contains the
' time limit of the simulation. This value is stored in order
' to stop the animation at the end of the data file.
Input #6, Time_Max%
frmGraphics.gTimeLimit = Time_Max

' Now reset the data file and cue it up to the first line of
' the animation data.
Close #6
Open filename$ For Input As #6
For Counter = 1 To 29 Step 1
  Input #6, Blank$
Next

' Now the data file is cued to the first line of the data
' that will change during the animation. Set the timer flag
' variable to 1 so that the timer subroutine will be enabled.

frmGraphics.gGoAnimate = 1
End If
End Sub

Private Sub cmdEndGraphics_Click()
' This section is activated when the user picks
' "Return to Main" button in the "Animation Information"
' frame.

FileNumber% = FreeFile
If FileNumber = 7 Then
  Close #6
End If

frmMain1.SetFocus
frmParent.Arrange vbCascade
frmGraphics.Width = 12720
frmGraphics.Height = 9030
frmHelp.Width = 12720
frmHelp.Height = 8340
frmMain1.Width = 12720
frmMain1.Height = 8340
End Sub

Private Sub cmdGetData_Click()

```

```
' This section is activated when the user picks  
' the "Select Output File" button in the  
' "Output File" frame.
```

```
frmDataLoad.Show  
frmDataLoad.SetFocus
```

```
End Sub
```

```
Private Sub tmrTimer1_Timer()  
    Dim Time As Integer  
    Dim Ebar As Double, AbsPow As Double, LostPow As Double  
    Dim MaxSurf As Double, MaxElement As Double  
    Dim MaxField As Double  
    Dim T(0 To 39, 0 To 7) As Single  
    Dim Field(0 To 39) As Single  
    Dim Space As String  
    Dim FormHeight As Integer  
    Dim TMax As Integer  
    Dim FMax As Long  
    Dim YValue As Single  
    Dim TScaleChange As Integer  
    Dim FScaleChange As Integer  
    Dim Changed As Integer
```

```
FormHeight = 3705  
TScaleChange = 0  
FScaleChange = 0  
tmrTimer1.Interval = 1  
MaxField = 0  
Flag% = frmGraphics.gGoAnimate  
' If Flag = 1 then animation is on.  
' If Flag = 0 then animation is off.  
If Flag = 1 Then
```

```
    ' Loop through the data display loop until the last data  
    ' set has been displayed. This loop is  
    ' suspended when the "Pause" button is clicked.
```

```
    ' Read in all of the data from the .dat file for one time step.  
    Input #6, Time, Ebar, AbsPow, LostPow, MaxSurf, MaxElement  
    For I% = 0 To 39 Step 1  
        ' Center elements are T(I,1) and surface elements  
        ' are T(I,8).
```

```

Input #6, Field(I), T(I, 0), T(I, 1), T(I, 2), T(I, 3), T(I, 4), T(I, 5), T(I, 6), T(I, 7)
' Check if the current field strength is larger than the
' value currently stored as the largest.
If Field(I) > MaxField Then
    MaxField = Field(I)
End If

Next
Input #6, Space
' The data file is now cued to the start of the next
' set of animation data (next time step).
' Now put take the temperature values that were just read
' in and display them in the table. 'I' is the counter
' to loop through rows, and 'J' is the counter to loop
' through the columns.
txtAnTime.Text = Time
txtAnAEFS.Text = Ebar
txtAnABSP.Text = AbsPow
txtAnLossPower.Text = LostPow
txtMET.Text = MaxElement
txtAnMST.Text = MaxSurf
For I% = 0 To 39 Step 1
    grdTable.Row = I
    For J% = 0 To 1 Step 1
        If J = 0 Then
            grdTable.Col = J
            grdTable.Text = T(I, J)
        Else
            grdTable.Col = 1
            grdTable.Text = T(I, 7)
        End If
    Next J
Next I

' Check to see if the temperature and field strength axis
' labels need to be updated. If so, change all of the axis
' labels. Switch to the next larger or smaller scale as needed.
' First see if the next larger scale is needed.
Do While TScaleChange = 0
    Changed = 0
    If MaxSurf > gTempScales(gTScale) Then
        If gTScale <> 5 Then
            TScaleChange = 1
            gTScale = gTScale + 1
            lblTempAxis(4).Caption = gTempScales(gTScale)
            gTempStep = gTempScales(gTScale) / 4
        End If
    End If

```

```

    For Counter = 3 To 1 Step -1
        lblTempAxis(Counter).Caption = gTempScales(gTScale) _
            - ((4 - Counter) * gTempStep)
    Next Counter
    Changed = 1
End If
End If
If gTScale <> 0 Then
    If MaxSurf < gTempScales(gTScale - 1) Then
        gTScale = gTScale - 1
        lblTempAxis(4).Caption = gTempScales(gTScale)
        gTempStep = gTempScales(gTScale) / 4
        For Counter = 3 To 1 Step -1
            lblTempAxis(Counter).Caption = gTempScales(gTScale) _
                - ((4 - Counter) * gTempStep)
        Next Counter
        Changed = 1
    End If
End If
If Changed = 0 Then
    TScaleChange = 1
End If
Loop
' Now check the field strength axis label values.
' Switch to the next larger or smaller scale as needed.
' First, see if the next larger scale is needed.
Do While FScaleChange = 0
    Changed = 0
    If MaxField > gFieldScales(gFScale) Then
        If gFScale <> 5 Then
            gFScale = gFScale + 1
            lblFieldAxis(4).Caption = gFieldScales(gFScale)
            gFieldStep = gFieldScales(gFScale) / 4
            For Counter = 3 To 1 Step -1
                lblFieldAxis(Counter).Caption = gFieldScales(gFScale) _
                    - ((4 - Counter) * gFieldStep)
            Next Counter
            Changed = 1
        End If
    End If
    If gFScale <> 0 Then
        If MaxField < gFieldScales(gFScale - 1) Then
            gFScale = gFScale - 1
            lblFieldAxis(4).Caption = gFieldScales(gFScale)
            gFieldStep = gFieldScales(gFScale) / 4
            For Counter = 3 To 1 Step -1

```

```

        lblFieldAxis(Counter).Caption = gFieldScales(gFScale) _
            - ((4 - Counter) * gFieldStep)
    Next Counter
    Changed = 1
End If
End If
If Changed = 0 Then
    FScaleChange = 1
End If

Loop
' Now that the axis scaling has been updated,
' move the temperature and field markers to their new positions
' corresponding to the updated values for this time step.
TMax = gTempScales(gTScale)
FMax = gFieldScales(gFScale)
For Counter = 0 To 39 Step 1
    ' First, do the temperature
    YValue = FormHeight * (1# - (T(Counter, 7) / TMax))
    linTemp(Counter).Y1 = YValue
    linTemp(Counter).Y2 = YValue
    ' Then, do the field strength
    YValue = FormHeight * (1# - (Field(Counter) / FMax))
    linField(Counter).Y1 = YValue
    linField(Counter).Y2 = YValue
Next Counter

' Increment the counter that
' keeps track of position in the file versus the end
' of the data sets.
frmGraphics.gCounter = frmGraphics.gCounter + 1
If frmGraphics.gCounter = (gTimeLimit + 2) Then
    frmGraphics.gGoAnimate = 0
    frmGraphics.gKeepTrack = 0
    cmdAnimate.Caption = "&Start"
    Exit Sub
End If
End If
End Sub

```

---

### **FrmHelp:**

```

Private Sub cmdEndHelp_Click()
    frmMain1.SetFocus
    frmParent.Arrange vbCascade
    frmGraphics.Width = 12720
    frmGraphics.Height = 9030

```

```
frmHelp.Width = 12720
frmHelp.Height = 8340
frmMain1.Width = 12720
frmMain1.Height = 8340
End Sub
```

```
Private Sub optAperHelp_Click()
    txtHelp.Text = "This simulator models a box-shaped cavity coupled by a rectangular
iris. The iris "
    txtHelp.Text = txtHelp.Text + "dimensions needed are the width and height of the
aperture. "
    txtHelp.Text = txtHelp.Text + "Changing the dimensions of the aperture will result in a
different "
    txtHelp.Text = txtHelp.Text + "distribution in the electric field along the heated part.
The "
    txtHelp.Text = txtHelp.Text + "original default values are for the aperture used at the
Los Alamos "
    txtHelp.Text = txtHelp.Text + "National Laboratory: 27.78 mm wide x 7.54 mm high."
End Sub
```

```
Private Sub optCavHelp_Click()
    txtHelp.Text = "This simulator is designed for waveguides with a rectangular cross-
section normal"
    txtHelp.Text = txtHelp.Text + " to the direction of wave propagation. The dimensions
required are"
    txtHelp.Text = txtHelp.Text + " the inside dimensions of the waveguide in the plane
normal to the "
    txtHelp.Text = txtHelp.Text + "direction of wave propagation. The default values that
correspond "
    txtHelp.Text = txtHelp.Text + "to the dimensions at Los Alamos National Laboratory
are: 254 mm "
    txtHelp.Text = txtHelp.Text + "long x 72 mm wide x 34 mm high and a rod distance
from peak of 0."
End Sub
```

```
Private Sub optFreqHelp_Click()
    txtHelp.Text = "This is the value, in GigaHertz, of the frequency of the microwave
source. Electro"
    txtHelp.Text = txtHelp.Text + "magnetic waves in the frequency range from 300 MHz
to 300 GHz are class"
    txtHelp.Text = txtHelp.Text + "ified as microwaves. The Magnetron is a common
source in home micro"
    txtHelp.Text = txtHelp.Text + "wave ovens and is ususally set at an operating frequency
of 2.45 GHz"
    txtHelp.Text = txtHelp.Text + " for the preparation of food. The source used at
VPI&SU also operat"
```

```

    txtHelp.Text = txtHelp.Text + "es at this frequency. The source used for the
experiments at Los "
    txtHelp.Text = txtHelp.Text + "Alamos National Laboratory was operating at a nominal
frequency of "
    txtHelp.Text = txtHelp.Text + "2.93 GHz."
End Sub

```

```

Private Sub optLossHelp_Click()
    txtHelp.Text = "Include wall loss to incorporate losses in the field due to non-ideal
interactions "
    txtHelp.Text = txtHelp.Text + "at the lateral walls of the waveguide. This does not
include the lo"
    txtHelp.Text = txtHelp.Text + "ss due to interactions with the iris, adjustable short, or
the varia"
    txtHelp.Text = txtHelp.Text + "ble coupler used at the Los Alamos National
Laboratory."
End Sub

```

```

Private Sub optMatHelp_Click()
    txtHelp.Text = "Choose the material you wish to simulate in the process. Only
materials listed are"
    txtHelp.Text = txtHelp.Text + " currently available for the simulation. This is due to the
limited"
    txtHelp.Text = txtHelp.Text + " amount of reliable property data currently available.
The results "
    txtHelp.Text = txtHelp.Text + "obtained for zirconia should be treated with caution
because of the "
    txtHelp.Text = txtHelp.Text + "fact that the emissivity of the substance is modeled with
the data "
    txtHelp.Text = txtHelp.Text + "from alumina. This should be corrected when data for
the emissivity"
    txtHelp.Text = txtHelp.Text + " of zirconia becomes available."
End Sub

```

```

Private Sub optModeHelp_Click()
    txtHelp.Text = "The convergence of the solution is dependent on how the waveguide
and aperture"
    txtHelp.Text = txtHelp.Text + " modes are truncated. The number of cavity modes
determines how"
    txtHelp.Text = txtHelp.Text + " well the Green's function is approximated. The
function is approxi"
    txtHelp.Text = txtHelp.Text + "mated as a truncation of an infinite series. Ideally, an
infinite "
    txtHelp.Text = txtHelp.Text + "number of modes should be used, but this is unrealistic
due to limi"

```

```

txtHelp.Text = txtHelp.Text + "tations on computational resources. The number of
aperture"
txtHelp.Text = txtHelp.Text + " modes determines how well the magnetic surface
current at the aperture"
txtHelp.Text = txtHelp.Text + " iris is approximated. The Default values, 10 in X and 5
in Y,"
txtHelp.Text = txtHelp.Text + "are sufficiently large to "
txtHelp.Text = txtHelp.Text + "ensure convergence in most cases without excessive
calculations."
txtHelp.Text = txtHelp.Text + "It is recommended that the number of cavity modes in
X be >= the "
txtHelp.Text = txtHelp.Text + "number of aperture modes in X times the ratio of the
cavity width to"
txtHelp.Text = txtHelp.Text + " the aperture width. Generally, the larger the dimensions
of the "
txtHelp.Text = txtHelp.Text + "aperture, the more aperture modes are required to
approximate the "
txtHelp.Text = txtHelp.Text + "magnetic surface current."
End Sub

```

```

Private Sub optPowerHelp_Click()

```

```

txtHelp.Text = "A field strength, in V/m, must be entered. Selecting the 'Constant Field
Strength' "
txtHelp.Text = txtHelp.Text + "option simulates a process where the microwave
generator supplies a "
txtHelp.Text = txtHelp.Text + "constant electromagnetic source. The absorbed power
level of the "
txtHelp.Text = txtHelp.Text + "material is then dependent on the material temperature
and thermal "
txtHelp.Text = txtHelp.Text + "runaway is possible. Selecting the 'Constant Absorbed
Power' option "
txtHelp.Text = txtHelp.Text + "simulates the use of feedback control of the microwave
source. It "
txtHelp.Text = txtHelp.Text + "varies the strength of the source to keep the absorbed
power of the "
txtHelp.Text = txtHelp.Text + "specimen constant and helps to avoid thermal runaway."
txtHelp.Text = txtHelp.Text + "A power level must be entered when using the 'Constant
Absorbed Power'"
txtHelp.Text = txtHelp.Text + " option. This is also the initial value used for the field
strength "
txtHelp.Text = txtHelp.Text + "when a uniform field shape is being used in 'Constant
Absorbed Power'"
txtHelp.Text = txtHelp.Text + "mode."
End Sub

```

```

Private Sub optProcessHelp_Click()

```

```

txtHelp.Text = "The 'Batch Process' option is used for cases with zero rod velocity. If
Rate "
txtHelp.Text = txtHelp.Text + "Process' is selected, a rod velocity must also be entered
or it "
txtHelp.Text = txtHelp.Text + "will default to zero."
End Sub

```

```

Private Sub optRunHelp_Click()
txtHelp.Text = "Select 'Run to Steady State' to continue the simulation as long as it takes
for"
txtHelp.Text = txtHelp.Text + " the material to reach a steady temperature distribution
for the"
txtHelp.Text = txtHelp.Text + " given power conditions. Select 'Run to Specified Time'
to run "
txtHelp.Text = txtHelp.Text + "the simulation for the length of time specified in the
appropriate"
txtHelp.Text = txtHelp.Text + " window. The 'Run to Steady State' option must be
selected in order"
txtHelp.Text = txtHelp.Text + " to run cases with non-zero rod velocities."
End Sub

```

```

Private Sub optSpecHelp_Click()
txtHelp.Text = "The length and diameter of the specimen are required. The length of
the sample "
txtHelp.Text = txtHelp.Text + "should be left at the default value of 34 mm."
End Sub

```

```

Private Sub optUpdate_Click()
txtHelp.Text = "This option is essential to providing fast and accurate results when the
enhanced fi"
txtHelp.Text = txtHelp.Text + "eld option is being used. Calculating the shape of the
electric field"
txtHelp.Text = txtHelp.Text + " distribution at every time step is really not necessary for
accurate "
txtHelp.Text = txtHelp.Text + "results. The maximum nodal temperature change can be
specified so that "
txtHelp.Text = txtHelp.Text + "the electric field shape is only re-calculated after a
sufficient tempe"
txtHelp.Text = txtHelp.Text + "rature change has occurred. This prevents excessive
calculations when "
txtHelp.Text = txtHelp.Text + "the dielectric properties of the material have not changed
significan"
txtHelp.Text = txtHelp.Text + "tly. A recommended value of 10 degrees Celcius greatly
improves the "
txtHelp.Text = txtHelp.Text + "run time required while virtually no change in the final
temperature "

```

```

txtHelp.Text = txtHelp.Text + "distribution occurs. This is partly due to the fact that,
while the "
txtHelp.Text = txtHelp.Text + "shape of the field distribution may not be updated at
every step, the"
txtHelp.Text = txtHelp.Text + " shape is scaled at every step to result in the desired
heating rate."
End Sub

```

---

**FrmIntro:**

```

Private Sub cmdOk_Click()
    Unload frmIntro

End Sub

```

---

**FrmMain1:**

```

Public gInputFile As String
Public gSaveFile As String

```

' End of general declarations section.

```

Private Sub cmdDefault_Click()
    'Read in each value from the data file and convert the
    'string data to integer, double, or boolean value.

    Open "D:\GRA\HTNew\defaults.dat" For Input As #9
    'Open "C:\Microsim\defaults.dat" For Input As #9

    Input #9, dataline$
    txtPowCheck.Text = CDbl(dataline$)
    Input #9, dataline$
    If dataline$ = "1" Then
        optSteadyState.Value = True
    Else
        optSteadyState.Value = False
    End If
    Input #9, dataline$
    If dataline$ = "1" Then
        optCavitySI.Value = True
    Else
        optCavitySI.Value = False
    End If
    Input #9, dataline$
    If dataline$ = "1" Then

```

```

    optSpecimenSI.Value = True
Else
    optSpecimenSI.Value = False
End If
Input #9, dataline$
txtCavityLength.Text = CDbI(dataline$)
Input #9, dataline$
txtCavityWidth.Text = CDbI(dataline$)
Input #9, dataline$
txtCavityHeight.Text = CDbI(dataline$)
Input #9, dataline$
txtRodLocation.Text = CDbI(dataline$)
Input #9, dataline$
txtDiameter.Text = CDbI(dataline$)
Input #9, dataline$
txtRodLength.Text = CDbI(dataline$)
Input #9, dataline$
txtModeXCav.Text = CInt(dataline$)
Input #9, dataline$
txtModeYCav.Text = CInt(dataline$)
Input #9, dataline$
txtModeXAper.Text = CInt(dataline$)
Input #9, dataline$
txtModeYAper.Text = CInt(dataline$)
optBatch.Value = True
Input #9, dataline$
If dataline$ = "Alumina" Then
    optAlumina.Value = True
ElseIf dataline$ = "Mullite" Then
    optMullite.Value = True
ElseIf dataline$ = "Nylon" Then
    optNylon.Value = True
Else
    optZirconia.Value = True
End If
Input #9, dataline$
txtPower.Text = CDbI(dataline$)
Input #9, dataline$
If dataline$ = "1" Then
    optAbsPower.Value = True
Else
    optAppliedPower = True
End If
Input #9, dataline$
txtAperWidth.Text = CDbI(dataline$)
Input #9, dataline$

```

```

txtAperHeight.Text = CDb1(dataline$)
Input #9, dataline$
If dataline$ = "1" Then
  optAperSI.Value = True
Else
  optAperUS.Value = True
End If
Input #9, dataline$
If dataline$ = "0" Then
  optUniField.Value = True
ElseIf dataline = "1" Then
  optEnhanceNo.Value = True
Else
  optEnhanceYes.Value = True
End If
Input #9, dataline$
txtFrequency.Text = CDb1(dataline$)
Input #9, dataline$
txtFieldStrength.Text = CDb1(dataline$)
Input #9, dataline$
txtTimeStep.Text = CDb1(dataline$)
Input #9, dataline$
txtDTStep.Text = CDb1(dataline$)
Input #9, dataline$
txtDTSS.Text = CDb1(dataline$)
Input #9, dataline$
txtWallTemp.Text = CDb1(dataline$)
Input #9, dataline$
txtAirTemp.Text = CDb1(dataline$)
Input #9, dataline$
If dataline$ = "1" Then
  optTempSI.Value = True
Else
  optTempUS.Value = True
End If
Input #9, dataline$
If CDb1(dataline$) = 0# Then
  optFUOeveryTS.Value = True
  txtFUOdT.Text = "0.0"
Else
  optFUOsomeTS.Value = True
  txtFUOdT.Text = dataline$
End If
Input #9, dataline$
If dataline$ = "1" Then
  optFUOC.Value = True

```

```

Else
    optFUOF.Value = True
End If

Close #9
End Sub

Private Sub cmdExit_Click()
    End
End Sub

Private Sub cmdGraphics_Click()
    ' Load the Graphics form and size the windows.
    frmGraphics.SetFocus
    frmParent.Arrange vbCascade
    frmHelp.Width = 12720
    frmHelp.Height = 8340
    frmMain1.Width = 12720
    frmMain1.Height = 8340
    frmGraphics.Width = 12720
    frmGraphics.Height = 9030
End Sub

Private Sub cmdHelp_Click()
    ' Load the Help form and size the windows.
    frmHelp.SetFocus
    frmParent.Arrange vbCascade
    frmGraphics.Width = 12720
    frmGraphics.Height = 9030
    frmMain1.Width = 12720
    frmMain1.Height = 8340
    frmHelp.Width = 12720
    frmHelp.Height = 8340
End Sub

Private Sub cmdPickSaveFile_Click()
    ' Load the Pick Save File form.
    frmPickSaveFile.Show

End Sub

Private Sub cmdRun_Click()
    Dim InFlag As Integer
    Dim InFileName As String

    ' Writes the input file for the Fortran program and starts the

```

```

' Fortran code with the Shell command
' All dimension output must be in units of meters for the Fortran
' program to work, so all inputs are properly converted here
' txtModeXCav is "mtot", number of cavity x-modes to include
' txtModeYCav is "ntot", number of cavity y-modes to include
' txtModeXAper is "ptot", number of Green's Function unknowns in X
' txtModeYAper is "qtot", number of Green's Function unknowns in Y

' Check for user interface problems that could crash the program.
' Make sure a "save file" has been specified.
If txtSaveFile.Text = "" Then
    MsgBox ("You MUST select a Save file first!")
    Exit Sub
End If
' If a rate process selected, make sure a rate is entered.
If optRate.Value = True Then
    If txtRateSpeed.Text = "" Then
        MsgBox ("You MUST specify a velocity to use Rate Process option!")
        Exit Sub
    End If
End If
' If Input File mode is selected, make sure a data file is selected.
If optInputFile.Value = True Then
    If txtInputFile.Text = "" Then
        MsgBox ("You MUST specify a file name to use Input File option!")
        Exit Sub
    End If
End If
' Make sure the Cavity Dimensions have been selected.
If txtCavityWidth.Text = "" Or _
txtCavityHeight.Text = "" Or _
txtCavityLength.Text = "" Or _
txtRodLocation.Text = "" Then
    MsgBox ("One or more elements in the Cavity Dimensions section is empty!")
    Exit Sub
End If
' Make sure the Specimen Dimensions have been selected.
If txtDiameter.Text = "" Or _
txtRodLength.Text = "" Then
    MsgBox ("One or more elements in the Specimen Dimensions section is empty!")
    Exit Sub
End If
' Make sure the Temperatures have been selected.
If txtWallTemp.Text = "" Or _
txtAirTemp.Text = "" Then
    MsgBox ("One or more of the environment temperatures is empty!")

```

```

Exit Sub
End If
' Make sure the Modes section is completed.
If txtModeXCav.Text = "" Or _
txtModeYCav.Text = "" Or _
txtModeXAper.Text = "" Or _
txtModeYAper.Text = "" Then
MsgBox ("One or more of the Modes is empty!")
Exit Sub
End If
' Make sure the Field Strength/Power Level is completed.
If txtFieldStrength.Text = "" Then
MsgBox ("You MUST enter a nominal Field Strength for ANY simulation!")
Exit Sub
End If
If optAbsPower.Value = True Then
If txtPower.Text = "" Then
MsgBox ("You MUST enter a Power Level to use the Absorbed Power option!")
Exit Sub
End If
End If
' Make sure the Frequency is specified.
If txtFrequency.Text = "" Then
MsgBox ("You MUST enter a nominal source frequency!")
Exit Sub
End If
' Make sure the Aperture Dimensions are specified.
If txtAperWidth.Text = "" Or _
txtAperHeight.Text = "" Then
MsgBox ("One or more Aperture Dimensions is empty!")
Exit Sub
End If
' Make sure the Convergence Criteria are specified.
If txtTimeStep.Text = "" Or _
txtPowCheck.Text = "" Or _
txtDTStep.Text = "" Or _
txtDTSS.Text = "" Then
MsgBox ("One or more of the Convergence Criteria is empty!")
Exit Sub
End If
' Make sure the Field Update Options are specified
If txtFUOdT.Text = "" Then
MsgBox ("One or more of the Field Update Options is empty!")
Exit Sub
End If

```

'Open the file to which the input parameters will be written. The  
'Fortran code will open this file and read in data from it.  
Open "D:\GRA\HTNew\interout.dat" For Output As #1  
'Open "C:\Microsim\interout.dat" For Output As #1

```
If optTimeLimit.Value = True Then
  SS% = 0
Else
  SS% = 1
End If
'change the temperatures into Absolute Kelvin
If optTempUS.Value = True Then
  TTUB# = ((Cdbl(txtWallTemp.Text) - 32) / 1.8) + 273.15
  TINF# = ((Cdbl(txtAirTemp.Text) - 32) / 1.8) + 273.15
Else
  TTUB# = Cdbl(txtWallTemp.Text) + 273.15
  TINF# = Cdbl(txtAirTemp.Text) + 273.15
End If
'configure convergence criteria for FORTRAN code
DT# = Cdbl(txtTimeStep.Text)
DIFF# = Cdbl(txtDTStep.Text)
DIFFSS# = Cdbl(txtDTStep.Text)
If optCavityUS.Value = True Then
  CavLength# = Cdbl(txtCavityLength.Text) / 254#
  CavWidth# = Cdbl(txtCavityWidth.Text) / 254#
  CavHeight# = Cdbl(txtCavityHeight.Text) / 254#
Else
  CavLength# = Cdbl(txtCavityLength.Text) / 1000#
  CavWidth# = Cdbl(txtCavityWidth.Text) / 1000#
  CavHeight# = Cdbl(txtCavityHeight.Text) / 1000#
End If
If optSpecimenUS.Value = True Then
  Diameter# = Cdbl(txtDiameter.Text) / 254#
  RodLength# = Cdbl(txtRodLength.Text) / 254#
Else
  Diameter# = Cdbl(txtDiameter.Text) / 1000#
  RodLength# = Cdbl(txtRodLength.Text) / 1000#
End If
If optRate.Value = True Then
  If optProcessUS.Value = True Then
    Speed# = Cdbl(txtRateSpeed.Text) / 254#
  Else
    Speed# = Cdbl(txtRateSpeed.Text) / 1000#
  End If
Else
  Speed# = 0#
```

```

End If
If optAperUS.Value = True Then
  AperWidth# = CDbI(txtAperWidth.Text) / 254#
  AperHeight# = CDbI(txtAperHeight.Text) / 254#
Else
  AperWidth# = CDbI(txtAperWidth.Text) / 1000#
  AperHeight# = CDbI(txtAperHeight.Text) / 1000#
End If
If optEnhanceYes.Value = True Then   `enhanced with loss
  Loss% = 1
  Field% = 1
ElseIf optUniField.Value = False Then `enhanced with out loss
  Loss% = 0
  Field% = 1
Else                                `uniform field
  Loss% = 0
  Field% = 0
End If
If optAppliedPower.Value = True Then
  Source$ = "ELECTRIC"
End If
If optAbsPower.Value = True Or _
  optInputFile.Value = True Then
  Source$ = "POWER"
End If
If optAlumina.Value = True Then
  MaterI$ = "ALUMINA"
ElseIf optMullite.Value = True Then
  MaterI$ = "MULLITE"
ElseIf optZirconia.Value = True Then
  MaterI$ = "ZIRCONIA"
Else
  MaterI$ = "NYLON"
End If

Mtot% = Int(txtModeXCav)
Ntot% = Int(txtModeYCav)
Ptot% = Int(txtModeXAper)
Qtot% = Int(txtModeYAper)
c2a# = AperWidth / CavWidth
v2b# = AperHeight / CavHeight
t2a# = Diameter / CavWidth
Pow# = CDbI(txtPower.Text)
pi# = 3.14159
`MUST LEAVE FREQUENCY IN GHz!!!!
Freq# = CDbI(txtFrequency.Text)

```

```

W# = Freq * 2 * pi * (10 ^ 9)
' Right now, I'm assuming the relative permeability of air is 1.0
' If I find later that it is not so, I must change the following
' calculation for the waveguide frequency...
' Essentially assuming c(propagation speed) in air = c in vacuum =
' the speed of light.
u# = 3# * 10 ^ 8
CutFreq# = u / W
Lambda# = u / W
GuideFreq# = Lambda / ((1 - (CutFreq / W) ^ 2#) ^ 0.5)

d2lg# = CavLength / GuideFreq
E# = CDb1(txtFieldStrength.Text)
PCheck# = CDb1(txtPowCheck.Text)

' Decide the value of the Input File Mode flag.
If optInputFile.Value = True Then
    InFlag = 1
    InFileName = txtInputFile
Else
    InFlag = 0
    InFileName = "NONE"
End If

' Change the value of the Field Update Options temperature
' step to SI if they are in English units and not zero...
If optFUOeveryTS = False Then
    If optFUOF.Value = True Then
        TLIMIT# = CDb1(txtFUOdT.Text) * 0.55555556
    Else
        TLIMIT# = CDb1(txtFUOdT.Text)
    End If
Else
    TLIMIT# = 0#
End If

' Now write all of the data from the input interface to a data file
' that the Fortran code can read from...
Write #1, SS, TLIMIT
Write #1, Mtot
Write #1, Ntot
Write #1, Ptot
Write #1, Qtot
Write #1, c2a
Write #1, v2b
Write #1, t2a

```

```

Write #1, Loss
Write #1, Field
Write #1, Source
Write #1, Pow
Write #1, d2lg
Write #1, Freq
Write #1, Speed
Write #1, Materl
Write #1, RodLength
Write #1, Diameter
Write #1, CavWidth
Write #1, CavHeight
Write #1, E
Write #1, TINF
Write #1, TTUB
Write #1, DT, PCheck
Write #1, DIFF
Write #1, DIFFSS
Write #1, txtSaveFile.Text
Write #1, InFlag, InFileName
Close #1
filename$ = txtSaveFile.Text

```

```

' Now call the Fortran program to run.
' The VB handling program can be terminated once the Fortran code
' is running... the only change is that the time stamp will not
' appear on the bottom of the data file. i.e. you won't know exactly
' how long the code took to finish running. The advantage is that
' the Fortran code runs faster, especially when you are running multiple
' simulatneous simulations.

```

```

frmRunning.Show
frmRunning.Top = 500
frmRunning.Left = 500
frmRunning.SetFocus
frmRunning.Width = 3810
frmRunning.Height = 1755
StartTime = Timer
RunShell "D:\GRA\HTNew\HTMain.exe"
'RunShell "C:\Microsim\HTMain.exe"
RunTime = Timer - StartTime
Open filename For Append As #2
Write #2, "Actual Simulation Run Time = "; RunTime; " seconds"
Close #2
Beep
Unload frmRunning
frmDone.Show

```

```

frmDone.SetFocus
frmDone.Top = 500
frmDone.Left = 500
End Sub

```

```

Private Sub RunShell(cmdline As String)

```

```

    Dim hProcess As Long
    Dim ProcessId As Long
    Dim exitCode As Long

```

```

    ProcessId = Shell(cmdline, 6)
    hProcess = OpenProcess(PROCESS_QUERY_INFORMATION, False, ProcessId)

```

```

    Do

```

```

        Call GetExitCodeProcess(hProcess, exitCode)
        DoEvents

```

```

    Loop While exitCode = STATUS_PENDING `new

```

```

    Call CloseHandle(hProcess)

```

```

    `Unload frmRunning
    `MsgBox "The shelled process " & cmdline & " has ended."

```

```

End Sub

```

```

Private Sub cmdSaveDefaults_Click()

```

```

    Open "D:\GRA\HTNew\defaults.dat" For Output As #9

```

```

    `Open "C:\Microsim\defaults.dat" For Output As #9

```

```

    Write #9, CDbl(txtPowCheck.Text)

```

```

    If optSteadyState.Value = True Then

```

```

        Write #9, "1"

```

```

    Else

```

```

        Write #9, "0"

```

```

    End If

```

```

    If optCavitySI.Value = True Then

```

```

        Write #9, "1"

```

```

    Else

```

```

        Write #9, "0"

```

```

    End If

```

```

    If optSpecimenSI.Value = True Then

```

```

        Write #9, "1"

```

```

    Else

```

```

    Write #9, "0"
End If
Write #9, CDbI(txtCavityLength.Text)
Write #9, CDbI(txtCavityWidth.Text)
Write #9, CDbI(txtCavityHeight.Text)
Write #9, CDbI(txtRodLocation.Text)
Write #9, CDbI(txtDiameter.Text)
Write #9, CDbI(txtRodLength.Text)
Write #9, CInt(txtModeXCav.Text)
Write #9, CInt(txtModeYCav.Text)
Write #9, CInt(txtModeXAper.Text)
Write #9, CInt(txtModeYAper.Text)
If optAlumina.Value = True Then
    Write #9, "Alumina"
ElseIf optMullite.Value = True Then
    Write #9, "Mullite"
ElseIf optNylon.Value = True Then
    Write #9, "Nylon"
Else
    Write #9, "Zirconia"
End If
Write #9, CDbI(txtPower.Text)
If optAbsPower.Value = True Then
    Write #9, "1"
Else
    Write #9, "0"
End If
Write #9, CDbI(txtAperWidth.Text)
Write #9, CDbI(txtAperHeight.Text)
If optAperSI.Value = True Then
    Write #9, "1"
Else
    Write #9, "0"
End If
If optUniField.Value = True Then
    Write #9, "0"
ElseIf optEnhanceNo.Value = True Then
    Write #9, "1"
Else
    Write #9, "2"
End If
Write #9, CDbI(txtFrequency.Text)
Write #9, CDbI(txtFieldStrength.Text)
Write #9, CDbI(txtTimeStep.Text)
Write #9, CDbI(txtDTStep.Text)
Write #9, CDbI(txtDTSS.Text)

```

```

Write #9, CDbI(txtWallTemp.Text)
Write #9, CDbI(txtAirTemp.Text)
If optTempSI.Value = True Then
    Write #9, "1"
Else
    Write #9, "0"
End If
Write #9, CDbI(txtFUOdT.Text)
If optFUOC.Value = True Then
    Write #9, "1"
Else
    Write #9, "0"
End If
Close #9
End Sub

```

```

Private Sub optAbsPower_Click()
' The absorbed power option must clear the input file selection
' if it is selected.
    If optInputFile.Value = True Then
        optInputFile.Value = False
        optBatch.Value = True
    End If
    If txtInputFile.Text <> "" Then
        txtInputFile.Text = ""
    End If
End Sub

```

```

Private Sub optAppliedPower_Click()
' The applied power option must clear the input file selection
' if it is selected.
    If optInputFile.Value = True Then
        optInputFile.Value = False
        optBatch.Value = True
    End If
    If txtInputFile.Text <> "" Then
        txtInputFile.Text = ""
    End If

End Sub

```

```

Private Sub optFUOeveryTS_Click()
    txtFUOdT.Text = "0.0"
End Sub

```

```

Private Sub optInputFile_Click()
    ' The input file option can not be used at the same time as
    ' the Absorbed Power of Constant Field options. If Input File
    ' is the selected option, the other options must be de-selected.
    If optAppliedPower.Value = True Then
        optAppliedPower.Value = False
    End If
    If optAbsPower.Value = True Then
        optAbsPower.Value = False
    End If
    If txtPower.Text <> "" Then
        txtPower.Text = ""
    End If
    txtPower.Text = "1"
    frmPickInputFile.Show
End Sub

```

```

Private Sub optRate_Click()
    ' Rate option must clear the value in the Input File box if
    ' it isn't already empty.
    If txtInputFile.Text <> "" Then
        txtInputFile.Text = ""
    End If
End Sub

```

---

### **FrmPickInputFile:**

```

Private Sub Form_Load()
    ' Size the form.
    frmPickInputFile.Height = 5900
    frmPickInputFile.Width = 5400

    ' Fill the cboFileType combo box.
    cboFileType.AddItem "Data Files (*.DAT)"
    cboFileType.AddItem "Text Files (*.TXT)"
    cboFileType.AddItem "All Files (*.*)"
    cboFileType.ListIndex = 0

    ' Update the lblDirName label with the path.
    lblDirName.Caption = dirDirectory.Path
End Sub
Private Sub drvDrive_Change()
    ' The next statement may cause an error so we
    ' set an error trap.

```

```
On Error GoTo DriveError
```

```
'Change the path of the directory list box to  
'the new drive.  
dirDirectory.Path = drvDrive.Drive  
Exit Sub
```

```
DriveError:
```

```
'An error occurred! So tell the user and  
'restore the original drive.  
MsgBox "Drive error!", vbExclamation, "Error"  
drvDrive.Drive = dirDirectory.Path  
Exit Sub
```

```
End Sub
```

```
Private Sub dirDirectory_Change()  
'A directory was just selected by the user so  
'update the path of the file list box  
'accordingly  
filFiles.Path = dirDirectory.Path
```

```
'Also update the lblDirName label.  
lblDirName.Caption = dirDirectory.Path
```

```
End Sub
```

```
Private Sub filFiles_Click()  
'Update the txtFileName text box with the file  
'name that was just selected.  
txtInputFile.Text = filFiles.filename
```

```
End Sub
```

```
Private Sub cmdAccept_Click()  
Dim PathAndName As String
```

```
On Error GoTo NotReady
```

```
'If no file is selected, tell the user and  
'exit this procedure.  
If txtInputFile.Text = "" Then  
MsgBox "You must first select a file!"  
Exit Sub  
End If
```

```
'Make sure that the Path ends with backslash (\)
```

```
If Right(filFiles.Path, 1) <> "\" Then
```

```
    Path = filFiles.Path + "\"
```

```
Else
```

```
    Path = filFiles.Path
```

```
End If
```

```
'Extract the Path and Name of the selected file.
```

```
If txtInputFile.Text = filFiles.filename Then
```

```
    frmMain1.gInputFile = Path + filFiles.filename
```

```
Else
```

```
    frmMain1.gInputFile = txtInputFile.Text
```

```
End If
```

```
Unload frmPickInputFile
```

```
frmMain1.txtInputFile.Text = frmMain1.gInputFile
```

```
Exit Sub
```

```
NotReady:
```

```
    MsgBox "The selected file is either in use or not available."
```

```
Exit Sub
```

```
End Sub
```

```
Private Sub filFiles_DblClick()
```

```
'Update the txtFileName text box with the file  
'name that was just double clicked.
```

```
'An error may result if the file is already
```

```
'open so we set an error trap.
```

```
On Error GoTo FileBusy
```

```
txtInputFile.Text = filFiles.filename
```

```
'Execute the cmdAccept_Click () procedure.
```

```
cmdAccept_Click
```

```
Exit Sub
```

```
FileBusy:
```

```
    MsgBox "That file is either already in use or not available."
```

```
Exit Sub
```

```
End Sub
```

```
Private Sub cmdCancel_Click()
```

Unload frmPickInputFile

End Sub

Private Sub cboFileType\_Click()

'Change the Pattern of the file list box  
'according to the File Type that the user  
'selected.

Select Case cboFileType.ListIndex

Case 0

filFiles.Pattern = "\*.DAT"

Case 1

filFiles.Pattern = "\*.TXT"

Case 2

filFiles.Pattern = "\*.\*"

End Select

End Sub

---

### **FrmPickSaveFile:**

Private Sub Form\_Load()

txtSaveFile.Text = frmMain1.gSaveFile

'Fill the cboFileType combo box.

cboFileType.AddItem "Data Files (\*.DAT)"

cboFileType.AddItem "Text Files (\*.TXT)"

cboFileType.AddItem "All Files (\*.\*)"

cboFileType.ListIndex = 0

'Update the lblDirName label with the path.

lblDirName.Caption = dirDirectory.Path

End Sub

Private Sub drvDrive\_Change()

'The next statement may cause an error so we  
'set an error trap.

On Error GoTo DriveError

'Change the path of the directory list box to  
'the new drive.

dirDirectory.Path = drvDrive.Drive

Exit Sub

DriveError:

'An error occurred! So tell the user and

```

'restore the original drive.
MsgBox "Drive error!", vbExclamation, "Error"
drvDrive.Drive = dirDirectory.Path
Exit Sub

End Sub
Private Sub dirDirectory_Change()
'A directory was just selected by the user so
'update the path of the file list box
'accordingly
filFiles.Path = dirDirectory.Path

'Also update the lblDirName label.
lblDirName.Caption = dirDirectory.Path

End Sub

Private Sub filFiles_Click()
'Update the txtFileName text box with the file
'name that was just selected.
txtSaveFile.Text = filFiles.filename

End Sub

Private Sub cmdAccept_Click()
Dim PathAndName As String

On Error GoTo NotReady

'If no file is selected, tell the user and
'exit this procedure.
If txtSaveFile.Text = "" Then
MsgBox "You must first select a file!"
Exit Sub
End If

'Make sure that the Path ends with backslash (\)
If Right(filFiles.Path, 1) <> "\" Then
Path = filFiles.Path + "\"
Else
Path = filFiles.Path
End If

'Extract the Path and Name of the selected file.
If txtSaveFile.Text = filFiles.filename Then
frmMain1.gSaveFile = Path + filFiles.filename

```

```

Else
    frmMain1.gSaveFile = txtSaveFile.Text
End If

Unload frmPickSaveFile
frmMain1.txtSaveFile.Text = frmMain1.gSaveFile

Exit Sub

NotReady:
    MsgBox "The selected file is either in use or not available."
Exit Sub

End Sub

Private Sub filFiles_DblClick()

    'Update the txtFileName text box with the file
    'name that was just double clicked.
    'An error may result if the file is already
    'open so we set an error trap.

    On Error GoTo FileBusy
    txtSaveFile.Text = filFiles.filename

    'Execute the cmdAccept_Click () procedure.
    cmdAccept_Click
Exit Sub

FileBusy:
    MsgBox "That file is either already in use or not available."
Exit Sub

End Sub

Private Sub cmdCancel_Click()

    Unload frmPickSaveFile

End Sub
Private Sub cboFileType_Click()

    'Change the Pattern of the file list box
    'according to the File Type that the user
    'selected.

```

```
Select Case cboFileType.ListIndex
Case 0
    filFiles.Pattern = "*.DAT"
Case 1
    filFiles.Pattern = "*.TXT"
Case 2
    filFiles.Pattern = " *.*"
End Select
```

```
End Sub
```

---

### **Module1:**

```
Option Explicit
```

```
Public Declare Function OpenProcess Lib "kernel32" _
    (ByVal dwDesiredAccess As Long, _
    ByVal bInheritedHandle As Long, _
    ByVal dwPcprocessId As Long) As Long
```

```
Public Declare Function GetExitCodeProcess Lib "kernel32" _
    (ByVal hProcess As Long, lpExitCode As Long) As Long
```

```
Public Declare Function CloseHandle Lib "kernel32" _
    (ByVal hObject As Long) As Long
```

```
Public Const PROCESS_QUERY_INFORMATION = &H400
Public Const STATUS_PENDING = &H103& `new
```

**The vita has been removed from  
the scanned document**